STATUS OF THESIS

Title of thesis: Estimation of Surface Moisture Content and Evapotranspiration Using Weightage Approach.

I ABDALHALEEM ABDALLA HASSABALLA

hereby allow my thesis to be placed at the Information Resource Center (IRC) of Universiti Teknologi PETRONAS (UTP) with the following conditions:

1. The thesis becomes the property of UTP
2. The IRC of UTP may make copies of the thesis for academic purposes only.
3. This thesis is classified as

☐ Confidential

☑ Non-confidential

If this thesis is confidential, please state the reason:

____

The contents of the thesis will remain confidential for __________ years.

Remarks on disclosure:

____

Endorsed by

Signature of Author	Signature of Supervisor
Permanent address: University of Khartoum, P. O. Box: 321, Khartoum, Sudan	Name of Supervisor Assoc. Prof. Dr. Abd Nasir B. Matori
Date: January 21, 2014	Date :

UNIVERSITI TEKNOLOGI PETRONAS

ESTIMATION OF SURFACE MOISTURE CONTENT AND EVAPOTRANSPIRATION USING WEIGHTAGE APPROACH.

By

ABDALHALEEM ABDALLA HASSABALLA

The undersigned certify that they have read, and recommend to the Postgraduate Studies Programme for acceptance this thesis for the fulfillment of the requirements for the degree stated.

Signature:

Main Supervisor: Assoc. Prof. Dr. Abd Nassir B. Matori

Signature:

Co-Supervisor: Assoc. Prof. Dr. Helmi Z. M. Shafri

Signature:

Head of Department: Assoc. Prof. Dr. Ir. Mohd Shahir Liew

Date:

ESTIMATION OF SURFACE MOISTURE CONTENT AND EVAPOTRANSPIRATION USING WEIGHTAGE APPROACH.

by

ABDALHALEEM ABDALLA HASSABALLA

A Thesis

Submitted to the Postgraduate Studies Programme

as a Requirement for the Degree of

DOCTOR OF PHILOSOPHY

CIVIL ENGINEERING DEPARTMENT

UNIVERSITI TEKNOLOGI PETRONAS

BANDAR SERI ISKANDAR,

PERAK

JANUARY 2014

DECLARATION OF THESIS

Title of thesis	Estimation of Surface Moisture Content and Evapotranspiration Using Weightage Approach.

I ABDALHALEEM ABDALLA HASSABALLA

hereby declare that the thesis is based on my original work except for quotations and citations which have been duly acknowledged. I also declare that it has not been previously or concurrently submitted for any other degree at UTP or other institutions.

	Witnessed by
Signature of Author	Signature of Supervisor
Permanent address: University of Khartoum, P. O. Box: 321, Khartoum, Sudan	Name of Supervisor Assoc. Prof. Dr. Abd Nasir B. Matori
Date : January 21, 2014	Date :

DEDICATION

I lovingly dedicate this thesis to my family, especially..

To my parents for instilling the meaning of hard work;

To my wife for the non-stop motivation and encouragement.

ACKNOWLEDGEMENTS

First and foremost, I would like to express my deep and sincere gratitude to my supervisor, Associate Professor Dr. Abdul Nassir Bin Matori, Geoinformatics and Highway Cluster, Civil Eng. Dept., for his encouragement and support in this work, providing me with valuable advice as a supervisor, derived from his knowledge as a professor and also for appreciable efforts in facilitating the research.

I am also grateful to my Field supervisor Associate Professor Dr. Helmi Zulhaeidi Bin M. Shafri Dept. of Civil Engineering UPM, for his guidance and advices in organizing and satisfying the research needs. Appreciation is also extended to him for proving the required data.

I highly acknowledge the support given by Universiti Teknologi PETRONAS in pursuing this study. I do never forget to acknowledge the assistant provided by the Malaysian Agency for Remote Sensing for access to the satellite images. Assistances provided by SITIAWAN meteorological station and FELCRA Berhad Perak represented in data collection, are highly acknowledged as well. Further, I gratefully acknowledges the financial support provided by Education Sponsorship Unit of PETRONAS and CGS-UTP as part of PhD scholarship.

Primary acknowledgement goes to those directly involved with the Remote Sensing and GIS knowledge as lecturers and colleagues for their valuable knowledge sharing.

On a personal note, I would like to thank my family and my parents in Sudan for their continuous support and patience throughout the whole study time..

ABSTRACT

Soil moisture (MC) and evapotranspiration (ET) are considered as the most significant boundary conditions controlling most of the hydrological cycle's processes. However, monitoring them continuously over large areas using the high temporal-resolution optical satellites is very demanding. Satellites such as the Advanced Very High Resolution Radiometer (AVHRR) and the Moderate Resolution Imaging Spectroradiometer (MODIS), have a coarse spatial resolution in their images. Thus it not only impedes the acquisition of an accurate MC and ET but also represents multispectral reflections from the holistic surface features. This beside their dependence on vegetation and ground coefficient when assessing MC and ET. The study aims to enhance the spatial accuracy by weighting the MC produced from different surface cover classes within the pixel. MC for each pixel is segmented into three (3) different classes namely urban, vegetation and multi surface cover according to their respective MC weightage. Secondly, to generate an improved actual ET_a map by overlaying the segmented MC with a rectified ETo. Images from AVHRR and MODIS satellites were selected in order to generate MC and ET maps. Two powerful MC algorithms were used based on land Surface Temperature (Ts), vegetation Indices (VI) and field measurements of MC; which were conducted at variable depths to examine the depth influence on MC and Ts magnitudes. The study area was divided into the three classes according to the nature of surface cover. ET images were produced based on two scenarios. Firstly, from energy budget principle using satellite's rectified Ts and VI. Secondly, from Jacobs algorithm strengthened by moisture weighted maps. The resultant MC and ET maps were considerably improved after a pixel segmentation method was used which represented their true MC value for each individual class of surface cover within the image pixel. The enhancement accuracy gained by this method ranged from 0.66 to 0.95 for MC and 0.62 to 0.88 for ET when a statistical validation was conducted to examine the homogeneity and

disparity in the produced results. A spatial validation was conducted using the success rate validation in order to examine the influence of MC in the actual ET assessment.

Energy Balance Algorithm for Land SEBAL models was also used in order to validate the proposed algorithm. The spatial validation assured the usefulness of the proposed Jacobs method with MC weighted approach in producing a valuable estimation of the actual evapotranspiration from the soil status and the available potential evapotranspiration. Accuracies of 0.66, 0.85 and 0.87 from NOAA 17, NOAA 18 and MODIS TERRA images respectively were produced.

ABSTRAK

Keadaan kelembapan tanah dan evapotranspirasi dianggap sebagai elemen yang amat signifikan dalam mengawal keseluruhan proses kitaran hidrologi. Walaubagaimanapun, pemantauan terhadap kelembapan permukaan (MC) dan evapotranspirasi (ET) menggunakan optikal temporal-resolusi tinggi ke atas suatu kawasan yang luas adalah begitu mendesak. Satelit seperti "Advanced Very high Resolution Radiometer" (AVHRR) dan "Moderate Resolution Imaging Spectroradiometer" (MODIS) mempunyai spatial resolusi yang agak kasar pada setiap imej. Oleh itu, ia bukan sahaja menghalang pemerolehan sebuah kelembapan permukaan dan evapotranspirasi dengan tepat tetapi juga mewakili pantulan multi-spektral dari ciri-ciri permukaan holistic selain kaitan kecekapannya terhadap tumbuh-tumbuhan dan tanah apabila menilai MC dan ET. Kajian ini bertujuan untuk meningkatkan ketepatan spatial dengan mengunakan kaedah pemberat iaitu MC yang dihasilkan dari kelas tutup bumi di dalam suatu piksel. MC untuk setiap piksel dibahagikan kepada tiga kelas (3) yang berbeza iaitu kawasan bandar, kawasan pertanian dan kawasan yang dilitupi pelbagai jenis permukaan mengikut pemberat MC. Seterusnya adalah untuk menghasilkan peta Eta yang lebih baik dengan melapisi MC bersegmen dengan Eto yang diperbetulkan. Imej satelit dari AVHRR dan MODIS telah dipilih untuk menjana peta MC dan ET. Dua MC algoritma telah digunakan berdasarkan suhu permukaan tanah (Ts), indeks tumbuhan (VI) dan ukuran keluasan kelembapan permukaan; yang dijalankan pada kedalaman yang pelbagai untuk mengkaji pengaruh MC dan magnitudes Ts. Kawasan kajian telah dibahagikan kepada 3 kelas asas berdasarkan keadaan litupan permukaan. Akhirnya, imej evapotranspirasi dihasilkan berasaskan dua senario. Senario pertama berasaskan prinsip bajet tenaga menggunakan rektifikasi Ts and NDVI daripada satelit. Manakala yang kedua melibatkan penggabungan kelembapan menggunakan algoritma Jacobs dengan peta kelembapan umum. Hasilnya, peta MC dan ET telah bertambah baik selepas kaedah

segmentasi piksel yang digunakan iaitu untuk mewakili nilai MC sebenar bagi setiap kelas individu litupan permukaan di dalam imej piksel. Ketepatan peningkatan yang diperolehi melalui kaedah ini adalah di antara 0.66 hingga 0.95 dan 0.62 hingga 0.88 untuk ET iaitu apabila pengesahan statistic dijalankan untuk mengkaji keseragaman dan perbezaan perbezaan untuk keputusan yang telah dihasilkan. Untuk tujuan validasi, pengesahan spatial telah dibuat menggunakan validasi kadar keberkesanan untuk mengkaji pengaruh MC di dalam penilaian ET yang sebenar.

Model “Energy Balance Algorithm of Land” atau SEBAL juga telah digunakan untuk tujuan validasi algoritma yang dicadangkan. Validasi spatial turut dilakukan terhadap kaedah Jacobs yang telah dicadangkan dengan pemberat MC untuk menghasilkan anggaran evapotranspirasi yang betul dari status tanah dan potensi evapotranspirasi yang ada dengan ketepatan setiap satunya adalah 0.66, 0.85 dan 0.87 daripada imej NOAA 17, NOAA 18 dan MODIS TERRA.

TABLE OF CONTENTS

LIST OF FIGURES

LIST OF TABLES

LIST OF ABBREVIATIONS

ALOS	Advanced Land Observing Satellite
AMSR	Advanced Microwave Scanning Radiometer
ASTER	Advanced Spaceborne Thermal Emission and Reflection Radiometer
ATI	Apparent Thermal Inertia
AUC	Area Under the Curve
AVHRR	Advanced Very High Resolution Radiometer
CLM	Common Land Model
DEM	Digital Elevation Model
DN	Digital Number
DOY	Day Of the Year
ENVI	Environment for Visualizing Images
EOS-PM	Earth Observing System - Post Meridiem
ERS	European remote sensing satellite
ESMR	Electrically Scanning Microwave Radiometer
ESRI	Environmental Sciences Research Institute
ESTAR	Electrically Scanning Thinned Array Radiometer
ET	Evapotranspiration
ET_a	Actual Eavpotranspiration
ET_c	Crop Evapotranspiration under standard conditions
ETM	Enhanced Thematic Mapper
EuDASM	European Digital Archive of Soil Maps
EVI	Enhanced Vegetation Index
FAO	Food and Agriculture Organization
FC	Field Capacity
Fr	fraction of vegetation
FLAASH	Fast Line-of-sight Atmosphere Analysis of Spectral Hypercubes
GCM	General Circulation Model
GIS	Geographical Information System
GMS	Geostationary Meteorological Satellite
GPS	Global Positioning System

HRPT	High Resolution Picture Transmission
IBM	International Business Machine
IES	Institute of Environment and Sustainability
JERS	Japanese Earth Resources Satellite
LAADS	Level 1 and Atmosphere Archive and Distribution System
LAI	leaf area index
LANDSAT	Land Remote Sensing Satellite System
LIDAR	Light Detection and Ranging
LSM	Land Surface Model
LST	Land Surface Temperature
LULC	Land Use/ Land Cover
MetOP-A	Meteorological Operational satellite
MMD	Malaysian Meteorological Department
MODIS	Moderate Resolution Imaging Spectroradiometer
MOSTI	Ministry of Science, Technology and Innovation
MSAVI	Modified Soil Adjusted Vegetation Index
NASA	National Aeronautics and Space Administration
NDVI	Normalized Difference Vegetation Index
NEDT	Noise Equivalent Differential Temperature
NOAA	National Oceanic and Atmospheric Administration'
PET	Potential Evapotranspiration
PM	Penman-Monteith
PSD	Particle Size Distribution
PWP	Permanent Wilting Point
RADAR	Radio Detection and Ranging
RadarSAT	An advanced Earth observation satellite project
RAR	Real Aperture Radar
RH	Relative Humidity
RMS	Root-Mean-Square
RS	Remote Sensing
S.Perak	Seberang Perak
SAR	Synthetic aperture radar

SAVI	Soil Adjusted Vegetation Index
SCS	Soil Conservation Service
SEBAL	Surface Energy Balance Algorithm for Land
SITI	Sitiawan city
SLAR	Side-Looking Airborne Radar
SMMR	Scanning Multichannel Microwave Radiometer
SONAR	Sound Navigation and Ranging
SPOT	Système Pour l'Observation de la Terre
SPSS	Statistical Package for the Social Sciences
SSM/I	Special Sensor Microwave/Imager
SST	Sea Surface Temperature
SVAT	Soil Vegetation Atmosphere Transfer
SWC	Soil Water Content
SWI	Soil Wetness Index
T_a	Air Tempreature
T_s	Surface Temperature
TB	Brightness Temperature
T_d	Differential Temperature
TDR	Time Domain Reflectometer
TI	Thermal Inertia
TM	Thematic Mapper
TIROS-N	Television Infrared Observation Satellite-National
TVDI	Temperature-Vegetation Dryness Index
TVX	Temperature Vegetation Contextual
USCS	Unified Soil Classification System
USDA	U.S. Department of Agriculture
USGS	United States Geological Survey
UT	Universal Triangle approach
UTM	Universal Transverse Mercator
UTP	Universiti Teknologi PETRONAS
VI	Vegetation Index
VMC	Vegetation and Moisture Coefficient

NOMENCLATURE

MC_g	Gravimetric soil moisture content
MC_v	Volumetric soil moisture content
ρ_w	Water density
ε_r	The dielectric constant
σ_o	Backscattered signal
W_q	The surface scattering albedo
T_{vq}	Microwave brightness temperature
τ_q	Vegetation optical depth
k_0	Free-space vegetation constant
s	Surface root mean square (RMS) height
θ	View angle
R_q	Fresnel reflectivity of the flat surface
T_4 and T_5	Brightness temperature for channel 4 and 5 respectively
$T_a^{\uparrow}$	The average temperature of radiance going upward
$T_a^{\downarrow}$	The average temperature to the downward radiance
σ	Stefan-Boltzmann Const. (5.67×10^{-8} $Wm^{-2}K^{-4}$)
T_B	Brightness temperature (^oK)
B	Amount of radiation emitted (Wm^2)
Lλ	The spectral radiance (W/m^2-ster-μm)
DN	The digital number of image pixels
QC_{max}	The maximum quantized calibrated pixel value
QC_{min}	The minimum quantized calibrated pixel value
Lmax	The spectral radiance which is scaled to QC_{max} (W/m^2-ster-λm)
Lmin	The spectral radiance which is scaled to QC_{min} (W/m^2-ster-λm)
MC_{min}	The lower limit of MC_v
MC_{max}	The upper limit of MC_v
F_c	Field capacity of the soil in sensing region [m^3m^{-3}]
W_p	Wilting point of the soil in the sensing region [m^3m^{-3}]

T_{GL}	Lower limit of the temperature gradient [°C/min]
T_{GU}	Upper limit of the temperature gradient [°C/min]
T_{G}	Surface temperature gradient [°C/min]
R_{a}	Extraterrestrial radiation in the hour period [MJ m^{-2} $hour^{-1}$]
G_{sc}	Solar constant = 0.0820 MJ m^{-2} min^{-1}
d_{r}	Inverse relative distance Earth-Sun
δ	Solar declination [rad]
φ	Latitude [rad]
w_{1}	Solar time angle at beginning of period [rad]
w_{2}	Solar time angle at end of period [rad]
$\cos\theta$	Cosine of the solar zenith angle.
Φ	Sun elevation angle in radian.
R_{s}	Solar or shortwave radiation [MJ m^{-2} day^{-1}]
n	Actual duration of sunshine [hour]
N	Maximum possible duration of sunshine or daylight hours [hour]
ω_{s}	The sunset hour angle in radians
R_{ns}	Net solar or shortwave radiation [MJ m^{-2} day^{-1}]
□	Albedo or canopy reflection coefficient
R_{nl}	Net outgoing longwave radiation [MJ m^{-2} day^{-1}]
e_{a}	Actual vapour pressure [kPa]
R_{so}	Calculated clear-sky radiation [MJ m^{-2} day^{-1}]
T_{mean}	The mean air temperature
RH	Relative humidity
$e^{o}(T)$	Saturation vapor pressure at temperature (T) [kPa]
Δ	The Slope of saturation vapor pressure curve [kPa $°C^{-1}$]
u_{z}	Measured wind speed at z m above ground surface [m s^{-1}]
z	Height of measurement above ground surface [m]
P	Atmospheric pressure [KPa]
γ	Psychrometric constant [kPa $°C^{-1}$]
λ	Latent heat of vaporization, 2.45 [MJ kg^{-1}]
c_{p}	Specific heat at constant pressure, 1.013×10^{-3} [MJ kg^{-1} $°C^{-1}$]

G	Soil heat flux [MJ m^{-2} day^{-1}]
c_s	Soil heat capacity [MJ m^{-3} °C^{-1}]
Δt	Length of time interval [day]
Δz	Effective soil depth [m]
H	The sensible heat
λET	The latent heat flux
ΔH_s	The change in energy storage for each unit time per unit area
ET_o	Reference evapotranspiration [mm day^{-1}]
α and β	Calibration factors
U	Seasonal consumptive use in inches
K	The seasonal consumptive use coefficient
f_i	Monthly consumptive use
ρ	Density of air
q_v	Specific humidity
K_p	Pan coefficient
E_{pan}	Pan evaporation [mm/day]
ET_{ins}	The rate of evapotranspiration at the time of the satellite overpassing
ε_a	The air emissivity
ε_s	The surface emissivity
τ_{sw}	Two way atmospheric transmissivity
c_p	The specific heat of air (29.3 J/mol/ ^{o}C)
r_{ah}	The aerodynamic resistance to heat transport (s/m)
u_*	The friction velocity (m/s)
h	The plant height (m)
z_m	The roughness length (m)
r_o	The hemispherical surface reflectance
L	The Monin–Obukhov length (m)
ET_{24}	The daily actual (mm/day)
LE ^ E	The evaporative fraction
^ λs	The thermal conductivity of the soil
ET_i	Actual ET for pixel i

VMC_i	Vegetation and moisture coefficient for pixel i
$'MC_i$ B	The moisture reduction coefficient
MC_{SUM_i}	Moisture Pixel's summation
MC_{SITI_i}	Moisture Pixel from SITIAWAN parameters
MC_{UTP_i}	Moisture Pixel from UTP parameters
MC_{SP_i}	Moisture Pixel from SEBERANG PERAK parameters
Fr_{SITI_i}	Fraction of SITIAWAN's Moisture pixel
Fr_{UTP_i}	Fraction of UTP's Moisture pixel
Fr_{SP_i}	Fraction of SEBERANG PERAK's Moisture pixel
W_{SITI_i}	The weightage of SITIAWAN surface cover
W_{UTP_i}	The weightage of UTP surface cover
W_{SP_i}	The weightage of SEBERANG PERAK surface cover
MC_i	The generalized moisture pixel
λ	the latent heat of vaporization (J/kg)

CHAPTER 1

INTRODUCTION

This chapter presents general information about surface moisture content (MC) as one of the most effective environmental and hydrological parameters that integrates the surface and sub-surface water activities with the surrounding atmosphere and the evapotranspiration (ET), which is a crucial assisting factor in determining the total water loss from surfaces. Moreover, this chapter highlights the importance of soil MC and ET in controlling and managing surface water activities and flood forecasting. The problems encountered in the measurements of MC and ET within the ground-based meteorological units are also discussed. Finally, the chapter outlines the objectives and significance of the study.

1.1 Overview

Water is an extremely essential and important ingredient for the improvement and nutrition of life [1]. Additionally, it is also present in a liquid crystal state near hydrophilic surfaces [2]. Water covers 71% of the Earth's surface of which oceans represent 96.5%, groundwater represents 1.7%, glaciers as well as the ice limit of Antarctica and Greenland represent 1.7% [3], a little fraction in other large water bodies, and 0.001% in form of air vapor, clouds and rainfall [4]. The freshwater takes up only 2.5% of the Planet's water and 98.8% of this water is situated in the shape of ice and groundwater. Lower than 0.3% of the fresh water comprises of lakes, rivers, and an even less of the Earth's freshwater (0.003%) is included within biological bodies and produced products [4]. Water on the planet is in continuing mobility throughout the so-called hydrological cycle that is made up of multi-systems of evaporation and evapotranspiration, condensation, runoff, and precipitation, normally attaining the sea. Evaporation and transpiration cause the precipitation over land [1].

Achieving an accurate estimation of soil moisture with acceptable resolution and revisit times is a key for an efficient hydrological modeling and for improved soil wetness forecasts. Surely, many of the environmental phenomena such as flooding and drought extent cannot be estimated by ground measurements alone, which explain the rising need to remote sensing in combination with ground-based observations in natural resource management and especially in water resources monitoring and forecasting. Furthermore, better evaluation of spatial and temporal variation of surface moisture meaningfully enhance the ability to accurately predict the degree and the timing of extreme events and natural hazards such as extreme weather, floods, and droughts [5]. Malaysia in particular, suffers from floods over many cities of the northern peninsular. As MC has the main influence on the soil saturation, this study intends to generate enhanced MC algorithms with locale parameters for daily monitoring, which could help in predicting the urban floods during the intense rainy periods. Moreover, landslides are also considered as one of the dangerous natural phenomena in Malaysia, by using high spatial resolution images on sloppy areas. Moisture content can assist in landslide's susceptibility study due to its direct influence on the pore water pressure so that moisture content plays as an interface between rainfalls and pore water pressure [6].

Moreover, this study provides an enhanced quantitative estimation of ET from remote sensing techniques in the most economical way through the use of the Advance Very High Resolution Radiometer (AVHRR) and the Moderate Resolution Imaging Spectroradiometer (MODIS) daily passing satellites. The accuracy of the predicted ET is enhanced through enclosing the MC's impact with the other ET parameters taking into account the effect of the satellite Ts corrected by field measurements.

1.2 Problem statement

MC and ET are critical hydrological parameters which have direct influence on agriculture, civil engineering, water resources management and crop system modeling. Furthermore, the MC's variability in space and time causes difficulty in its measurements and modeling [1]. Likewise, spatial estimation of the actual ET in a regional scale is also problematic because of its correlation to the MC in the soil and crops coefficient. This phenomenon becomes more complex when determining ET values in tropical areas due to the high density of vegetation canopies as well as the variety of the species[7-11].

There have been considerable advances in the monitoring and retrieval of MC and ET from optical/Infrared (IR) remote sensing sensors. These advances are found in sensors with a high temporal resolution to meet the dynamic nature of MC [12]. Two of the most applicable sensors which are being applied for MC and ET assessment at a regional scale, are AVHRR and MODIS due to their wide area coverage and high temporal resolution. However, the optical/IR remote sensing techniques still have serious drawbacks that hinder the accuracy of MC and ET assessment. Thus, the study intends to surpass these problems considering them as the most influencing conditions on MC and ET estimation which are:

- The coarse spatial resolution in AVHRR and MODIS affects the MC and ET estimation accuracy by producing maps from spectral reflections that are generated by a holistic surface cover classes within a single pixel. This holistic contribution does not represent the real MC value of some classes. This in turn, diminishes the advantage of the mentioned satellites as open-source data providers.

- Optical signal's capability limitation represented in clouds and atmospheric attenuation which considered as one of the most troublesome problems in the assessment of surface parameters from the optical/IR RS.

- The effect of soil formula and its physical structure in turn make it harder to accurately assess the MC and ET of the specific location from the optical/IR satellites.

Studies by De Troch, Engman, Walk er [13-15] and others denoted that, the optical sensing approach is rarely used because the reflected radiation can be simply affected by many variables. Those variables represented in organic matter, soil texture, surface roughness, angle of incidence, plant cover and color. All these cause large variation in albedo of different soil types [16]. Thus, it will not give high precision and perfection in MC calculation due to these variations.

The MC observation depth also remains a challenging issue for the optical/IR sensors since they have passive spectral properties. As shown by a lot of researches, the observable depth of moisture of soil is relative to the wavelength employed in remote sensing method. The visible region of the electromagnetic spectrum merely allows the recognition of the top few millimeters of the soil profile [17].

1.3 Objectives of the study

In order to determine a better accuracy of the MC and ET values, the following objectives have been drawn:

(i) To obtain enhanced MC values using the weightage approach on the land use/land cover (LULC) of AVHRR and MOIS image's pixel.

(ii) To evaluate the effect of soil formula, physical structure and the depth of MC measurements using the thermal inertia algorithm (TI) in which, the enhanced vegetation index (EVI) is used.

(iii) To analyze and evaluate the impact of the surface MC that generated by the weightage method on the quantification of the actual ET in which, the MC is applied as a substitute of the crop coefficient in the ordinary algorithms for better assessment's accuracy.

1.4 Scope of the study

The research was applied at a study area within Perak state in which, two basic classes of the surface cover were easily interpreted and processed. Those classes are, the urban area and vegetation cover; while the rest of the available surface cover classes were assigned a one general class named as multi-surface cover. For each class, ground meteorological station and testing field were allocated. Any spatial computation was assumed to represent the average value of the image's pixels of the subset area surrounding each station.

The study used only optical/IR satellite images from NOAA/AVHRR and MODIS sensors because of their high temporal resolution, which avail intensive data for MC and ET correlation. In addition, images from LandSAT ETM+ were used in order to examine the relevancy of the produced algorithms to the relatively-high resolution images.

Due to the large ground cover of every AVHRR or MODIS's pixel (almost 1 km^2), the assumed assumption that, there is no homogeneity in surface cover throughout each area captured by the pixel. Mainly, every single area could be a mixture of vegetation, wet soil and dry soil. Finally, the measurements of MC in-situ were also conducted in soil depths ranged from 0 cm to 15 cm according to the capability and specifications of the available instruments.

1.5 Thesis contribution

Based on the results, the study has contributed to the spatial application through implementing the image pixel's segmentation technique in coarse resolution's optical images, where the different surface covers within the single pixels were spatially processed according to their weights. Eventually, the study managed to provide a new advantage of those coarse spatial resolution satellite images beside their high temporal resolution. The study has also highlighted the use of Enhanced Vegetation Index (EVI) from MODIS as an alternative index to the Normalized Difference Vegetation Index (NDVI) in the moisture assessment. All applied algorithms within the study, were enriched by rectified surface temperature through field measurements of Ts. On the other hand, the study provided local moisture parameters for the universal triangle method applications throughout variable moisture measurement depths.

1.6 Organization of thesis

The thesis contains a total of five chapters; chapter 1 conducts general briefing about the MC and the ET. The chapter also emphasizes on the importance of MC as one of the most effective meteorological parameter and the ET with highlighting their applications in all aspects of life. Furthermore, the chapter contains an overview of the problems encounter the measurements of those two parameters. Finally the contributions made by this study are addressed.

Chapter 2 presents extended description of the remote sensing techniques, their general applications literature beside the standard measurements. In addition to that, the knowledge of remote sensing applications on MC is highlighted. The spatial parameters that influence the MC status are studied. In the second part of the chapter, the ET with its characteristics and measurements techniques are expressed in details. Finally, the chapter evaluates the techniques of remote sensing in ET assessment in conjunction with related algorithms from the literature.

Chapter 3 includes general information about the study area and its characteristics and also handles the ways of collecting and analyzing the particular terrestrial and spatial data. The implementation of algorithms is also included in the chapter and finally, all softwares and programs that were used along the study are highlighted.

Chapter 4 presents all results gained from the study of algorithms in terms of tabulated results and figures. The chapter also encloses new proposed methodologies proved by different kinds of validations with discussions at the end of each section.

Finally, chapter 5 portrays a summary of the overall work conducted regarding the soil MC and ET estimation, focusing on their final results and validations. In addition, the chapter addresses and recommends the future work that could be performed in order to enhance this study’s finding for supporting more valuable researches.

CHAPTER 2

LITERATURE REVIEW

This chapter deals with an extended description of remote sensing techniques and their environmental and meteorological applications in general. Moisture content MC in its two main parts of estimation is also mentioned extensively. These parts include the conventional approaches which are point-based measurement devices and also the remote sensing techniques, which have been used intensively for moisture assessment over field, landscape and regional scales. Detailed description of the basic categories of remote sensing techniques that are used for moisture estimation, are included with the spatial and meteorological parameters that are being used for modelling the MC. The chapter also highlights some well-known approaches which have been used widely within the optical/infrared remote sensing of moisture. In addition, the chapter also mentions the ET as one of the most effective meteorological parameters and also as one of the targeted issues of this study. Fundamentals and characteristics of ET are discussed besides the affecting factors, atmospheric and meteorological parameters that are used in ET generation. Finally, some of the conventional and the remote sensing-based methods, which have been used for the ET assessment, are mentioned as well.

2.1 Global Water Cycle

The hydrologic cycle or also known as water cycle is the continuous water movement system, above the surface of the Earth and below it, in a closed path as in Figure 2.1. Within this cycle, water transfers and converts from one state into another among the ocean, land and atmosphere. The light and the heat of the Sun which are considered as effective forms of energy, control the hydrologic cycle processes so that the state of water changes among liquid, vapor and ice inside the cycle. The main processes in the water cycle can be classified into five types which are: (a) condensation, (b) precipitation, (c) infiltration, (d) run-off and (e) ET. Condensation is the process when the water vapor condenses on particles in the atmosphere to form cloud. This occurs as a result of drop in air temperature when it rises upwards from the Earth's surface. The wind conveys this cloud across the globe. Precipitation is the release of water from the cloud in liquid or solid form (rain, snow, hail, sleet etc.). Precipitation begins after the condensed water becomes heavier to be held in the atmosphere. After that the water is transported from the atmosphere to reach the Earth's surface through precipitation. Infiltration is another process where some portion of the perceptible water permeates into the ground underneath the Earth's surface. The infiltrated water supplies and constitutes the ground water or subsurface water. The amount of infiltrating water depends on soil type, vegetation type and cover and rock type on the surface, saturation percent of soil, slope and permeability. Run-off takes place when the soil reaches saturation state of water. In the cold regions, it can happen in the form of snow melting. Run-off normally falls into streams, creeks and rivers which finally flow down usually to bigger pans like lakes, seas and oceans. ET is the transmission of water from the ground and vegetation back to the atmosphere again to complete water cycle. When the solar energy reaches the Earth's surface, it warms and heats the water causing the water evaporation to the atmosphere. Vegetation absorbs water from the sub-surface through their roots and transfers it to the atmosphere through the leaves which is called transpiration. Some water also gets evaporated before reaching the ground or from run-off while flowing in rivers or from some other water bodies that hold the perceptible water in the form of depression storage [1].

2.2 Global Energy Budget

The global energy budget explains the concept of how the incoming and outgoing energy to and from our earth-atmosphere system is distributed between different kinds of processes [18]. Basically, the incoming solar radiation is in the ultraviolet, visible and infrared region of the spectrum (represented by shortwave radiation) whereas the

Earth’s emitted radiation from the surface and the atmosphere as well, with wave length that is greater than 3 microns in the infrared region of the spectrum (represented by long wave radiation). The incoming solar radiation which is about 342 W m^{-2}. Some portion about 107 W m^{-2} is either reflected back into space directly, absorbed by the atmosphere 67 W m^{-2} or absorbed by the surface compounds 168 W m^{-2}. Some of this heat which is absorbed by the Earth’s surface is returned to the atmosphere in the form of sensible heat and latent heat flux. Sensible heat flux represents the transference to the atmosphere by convection and conduction while latent heat flux is related to the movement of water from the Earth’s surface to the atmosphere upon the change in water state among solid, liquid and vapor. The two forms of this heat (sensible and latent heat flux) are absorbed by the atmosphere. The outgoing emission from the Earth's surface is about 350 W m^{-2} as the long wave radiation and is mostly absorbed and radiated back by the atmosphere 324 W m^{-2} to the Earth’s surface [1]. A brief description is given in Figure. 2.2.

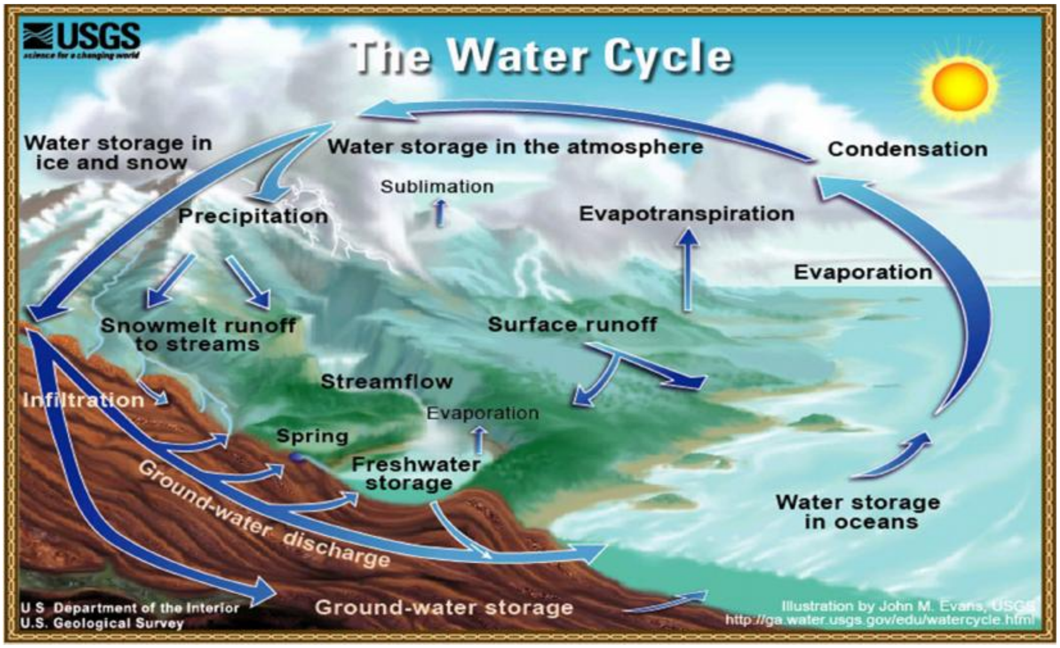

Figure 2. 1: The water cycle and the forming processes [18].

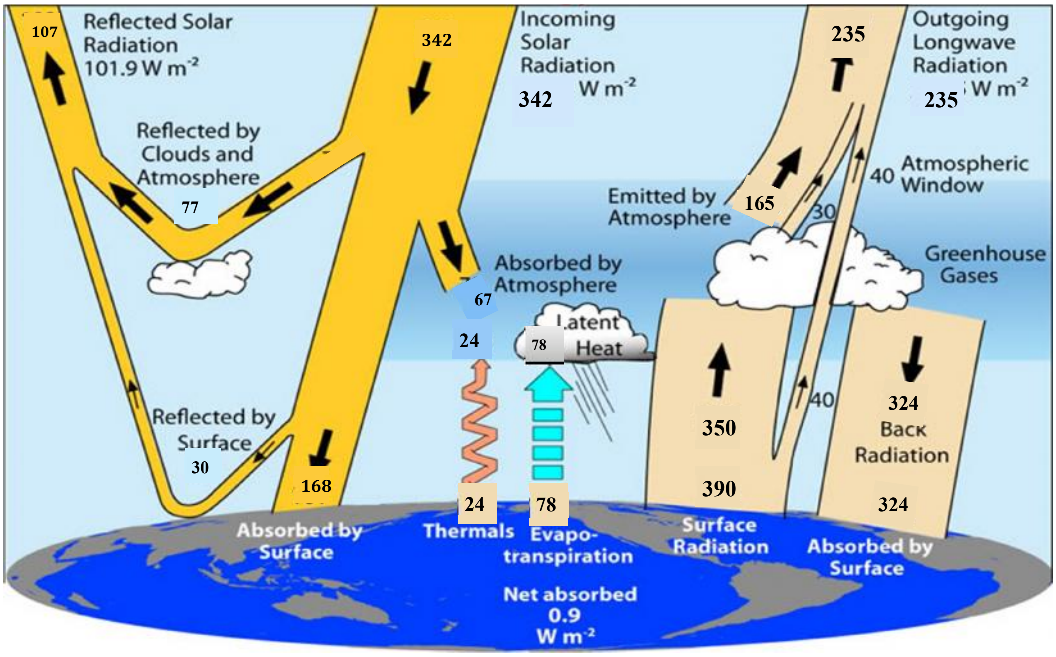

Figure 2. 2: The global annual mean energy budget at Earth's surface [1].

2.3 Definition of Soil Moisture

Soil moisture is not clearly defined in literature; however, it can be described in many ways depending on the application that it is used for. In some areas, it is defined as water stored in a farm scale for crop production from agriculture point of view [19]. Hydrologists define it as a precondition in the watershed scale to affect the surface runoff, source of contamination and aquifer recharge. Meteorologists define soil moisture when considered over a large area which can interact with the atmosphere to affect the precipitation over land [20]. Some researchers define it as the amount of water that is held by soil. For this thesis, the definition of soil moisture used by the meteorologists is the most considerable and is expressed as a dimensionless ratio of mass or volume of water by total mass or volume of soil which contains this water. This ratio is reported as decimal fraction or percentage after multiplied by 100 [21].

2.4 Importance of Surface soil moisture

Surface Soil moisture plays a very significant role in land surface hydrology as it controls the portioning of rainfall into run off and infiltration. Along with surface temperature, it affects the depth of planetary boundary layer, circulation/ wind patterns [22, 23] and regional water energy budgets. Soil moisture tracks the perceptible evaporative water over period of weeks and provides a historical record of atmospheric-land interaction. Moreover, it integrates the land surface hydrology and also acts as an interface between the land surface and the atmosphere. The primary factor in the persistence of dry or wet anomalies over large continental regions during summer is due to the recycling of the water through MC, ET and precipitation [24]. Soil moisture can be considered as the most significant boundary condition controlling summer precipitation in the semi-arid zones [25]. On a regional scale, the importance of soil moisture appears in agricultural assessment (crops yield management, irrigation management, etc.), flood and draught control. Evapotranspiration, in turn, depends on soil moisture (together with incoming radiation and a host of other meteorological factors) and they assist in determining surface pressure, rainfall and motion [26].

2.5 Definition of Evapotranspiration

Evapotranspiration can be defined as the transference of water from earth's surface into the atmosphere. This process includes the evaporation from soil and water surface besides the transpiration from vegetation. It has been quantified as 60% of the falling precipitation that leaves the surface in terms of ET [27].

2.5.1 Importance of Evapotranspiration

Assessment and estimation of the hydrologic budget is mainly based on the quantification of ET, therefore, its consideration is very important in the planning, development of a water resources area and the estimation of water-supply potential and the ecological effect of a development. The study of ET is required in order to address the following issues;

- Studying the global change because monitoring of ET at regional scale has become an important matter [28].
- Developing water supplies for agricultural schemes or and other related activities as well as the hydrological modeling. Those applications are often done at a scale that involves the analysis of ET for a region.
- ET patterns at regional scale can integrate factors related to the change in land use, runoff, and rainfall distribution.

2.6 Application of Soil Moisture MC

Along with the hydrologic cycle, the most important component is MC because it has an impact on climate change over land and plays the same role over land as sea surface temperature plays over oceans and seas. In some circumstances, it has a good potential for storing the atmospheric signature/energy transferred to it through precipitation (order of months), in turn transferring it back to the atmosphere through evaporation and affecting the climate [29]. MC assists in the determination of the redistribution of rainfall into surface runoff and subsurface run off [30, 31], so that it controls the portion of energy at the surface as well as the feedback of the water to the atmosphere. Further, it divides the up-willing energy into sensible heat and latent heat fluxes. In addition, soil moisture influences the soil erosion, soil aeration, distribution and growth of vegetation, soil microbial activity, the concentration of toxic substances, the movement of nutrients in the soil to the roots and weather prediction at a local to regional scale [32]. Apart from these, there are many other real life applications that soil moisture controls, which make it a very important parameter. The following examples have been mentioned due to their influences on human life to a very far extent:

Drought and flood monitoring – the amount of MC can directly affect the hydrologic drought and flooding because they are closely related to its availability in specific region. The deficit in root zone soil moisture for some period of time leads to hydrologic drought and then later results in agricultural drought (no vegetation). On the other hand, when rain falls for a longer period of time, the soil gets saturated with water leading to floods, especially for instant heavy precipitation which does not give enough time for the perceptible water to percolate underneath soil and hence generates high run-off and flash flooding [1].

Hydrologic modeling – the assessment of soil water change due to natural and anthropogenic causes is very necessary. Since MC is a main component of water cycle, it will be very helpful to study water cycle processes, precipitation and discharge pattern analysis through determining the amount of MC.

Modeling of climate and weather - In a climate system, MC is considered as a water reservoir, so that MC coming from the precipitation or snow melting during wet seasons is stored in soil and is evaporated during the summer time (dry season) when the soil gets warmer due to strong solar illumination. Soil moisture acts as an interface between wet season and dry season processes to drive the climate. The knowledge of MC attitude helps in understanding the seasonal processes and modeling the climate system. The weather as is also controlled by the soil moisture. MC quantifies the amount of water available to be transported to the atmosphere though ET. It controls the sensible and latent heat flux amounts that are going to the atmosphere. The intensity and genesis of severe storms and heating and cooling of the atmosphere and all those local weather depend on the evaporated portion of MC to the atmosphere.

Civil Engineering – the important structural properties are highly influenced by soil water because it makes soil heavier and softer to hold them. So, it is important to know and address the moisture amount and variation of the soil water over the years. This can assist in maintaining the engineering structures like dams, bridges, roads, etc. that are adequately suitable for the soil conditions. Among the wide range of MC applications in urban areas, the flood prediction is based on the spatial distribution of the saturation of ground soil [33, 34].

Management of watersheds and reservoirs – Watershed is defined as a portion of the land where all the water beneath it or draining off it goes to a common place such as streams, lakes or rivers. The watershed is highly controlled by the moisture available within the root zone of the soil. It is necessary to know the properties of the soil and the amount of water it can hold for the perfect management of watersheds and reservoirs.

Ecosystem and forest modeling – The balance of the ecosystem is too important for all the living beings. Vegetation requires water from soil to survive. In a closed environment such as forests, insufficient availability of water will lead all the trees to compete among themselves and dispute to survive. MC also controls the nutrients and chemicals uptake by the trees and sediment transportation by the rivers. MC is a major cause of deforestation. All the living beings in the ecosystem also depend on soil water, especially in the arid environment where people dig deeper into aquifers to find some water to survive. Knowledge of the MC assists accurately in modeling the ecosystem.

Agriculture and crop system modeling – Agriculture is the most dependent on MC and irrigation, especially in the dry season when the rainfall is scarce. It is highly important to know the amount of moisture in the root zone before cultivating any crop and can help farmers to decide whether they want to plant a crop type which intakes lot of water, but yields food very fast or a crop type which intakes less water and takes longer time to yield food.

Soil conservation – one of the major geohazards which threatens the crop production systems in Malaysia, is the soil erosion. MC holds the soil tightly and controls the soil erosion positively and negatively through reducing the mass movements (soil particles) and the transportation of soil components by water respectively [35].

Fire risk management – Many trees along the regions die due to the low rate of MC. They provide an excellent fuel (dry trees and wood) for wild land fires. So, the regions with low MC are highly prone to wild land fires.

2.7 Fundamentals and Characteristics of soil moisture

Soil moisture is understood to be water that is locked in the spaces between contaminants of soil. While surface MC could possibly be the water that is found within the upper 10 centimeters of soil, whereas root zone MC stands out as the water that is available to plants, which is generally considered being within the upper 200 centimeters of soil (http://worldwideweb.ghcc.msfc.nasa.gov/landprocess/lp_home.html). Soil MC can be expressed gravimetrically or volumetrically, i.e.,

$$MC_g = \frac{M_{water}}{M_{solid}} \times 100\%, \tag{2.1}$$

$$MC_v = \frac{V_{water}}{V_{solid}} \times 100\%, \tag{2.2}$$

Where MC_g and MC_v represent the gravimetric and volumetric MC content respectively, M_{water} and M_{solid} represent the mass of water and solid materials in the soil respectively, and V_{water} and V_{solid} represent the volume of water and solid materials in soil respectively [36].

Soil moisture within the top one or two meters from the surface is one of the key variables in managing the water-heat energy exchange between land surface and the surrounding atmosphere simply by evaporation and plant transpiration [37, 38]. In comparison to the quantity of water around the globe, the amount of soil moisture is small nevertheless; it's of elementary importance to a lot of hydrological, biological and biogeochemical processes (http://world wide web.ghcc.msfc.nasa.gov/land process/lp_home.html). Consequently, soil moisture plays a huge role in developing the weather forecasting algorithms and precipitation methods [39]. Regardless of its importance, continuous measurement of soil moisture is basically nonexistent (http://world wide web.ghcc.msfc.nasa.gov/land process/lp_home.html). The possible lack of an effective approach of global measurement of soil moisture is really a serious issue [40].

All soils contain three composites: solid (mineral and organic), water and gas. Their mechanical, physical and chemical pursuits are complicated, and therefore are frequently impacted by the proportion of water within the soil voids. Estimation of MC is thus an essential facet of soil research [41-44].

Due to its porous characteristics, soil is ubiquitous container of water that it supplies to the plants. As the three natural activities (evaporation, drainage and uptake by plants) take out water in the container, what remains becomes progressively inaccessible to plant roots. This leads to stress in plants and their growth is threatened. However, when the soil tank reaches capacity or near capacity, any extra water placed in the top will lead to run off, thus leading to hazardous flood and erosion. Therefore, information on soil moisture is highly significant, especially regarding the hydrological modeling and agricultural management [45].

Water is generally held in soil in one of two states. First, free water is within the pores of the soil structure and flows within that structure. Thus free water drains effortlessly which is easily available to crop roots. Secondly, water could be bound to the soil contaminants because of chemical and physical attractive forces. Since these kinds of forces decrease quickly with distance from the specified particle, bound water may exist such as a layer merely a couple of molecules thick around each aggregate [45]. Soil-water relationship could be splitted into three types based on the potential energy existing dry, moist, and wet. Dry soils are those types in which the soil reaches the welting point where tension equals to fifteen bars (1500 kpa). This really is greater MC than "air dry" soils, but it is so low that regular mesophytic plants can't survive [45]. Moist soils are those in which the moisture exists under some kind of a tension which is between 1/3 and 15 bars (33-1500 kpa), while extremely moist soils are those in which the moisture is within tension between .01 and 1/3 bars (1-33 kpa). Soil is wet if it consists of free water, or where tension does not realize 1 kpa [45].

2.7.1 Typical soil moisture measuring techniques

A multiplicity of algorithms and techniques have been established and availed for MC measurement. The way of selecting the method and equipment is mostly depending on ease of use, equipment expenses, plus a need to monitor continuous alterations in MC. The following examples show some typical MC content measuring techniques:

Gravimetric method: It is a direct way to estimate the total MC of soils. In this method, soil sample is dried in an oven (105°C for 24 hours) in order to determine the MC. Moisture content (grams of water in the sample) equals the primary soil weight without the oven-dry weight. Water content (%) may then be calculated by dividing the sample water content (grams) by the primary soil weight (grams) and scaling to100.

$$W_m = \frac{\text{mass of water}}{\text{mass of soilds}} \tag{2.3}$$

$$W_v = \frac{\text{volume of water}}{\text{volume of soil}} \tag{2.4}$$

W_m is based on dry soils, while W_v is based on the volume of the soil (solids, water and gas) at the measurement of MC. The relationship between W_m and W_v can be stated as follows:

$$W_v = \frac{W_m \rho_b}{\rho_w} \tag{2.5}$$

Where ρ_w is water density.

Advantages: This method is comparatively affordable, simple, and accurate [45]. Disadvantages: This method is time-consuming, destructive towards the soil, labor-intensive and stressful in rocky soils. A lab oven or microwave, soil sampling equipment, and lab scale are needed.

Neutron Probe: A radioactive source is placed in the soil that fast neutrons sent in a form of emission to the soil. When those fast neutrons act with the surrounding hydrogen atoms within the water molecules, they lose their energy and get slow. Those neutrons are out of charge and hard to be directly detected. Therefore, a gas (boron tri-fluoride) can be used to soak up the slow neutrons which will make the gas nucleus emit photons that are proportional to the amount of absorbed neutrons. The resulting photons are identified through an electronic device. The number of photons is measured via the electronic device, that is proportional to the amount of slow neutrons, then that is proportional to the quantity of moisture contained by the soil.

Advantages: The neutron probe provides an immediate, accurate, multi-times measure of soil MC to enable the achievement of a number of depths and locations. Disadvantages: The main disadvantages are that application of radioactive material needs a licensed and extensively trained operator, a high connection with the soil, a high equipment cost is required and also an extensive calibration is needed for every site.

Gypsum-porous blocks: This type operates based on the principle that the electrical resistance for each porous block is relative to its MC. Ceramic thermal dissipation determines the amount of heat dissipation inside the soil, which fits to MC.

Advantages: The technique is rapid, repeatable, and relatively inexpensive. Disadvantages: The blocks fail to work well in coarse-textured, high shrinks well or saline soils which are harmful to the soil. Accuracy of gypsum porous blocks is weak. The blocks need to be replaced every 1 to 3 years. The sensitivity of the blocks is inadequate in dry soil conditions and they need to be drenched in water for a variety of hours before setting them up at field.

Tensiometers: A Tensiometer is usually an airtight hollow tube stuffed with water. A permeable ceramic cup is connected to the end of the tube that is then inserted inside the soil, and then a vacuum measure is connected to the upper end. The tensiometer measures soil moisture tension, and gives an index of strength of water retentions in the soil. A soil moisture retention curve is drawn for each horizon of the soil to figure out MC [46].

Advantages: Tensiometers are not affected by the level of salts dissolved inside soil water. Tensiometers measure soil moisture tension with good accuracy within the wet range.

Disadvantages: Tensiometers only function between saturation and approximately –

70 KPa amount of MC causing them to be unsuitable for measurements in dry soils. Moreover, tensiometer are harmful to the soil surface.

Time-Domain Reflectometer (TDR): The TDR is a mobile device that is used to conduct measurements of MC at a point based or could be connected to a multiplexer in case of measurement for a variety of buried waveguides [47]. An electromagnetic wave is transmitted via probes. Reflectivity of the placed signal will take place where there are impedance changes. The value of the impedance relates to the geometrical arrangement of the probe which is inversely correlated to the dielectric constant of the soil. A general change in volumetric MC of soil around the probe leads to an alternation in the dielectric constant. The alteration of the dielectric constant of the soil changes the impedance of the probe which influences the form of the reflected signal that contains information which is used to figure out MC. A normal TDR soil moisture measuring probe is presented in (Figure. 2.3) the MC is usually estimated ever since the dielectric constant of a soil increases with the water percentage.

Figure 2. 3: Soil moisture probe (Time Domain Reflectometer TDR) [5].

Advantages: TDR is precise, supplies continuous measurements does not require calibration and is unaffected by salts.

Disadvantages: TDR damages the soil, contains difficult electronics, and expensive devices are required for successful measurements [46].

The measurement of MC over large areas via conventional field methods is neither ideal nor economical. Moreover, these conventional methods produce point measurement data which does not usually signify the spatial distribution of MC content within the region, as regard to MC varies in space and time and its value is mostly influenced by the variation of soil components, terrain, land cover, ET and precipitation. Hence, it's important to search for technologies like remote sensing as an option to produce spatial distribution of MC estimations [5]. Since the early sixties, satellite remote sensing has improved a notable tool to observe and determine environmental processes both in spatial and temporal conditions. Opposing the point measurements, remote sensing techniques can acquire spatial information over large areas with a routine basis, offering a possible capacity to make spatially and temporally extensive measurements of the near-surface MC along with other ecological variables [5].

2.8 Remote sensing techniques

Remote sensing is a term that is used for the study of objects sensed from a distance. It denotes the employment of modern sensors and data processing [46]. The use of remote sensing has replaced some contact and destructive methods in sensing environmental and agricultural phenomena. There are many remote sensing techniques that can be used in the infrared and microwave spectral regions in order to collect data from targeted locations. Lunel and Dill [48] reported that remote sensing can be used for the detection and characterization of agricultural and land phenomena.

2.8.1 General applications of remote sensing

Remote sensing as a sophisticated system today has become the best performing, effective and precise source for the mapping and monitoring of environmental conditions over earth surface at all levels and scales. All those systems have been used intensively for field’s spectroscopy and spectroradiometer studies which issue the subsequent activities as examples: the analysis of the common relationship among the spectral characteristics of surface targets and their environmental qualities and features in the field. Ground truthing, which is an in situ field measurement of physical environmental parameters with equivalent illumination and viewing geometry for reasonable correlation to satellite and aircraft sensor data. Analysis of Multispectral and hyperspectral imagery, which are a collection of visible, near infrared, and short wave infrared images for the recognition, detection, and quantity assessment of surface substances, organic, and chemical activities for analysis and research in several ecological and security purposes. Research on soil and crop, which is a detailed identification of soil nutrients, its structure, hydrological parameters acting on soil profile and surface as well as the topographical aspect of soil surface, while research on crops includes the monitoring of crop growth stages and heath, irrigation water requirements besides the photosynthetical activities and many other plant processes. Researches on ice characteristics and snow, which entails the monitoring of ice and snow properties to improve the understanding of the phenomena in a clear way, such as the balance in radiation between the Earth and the atmosphere and correlations between the size of the snow grain's configuration and its reflection, hardness index, density, liquid water content, and temperature. Landscape ecology and ecology researches also involve the capability to precisely achieve reflectance and radiometric measures of green canopy and soil within the field [46]. Airborne remote sensing measurements, is mostly applied over areas that are inaccessible or relatively large for in situ data collection. Atmospheric remote sensing and spectral irradiance research provides information in direct, diffusion, and complete irradiance from spectrum. In addition, to sky and cloud radiance are crucial for environmental research in a lot of climate and ecosystem energy balance researches. Researches on climate, which concerns the global change is conducted daily and data is collected via remote sensing which can be utilized effectively in climatic change studies. Remote sensing of geology researches contains studies of the formula, material, structure, processes, and history of our planet, usually for the detection of minerals and new energy resources. Remote sensing of water, oceans coastal and inland water bodies involves the reflected radiance from water surface to affect water leaving radiometrical properties with no need to study and measure the in-water to interpret and validate the satellite imagery and much more. Furthermore, other variable applications in urban planning, urban heat island, natural disasters, environmental and meteorological observations which are extended at the earth surface are also involved. Lunel and Dill [48] mentioned the primary uses of remote sensing in agricultural and water management sectors as the following:

Land-Use Assortments: In numerous countries, air photos are widely-used to produce maps illustrating the distribution of plants, specific crops, and land use.

Soil Surveys: Before 1930, soil surveys in the USA took a quite long time due to the use of traditional field-methods for soil classification and land mapping. With the use of air photos, soil information could be acquired quickly and efficiently [49].

Estimation of crop Condition and Yield Forecasting: Remote sensing offers the process of obtaining data on crop yields and also forecasts throughout the growing season. This data is useful to agriculture as it affects all phases of agricultural production, processing, and storage.

Management of water-Supply: Remote sensing is employed for the management of water resources. It is widely used for the discovery of fresh water at low sensing cost, to forecast the future supply, and control the location, amount, level of quality, and timing of that supply.

Irrigation Management: Remote sensing techniques can be used to study the changes of moisture levels in the soil and detect the water-table depths with enough confidence [50]. This information is then used to advise the farmers on irrigation scheduling and the quantity of moisture within the soil, so that they can avoid overtopping or drying the irrigated field [46].

2.9 Remote sensing of soil moisture content

The distributions of MC condition spatially and temporally at the surface and root zone throughout large land present a crucial input for several agricultural, hydrological, as well as meteorological uses [51]. Additionally, evaluation of surface and root zone MC at numerous temporal and spatial scales is often a critical factor to strategic management of water resources. Surface MC is an essential storage factor, which usually regulates partitioning of energy and mass relevant to ET and runoff [52]. Numerous studies in the SGP97 (Southern Great Plains 1997 hydrology experiment) site have analyzed the parameters that affect the spatio-temporal circulation of MC in addition to surface fluxes [53-60]. The estimation of MC of soil and energy/mass exchange is mostly simulated through Soil Vegetation Atmosphere Transfer models (SVAT). The precision of SVAT models is normally confined by undependable estimations of surface and root zone MC [61]. In spite of the importance of MC in hydrological and meteorological forecasts, comprehensive spatio-temporal modeling of soil MC at the local and global range is usually missing. Distributions of MC would be best evaluated by regular gravimetric sampling or through adjusted TDR approaches. For a specific location, MC could be frequently monitored simply by calibrating segmented TDR probes e.g., [62] or through multi-sensor capacitance probes e.g., [63]. Root zone MC estimations were retrieved via surface measurement for dried out soil along with completely grown roots by using a linear relationship between MC in a couple of soil layers [64]. These methods assist effectively for field portion or local-scale monitoring but aren't practical for watershed or regional scale. Remote sensing of MC from satellites has the capacity to surpass this issue and offer huge spatial coverage and temporal continuity. Within the last 30 years researchers have effectively proven the usage of passive microwave remote sensing to determine the surface wetness [65-68]. These types of measurements explained soil moisture within a thin soil layer, normally up to a depth of 0.05 m underneath the soil surface [41, 69, 70]. Nevertheless, a related problem, that obstructed the measurement of soil moisture from air/space using passive microwave methods, is its low spatial and temporal resolution that is not in conjunction with the scale of hydrologic processes of interest.

Prevot et al. [71] revealed that the soil water balance could possibly be established with equivalent precision using remotely sensed surface soil moisture estimations substituted for in situ observations. Smith et al. [72] published a soil water simulators model that made use of remotely sensed data to predict profile MC. Recently, researches have been carried out on enhancing evaluation of profile soil moisture with the aid of surface MC observations [33, 73]. Four techniques were elaborated using surface soil moisture data to estimate profile soil moisture: (i) statistical extrapolation of surface observation, (ii) incorporation of surface observations in the profile water budget model, (iii) inversion of radiative transfer model, and (iv) the parametric profile model technique [38]. Kostov and Jackson [73] introduced a comprehensive write-up on these basic methods for estimating profile MC using remotely sensed surface moisture data and figured that essentially the most encouraging method of the problem of profile MC estimation has been the incorporation of remote sensing and computational modeling. An illustration of this principle has been supplied by Entekhabi et al. [33] in their theoretical method for fixing the inverse problem for MC using consecutive assimilation of remotely sensed surface data. Houser et al. [74] studied the application of four-dimensional data assimilation techniques in a macro-scale land hydrology model to create root zone MC fields on typical space and periods of time. Jackson et al. [68] examined these principles within the point scale [75-78]. Walker and Houser [79] investigated the consequences of observation depth and update phases on MC profile retrieval and made an evaluation of two widely used assimilation methods (i.e., direct insertion and Kalman filter) using synthetic data. They figured that, Kalman filter assimilation system provides improvement over the direct insertion assimilation system, and profile retrieval seemed to be unsuccessful for direct insertion using the surface node only, with observations over some non-zero depth being essential. The efficiency of the Kalman filter is based on its capability to adjust the whole profile, while direct insertion could only affect the profile within the observation depth. On the other hand, Heathman et al. [77] investigated profile MC using direct data assimilation in Root Zone Water Quality model at four field sites in the Little Washita (LW) River Experimental Watershed during SGP97, and discovered that direct insertion assimilation enhanced model estimations down to a depth of 0.30 m at all the sites considered in their study, however no significant improvement in soil water estimates below the 0.30 m depth. Crosson et al. [75] applied the Kalman Filter based method for assimilating remotely sensed (ESTAR-based, during SGP97) MC estimates in a point-scale testing scheme and observed that even in the existence of extremely inaccurate rainfall, the model results in good agreement with observed MC. Crow and Wood [78] expanded Ensemble Kalman Filter (EnKF) technique to assimilate remotely sensed (ESTAR, SGP97) MC data into a land surface model and verified by independent observations. They discovered that root zone MC forecasts made with the EnKF are more precise than predictions produced from direct assimilation of ESTAR surface MC imagery. Lately, Dunne and Entekhabi [80] used ESTAR pixel and field data of SGP97 to research an ensemble-based reanalysis (ensemble based smoother) method of land data assimilation. They demonstrated that smoothing improved the estimated MC at the soil surface and in depths over EnKF estimation. The performance of EnKF was also studied by Reichle et al. [64] and Margulis et al. [81], where MC estimation was assessed by assimilating L-band (1.4 GHz) microwave observations into a land surface model. They showed that EnKF is an adaptable and powerful data assimilation technique that provides satisfactory estimates even for moderate ensemble size. From these, it is evident that EnKF provides several positive aspects over conventional methods of data assimilation for retrieving soil moisture from microwave remote sensing.

In addition, data assimilation is utilized along with a SVAT (land surface model, LSM) model. This model could be treated as a stand-alone program, which communicates with the filter through its input and output files. The filter provides a set of random initial conditions, parameters, and forcing variables to the land surface model. In turn, the model originates a time-dependent state vector that is definitely passed to the filtering algorithm. This modularity makes it possible to use nearly any land surface model in a data assimilation process depending on an EnKF. The most frequently used SVAT model with data assimilation are NOAH model [82], Variable Infiltration Capacity (VIC) model [83], Mosaic model [84], and Common Land Model CLM [85]. The SVAT models usually incorporate a thin surface soil layer and another one or more thicker layers as root zone and approximate MC content of each soil layer within the land-atmosphere boundary and also the connections between those soil layers. The SVAT models operate usually within an uncoupled trend by using a variety of simple tools to handle the input as well as output data. From the vadose zone hydrology viewpoint within the landscape scale or greater, there is a necessity for easy and strong incorporation of surface remote sensing data into a powerful soil water model within a dispersed processing platform (e.g., geographical information systems [GIS]) to enhance the simulation of root zone soil moisture. For dispersed models, GIS is most likely the best readily available tool for arranging and control data for the watershed/regional scale [86-89].

2.9.1 Spatial properties of surface Moisture

Gates [90] noted that, there are two attributes of the soil surface that are of basic interest in remote sensing. First, is the soil reflectance of incident radiation, and the other one is related to its long-wave emittance and surface temperature. Based on [90], the reflectance of the soil depends on its color, structure, roughness, MC, substance and chemical formula, direction of illumination, and level of shadowing by vegetation or buildings.

Since MC is certainly one parameter that influences the reflectance and emittance of soil, then the effect signifies that an alteration of water content in the soil leads to an alternation in its reflectance and/or emittance. A proper remote sensing approach could be used to discover and evaluate the alternation in reflectance and/or emittance of the soil and link it to the quantity of moisture within the soil. A calibration model could be developed to anticipate MC content which correlates MC to soil reflectance [69, 91] as well as to differential temperature (Td) and weather meteorological parameters [92].

Standard remote sensing techniques for MC appraisal include the gathering and presentation of satellite imaging, aerial photography or surface monitoring station data concerning the nature, components and state of the soil. These distinctions and variations in the soil nature, properties and state are shown and chosen by the sensors attached to the satellites according to their various electromagnetic spectrum properties. Presently, a number of remote sensing approaches for MC assortment have been developed based upon their various electromagnetic spectrum properties.

Every remote sensing method employed has its own pros and cons, depending on how susceptible the soil surface would be to the electromagnetic radiation and how robust the reflected radiation, in the soil surface, could be received through the sensor. So that, the satellite sensor records solar energy reflected or emitted through the Earth‘s surface. One class of satellite sensors has its own source of energy as certain wavelengths are transmitted in the direction of ground objects, a part of that is scattered back to an antenna on the same platform. The quantity of energy which is recorded by the satellite sensor is dependent upon the MC of the Earth‘s surface and also other elements, such as roughness and thereby provides basis for remote sensing of soil moisture.

Table 2.1 shows a summary including benefits, drawbacks, as well as a comparability among the four distinctive remote sensing group of techniques that have been widely utilized for field of soil moisture assessment [93]. Amongst abovementioned four approaches, calculating MC by passive microwave and optical/IR remote sensing have attracted more interest [94].

Table 2. 1: Review of remote sensing approaches for measurement of near-surface soil moisture content [13, 94, 95].

	Active Microwave	Passive Microwave	Visible	Thermal Infrared
Property Concerned	Backscatter coefficient Dielectric properties	Brightness temperature. Dielectric coefficient. Soil temperature.	Soil albedo. Index of refraction.	Surface temperature.
Advantages	Low atmospheric noise. High resolution. All weather conditions. Polarization changeable. Good physical bases.	Low atmospheric noise. Moderate vegetation's penetration. All weather conditions. Good physical bases. Daily bases acquisition.	Lots of data. Simple to operate. Applicable at a range of spatial and temporal resolutions.	High resolution. Large swath coverage frequency. Physical well understood. Provides an integrated soil moisture value for the root zone. Applicable at a range of spatial and temporal resolutions.

				Cost effective technique.
Disadvantages	Limited swath width. Calibration of SAR. Moisture estimates affected by surface roughness. Limited penetration depth when aircraft used. Very expensive.	Very low resolution. Manmade radiation. Limited operating range. Soil moisture only observable on top few centimeters and for spares vegetation. Expensive.	Many noise sources. Cloud free condition required. Strong empirical character.	Cloud cover. Depth of the root zone is variable across an image.
Source of Noise	Roughness. Surface slope. Vegetation cover.	Roughness. Surface slope. Vegetation cover.	Numerous	Meteorological conditions. Topography. Vegetation cover

Previously, the most important factor for avoiding wide spread utilization of remotely sensed soil moisture information in hydrology was having less data sets and ideal satellite systems. As a result, researchers have been limited to data from limited duration aircraft activities, or analysis of the passive microwave satellites. Currently, daily soil moisture observation data like from AMSR-E, NOAA/ AVHRR AND MODIS are quickly and freely accessible [96].

2.9.2 Sensors developed for moisture measurements

Table 2.2 briefly explains the growth of a number of the satellites which have been widely used for soil moisture estimation since 1991.

Table 2. 2: Satellites' Sensor Developments for soil moisture Evaluation [93].

Satellite	Sensor	Year launched	Owner	Data type
Landsat	Landsat (series)	1975(first)	NASA	Passive
ESRI-1	SAR-C band	1991	European space agency	Active
JERS-1	SAR-L band	1992	Japanese agency	Active
SIR-C/X-SAR	SAR	1994	U.S-Germany-Italy	Active
ERS-2	SAR	1994	European space agency	Active
Radarsat-1	SAR-C band	1995	Canadian space agency	Active
Terra	MODIS-Terra ASTER-Terra	1999	NASA/ Japan	Passive
Aqua	AMSR-E-Aqua MODIS-Aqua	2002	NASA/ Japan	Passive
ALOS-PALSAR	SAR-L band PRISM &AVNIR-2	2006	JAPAN	Passive/ Active
Radarsat-2	SAR-C band	2007	Canadian space agency	Active
SMOS	MIRAS (interferometric radiometer)L-band	2009	European space agency	Passive

2.9.3 Optical Remote Sensing

The visible parts of the electromagnetic spectrum are the most popular and widely used in remote sensing of planetary surfaces mainly because of this spectral region is highly illuminated by the sun and is also accessible widely by most of the sensors [97]. The visible remote sensing of MC relies on the measurement of the sun radiation reflected (i.e. albedo) from the earth's surface. Making use of the known partnership between albedo and MC, soil moisture is obtainable. Soil albedo is described as the ratio of reflected to arriving radiation [98], and it has long been recognized to be affected by MC together with several additional factors.

There are several physical models to link soil biophysical and geophysical variables with sensor measurements in optical/IR region. Inversion and sensitivity evaluation of those models offer physical basis for soil moisture evaluation [99]. The SVAT model and also the 'Universal Triangle' method are actually most widely used.

Vegetation and land surface temperature have a very complicated reliance on MC. Careful examination of spatial data by Carlson et al. [100] and Gillies et al. [101] indicated that there is a special connection often known as the 'Universal Triangle' among MC, the Normalized Difference Vegetation Index (NDVI), and the Land Surface Temperature (Ts) for a specific region. The outcomes were afterwards verified by theoretical researches utilizing the SVAT model, that was first named by Gillies and Carlson [102] and built to describe the fundamental evaporation processes in the surface, along with the water partitioning between transpiration from vegetation, drainage, surface runoff and MC variations. Carlson analyzed NDVI and fractional vegetation cover in particular and stated that the triangle relationship is applicable for a wide range of surface forms [103]. The relationship between fractional vegetation cover and scaled NDVI, however, is extremely complicated. The triangle technique is usually a simplification depending on empirical associations between NDVI and fractional vegetation cover, and thus it is just a semi-physical method [99]. Additionally, the relationship between MC content and optical/IR proportions is rather complex since soil reflectance can also be influenced by soil organic matter, soil texture, surface roughness, incidence angle, plant cover and color [14, 65], which result in a wide fluctuation in the reflected spectrum from the soil, regardless the moisture condition of soil [16]. These types of complicating variables, and also the fact that the reflected solar radiation takes action to simply the top few millimeters on the soil profile [98], minimize the effectiveness of solar reflectance measurements for MC assessment [95].

As the radiative transfer model is perhaps all but nonexistent to mimic reflectance with soil variables to date, 'Universal Triangle' method is still the main approach for MC estimation with optical/IR measurements [36].

Moisture content MC greatly affects the reflection of shortwave radiation coming from soil surfaces within the visible and near infrared VNIR (0.4 - 1.1 µm) and also the shortwave infrared SWIR (1.1 - 2.5 µm) parts of the spectrum. Lobell and Asner [104] produced quantitative model characterizing relationships between MC and reflectance, which is often used in functional MC retrieval formulas. Their model is actually based upon the measurement of reflected shortwave radiation (.4 - 2.5 µm) in the laboratory setting for various soils at various MC. They discovered that reflectance diminished with the boost in moisture and the moisture level of sensitivity of reflectance raises as the wavelength rises from the VNIR to the SWIR. Additionally, they found out that the SWIR region is better fitted to MC measurement compared to VNIR. Sellers et al. and Smith et al. [105, 106], found out that the latent heat flux, the energy employed to evaporate water, is related to MC through a standard regression curve that is independent of soil and vegetation type. In order to exploit this empirical relationship for MC approximation, it is crucial to partition the surface heat fluxes into its elements. This involves a sufficient explanation on the surface energy balance that dominates under normal environmental circumstances. The Surface Energy Balance Algorithm for Land (SEBAL) is a formula that explains these procedures and figures latent heat flux [107]. This model utilizes digital image information within the visible, near-infrared and thermal infrared parts of the spectrum gathered by remote sensing satellites like Landsat, ASTER (Advanced Spaceborne Thermal Emission and Reflection Radiometer), AVHRR (Advanced Very High Resolution Radiometer) and MODIS (Moderate Resolution Imaging Spectroradiometer).

The optical signal has limited capability to pass through clouds and vegetation cover, and it is highly attenuated by the Earth's atmosphere. As well as MC, optical soil reflectance measurements are generally strongly impacted by the soil formula, physical structure (soil texture beside the other properties), and observation situations, causing poor predictors of MC on combined soil type [108].

2.9.4 Thermal Infrared Remote Sensing

Infrared radiation can be an electromagnetic radiation on the wavelength longer than the visible portion of the light and shorter than that of radio waves. Infrared radiation has wavelengths value in between roughly 750 nm and 1 mm [109]. The infrared part of the spectrum has a variety of scientific uses, which includes target acquisition and monitoring by the military, remote temperatures detecting, wireless communication, spectroscopy, and climate forecasting. Thermal infrared sensors measure the infrared radiation emitted via object and then energy is directly related to the object's temperature [46].

Objects which have a temperature higher than absolute zero (0 ^{o}K) produce electromagnetic energy at whole wavelength. For that reason, all the features in surroundings (i.e. vegetation, soil, animals, water) release thermal infrared electromagnetic radiation within the 3.0-14 μm part of spectrum [110]. The opportunity for the evaluation of soil moisture is dependent on great thermal emission capability of earth surface.

There are specific distinctions between the thermal properties of soil and water, which includes Heat Capacity (C), Thermal Conductivity (K) and Thermal Inertia (P). Consequently, a bit change in the soil-water portion provides a large alternation in the thermals properties. By sensing the thermal properties of the surface, the MC will then be acquired through the use of the founded models or techniques. Since the observable radiation released by the earth's surface is not exclusively dependent upon the surface temperature but also the dependent on soil surface emissivity, therefore the emissivity needs to be assumed or empirically identified when utilizing the models. Besides emissivity, numerous external variables can also be considered when using thermal infrared approach. As thermal part of electromagnetic spectrum has minimal penetrating capability, atmospheric effects are considered as large obstacles. Moreover, ground vegetation also obstructs the thermal spectrum to pass through. When the vegetation cover contains thick canopy, and obscures a lot more than about 10 to 20% of the soil surface, then a resulting image generated by the thermal remote sensor might have no relation to the radiation temperature of the earth's surface beneath. When the vegetation cover is mainly low grass, then a resulting image is tightly related to the earth's surface temperature [111]. Presently, when the vegetation cover is important within the targeting region, as opposed to measuring the soil surface thermal properties, the thermal properties of vegetation could be obtained. Areas with minimal vegetation (i.e. bare soil) will probably be much better for the thermal infrared remote sensing. Besides the vegetation issue, thermal techniques involve some other disadvantages like reduced surface penetration depth, high perturbation of the signal by atmosphere and bushfires and signal attenuation by the earth's atmosphere. A number of complicated noise removal systems tend to be utilized prior to the utilization of the thermal data. Nonetheless, the capabilities for higher spatial resolution, wide coverage, multi-satellite sensor accessibility, high and standard revisit frequencies, the likelihood for real-time applications and also the robust connection between surface MC content and temperature are however very promising [112]. To date, analysts using thermal infrared data for MC assortment prevailingly concentrate on the thermal inertia associated theory [111-114].and the theory related to heat fluxes exchange in energy balance [115], which might be introduced as the following.

2.9.4.1 Use of thermal Infrared to estimate soil moisture content

The application of thermal infrared sensors to calculate MC content has been well studied. MC content and soil surface-minus-air temperatures could be associated together via thermal attributes of the soil [92].

The infrared thermometry process demands the measurement of soil surface temperature and air temperature using a thermal infrared sensor. After that, the soil surface-minus-air temperature (Td) is determined. The computed soil surface-minus air temperatures are associated with the quantity of soil water existing where soil surface and air temperatures are obtained. Additional meteorological parameters such as solar radiation, relative humidity, and wind speed, can also be measured concurrently. Measurements of such variables are achieved at various levels of MC, soil surface and air temperatures, along with other weather relevant meteorological parameters. A calibration model will then be produced which correlates MC content as being the dependent variable to Td, and the remainder of weather parameters could be integrated into the calibration model to improve prediction efficiency. Shih and Chen [116] utilized multiple linear regressions to examine the significance of using air and grass/soil temperature, solar radiation, wind speed, and relative humidity in calculating soil water content.

Modeling MC through Optical/IR remote sensing data has produced a big influence on mapping the global soil moisture, because it is the best way for symbolizing the global MC distribution [117]. This number of techniques retrieves MC information individually regardless if there's a vegetation canopy available [118]. It gives details about the land properties like surface temperature and Normalized Difference Vegetation Index (NDVI). Some researchers show that the Optical/IR technique has the advantage of offering fine spatial resolution for MC evaluation [119]. The thermal infrared band is definitely the electromagnetic wavelength which measures the land features on this group of strategies. These techniques have established their capability to retrieve MC information separately by providing direct measurements for MC [95]. The primary attempt to estimate MC via Optical/IR sensing information was proposed by Jackson [79], whose technique was applied to determine MC retrieval for the top meter of the soil surface. Later on, several applications have been offered based on creating a relationship among land parameters, vegetation indices, and surface radiant temperature measurements [120, 121].

The following selection of methods, utilizing passive remote sensing data, is traditionally used for MC estimation: Universal triangle relationship method [93], brightness models [93], thermal inertia (TI) Method [17], heat flux balance Method and the presumed TIR-SM conversion model by Pegram [122].

2.10 Spatial Parameters for moisture estimation

The condition of surface cover parameters provides important information on MC status, which could be used to describe the moisture behavior via optical/IR techniques. Among those parameters, the followings have the strongest effect on moisture statement estimation.

2.10.1 Vegetation Indices

Vegetation indices tend to be dimensionless, radiometric measures that act as signals of the comparative abundance and activity of green vegetation. Remotely sensed spectral vegetation indices are commonly used and also have been of great benefit for various disciplines considering the evaluation of vegetation biomass, water use, plant stress, plant health, crop production, and detection of biome kinds. VIs can also be beneficial in calculating emissivities from space [123, 124]. To use these vegetation indices efficiently, one should understand the input parameters employed to make up the indices. In addition, knowledge of the way the external ecological elements and the architectural areas of the vegetation cover impact and modify the calculated index values is additionally required. The primary thrust of the vegetation index (VI) is its capability to react to subtle alterations in plant health condition for variable view, illumination and atmospheric circumstances. VIs could be determined from sensor voltage results, radiance values, reflectance values and satellite digital numbers. Both ways therefore, will produce an alternative VI value for the similar surface conditions. Likewise, a VI determined from data acquired within the same target, however with different devices, might not be exactly the same due to variations in the detector and filter qualities of the instruments. Even though VIs were designed to extract only plant signals. Other variables like the soil background, moisture conditions, solar zenith angle, and the atmosphere change the index values in complicated means. Therefore, any study related to the MC status must carefully evaluate and interpret the signatures of vegetation indices to improve the understanding of moisture distribution pattern. Study of spatial distribution and temporal trends of the vegetation indices over for a longer time (for example two years of study period) is beneficial and gives substantial understanding of regional scale moisture application [96].

The theoretical understanding of the VI is situated with the red (wavelength = 0.60-0.70 μm) and NIR or reflected IR (wavelength = 1.35-2.10 μm) contrast with the vegetation spectral reflectance signatures. Whenever light hits the vegetation surface, portion is reflected, transmitted and the rest is absorbed. The relative quantities of reflected, transmitted and absorbed light are a function of the surface and fluctuate together with the wavelength of the light. For instance, almost all of the light in the NIR wavelengths is transmitted and reflected, with minimal assimilated. On the other hand, light in the visible wave lengths (e.g. red) is mainly assimilated, with a few reflected and minimal transmitted. The reduction in red reflectance as a result of increase of live, green vegetation inside a pixel is a result of the assimilation by chlorophyll. Nearly all light hitting the soil, however is either reflected or absorbed, with minimum changes in wavelength. The quantity of radiation reflected from the vegetation surface is estimated by the quantity and composition of solar irradiance that hits the vegetation, and also the reflectance properties of the vegetation surface, due to which the data from two or more spectral bands can be used to form a vegetation index. VI could be calculated by fractioning differences and sums, and also by developing linear combinations of spectral band data. These methods usually are meant to improve the vegetation signal, while reducing solar irradiance and soil background consequences [96].

2.10.1.1 The Normalized Difference Vegetation Index (NDVI)

The Normalized Difference Vegetation Index (NDVI) is the distinction between near infrared and red reflectance values stabilized within the sum of both [125]. In a shape of mathematical formula the NDVI is given by,

$$NDVI = \frac{NIR-RED}{NIR+RED} \qquad 2.6$$

The upper bound of the NDVI is certainly one, while the lower bound is normally close to zero. With respect to the sensor features and also the units of the input factors (like radiance, digital numbers, etc) the fewer bound value might be a bit positive or a bit negative. The effectiveness of the NDVI is within its ratioing concept, which decreases the multiplicative noise within multiple bands. The NDVI is adequately steady to allow for significant comparisons of seasonal and inter-annual alterations in vegetation development and activity. It's a great measure of landscape patterns of green biomass and could be employed to estimate landscape patterns of principal productivity [105]. It is also employed to estimate crop yields, crop phenology [126], and also to assess leaf area index. NDVI has been shown to be considered a good predictor of evapotranspiration (ET) over grassland [127] as well as a great estimator of vegetation water stresses [128]. Nevertheless, NDVI demonstrates scaling difficulties, and saturated signals over high biomass situations, and it's also very sensitive to canopy background variations, with NDVI values specifically high with darker canopy backgrounds. A few of these difficulties have been studied by establishing indices like the soil adjusted vegetation index as well as the enhanced vegetation index.

2.10.1.2 The Enhanced Vegetation Index (EVI)

The Enhanced Vegetation Index (EVI) [129] was created to enhance the vegetation signal with enhanced sensitivity in higher biomass regions and enhanced vegetation tracking via de-coupling of the canopy background signal along with a decrease in environment influences. EVI is among the vegetation products offered by MODIS and it is described as:

$$EVI = G\frac{\rho_{NIR}-\rho_{RED}}{\rho_{NIR}+C_1\rho_{RED}-C_2\rho_{BLUE}+L} \qquad 2.7$$

where: ρ_{BLUE} is Blue (0.44-0.50 µm) reflectance, ρ_{RED} is Red (0.60-0.70 µm) reflectance, C_1 is the correction coefficient for environmental resistance in Red channel, C_2 is the correction coefficient for atmospheric resistance in Blue channel, L is canopy background brightness correction factor, and G is the gain factor. The C_1 and C_2 coefficients reveal the "atmospheric resistance" concept that is in accordance with the wavelength reliance of aerosol effects, using the more atmosphere-sensitive blue band to improve the red band for aerosol impacts. The atmospheric resistance coefficient values used in the MODIS EVI formula are $C_1=6$ and $C_2=7.5$ (found to best decrease aerosol impacts). The remaining terminology in above formula are L=1 (works well with global applications) and G = 2.5. The removal of the background soil impact in EVI resembles those of SAVI. Consequently, EVI might be presumed as a much better form of the NDVI.

2.10.2 Land Surface Emissivity (ε)

Emissivity For split-window algorithms

Emissivity has been calculated through an empirical formula based on the relationship between emissivity and the logarithm of NDVI [130] within the range [0.955, 0.985]. The emissivity of channel 4, ε_4, the emissivity of channel 5, ε_5 and also the emissivity variance of channels 4 and 5 ($\Delta\varepsilon$), are as follows:

$$\varepsilon_4 = 0.9897 + 0.029\,Ln(NDVI) \tag{2.8}$$

$$\Delta\varepsilon = 0.01019 + 0.01344\,Ln(NDVI) \tag{2.9}$$

$$\varepsilon_5 = \varepsilon_4 - \Delta\varepsilon \tag{2.10}$$

$$\varepsilon = \frac{(\varepsilon_4 + \varepsilon_5)}{2} \tag{2.11}$$

Emissivity for Planck Equation

Land surface emissivity ε for land surface temperature from Landsat is related to logarithmic value of NDVI [131] and it also could be indicated as;

$$\varepsilon = 1.0094 + 0.047 \times Ln(NDVI) \tag{2.12}$$

Value of ε within the 8-14 μm atmospheric window utilized by the ETM+ thermal sensors varies from about 0.8 to 1.0 for the majority of (natural) surface forms.

2.10.3 Satellite's Surface Temperature (Ts)

Land surface temperature (Ts) is often a crucial parameter for understanding the energy and hydrological balance in the earth surface's atmosphere system [132]. Moreover, it is the most beneficial land surface variable which can be produced from thermal remote sensing. It is of basic significance to the net radiation budget on the Earth's surface also to monitoring the condition of crops. Excluding solar irradiance components, almost all of the energy fluxes on the surface/atmosphere interface are only able to be parameterized using Ts [133]. It could possibly play either a direct role (e.g. when calculating long-wave fluxes) or an indirect role as when calculating latent and sensible heat fluxes. Moreover, a number of other modeling programs such as in hydrology, geology, vegetation monitoring, and global circulation models depend on the knowledge of land surface temperature. Remotely sensed Ts's are actually used in variety of applications including moisture availability to vegetation [130, 134-136]. Other Ts purposes incorporate modelling of regional scale ET [137] and land surface turbulent flux forecast [138].

A long-term observation of satellite-extracted land-surface temperature, for example that from MODIS could be used to study the greenhouse effect and climate change within the polar area. Additionally, canopy temperature could be used to approximate sensible heat flux [139], soil surface temperature also helps in the estimation of sensible and latent heat fluxes [140], and satellite-measured surface temperature could be used to improve models and techniques for assessing land-surface energy balance [141, 142]. Moreover, atmospheric general circulation model (GCM) simulations reveal that tougher summer monsoons are related to higher land temperatures [143]. Radiative transfer simulations depending on observed surface temperature information show a good correlation between the normalized greenhouse effect and the surface temperature [144]. For agriculture, the canopy temperature might be also employed to assess water needs of wheat [145], to find out frosts in orange groves [146] as well as the frost-damaged area [147].

The truth is, soil temperature carries a strong relationship with the MC. For instance, dry soil shows higher day-night temperature fluctuations compared to wet soil under similar environmental circumstances. Likewise, throughout mid-day, while dry areas seem as ‘hot spots’, wet areas seem as ‘cool spots’ because of the higher specific heat of water substances. The supply of spatially averaged Ts around large areas produced from remotely sensed data as well as the robust relationship between Ts and MC provide a perfect possibility to use remotely sensed Ts data for MC scaling research. This can be achieved by using remotely sensed Ts as being a surrogate variable to obtain spatial MC patterns. Nevertheless, due to the narrow range of temperature variations and MC, precise estimation of Ts is vital [132]. When inferring Ts from remotely sensed data, the initial problem to solve could be the translation of observed radiance into surface brightness temperature. Following calibration and conversion of radiance into temperature, using the inverse Plank’s law, it's important to take into account the atmospheric contribution. Then the surface brightness temperature has to be transformed into surface temperature, taking into consideration emissivity and directional effects. In fact, the issue is more complex simply because atmospheric, emissivity and directional effects are combined and these modulating elements are not approached independently [133].

2.10.3.1 Split-window algorithm for Ts (NOAA) product

The AVHRR channels 4 and 5 (10.3-11.3 µm and 11.5-12.5 µm) are being used broadly for deriving surface temperature with regard to daytime passes. The temperatures produced from channels 4 and 5 are somewhat different because of atmospheric water vapour assimilation. A strategy depending on the differential absorption in two neighboring infrared channels, known as the ‘split window’ technique, is employed for estimation of surface temperature. An additional problem arises since the land surface, generally, doesn't represent an ideal emitter of infrared radiation and provides a high variability. A number of Ts techniques have been developed to fix these difficulties. Various authors Harris and Mason; Sobrino et al. [148, 149] demonstrated that the addition of the total water vapor within the algorithm to allow for atmospheric variability enables the removal of a substantial quantity of errors in the retrieval of sea surface temperature (SST). Several approaches have been suggested to obtain the perceptible water and also the channel transmittance ratio from split window channels [150, 151]. Even so, these methods have been restricted to SST and are highly dependent on the atmospheric circumstances considered.

2.10.3.2 Split-window algorithm for Ts (MODIS) product

The accuracy standards for MODIS Ts are 1 °K at 1km resolution under clear-sky situations. It could be confirmed by field measurements in a flat homogeneous land surfaces. The accuracy standards for land surface emissivity gathered from MODIS information is 0.02 for bands 29, 31 and 32, and 0.05 for bands 20, 22, and 23 [Earth Observing System Output Data Products and Input Requirements, version 2.0, Science Processing Support Office, Goddard Space Flight Center, August 1992]. Following the calibration of MODIS, TIR information is validated by precise ground-based measurements, and it could be simple to achieve a complete accuracy of 0.5 °K for calm lake water and playa surfaces in dry atmospheric situations [132].

A view-angle reliant split-window Ts method has been produced by Wan and Dozier [152] for atmosphere and emissivity effects correction for land cover kinds with identified band emissivities. In the progression of this generalized split window Ts algorithm, a data source for MODIS atmospheric thermal radiance values in bands 31 and 32 has been set up from exact atmospheric radiative transfer simulations for 12 atmospheric temperature profiles, that go over the range of surface air temperatures, T_{air}, from 256 °K to 310 °K (it will be extended to 210-325 °K in the at-launch code). The water vapor profile was scaled from the near saturated level right down to 5% of the saturated level for every temperature profile. The land-surface temperature, Ts, ranges from T_{air} - 16 °K to T_{air} +16 °K, and the surface emissivity ranges from 0.8 to 1.0 for each atmospheric temperature profile. According to this simulated data source, a look-up table and interpolation scheme has also been developed with accuracy better than 0.05 °K, the specification for the MODIS noise equivalent differential temperature (NEDT). Comprehensive error analysis has been created in wide ranges of atmospheric and surface conditions. Generally, the accuracy of the general multi-channel Ts algorithm is preferable to 1 °K for land cover types with known emissivities by optimization of its variables for viewing angle and column water vapor ranges. MODIS products of land-cover, snow, and vegetation index will likely be used to infer band average emissivities of land-surface pixels. When the pixel is of dense evergreen cover, lake surface, ice/snow cover, the related values of the band average emissivities of MODIS bands 31 and 32 in the emissivity knowledge base is going to be used as inputs for the generalized split-window Ts formula [132].

The derivation of split-window algorithm formula is dependent on radiance transfer equation. Qin et al. [153] determined a detailed derivation to the Ii q and Ii Q, which is often depicted as follows:

$$I_i^{\uparrow} = (1 - \tau_i(\theta'))B_i(T_a) \qquad 2.13$$

$$I_i^{\downarrow} = (1 - \tau_i(\theta'))B_i(T_a^{\downarrow}) \qquad 2.14$$

T_a is the average temperature of radiance going upward the atmosphere. $T_a^{\downarrow}$ is the average temperature to the downward radiance of atmosphere. Using $I_i^{\uparrow}$ and $I_i^{\downarrow}$ represent equation (1),

$$B_i(T_i) = \tau_i(\theta)[\varepsilon_i B_i(T_S) + (1 - \varepsilon_i)(1 - \tau_i(\theta))B_i(T_a^{\downarrow})] + (1 - \tau_i(\theta')B_i(T_a) \qquad 2.15$$

To be able to shorten the Equation 2.15, Qin et al. [153] developed sensible simplifications and evaluation; they determined that it doesn’t have much impact if using T_a rather than $T_a^{\downarrow}$, therefore the equation could be shown as Equation 2.16

$$B_i(T_i) = \tau_i(\theta)\varepsilon_i B_i(T_S) + [1 - \tau_i(\theta)][1 + (1 - \varepsilon_i)\tau_i(\theta)]B_i(T_a) \qquad 2.16$$

For MODIS 31/32, the relation can be written as:

$$B_{31}(T_{31}) = \tau_{31}(\theta)\varepsilon_{31}B_{31}(T_S) + [1 - \tau_{31}(\theta)][1 + (1 - \varepsilon_{31})\tau_{31}(\theta)]B_{31}(T_a) \qquad 2.17$$

$$B_{32}(T_{32}) = \tau_{32}(\theta)\varepsilon_{32}B_{32}(T_S) + [1 - \tau_{32}(\theta)][1 + (1 - \varepsilon_{32})\tau_{32}(\theta)]B_{32}(T_a) \qquad 2.18$$

In Equation 2.16, the Planck function makes the equation complex. So, some simplification should be there prior to solving the equation. In the earlier research, researchers frequently use Taylor extension to Planck function.

$$0.13787\varepsilon_{31}\tau_{31}T_s = 0.13787T_{31} + 31.65677\varepsilon_{31}\tau_{31} - (1 - \tau_{31}) \qquad 2.19$$

$$[1 + (1 - \varepsilon_{31})\tau_{31}](0.13787T_a - 31.65677) - 31.65677$$

$$0.11849\varepsilon_{32}\tau_{32}T_s = 0.11849T_{32} - 26.50036\varepsilon_{32}\tau_{32} - (1 - \tau_{32}) \qquad 2.20$$

$$[1 + (1 - \varepsilon_{32})\tau_{32}](0.11849T_a - 26.50036) - 26.50036$$

For convenient calculation, the coefficients of Equations 2.19 and 2.20 could be simplified as follows:

$$A_{31} = 0.13787\varepsilon_{31}\tau_{31}$$

$$B_{31} = 0.13787\tau_{31} + 31.65677\varepsilon_{31}\tau_{31} - 31.65677$$

$$C_{31} = (1 - \tau_{31})(1 + (1 - \varepsilon_{31})\tau_{31})\ 0.13787$$

$$D_{31} = (1 - \tau_{31})(1 + (1 - \varepsilon_{31})\tau_{31})\ 31.65677$$

$$A_{32} = 0.11849\varepsilon_{32}\tau_{32}$$

$$B_{32} = 0.11849\tau_{32} + 26.50036\ \varepsilon_{32}\tau_{32} - 26.50036$$

$$C_{32} = (1 - \tau_{32})(1 + (1 - \varepsilon_{32})\tau_{32})\ 0.11849$$

$$D_{32} = (1 - \tau_{32})(1 + (1 - \varepsilon_{32})\tau_{32})\ 26.50036$$

The equations (2.19) and (2.20) could be described as:

$$A_{31}T_s = B_{31} - C_{31}T_a + D_{31} \qquad 2.21$$

$$A_{32}T_s = B_{32} - C_{32}T_a + D_{32} \qquad 2.22$$

By merging Equations 2.21 and 2.22, the T_s could be assessed as:

$$T_s = (C_{32}(B_{31} + D_{31}) - C_{31}(D_{32} + D_{32}))/(C_{32}A_{31} - C_{31}A_{32}) \qquad 2.23$$

From the Equation 2.23, the coefficient of A_i. B_i. C_i. D_i could be calculated when the transmittance and emissivity of land surface.

$$T_s = T_{31} + A(T_{31} - T_{32}) + B \qquad 2.24$$

MODIS Land Surface Temperature and Emissivity (Ts/ε) product by Aqua MODIS (e.g. MYD11A1 products) and Terra-MODIS (e.g. MOD11A1 products) offered per-pixel temperature and emissivity values every day. Temperatures are produced in Kelvin (K) with a view-angle reliant formula applied to direct observations. MODIS LST algorithm claims producing 1 K accuracy for materials with identified emissivities [132]. The view angle details are a part of each Ts/ε product. Emissivities are estimates that are produced from implementing algorithm output to database information. The Ts/ε algorithms use MODIS data as input, such as geolocation, radiance, cloud masking, atmospheric temperature, water vapour, snow, and land cover. The theoretical foundation in MODIS Ts is outlined in detail by Wan [132]. Equally Aqua MODIS and Terra-MODIS Ts/ε products are supplied daily as a gridded level-3 product in the sinusoidal projection at (http://ladsweb.nascom.nasa.gov/). The availability of daily Ts as a MODIS technique is very beneficial for MC scaling research for around two major causes. First, the Ts inversion algorithm used by MODIS has been extensively recorded and also the technique is obtainable for assessment. Second, the data is readily obtainable through the internet.

2.11 Observation depth of MC

Nearly all hydrological and agricultural interests are in the root-zone soil moisture, which is much deeper than the top several centimeters and cannot be penetrated by current microwave remote sensors [154]. The issue was, is it possible to assess the root-zone soil moisture via optical remote sensing techniques? The fact is that, in vegetated areas, root-zone soil moisture is considered as a link between surface phenology and subsurface water storages, and it strongly influences surface water balance and energy partitioning because of evapotranspiration [154]. Referred to the capability of optical remote sensing to extract soil moisture, a depth of 50 cm under diverse land use and cover types was sampled earlier by Wan et al. [155]. Results by Wan et al. [155] revealed that NDVI has substantial correlation with root-zone soil moisture at different depths for shrub and grass vegetation at humid and semi-arid conditions. this correlation between soil moisture and NDVI was found to be statistically significant at the 5 cm, 10 cm, and 20 cm depths (near surface and major root zone) so that, significant regression equations for the relationships between VI (in general)-Ts and soil moisture in the two layers: 0 to 10 cm and 10 to 20 cm could be developed [156]. On the other hand, at the 50 cm and probably the 100 cm depths, the correlation is not statistically significant. At the 50 cm and 100 cm depths, the soil moisture has little fluctuation throughout the year compared with the larger fluctuation in the root zone. This means that soil moisture at 50 is less affected by rainstorm events or evapotranspiration. Some findings by Wang et al. [156] indicate that the soil moisture at depths of 0 to 10 cm and 10 to 20 cm could be estimated using the relationship between VI-Ts and soil moisture [156].

2.12 MC estimation from optical –multi sensors and ground measurements

The majority of the researchers have shown the significant possibilities of microwave and optical/IR frequency regimes for MC retrievals, all with their own pros and cons. Chauhan et al. [94] suggested a complete method of estimation for MC by merging the advantages of microwave and optical/IR measurements. Nevertheless, the poor spatial resolution of microwave sensors, along with the surface heterogeneity caused it to be challenging to set up strong relationships among optical/IR measurements and MC determined from microwave remote sensing [99]. The current research is made to develop a MC estimation formula at reasonable resolution by connecting MC measurements from multiple space-borne systems (optical/IR), and ground stations using the ‘Universal Triangle’ relation among soil moisture, land surface temperature and vegetation cover.

2.12.1 Universal Triangle

Vegetation and land surface temperature have a very complex reliance upon soil moisture. Earlier explanation of the vegetation and atmosphere relationship comes from the vegetation index/temperature trapezoid [130]. Precise studies of information by Carlson et al. [100] and Gillies et al. [101] demonstrated that there's a distinctive connection amongst soil moisture, vegetation cover, and surface temperature for a specific area. The outcomes were later on verified through theoretical research using the SVAT model that was first named by Gillies and Carlson [102]. Figure 2.4 shows a schematic explanation of the relationship often known as the ‘Universal Triangle’ [157]. The abscissa and the ordinate are scaled temperature and NDVI respectively

$$Ts^{*} = \frac{T - T_o}{T_S - T_o} \qquad 2.25$$

$$NDVI^{*} = \frac{NDVI - NDVI_o}{NDVI_S - NDVI_o} \qquad 2.26$$

Where, Ts and NDVI are observed land surface temperature and NDVI, respectively, and the subscripts *o* and *s* stand for minimum and maximum values

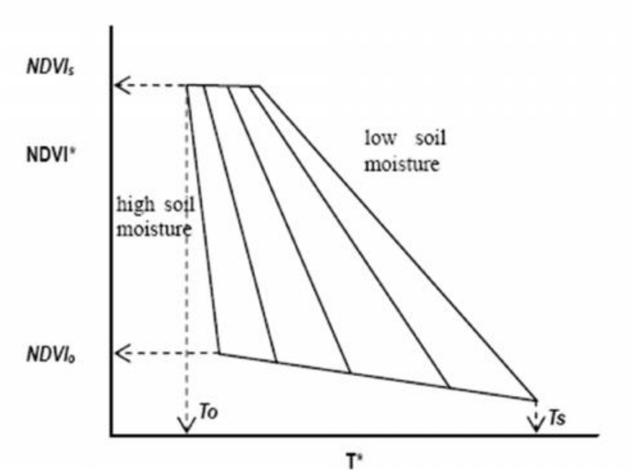

Figure 2. 4: Universal triangle’ relation between MC, Ts and NDVI [157].

The concept regarding the triangle could be that, the vegetation radiometric temperatures are usually near to air temperature; however, the surface radiant temperature over uncovered soil (bare soil) can vary based on the soil water content. This means that the spatial deviation in surface radiant temperature will likely be small (except for emission from underlying bare soil) over a full vegetation but can vary from warm to cold as the surface moisture accessibility goes from zero to one for bare soil (http://www.essc.psu.edu/~tnc/howto.html) [36]. Therefore, this triangle does not show a clear vertex is because of the simple fact that some emission of long wave radiation at complete vegetation cover has the capacity to penetrate the canopy and attain the radiometer. Therefore, even though NDVI* = 1, the actual dryness of the soil generates a spatial difference in surface radiant temperature which can be proved within the above figure as a lateral difference within the MC isopleths. Since the lateral variation at NDVI* = 1 is so significantly less than that at NDVI* = 0, the figure is similar to a triangle, though it is more properly known as a trapezoid [36]. Carlson et al. [100] found out that the relationship between MC, NDVI*, and Ts* could be indicated via a regression solution like:

$$MC = \sum_{i=0}^{i=n} \sum_{j=0}^{j=n} a_{ij} NDVI^{*(i)} Ts^{*(j)} \qquad 2.27$$

a_{ij}: The local parameters generated from the satellite-ground MC interpolation.

The flowchart of the MC evaluation formula is given in Figure 2.5. The regression relations are recognized by merging the ground measurements of MC and MODIS/AVHRR scaled NDVI and Ts. This MC strategy is later on used on a different set of MODIS/AVHRR, NDVI and Ts images. In-situ MC is compared against the estimations. A statistical examination has been carried out for the calculation process. Finally, the benefits and constraints of the approach were discussed [36]. Since suggesting the technique, it's been positively utilized in estimating outcomes of different soil water uses, for example estimating evaporation and transpiration.

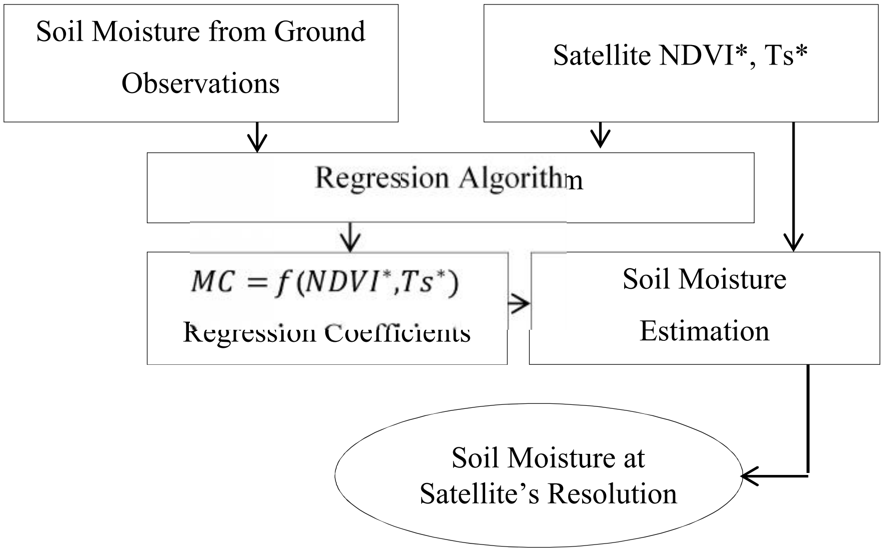

Figure 2. 5: Simple flow diagram for soil moisture estimation algorithm [36].

2.12.1.1 Current Applications of Universal Triangle Method

The technique is extensively suitable for any area that includes a combination of vegetated soil and bare soil. The two major input variables with the method are the surface temperature and the fraction of vegetation index. Thus, researchers work with different methods with remote sensing information to determine the method's input variables, and these various techniques produce different evaluation outcomes. Numerous researchers have applied this triangle method. Gillies et al. [101] applied an airborne multispectral radiometer data to acquire the method with two primary parameters. Nishida et al. [158] made use of the principles of triangle approach to approximate the evaporation fraction which is indicated as a percentage of actual (ET) for the available energy using NOAA/AVHRR data. Jiang and Islam [159] suggested a basic plan for the distribution of surface latent heat flux according to an interpretation of the triangle method utilizing vegetation index data and radiometric surface temperature. Wang et al. [160] incorporated a thermal inertial technique with triangle method to produce a modified day-night surface temperature with NDVI. They plotted the two variables in a triangular space using MODIS Aqua and MODIS Terra data to calculate the ET. Hassan et al. [161] suggested a brand new wetness index using terrain-corrected surface temperature and normalized difference vegetation index produced by MODIS products depending on the principles of the triangle technique. Stisen et al. [162] applied the initial principles of the triangle method using MSG-SEVIRI data to determine all Ts and NDVI, and then they plotted both parameters in a single space to calculate the air temperature. Yao et al. [163] applied the simple concepts of the triangle technique using Albedo- vegetation index space to ascertain the Priestley-Taylor factor for estimating evaporative fraction and ET in dry and semi-arid regions using MODIS data [163]. Lately, Nieto et al. [164] have calculated air temperature using thermal infrared and optical wavelength data by obtaining a relationship between the observed land surface temperature (Ts) and a spectral vegetation index (NDVI). Some of those presented studies have overlooked the impact of either the atmospheric circumstances or even the impact of topographic variations. Fixing both effects could possibly be challenging, however they both considerably affect evaluation of soil water applications.

2.12.1.2 Challenges of Applying Universal Triangle Method

A crucial concern that should be considered in remote sensing data before using the universal relationship technique is how the data must be atmospherically and topographically corrected by using free cloud-cover images, free atmospheric gases or vapor, and free solar illumination. This process mostly depends upon the imagery's pixel values; the more precise the pixel values are, better the estimated results. Also, employing this technique is represented in selecting the proper pixels that contain the wet edge or the dry edge. For example, once the method was suggested first, picking out the dry edge was merely showed from the best fit line of the pixels which have the greatest surface temperature value in the Ts-VI plot. Likewise for the wet edge, it was simply shown by a horizontal line at least value of surface temperature. Nevertheless, as the technique has changed, some changes have occurred in determining both the wet and the dry edges. These types of changes are occurred from the flexible principles of detailing both edges; like using different methods to identify the dry edge taking into consideration pixels location within the Ts-VI scatter plot and the pixels tend to create a linear regression line. There are not any pre-defined mathematical principles to determine the wet or dry edge; it is actually symbolized by a best fit line for a group of pixels at the wet or dry edge. The pixels that form a wet or a dry edge are usually chosen depending on how related they are to one another with regards to their location within the Ts-VI scatterplot. For instance, the pixels which have an identical pattern (found at a relatively close distance) are going to be represented within the formula of the best fit line as the dry edge pixels; nevertheless, the pixels which are spread or deviated from the trend, because of having very high or low Ts or very high or low VI are going to be omitted and will not be represented in the line's formula, as shown in Figure 2.6 [93].

An additional uncertainty which can be included with the method's applicability is that various vegetation indexes could be used to draw the Ts-VI scatterplot, and a vegetation index can produce different results at various areas' circumstances. Consequently, it is sometimes complicated to select the right vegetation index that could provide the best estimation outcomes. Additionally, MODIS, Landsat, or AVHRR are the most widely used optical data within this technique; they usually have a coarse resolution that may be hard to precisely identify the wet or the dry areas within the image because some pixels could be splitted among wet and dry areas, however the pixel value could only be represented in a single position in the Ts-VI space. Finally, present experiments have used low resolution images to appraise MC distribution on large scale areas [93].

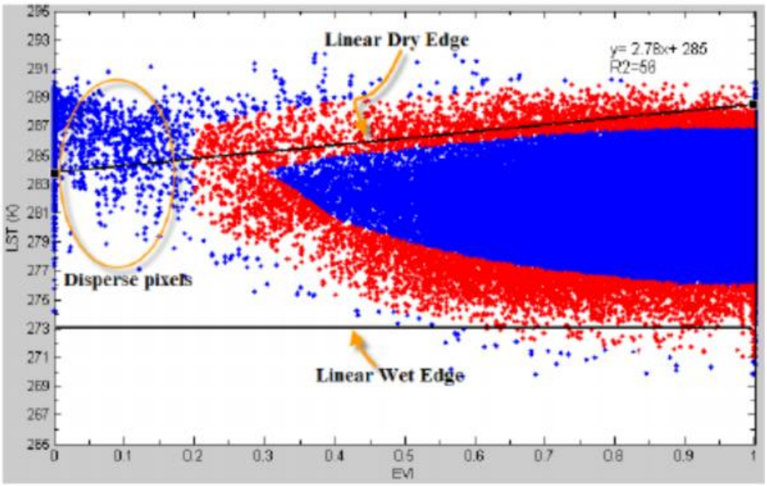

Figure 2. 6: Pixels distribution within the Ts-VI Scatterplot [93].

The plot implies that there is certainly inaccuracy in selecting the amount of pixels that determines both of the dry or the wet edge. Pixels positioned outside the trend of dry and wet edge are ignored and not thought to be in the formula of best fit line [93].

2.12.2 Thermal Inertia (TI) Method

This technique is dependent on the concept that water bodies possess a higher thermal inertia (TI) than dry soils and rocks and demonstrate a lesser diurnal temperature variation. When soil water content increases, thermal inertia relatively raises also, therefore decreasing the diurnal temperature variation range TI could be extracted, starting with the temperature diffusion formula. Many models have been produced using the thermal inertia technique by Xue and Cracknell [165], Sobrino and El kharraz [166] and Mitra and Majumdar [167] for MC extraction depending on the above mentioned theory, however with a little different methods. Among that, Mitra and Majumdar's [167] method is considered as essentially the most direct method and comparable to the assumed model by Pegram [122]. Within their method, apparent thermal inertia (ATI, presumed homogeneous layer for TI) is utilized. ATI is inferred through the measurements of spectral surface albedo and also the diurnal temperature range. It signifies the temporal and spatial variation of soil and canopy moisture [168]. The greater ATI, the greater the MC of the surface. The basic to derive soil water content is based on the idea that high/low ATI values match maximum/minimum MC contents [112] by including the soil wetness index (SWI).

In the triangular relationship of LST-NDVI Figure 2.7, maximum Ts (Ts_{max}) within the dry edge signifies the driest surface soil situations while surface soil wetness is actually zero. The wettest (saturated) soil statements are symbolized throughout the minimum Ts (Ts_{min}) across the ‘wet edge’ when surface soil wetness is the maximum [169]. The assumption is that, moisture availability ranges linearly from the dry edge to the wet edge. This can be in complete agreement with the understanding of LST- NDVI space [119, 162]. The soil wetness index (SWI) for a given day or time (t), which represents relative surface soil moisture, is described as:

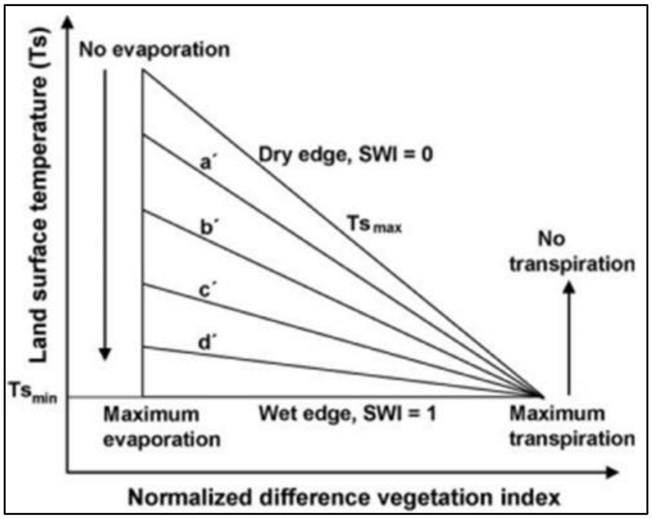

Figure 2. 7: Conceptual diagram of Ts-NDVI triangle for determining SWI [169].

$$SWI_{(t)} = \frac{Ts_{max(i)} - Ts_{(i)}}{Ts_{max(i)} - Ts_{min}} \tag{2.28}$$

Where $Ts_{(i)}$ is the land surface temperature of ith pixel. Ts_{hin} is the minimum Ts while in the triangle which specifies the wet edge. Ts_{max} would be the maximum Ts for i^{th} NDVI. Carlson [119] fairly found that, the dry edge as the least square fit to NDVI by using a polynomial (of the 3rd or 4th order) using fine resolution thermal information in addition to simulated data from soil vegetation atmosphere transfer model works. Today, the majority of the Ts-NDVI scatters from 927 m spatial resolution confirmed an obvious triangle with prominent linear dry edge and horizontal wet edge. The Ts-NDVI scatters at 90 m pixel resolution confirmed a non-linear pattern over the dry edge at higher NDVI values along with a sloping wet edge. Nevertheless, to maintain simplicity and consistency in method across various scales, the dry edge was modeled using a linear empirical fit to NDVI:

$$Ts_{max(i)} = a + bNDVI_{(i)} \tag{2.29}$$

Here, NDVI is the normalized difference vegetation index of the i^{th} pixel, 'b' is the slope and 'a' is the intercept of the linear dry edge. Ts_{max} values for several NDVI classes have been extracted using a NDVI interval of 0.05. After that 'dry edge' variables were calculated via regression analysis. The 'wet edge' is the horizontal line expressed by Ts_{min}.

Along the dry edge, SWI = 0, whereas it equals 1 along the wet edge. Isolines (a', b', c' and d') of SWI in Figure 2.7 represent equal surface moisture accessibility. By having the upper (MC_{max}) and lower (MC_{min}) boundaries of volumetric MC within the surface, the wetness index (SWI) over a given day or time could be transformed into a complete estimate of volumetric surface soil moisture (MC_v) making use of the following relationship [95]:

$$MC_v = MC_{min} + SWI_{(t)}(MC_{max} - MC_{min}) \tag{2.30}$$

MC_{max} is the upper limit of MC_v and will undertake values between field capacity (FC) and saturated MC. Generally, except right after a heavy rainfall event or irrigation MC_{max} could be set similar to FC. For additional practical purposes, MC_{max} could be represented as arithmetic mean of FC and maximum retentive capacity [112, 170]. The MC_{min} is the lower limit of MC_v and could be symbolized as permanent wilting point (PWP). These limits are soil type specific. The gap ($MC_{max} - MC_{min}$) between both two boundaries represents total water capacity (TWC) of soil [169].

2.13 The previously applied moisture Optical/IR-Models

During the last twenty years, optical and thermal RS sensors have been used for assessing MC in soils and vegetation. A summary by Moran et al. [12] discloses that a robust relationship is present between MC and index values produced from surface temperature-vegetation index (Ts-VI) techniques that employ optical and thermal RS data as input. Even though demonstrating promising outcomes, the penetrating abilities of optical and thermal RS sensors to sample the earth's surface minimize with the existence of clouds, vegetation cover, as well as other non-transmitting surfaces. Currently, many difficulties remain to be with utilizing remote sensing data to understand earth-system processes. The relation between Ts and VI has been earlier explained in scatterplots of Ts vs. VI, generally producing either "triangular" [128, 171] or "trapezoidal" forms [130, 172]. The edges of these styles give the basis for modelling MC in bare soils and in vegetation. A negative slope of the Ts-VI plot is usually noticed and interpreted using micro-meteorological concepts. For example, low Ts's typically happen over dense vegetation with higher MC, and relatively higher Ts's, over sparse vegetation with minimal MC. From the literature, Ts-VI plots have been given a variety of names, like the surface moisture status [173], triangular approach to indirect evaluation of MC [174], surface temperature-vegetation index [172], moisture index (MI; [175]), temperature vegetation contextual (TVX; [176]), and temperature-vegetation dryness index (TVDI; [128]). The Ts-VI technique has been applied using different remote sensing data over a variety of environments globally (Table 2.3). The technique has additionally been applied in different applications, like in quantifying (i) the evaporative fraction [158, 177], (ii) ET [171, 178], (iii) crop water deficit [130], (iv) forest fire hazard [179], and (v) drought period and intensity [180]. The favored Ts-NDVI relationship has restricted application in variable topography [119]. As an example, remotely-sensed Ts could only be estimated under clear-sky circumstances and Ts in variable terrain is usually lower in upland locations when compared with low-lying locations within the identical climatic and land use zonation. Obviously, using a response function depending on firmly Ts could improperly report that land-surface status in upland areas is wetter in comparison to low-lying areas. In order to enhance MC computations in high elevation areas, corrections are applied to Ts by applying grid, digital elevation model

(DEM) based mostly calculations of vertical atmospheric pressure to computations of surface possible temperature [181]. Here, surface possible temperature adjusts Ts to some value representing the temperature that might be at mean sea level (i.e., ~101.3 kPa) in a neutrally-stratified atmosphere [181]. Table 2.3 displays and summarizes the critical analysis of some of the previous MC estimation algorithms that have been applied using the optical sensors based on TS-VI relationship.

Table 2. 3: Examples of Ts-VI techniques available in the literature [161].

Researcher & Date	Sensor	Targeted Parameter	Method followed	Remarks
Sandholt et al. [128]	NOAA-AVHRR	Moisture Content via TS-VI technique	Moisture estimates from hydrological models using ground-based climate information as input	The method did not consider the atmospheric attenuation as well as the observation depth influence.
Carlson and Ripley; Carlson [103, 119]	Airborne Sat.	Moisture Content via TS-VI technique	Displayed moisture by using a "triangular" method	In this method, the ground measurements produced error of 16% between Ts-NDVI
Dupigny-Giroux and Lewis [175]	LANDSAT	Moisture Content via MI Modeling	Method modeled the periodic variations of MC because of alterations in vegetation growth	In this algorithm, there is no abrupt connections between MI and ground-based measurements of MC
Goward et al. [176]	NOAA-AVHRR	Moisture Content via TS-VI technique	Used TVX metrics to estimate daily soil	TVX metrics produced a wide range of standard

			moisture difference up to 2-cm depth	error ranged between 6-27%
Mitra and Majumdar [167]	MODIS	Moisture Content via TI technique	Apparent thermal inertia ATI was utilized	The study presumed homogeneous layer for TI, which overlooked the variety in surface cover classes
Pegram [122]	--	Moisture Content via TIR technique	Used the thermal infrared-soil moisture transformation model	The study depended on surface parameters that are difficult to measure like: heat capacity, Thermal conductivity and TI.
Moran et al. [12]	--	Moisture Content via Optical/IR-Model	The techniques have employed optical and thermal RS data as input	The method did not consider the atmospheric attenuation as well as the non-transmitting surfaces
Engman; Jackson; Njoku and Entekhabi; Jackson et al. [13, 66-68]	Airborne sensor	Moisture Content via TS-VI technique	The study used passive microwave remote sensing to measure the surface wetness	The technique was applicable for local-scale monitoring but not appropriate for watershed or regional scale

*Note: NOAA-National Oceanic and Atmospheric Administration; AVHRR-Advanced Very High Resolution Radiometer; NDVI-normalized difference vegetation index; FR- fraction of vegetation coverage produced from NDVI; SVAT-soil vegetation atmosphere transfer model; SWC-soil water content; GMS-Geostationary Meteorological Satellite; MODIS-Moderate Resolution Imaging Spectroradiometer [161].

2.14 Evapotranspiration, fundamentals & characteristics

Researches on ET include the study of equally ET by soil free water surfaces and transpiration from stomata of live vegetation. The complicated ET procedure entails radiation exchanges, vapor transport, and transfer structure and growth status of vegetation. There were many ET scientific studies; nonetheless a lot of them were focused on crop ET. Standard ET estimation strategies have been extracted fundamentally from an energy balance viewpoint, aerodynamic vapor transport viewpoint, or mixture of the two [182].

Evaporation and transpiration take place concurrently and there is not any smart way of differentiating between two of them. In addition to the water availability within the topsoil, the amount of evaporation from a cropped soil is principally based on the fraction of the solar radiation that hits the soil surface. This fraction decreases over the developing period as the crop evolves and grows and its canopy shades increase and cover most of the ground area. Once the crop is small, water is mainly lost by soil evaporation, but when the crop is well toned and totally covers the soil surface, the transpiration becomes the main process that acts at the plant's leaf and stomata [183].

2.14.1 Units

The ET rate is usually expressed in millimeter (mm) for each unit time. The rate states the amount of water lost from a cropped surface in units of water depth. The unit of time is often an hour, day, decade, month or perhaps whole growing period or year. Water depths may also be stated with regard to energy received for each unit area. The energy signifies the heat energy necessary to vaporize free water. This energy, referred to as latent heat of vaporization (λ), can be a function of the water temperature [183].

2.14.2 Factors affecting evapotranspiration

Weather variables, crop characteristics, management and ecological aspects tend to be factors influencing evaporation and transpiration.

2.14.2.1 Weather parameters

The main weather variables influencing evapotranspiration are radiation, air temperature, humidity and wind speed. Numerous techniques have been developed to measure the evaporation rate from all of these parameters. The evaporation power of the atmosphere is indicated by the reference crop evapotranspiration (ET_o). The reference crop evapotranspiration signifies the evapotranspiration from a standard vegetated surface.

2.14.2.2 Crop factors

The crop kind, assortment and development phase should be considered when evaluating the ET from crops developed in big, well-managed fields. Variations in resistance to transpiration, crop height, crop roughness, reflection, ground cover and crop rooting characteristics lead to diverse ET levels in various forms of crops under similar environmental circumstances. Crop ET under standard conditions (ET_c) means the evaporating need from crops which are grown in large fields under ideal soil water, great management and environmental conditions, and achieve complete production within the given weather conditions. The issue of soil water content on ET is conditioned mostly by the degree of the water deficit and the kind of soil. Alternatively, too much water can lead to waterlogging that might harm the root and reduce water uptake by suppressing respiration [183].

2.15 Reference ET

Potential ET, mentioned as ET_o, is the rate at which water, if available, could be taken off from wet soil and plant surfaces [182]. This concept was developed to study the evaporative need for the climate separately of crop type, crop development and management practices. As water is much available at the reference evapotranspiring surface, soil components usually do not impact ET_o. Relating ET to a particular surface gives a reference to that ET from other surfaces can be associated. ETo values calculated or assessed at various locations or in various seasons are equivalent as they refer to the ET from the same reference surface [184]. The only factors influencing ET_o are climatic parameters. As a result, ET_o is a climatic parameter which could be calculated from weather data. ET_o expresses the evaporating power of the atmosphere in a certain location and season and does not take into account the crop characteristics and soil elements [183].

2.16 Meteorological Data for ET Determination

The meteorological variables identifying ET are weather variables which give energy for vaporization and take off water vapour from the evaporating surface. The key weather variables to take into consideration are introduced below.

2.16.1 Solar radiation

The ET process depends on the quantity of energy accessible to vaporize water. Solar radiation could be the largest source of energy and is capable of changing large volumes of liquid water into water vapour. The possible quantity of radiation that may reach the evaporating surface is estimated by its location and the time. Because of differences in the position of the sun, the possible radiation varies at various latitudes and in various seasons. The exact solar radiation excessing the evaporating surface is dependent upon the turbidity of the atmosphere as well as the existence of clouds which reflect and soak up significant portions of the radiation while determining the effect of solar radiation on ET.

2.16.1.1 Extraterrestrial radiation (R_a)

The radiation excesses a surface vertical with respect to the rays of the sun on top of the earth's atmosphere, known as the solar constant, which is around 0.082 MJm^{-2} min^{-1}. The local intensity of radiation is, on the other hand, dependent on the angle between the direction of the sun's rays plus the normal rays to the surface of the atmosphere. This angle changes throughout the day and will also be different at different latitudes as well as in different seasons. The solar radiation acquired at the top of the earth's atmosphere on a horizontal surface is known as the extraterrestrial (solar) radiation, R_a. The extraterrestrial radiation, R_a, for every day of the entire year as well as for different latitudes could be approximated through the solar constant, the solar declination as well as the time of the year by Allen et al. [183]:

$$R_a = \frac{12(60)}{\pi} G_{sc} d_r \left[(w_2 - w_1)\sin(\varphi)\sin(\delta) + \cos(\varphi)\cos(\delta)\left(\sin(w_2) - \sin(w_1)\right)\right] \quad 2.31$$

Where

R_a	Extraterrestrial radiation in the hour (or shorter) period [MJ m^{-2} hour^{-1}],
G_{sc}	Solar constant = 0.0820 MJ m^{-2} min^{-1},
d_r	Inverse relative distance Earth-Sun
δ	Solar declination [rad]
φ	Latitude [rad]
w_1	Solar time angle at beginning of period [rad]
w_2	Solar time angle at end of period [rad].

The next relations are used for determining the inverse relative distance of Earth-Sun, as well as the solar declination:

$$dr = 1 + 0.033 \cos\left(DO^{Y}\frac{2pi}{365}\right) \quad 2.32$$

$$\cos\theta = \cos\left(\frac{pi}{2-\Phi}\right) \quad 2.33$$

G_{sc}	The solar constant (1367 w/m^2).
dr	Inverse squared relative distance earth-sun (dimensionless).
$\cos\theta$	Cosine of the solar zenith angle.
Φ	Sun elevation angle in radian.

$$\delta = 0.409 \sin\left(\frac{2\pi}{365} DOY - 1.39\right) \qquad 2.34$$

Where DOY is the number of the day in the year between 1(1 January) and 365 or 366 (31 December).

2.16.1.2 Solar radiation (R_s)

If the solar radiation, R_s, is not calculated, it could be determined using the Angstrom formulation that associates solar radiation to extraterrestrial radiation and relative sunshine duration [183]:

$$R_s = \left(a_s + b_s \frac{n}{N}\right) R_a \qquad 2.35$$

R_s	Solar or shortwave radiation [MJ m^{-2} day^{-1}],
n	Actual duration of sunshine [hour],
N	Maximum possible duration of sunshine or daylight hours [hour],
$\frac{n}{N}$	Relative sunshine duration [-],
R_a	Extraterrestrial radiation [MJ m^{-2} day^{-1}],
a_s	Regression constant, expressing the fraction of extraterrestrial radiation reaching the earth on overcast days ($n = 0$),
$a_s + b_s$	Fraction of extraterrestrial radiation to the earth on clear days ($n = N$).

2.16.1.3 Daylight hours (N)

The daylight hours, N, could be given as

$$N = \frac{24}{\pi} \omega_s \qquad 2.36$$

Where ω_s is the sunset hour angle in radians.

2.16.1.4 Net solar or net shortwave radiation (R_{ns})

The net shortwave radiation as a result of the balance between incoming and reflected solar radiation could be written by the following formula [184]:

$$R_{ns} = (1-\alpha)R_s \tag{2.37}$$

R_{ns} Net solar or shortwave radiation [MJ m^{-2} day^{-1}],

α Albedo or canopy reflection coefficient, which is 0.23 for the hypothetical grass reference crop [dimensionless],

R_s The incoming solar radiation [MJ m^{-2} day^{-1}].

If the net solar radiation required in the calculations when computing ET_o, the fixed value of 0.23 is used for the albedo in Equation 2.48.

2.16.1.5 Net longwave radiation (R_{nl})

$$R_{nl} = \sigma\left[\frac{T_{\max k^4}+T_{\min k^4}}{2}\right]\left(0.34-0.14\sqrt{\epsilon_a}\right)\left[1.35\frac{R_s}{R_{so}}-0.35\right] \tag{2.38}$$

R_{nl} Net outgoing longwave radiation [MJ m^{-2} day^{-1}],

σ Stefan-Boltzmann constant [$4.903*10^{-9}$ MJ K^{-4} m^{-2} day^{-1}],

$T_{\max k^4}$ Maximum absolute temperature during the 24-hour period [K = °C + 273.16],

$T_{\min,k^4}$ Minimum absolute temperature during the 24-hour period [K = °C + 273.16],

e_a Actual vapour pressure [kPa],

$\frac{R_s}{R_{so}}$ Relative shortwave radiation (limited to ≤ 1.0),

R_s Measured or calculated solar radiation [MJ m^{-2} day^{-1}],

R_{so} Calculated clear-sky radiation [MJ m^{-2} day^{-1}].

2.16.1.6 Net radiation (R_n)

The difference between the incoming net shortwave radiation (R_{ns}) and the outgoing net long wave radiation (R_{nl}), results in the net radiation (R_n) which is expressed as follow:

$$R_n = R_{ns} + R_{nl} \quad 2.39$$

Where

R_{ns} Net shortwave radiation

R_{nl} Net long wave radiation

2.16.2 Air temperature

The solar radiation assimilated by the atmosphere and also the heat released from the earth raise the air temperature. The sensible heat of the encompassing air conveys energy to the crop and consequently has a controlling impact on the rate of ET. In sunny warm weather, the loss of water by ET is larger compared to cloudy and cool weather. The mean air temperature is written by:

$$T_{mean} = \frac{T_{max} + T_{min}}{2} \quad 2.40$$

2.16.1 Air humidity

As the energy supply from the sun and surrounding air could be the main motivator for the vaporization of water, the gap between the water vapour pressure in the evapotranspiring surface and the surrounding air is the determining issue for the vapour removal. Well watered fields in hot dry arid regions consume large amounts of water due to the abundance of energy and the desiccating power of the atmosphere. In humid tropical areas, in spite of the high energy input, the high humidity from the air will decrease the ET need. In this environment, the air is definitely near to saturation, in order that significantly less additional water could be stored and therefore the ET rate is less than in arid regions. Relative humidity and saturated vapor pressure could be expressed as:

$$RH = 100\frac{e_a}{e^o(T)} \qquad 2.41$$

e_a	Vapor pressure at air
$e^o(T)$	Saturation vapor pressure at temperature (T) [kPa],

$$e^o(T) = 0.6108 exp\left[\frac{17.27T}{T+237.3}\right] \qquad 2.42$$

Actual vapor pressure (e_a) derived from relative humidity based on the humidity potential data, different formulas are used:

$$e_a = \frac{e^o(T_{min})\frac{RH_{max}}{100} + e^o(T_{max})\frac{RH_{min}}{100}}{2} \qquad 2.43$$

e_a	Actual vapor pressure [kPa],
$e^o(T_{min})$	Saturation vapor pressure at daily minimum temperature [kPa],
$e^o(T_{max})$	Saturation vapor pressure at daily maximum temperature [kPa],
RH_{max}	Maximum relative humidity [%],
RH_{min}	Minimum relative humidity [%].

2.16.1.1 Slope of saturation vapour pressure curve (Δ)

For the computation of the reference evapotranspiration, the slope of the relationship between saturation vapour pressure and temperature, Δ, is needed. The slope of the curve in a given temperature is provided by Raes [184]:

$$\Delta = \frac{4098\left(06108\,exp\left[\frac{17.27T}{T+237.3}\right]\right)}{(T+237.3)^2} \qquad 2.44$$

Where Δ is the Slope of saturation vapor pressure curve [kPa °C^{-1}]

2.16.1.2 Vapour pressure deficit (e_s - e_a)

The vapour pressure deficit is defined as the difference between the saturation (e_s) and actual vapour pressure (e_a) for a particular period of time.

2.16.2 Wind speed

The entire process of vapour elimination is dependent particularly upon wind and air turbulence that transfers large volumes of air within the evaporating surface. When vaporizing water, the air over the evaporating surface gets steadily saturated with water vapour. If the air isn't constantly substituted for drier air, the driving force for water vapour removal as well as the ET rate decreases.

The ET need is high in hot dry weather because of the dryness and also the quantity of energy readily available as direct solar radiation and latent heat. In these situations, a lot of water vapour might be kept in the air although wind may promote the transfer of water permitting more water vapour being taken up. Alternatively, under humid climate conditions, the high humidity of the air and also the existence of clouds result in a lower ET rate. The more dry the atmosphere, the greater the influence on ET and steeper would be the curve. For humid conditions, the wind could only replace saturated air with somewhat less saturated air and take off heat energy. As a result, the wind speed impacts the ET rate to some far lesser degree than under arid situations where small variations in wind speed may lead to bigger variations in the ET rate. To regulate wind speed, data is extracted from instruments positioned at elevations apart from the typical height of 2 m:

$$u_2 = u_z \frac{4.87}{ln(678z-5.42)} \qquad 2.45$$

u_2 Wind speed at 2 m above ground surface [m s^{-1}],

u_z Measured wind speed at z m above ground surface [m s^{-1}],

z Height of measurement above ground surface [m].

2.17 Atmospheric parameters

A number of relationships are available to present climatic parameters. The consequence of the primary weather parameters on ET could be evaluated with the aid of the forthcoming equations. A few of the relationships need parameters that express a particular characteristic of the atmosphere. Prior to examining the four primary weather parameters, some atmospheric parameters are discussed as follow.

2.17.1 Atmospheric pressure (P)

The atmospheric pressure, P, is the pressure applied by the weight of the earth's atmosphere. Evaporation at high altitudes is promoted because of low atmospheric pressure as indicated in the psychometric constant. The consequence is, even so, small, and in the computation procedures, the average value for a location is enough. A generality of the ideal gas law, supposing 20°C for the standard atmosphere, can be utilized to determine P:

$$P = 101.3\left(\frac{293-0.0065z}{293}\right)^{5.26} \qquad 2.46$$

P Atmospheric pressure [KPa]

z Station elevation above sea level [m]

2.17.2 The psychrometric constant, (γ)

Is given by:

$$\gamma = \frac{c_p P}{\varepsilon \lambda} = 0.665 \times 10^{-3} P \qquad 2.47$$

γ Psychrometric constant [kPa $°C^{-1}$],

P Atmospheric pressure [kPa],

λ Latent heat of vaporization, 2.45 [MJ kg^{-1}],

C_p Specific heat at constant pressure, $1.013x10^{-3}$ [MJ kg^{-1} $°C^{-1}$],

ε Ratio molecular weight of water vapor/dry air = 0.622

The specific heat at regular pressure is the quantity of energy necessary to raise the temperature of a unit mass of air by one degree at regular pressure. Its value depends upon the composition of the air, i.e., on its humidity. For average atmospheric situations a value $C_p = 1.013x10^{-3}$ MJ kg^{-1} $°C^{-1}$ can be utilized. Being an average atmospheric pressure is used for every location, the psychrometric constant is maintained constant for every location [183].

2.17.3 Latent heat of vaporization (λ)

The latent heat of vaporization, λ, represents the energy necessary to change a unit mass of water from liquid to water vapour within a constant pressure and temperature in a course of action. The value of the latent heat can vary as a function of temperature. At high temperatures, less energy is needed compared to lower temperatures. As λ differs only slightly over typical temperature ranges, a single value of 2.45 MJ kg^{-1} is drawn in the generality of the FAO Penman-Monteith equation. This is actually the latent heat for an air temperature of around 20°C.

2.17.4 Soil heat flux (G)

Complex models have a potential of describing soil heat flux. Simply because soil heat flux is smaller compared to R_n, especially when the surface is covered by vegetation and computation time steps are 24 hours or longer, an easy calculation process is introduced here for period of time steps, depending on the concept that the soil temperature follows the air temperature:

$$G = c_s \frac{T_i + T_{i-1}}{\Delta t} \Delta z \qquad 2.48$$

G Soil heat flux [MJ m^{-2} day^{-1}],

c_s Soil heat capacity [MJ m^{-3} °C^{-1}],

T_i Air temperature at time i [°C],

T_{i-1} Air temperature at time i-1 [°C],

Δt Length of time interval [day],

Δz Effective soil depth [m].

Because the soil temperature lags air temperature, the average temperature for any period should be considered when evaluating the daily soil heat flux, i.e., Δt should exceed 1 day. The depth of penetration of the temperature wave is estimated by the length of time interval. The powerful soil depth, Δz, is just 0.10-0.20 m for a time period of one or maybe a couple of days but could be 2 m or higher for monthly periods. The soil heat capacity is related to its mineral composition and water content.

For day and ten-day periods:

As the magnitude for the day or ten-day soil heat flux underneath the grass reference surface is comparatively small, it could be overlooked and therefore:

$$G_{day} \approx 0$$

For monthly periods:

By supposing a constant soil heat capacity of 2.1 MJ m^{-3} °C and a sufficient soil depth, Equation 2.59 could be used to estimate G for monthly periods:

$$G_{month,i} = 0.07(T_{month,i+1} - T_{month,i-1}) \qquad 2.49$$

$T_{month,i-1}$: Mean air temperature of previous month [^{o}C]

$T_{month,i+1}$: Mean air temperature of next month [^{o}C]

For hourly or shorter periods:

For hourly period (or shorter) assessments, G underneath a dense vegetation cover does not correlate in a good way with air temperature. Hourly G can then be approximated during daylight periods as:

$$G_{hr} = 0.1R_n$$

And during night time period as:

$$G_{hr} = 0.5R_n$$

When the soil is warm, the soil heat flux G value is positive. The quantity of energy needed for such process is extracted from Rn when assessing ET.

2.18 Evapotranspiration measurements

Two basic ways to measure the ET, which are the ordinary methods as well as the satellites-based one. The ordinary methods depend mainly on the weather potentials represented in the variable parameters that acquired from meteorological stations. The spatial methods in turn, depend mainly on the spectral signature from the ground vegetation entities beside some weather parameters.

2.18.1 Conventional measurement methods

Evapotranspiration is difficult to measure due to its dependency on very dynamic variables. Particular systems and precise measurements of numerous physical variables or the soil water balance in lysimeters are needed to figure out ET. The techniques tend to be expensive, demanding when it comes to accuracy of measurement and might only be fully exploited by well-trained investigation personnel. Even though the techniques are improper for routine measurements, they continue to be essential for the evaluation of ET estimations acquired by more indirect approaches.

2.18.1.1 Energy balance and microclimatological methods

Evaporation of water demands relatively considerable amounts of energy, either in the type of sensible heat or radiant energy. Hence the ET process is controlled by energy exchange at the vegetation surface and it is restricted to the quantity of energy available. Due to this constraint, it is easy to predict the ET rate by utilizing the energy conservation strategy. The energy reaching the surface must be similar to the energy leaving the surface for the same period of time. All fluxes of energy should be taken in consideration when deriving an energy balance formula. The equation for an evaporating surface could be given as:

$$R_n - G - \lambda ET - H = 0 \qquad 2.50$$

Where R_n represents the net radiation, H is the sensible heat, G is the soil heat flux and λET is the latent heat flux. The different terms could be either negative or positive. Positive Rn provides energy to the surface and positive G, λET and H take away energy from the surface.

Throughout daytime, the surface receives more radiative energy than it produces, and this excess is transformed into sensible heat conducted to the atmosphere (H) and also to the ground (G) and into latent heat (λET). The dividing between the three substances depends upon several elements including the surface characteristics, the geographic location, the time and the climate. Throughout night time, the surface emits much more radiative energy than it receives, and this decrease of energy is compensated by sensible heat conducted from the air and the ground into the surface, and perhaps additionally latent heat from condensation (dew formation). The absolute value of G during nighttime is approximately corresponding to its daytime value, thus G over 24 hours could be assumed to equal zero. Other ingredients normally have greater value during day compared to night.

The earth's surface isn't a perfect surface because it consists of horizontal in homogeneities (like vegetation, buildings and hills). Therefore, it is often better to treat it as being a finite layer with its own mass and heat capacity to ensure that energy could be kept in the layer. When considering vegetated surfaces, it's most suitable to incorporate the entire canopy layer inside the energy balance [185]:

$$R_n = H + LE + G + \Delta H_S \qquad 2.51$$

Where ΔH_S is the change in energy storage for each unit time per unit area within the depth of the layer, and H and LE tend to be assessed above the canopy.

The percent of energy storage in a vegetative canopy includes two parts (physical and biochemical) and it is rather complex to determine and calculate; it is usually included with the ground heat flux to generate a mixed storage compound. The latent heat exchange can also be difficult since in addition to evaporation from the surface, it contains transpiration from plant leaves as well [185].

2.18.1.2 Penman- Monteith

The United Nations Food and Agriculture Organization (FAO) has implemented the Penman-Monteith approach being a global standard for estimating ETo from four meteorological data (temperature, wind speed, radiation and relative humidity), with particulars introduced in the Irrigation and Drainage Paper no. 56 by Allen et al. [183], described hereafter as PM:

$$ET_o = \frac{0408\Delta(R_n - G) + \gamma \frac{900}{T+273} u_2 (e_s - e_a)}{\Delta + \gamma(1 + 034 u_2)} \qquad 2.52$$

ET_o	Reference evapotranspiration [mm day^{-1}],
R_n	Net radiation at the crop surface [MJ m^{-2} day^{-1}],
G	Soil heat flux density [MJ m^{-2} day^{-1}],
T	Mean daily air temperature at 2 m height [°C],
u_2	Wind speed at 2 m height [m s^{-1}],
e_s	Saturation vapour pressure [kPa],

e_a	Actual vapour pressure [kPa],
$e_s - e_a$	Saturation vapour pressure deficit [kPa],
Δ	Slope vapour pressure curve [kPa °C^{-1}],
γ	Psychometric constant [kPa °C^{-1}].

The PM model utilizes a theoretical green grass reference surface which is positively growing and is sufficiently watered with an assumed height of 0.12 m, having a surface resistance of 70s m^{-1} as well as an albedo of 0.23 which usually bears resemblance to ET from a comprehensive surface of green grass cover of standard height, completely shading the ground and without water shortage. This technique is usually considered to be the most reliable, in a wide range of environments and locations, since it is based on actual physical concepts and considers the primary climatic factors, which influence ET [186].

2.18.1.3 The Hargreaves- Samani methodology

Hargreaves, made use of grass ET data from the accurate lysimeter and climate data from Davis, California, during a period of eight years. He noticed, via regressions that for five-day time steps, 94% of the deviation in measured ET could be described through average temperature and global solar radiation R_s. Consequently, in 1975, he published a formula for predicting ET_o dependent only on these parameters:

$$ET = 0.0023\left(\frac{R_a}{\lambda}\right)(T + 17.8)(T_{max} - T_{min})^{05} \qquad 2.53$$

Where

ET	Daily potential evapotranspiration rate [mm/day]
R_a	Extraterrestrial radiation in the hour period [MJ m^{-2} day^{-1}],
T	Mean temperature [^{o}C]

λ Latent heat evaporation [kj/kg]

T_{max} Daily maximum temperature [^oC]

T_{min} Daily minimum temperature [^oC]

Where R_s is given in units of water evaporation in mm day^{-1}, and T in ^oC. Following tries to use wind velocity, U_2, and relative humidity, RH, to enhance the outcomes were not encouraging so, these variables have been omitted [187].

The quality index, or the fraction of the extraterrestrial radiation that really goes through the clouds and reaches the earth's surface, is the principal energy source for ET. Research by Hargeaves and Samani [188] revealed that it could be calculated through the difference between the maximum, T_{max}, and the minimum, T_{min} daily temperatures. Under clear skies the atmosphere is transparent to excess solar radiation therefor the T_{max} is higher, while night temperatures are lower as a result of outgoing longwave radiation.

2.18.1.4 The Turc method

Also referred to as the Turc-Radiation equation, this technique was provided by [189], using data from the humid climate of Western Europe (France). This technique only uses two variables, average daily radiation and temperature and then for RH > 50 % could be expressed as:

$$ET_p = \square\ ((23{,}9001R_s) + 50)\left(\frac{T}{T+15}\right) \qquad 2.54$$

And for RH < 50 % as:

$$ET_p = \square\ ((23{,}9001R_s) + 50)\left(\frac{T}{T+15}\right)\left(1 + \frac{50-RH}{70}\right) \qquad 2.55$$

Where

□: is 0.01333 and R_s is expressed in MJm^{-2}day^{-1}

Lu et al. [190] compared six distinct ET equations in humid southeast United States, and found that, the Turc formula is generally the second best only to the entire PM. Jensen et al. [191] examined the properties of twenty various methods against very carefully chosen lysimeter data from eleven stations, located globally in different climates. They noticed that the Turc method in comparison the others, is very positively with combination techniques for the humid lysimeter places. The Turc technique was positioned second when only humid locations were regarded, with simply the Penman-Monteith method performing much better.

2.18.2 Remote sensing techniques in evapotranspiration measurements

Since the beginning of Earth remote sensing from satellites, remotely sensed studies of the Earth's surface have introduced an encouraging supply of data for evaluating the characteristics over land surfaces. Principle of satellite remote sensing is found on the knowledge of the spectral response from materials on the ground. Spectral measurements using spectral radiometer are of essential significance in remote sensing, equally at the level of principal study as well as in functional applications. For vegetation property study or even to aid the interpretation of satellite information, a relationship should be formulated between satellite detected data and field measured spectral data [192].

Surface temperature and vegetation index are a couple of the most basic surface parameters that could be extracted from the thermal and optical part of the satellite remote sensing, correspondingly. Nevertheless, the relationship of surface temperature and vegetation index regarding land cover/use has to be substantially analyzed. Both of these parameters are correspondingly related to the moisture availability and the vegetation situation that are the most significant and hard surface elements being assessed in the ET process. Price [193] documented that there is no benefit of using advanced simulation model for ET evaluation in the event of unavailability of the needed surface parameters for the region.

Studies of remote sensing in ET estimation include four basic types which are often mentioned as follows.

2.18.2.1 The energy balance equation

Evapotranspiration estimation (equivalent to the latent heat flux LE) by remote sensing is dependent on evaluating the energy balance by way of various surface properties like albedo, leaf area index, vegetation cover, and surface temperature (Ts). When evaluating instantaneous conditions, the energy balance formula is written as:

$$Rn = LE + H + G \qquad 2.56$$

The accessible net radiant energy R_n is contributed between the soil heat flux G and also the atmospheric convective fluxes (sensible heat flux H and latent energy exchanges LE). Radiant and convective fluxes could be explained either along with the observed surface being a single aspect (single layer methods) or discerning soil and vegetation elements with some other levels of canopy description based on the number of vegetation layers (multilayer techniques, with those determined by two sources which are commonly used) [194].

With regards to immediate conditions, the energy balance formula is written as:

$$\lambda ET_{ins} = Rn - G - H \qquad 2.57$$

λET he instant latent heat loss (Wm^{-2}), which is calculated as a residual of the energy budget.

λ The heat loss when a gram of water evaporates.

ET_{ins} TThe rate of evapotranspiter at the time of the satellite overpassing.

Rn Net solar raids (wm^{-2}).

G Soil heat flux into the soil (wm^{-2}).

H Sensible heat into the air (wm^{-2}).

Satellite based Net Radiation (R)

$$R \quad R_{ins} - R_n =+ R_{s\downarrow} \quad R_{s\uparrow} \quad (wm^{l\downarrow} - \qquad 2.58$$

$$R_n = (1-\square)R_{s\downarrow} + \varepsilon_a \sigma T_a^4 - \varepsilon_s \sigma T_s^4 \quad (wm^2) \qquad 2.59$$

$R_n, R_{s\downarrow}, T_a^4, T_s^4, \varepsilon_s$ have been defined previously, □ the surface short-wave albedo, σ the Stefan–Boltzman constant (5.67 x 10^{-8} w m^{-2} K^{-4}), ε_a is the air emissivity taken as in Bastiaanssen [195]:

$$\varepsilon_a - 1.08(-\ln \tau_{sw})^{0.265} \qquad (wm^{-2}) \qquad 2.60$$

$$\tau_{sw} = 0.75 + 2 \times 10^{-5} z \qquad 2.61$$

τ_{sw} (−) two way atmospheric transmissivity.

z Elevation in meter.

The incoming short wave radiation ($R_{s\downarrow}$) was estimated from the equation as a function of solar zenith angle, atmospheric transmissivity, the solar constant and the sun-earth distance.

Digital Elevation Model DEM

In order to evaluate the atmospheric water vapor based on image pixel's elevation, DEM raster dataset is required considering the pixel's size compatibility with the processed image. Some studies tend to assume fixed rate of the atmospheric water vapor over the study areas due to its small effect on the quantification of ET_o.

$$R_{s\downarrow} = G_{sc} * \cos\theta \square dr * \tau_{sw} \quad (wm^{-2}) \qquad 2.62$$

$$dr = 1 + 0.033 \cos\left(DOY \frac{2pi}{365}\right) \qquad 2.63$$

$$\cos\theta = \cos\left(\frac{pi}{2-\Phi}\right) \qquad 2.64$$

G_{sc} The solar constant (1367 w/m^2).

dr Inverse squared relative distance earth-sun (dimensionless).

$\cos\theta$ Cosine of the solar zenith angle.

Φ Sun elevation angle in radian.

The outgoing longwave radiation (R_{L^a}) is computed using the Stefan-Boltzmann equation:

$$R_{L\uparrow} = \varepsilon_o \times \sigma \times T_s^4 \tag{2.65}$$

Where; ε_o is the broad-band surface emissivity (dimensionless), σ is the Stefan-Boltzmann constant (5.67*10^{-8} W/m^2/K^4), and Ts is the surface temperature (K). The excess Longwave Radiation ($R_{L\uparrow}$)

$$R_{L\downarrow} = \varepsilon_a \times \sigma \times T_a^4 \tag{2.66}$$

Where; ε_a is the atmospheric emissivity (dimensionless), σ is the Stefan-Boltzmann constant (5.67 × 10^{-8} W/m^2/K^4), and Ta is the near surface air temperature (K). The subsequent empirical formula for ε_a by Bastiaanssen [195] is used using data from alfalfa fields in Idaho.

Soil Heat Flux (G)

$$G = R_n\left[\frac{T_s}{\alpha}\right](0.0038\ \square + 0.0074\ \square^2)(1 - 0.98NDVI^4) \tag{2.67}$$

Sensible Heat Flux (H)

In case of dry image pixels: λE is assumed to have the value of 0.

$$H = Rn - G \quad (wm^{-2}) \tag{2.68}$$

$$H = \frac{\rho c_p dT}{r_{ah}} \tag{2.69}$$

Where

ρ The air density (mol/m^3).

c_p The specific heat of air (29.3 J/mol/ ^{o}C).

dT The near surface temperature difference (K).

r_{ah} The aerodynamic resistance to heat transport (s/m),

$$r_{ah} = \frac{\ln(\frac{z_2}{z_1})}{u^* k} \tag{2.70}$$

z_1 A height just above the zero displacement distance height of plant canopy set to 0.1 m for each pixel.

z_2 The reference height just above the plant canopy set to 2 m for each pixel.

u^{*} The friction velocity (m/s).

k The von Karman constant (0.4).

$$u^{*} = \frac{u(z)k}{\ln\left(\frac{z-d}{z_m}\right)} \quad \left(\frac{m}{s}\right) \qquad 2.71$$

$$d = 0.65h \qquad 2.72$$

$$z_m = 0.1h \qquad 2.73$$

$u(z)$ Wind speed at height of z.

d The zero displacement height.

h The plant height (m).

z_m The roughness length (m).

2.18.2.2 Surface Energy Balance Algorithm for Land (SEBAL)

Surface Energy Balance Algorithm for Land (SEBAL) originated by Bastiaanssen et al. [107] to produce ET maps using high resolution satellite images over large areas. Within the SEBAL model, ET is calculated from satellite images and climate data making use of the surface energy balance [196]. The formula estimates surface albedo, Normalized Difference Vegetation Index (NDVI), and surface temperature making use of visible, near infra-red (NIR), and thermal IR bands from satellite sensors. The calculated variables are employed to figure out different elements of the energy balance formula. Using NDVI they determine emissivity, which often is utilized to calculate Rn via a linear regression model. They determine the ratio of G to Rn (corrected for any errors) using NDVI, hemispherical reflectance, and surface temperature, which often provides the value for G. To calculate the H, they take into account two excessive cases of evaporative fraction or EF (rate of latent heat to the total of latent and sensible heat), the warmest pixel (when latent heat goes to zero) as well as the coolest pixel (when sensible heat goes to zero) [197].

As the satellite image offers data for the overpass time only, SEBAL determines an instant ET flux for the image time. The ET flux is determined for every pixel in the image being a "residual" of the surface energy budget formula [196]. This model continues to be built in order to determine the energy partitioning within the local scale with lowest ground information. Atmospheric parameters (air temperature and wind speed) are calculated via remote sensing data by taking into consideration the spatial variability brought on by hydrological and energetic differences. The estimation of wet and dry surfaces within the studied area is important to extract threshold values. The model demands incoming radiation, Ts, NDVI and albedo maps. Semi-empirical relationships are utilized to calculate emissivity, roughness length from NDVI. The sensible heat flux is calculated by inverting sensible heat flux expression over equally dry (LE = 0) and wet (H = 0) land. Latent heat flux is calculated as being the residual of energy balance [194]. The model was verified for both intermediary parameters and surface energy fluxes by Jacob et al. [198]. It had been additionally utilized for various applications to approximate monthly and seasonal ET [194].

SEBAL describes λE as the rest term of the instantaneous surface energy balance, λE. The general form could be expressed as:

$$\lambda E(x,y) = F_1\{r_0(x,y), K^{\downarrow}(x,y), \varepsilon'_2, \varepsilon_0(x,y), \times T_0(x,y), G_0(x,y), Z_{0m}(x,y), KB^{-1}, \times u_{\square}(x,y), L(x,y), \delta T_a(x,y)\}, \qquad 2.74$$

Where

r_0	The hemispherical surface reflectance,
$K^{\downarrow}$	The incoming solar radiation, (Wm^2)
ε'	The apparent thermal infrared emissivity of the atmosphere,
ε	The surface thermal infrared emissivity,

T_0	The radiometric surface temperature, (K)
G_0	The soil heat flux, (Wm^2)
Z_{0m}	The surface roughness length for momentum transport (m)
KB^{-1}	The relationship between Z_{0m} and the surface roughness length for heat transport,
u_*	The friction velocity, (ms^{-1})
L	The Monin–Obukhov length (m)
δT_a	The near-surface vertical air temperature difference. (K)

The (x,y) notation denotes that a particular parameter is variable in the horizontal space domain with a resolution of one pixel.

The NDVI is determined via bands RED and NIR of the optical images, and also the broadband albedo is determined using weighing factors of the visible, near infrared and short wave infrared bands [199]. Surface emissivity of the sensor is determined through the NDVI logarithmic relationship or acquired as ready product in case of MODIS data [200].

The ET is determined in SEBAL [201] with the instantaneous evaporative fraction Λ as well as daily averaged net radiation, Rn24.

$$ET_{24} = \Lambda \times [R_{n24} \times ((2.501 - 0.002361 \times T_s) \times 10^6)] \tag{2.75}$$

Where

ET_{24}: The daily actual (mm/day)

R_{n24}: Average daily net radiation (W/m^2)

T_s: Surface temperature (^oC)

The evaporative fraction Λ is normally computed from the instantaneous surface energy balance at time of satellite overpassing for each pixel as the follow:

$$\Lambda = \frac{\lambda E}{R_n - G_o} = \frac{\lambda E}{\lambda E + H_o} \qquad 2.76$$

Where λE = latent heat flux (the energy assigned for water evaporation). λ could be viewed in irrigated areas as being the ratio of actual evaporation to crop potential evaporation. It is reliant on the atmospheric and soil moisture conditions balance. G_o is the soil heat flux (conduction) W/m^2 and H_o is the sensible heat flux (convection) (W/m^2).

Hot and cold pixel of SEBAL

Two distinguished pixels within the image are significantly utilized by the model to fix the boundary conditions of the energy balance. Which are the hot and cold pixels, mostly located in the area of interest. The "cold" pixel is always selected as being a wet, well-irrigated crop surface possessing full surface cover via vegetation in which, surface temperature and near-surface air temperature are assumed to be near for the mentioned pixel. On the other hand, the hot pixel is always chosen as dry bare land in which the ET is assumed to be zero for this pixel. The selection of these pixels assist deeply in raising the ET computation quality, especially when these pixels are carefully selected [196].

2.18.2.3 Moisture-evapotranspiration relationship

Jacobs et al. [202] made use of Soil water parameterization method, which is widely used for the determination of the actual ET based on potential ET along with soil moisture. Moisture content is basically used in terms of reduction coefficient B incorporated with the potential evapotranspiration ET_o in order to determine the actual evapotranspiration ET_a [202].

$$ET_a = BET_o \qquad 2.77$$

The reduction coefficient B used for the relationship above was generated through regressing the ration of measured actual ET to the modeled Penman-Monteith ET to the MC. According to the aforementioned, the reduction coefficient is calculated from the relation below:

$$B = 2.77MC^{0427} \tag{2.89}$$

With accuracy of regression represented by R^2 equal to 0.93.

2.18.2.4 Models summary

Table 2.4 below, represents a selected set of ET assessment approaches according to Earth Observation approaches [203].

Table 2. 4: A fixed set of evapotranspiration evaluation approaches [203].

Concept	Method	Parameters	Advantages	Disadvantages	Ref.
Parameterization of the energy balance	SEBAL	$LST, T_a, V_a, RH, \varepsilon_0$ α_0, $NDVI$, surface roughness	Data requirements are minimal; Physical concept; no land use needed; multi-sensor approach.	Dry and wetland requirement to estimate H, hence heterogeneous surface needed; only applicable for flat terrain.	[107, 204] [205, 206]
	SEBS	$LST, T_a, V_a, LAI, \varepsilon_0$ $\alpha_0, e_{sat}, NDVI$ surface roughness	No a-priori knowledge of the actual turbulent heat fluxes needed.	Dry and wetland required to estimate H; combined with Penman Monteith equation.	[207] [208]
	RMI	LST, α_0 Meteorological data	Based on geostationary satellites with high temporal resolution.	Monin - Obukhov lengths require detailed meteorological data.	[209]
	S-SEBI iNOAA	$LST, \alpha_0, T_a, \varepsilon_0, RH$ $NDVI, \alpha_0$	Data requirements are minimal; No need for land use; no need to estimate H, multi-sensor.	Dry and wetland requirement to estimate evaporative fraction (dependent on ROI).	[210] [211]
Penman-Monteith based	Trapezoi-dal shp.	$LST, SAVI, T_a, \varepsilon_0$, LAI vapor P. deficit	Minimal meteorological data requirement, ET estimation at regional scales.	Requirement for biome map, surface roughness, vegetation height.	[212]
	Promet	α_0, LAI, resistance Values, soil type	Across scales, physiologically based (SVAT).	Requires a plant physiological model, land use, extensive meteorological dataset.	[213]
	Granger	$LST, \alpha_0, T_a, NDVI$ Sat. vapor pressure	Feedback relationship: LST is used to obtain the vapour pressure deficit in the overlying air.	Requires long term Ta and a conventional ET model including vapour transfer coeff.	[214]
	Wang	LST, α_0, VI, meteo.	Gradients of Ta and LST not required.	Day and night LST required.	[160]

	Cleugh	LST, α_0, VI Meteorological data	Linear relationship surface conductance and MODIS-LAI.	Extensive meteorological data and estimations of canopy cover required.	[215]
Water balance based	SWAP	LST, α_0, VI, data of: Meteorology, soil, ground water table	A mechanistic model simulating plant growth both temporal as spatially (GIS, EO).	Requires extensive datasets. Relationships between RS, vegetation data, soil profile and groundwater fluxes.	[216]
	Price	LST, VI, data of: Meteorology, soil, ground water table	Point method is extended spatially based on pixels of completely vegetated and bare soils.	Independent ET estimates required for a completely vegetated area and for a non-vegetated area; non-uniform area.	[193]
VI/LST based	Nagler	LST, EVI, T_a Calibration coeff.	Simple and minimal input requirements.	Need for site specific calibration, sensor type sensitive.	[217] [218]
	Jackson	$LST, VI, T_a, (T_a)$ Calibration coeff.	Simple relationship between VI and LST. Minimal input datasets.	Calibration parameter depends on surface roughness and wind speed.	[145]

CHAPTER 3

MATERIALS AND METHODS

This section entails general information about the study area in terms of geographical location, site characteristics and surface cover types. The chapter also covers description of the data collection, instruments and hardware and softwares that have been applied to achieve the results. Furthermore, it also highlights the methodology that has been used for moisture extraction, beginning with the ground observations preparation and arrangements as well as the spatial data management, which includes preprocessing of satellite images in terms of images correction, enhancement and calibration. In addition, the processing section includes the estimation of vegetation indices as well as the land surface temperature.

The chapter also encloses the strategies that have been used for MC and ET results realization in the form of charts. The validation contains two parts, he first one using a statistical validator, and the other validation is a spatial validation, which validates the extracted maps with the pixel based values.

3.1 Background

Malaysia is situated in Southeast of Asia, occupying an area of about 330,200 km^2. The entire country is split into two main regions, namely Peninsular Malaysia and East Malaysia. Peninsular Malaysia is just south of Thailand and north of Singapore; while East Malaysia is at the northern one-third of the island of Borneo adjoining Indonesia and Brunei as it is seen in Figure 3.1. Their positions as a tropical climate provides hot and humid weather throughout the year- with yearly monsoons at the southwest from April-October and at northeast from October-February and intense downpours are frequent.

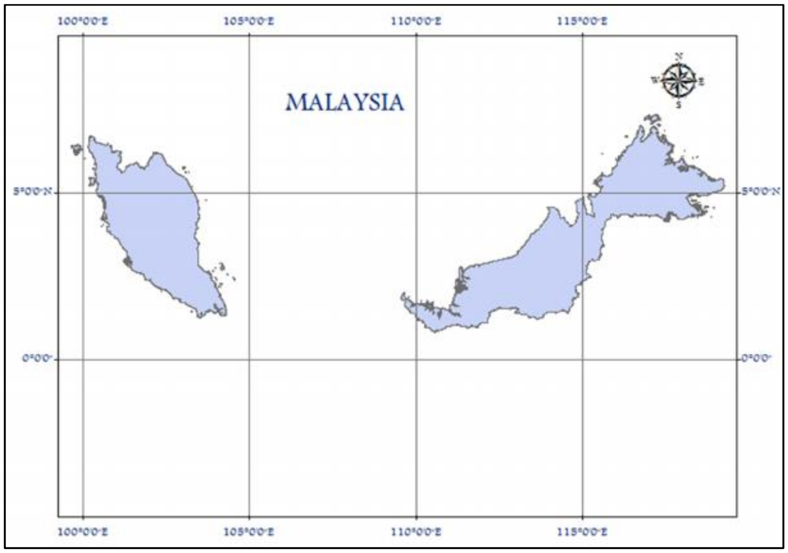

Figure 3. 1: Map of Malaysia

3.2 The study area

The description of the study area was handled from different anchors, with a focus on the climate description, topography and land use/cover of the area.

3.2.1 Geographical boundaries

The study area covers two distinctive districts of Perak state, which are Perak Tengah & Manjung. The two neighbor districts lay between latitude 4^{o}00` – 4$^{o}$30` N and longitude 100^{o}30` – 101$^{o}$00` E and separated by Sungai Perak (Perak River) which runs along the study area from the north to the south and runs surrounding Manjug district from the southern side to the coast downstream. Figure 3.2 shows a thematic map of the study area generated from classified LandSAT image [219].

Perak Tengah is bordered with the district of Kuala Kangsar in the north, the districts of Kinta and Batang Padang in the east and the district of Manjung in the west and Hilir Perak at the south. The Perak Tengah district encompasses an area of 1282.05 km^{2} comprising 11 localities. This district is located in the center of the state of Perak, in an elongated shape from north to south, with the Sungai Perak splitting it in half on the left and right.

Manjung district lays in the southwestern part of the state. It is well known for Pangkor Island. Manjung is surrounded by only two districts Kerian from the north and Perak tengah from the east while the coastline occupies the remaining directions. The total area is 1,074 km^2 [220].

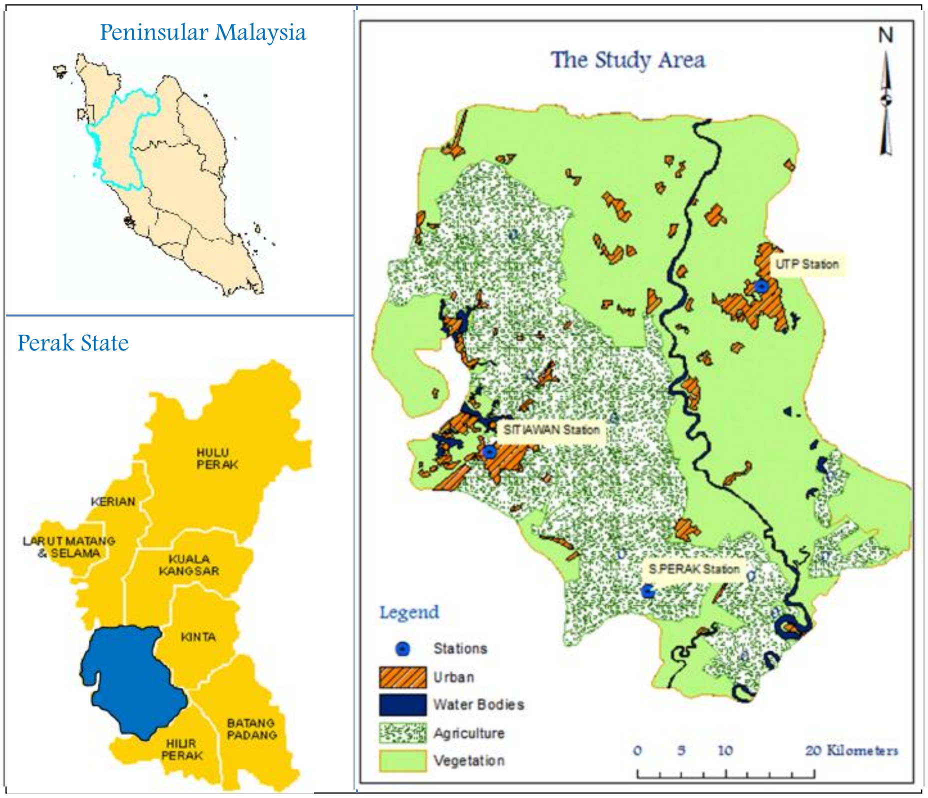

Figure 3. 2: The study area with classified map for surface cover representation [219].

3.2.1 Topography

The land is occupied mainly by four types of land use/cover type which are:

- The urban areas represented in some cities and rural areas scattered along the Ipoh-Lumut express way as well as along the fundamental water supply Sungai Perak. Some villages are within the agricultural land and the forest areas.

- Bare soils scattered beside the residential areas by some hilly areas.
- The vegetation cover takes the big portion of the area and is divided into two types of ordinal vegetation cover which includes the jungles, natural trees, grassland and some pasture lands while the second portion of the vegetation cover is agricultural fields of paddy, oil palm and coconut managed by two of the biggest agricultural companies in Malaysia which are Felcra and Sime Darby.
- Water bodies, which is represented mainly by Sungai Perak (Perak River) beside random distribution of some lakes over the area, which are abandoned in Tin mines.

3.2.2 The climate

Daytime at the study area is warm and sunny, although at night it is cool throughout the entire year with periodic rains in the evenings. Temperature is relatively constant, from 23 °C to 33 °C, with humidity typically greater than 82.3 percent. Annual rainfall measures at 3,218 mm [221].

The periodic wind flow patterns along the local topographic characteristics determine the rainfall distribution patterns across the country. Throughout the northeast monsoon season, the exposed place such as the east coast of Peninsular Malaysia, Western Sarawak and also the northeast coast of Sabah experience heavy rain spells. Conversely, inland parts or areas which can be sheltered by mountain ranges are comparatively free of its impact.

3.2.3 The soil

Several partitions of the soil types in the study area are integrated. The eastern part of the area and slightly to the central region are red-yellow Podzolic soils with Lithosols on acid to intermediate Igneous rocks as could be seen in Figure 3.3. Also scattered spots of red-yellow Podzolic soil shares with reddish-brown Lateritic soil on residual materials from acid as well as Gley soils on subrecent alluvium. Along the stream of Sungai Perak (Perak river), the soil layer is Alluvial and Gley on recent riverine alluvium. At the agricultural lands of Seberang Perak, Lekir and Hilir, the soil is Organic with Gley soil. At the coastal areas of Manjung, soils are Gley with alluvial on recent marine, riverine alluvium and subrecent alluvium beside, Organic soils with Gley at the beach [222].

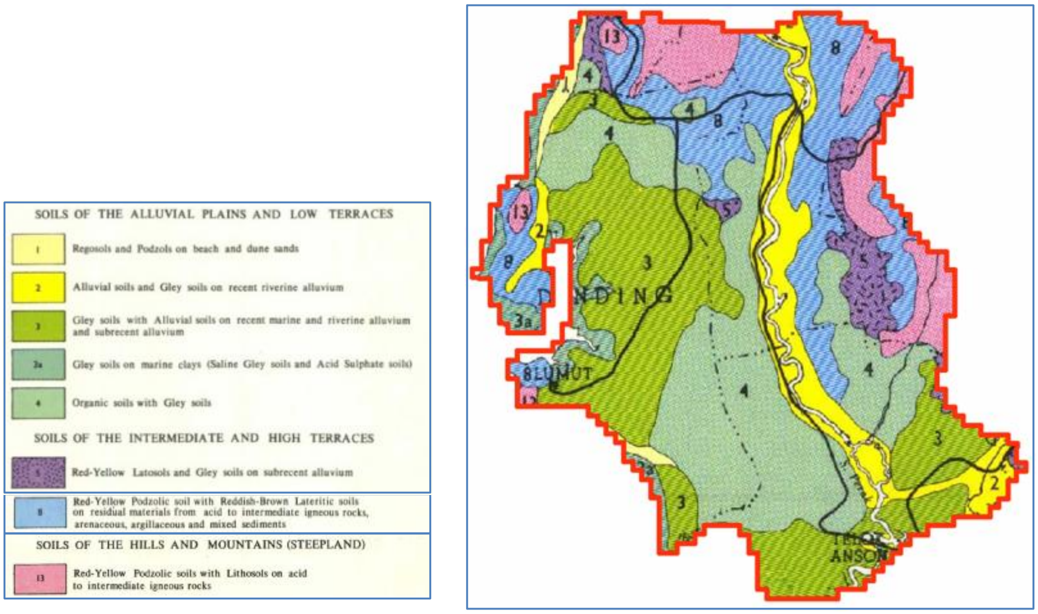

Figure 3. 3: The distribution of the soil and rock classes [222].

3.2.1 Land use/ cover (LULC)

Agriculture is one of the Perak's main industries, particularly rubber, coconut and palm oil. Tourism is a rising industry because of the state's abundant natural attractions. The main sectors of economy in Manjung District certainly are agriculture, services and manufacturing. Agriculture remains the main economic sector that offers the employment for the most of the populations. Manjung District is well known for its livestock, specifically chicken. Sea fishing and fish/prawn farming are the most crucial economic activities of some communities.

Felcra and Sime Darby agricultural companies have been developing new lands in the area, for oil palm cultivation, cocoa, rice (by Felcra) as a new crop with cultivation area reaches 4482 hectares.

3.3 Data collection

Two sets of data were used namely, terrestrial and spatial data. The terrestrial set represented in ground data collection and in-situ measurements, while the spatial dataset were acquired from the satellites.

3.3.1 Sources of spatial and meteorological data

Most of the spatial and the meteorological data used were requested from governmental authorities, such as:

3.3.1.1 Malaysian Agency for Remote Sensing (ARSM)

ARSM is a department under the Ministry of Science, Technology and Innovation (MOSTI). It was established as a center of remote sensing and associated technologies in August 1988 and was completely functional in January 1990. It has played the necessary part as being the national agency to guide the country in remote sensing technologies applications development, underlying its pursuit to offer complete solution in remote sensing and associated technologies for maintainable development, disaster control and strategic planning of the nation. Presently, ARSM operates with system for satellite data image processing, geographical information system (GIS) and global positioning system GPS, Satellite Ground Receiving Station for real time data acquisition, Remote Sensing Digital Laboratory, Remote Sensing Data Preserving and Assortment Centre [223]. During the research, NOAA/AVHRR, LANDSAT ETM+ and SPOT 5 satellite images over the study area were acquired from ARSM and used according to their time concurrency to the in-situ measurement of the required parameters. Table 3.1 shows the quantity and characteristics of the satellite images provided by ARSM for the study.

3.3.1.2 Malaysian Meteorological Department (MMD)

The Malaysian Meteorological Department devotes efforts to supply good quality meteorological and geophysical services to fulfill the socio-economic and security requirements of the Malaysian nation. This department even offers seismological and tsunami alert solutions, cloud seeding activities, marine meteorology and oceanography services, climatological services, agro-meteorological services and environmental meteorological services. (http://www.mosti.gov.my/index.php).

From MMD, daily air temperature data (through June-August 2009), mean daily wind speed and mean daily relative humidity over Sitiawan station (covers Seberang Perak also), were collected for periods of February 2011 – April 2011 and June 2012 – August 2012. These data were used for ET calculation and other applications concerning the temperature correction.

Table 3. 1: An image data provided by ARSM.

Sensor	Qty	Period of acquisition	Processing level	Type
NOAA/ AVHRR 17,18	90	1st June – 30th August 2009	(Level 1B)	Daily
	60	2nd Feb– 30th Apr 2011		
	60	1st June – 30th August 2012		
Landsat ETM+	2	20th September 2001 19th June 2002	*System corrected	16 days

*System corrected: Image is geometrically corrected using Satellite Orbital Parameters.

3.3.1.3 UTP Weather station

A small computerized weather station is placed at Universiti Teknologi PETRONAS (UTP) campus, which is an automated form of the regular weather station. The station typically contains a weather-proof enclosure which contains the data logger, rechargeable battery, telemetry (optional) as well as the meteorological sensors through an attached cell or wind generator and mounted on a mast.

Mainly, the station has a temperature gauge for measuring temperature, anemometer for measuring wind speed, wind vane to measure wind direction, hygrometer for measuring humidity, barometer for measuring atmospheric pressure, Rain gauge for measuring liquid-equivalent precipitation, pyranometer for measuring solar radiation. Some instruments for measuring soil temperature and Soil moisture at depth of 0.3 m also provided. The required weather parameters were collected for the entire period of ET estimation.

3.3.2 Data extraction

Three basic optical satellites were used, some used to provide daily images over the area and others for semi-monthly ones.

3.3.2.1 Spatial data source

MODIS is indeed a valuable plan for spatial data spreading using sensors on two platforms and each of them provides complete daily coverage of the world. The MODIS site, (http://modis.gsfc.nasa.gov/index.php), is a great starting point for researching this vital program. This website has links towards the category of MODIS that is, Atmospheres, Land and Oceans. Since the MODIS sensor is propelled on the Terra and Aqua satellites, it is commonly easy to obtain images each morning (Terra) and also the mid-day (Aqua) for almost any particular location.

MODIS (Terra & Aqua) images (from June – September 2012) were acquired for MC algorithms generation and the estimation of ET as well. Table 3.2 shows the types and quantities of MODIS image acquired from the source. All images were captured in concurrent times of field measurements conduction.

Table 3. 2: Web-based MODIS images downloaded for the study area.

Sensor	Quantity	Period of acquisition	Processing level	Type
MODIS Terra/Aqua	22	1st June – 30th August 2012	(Level 1B)	Daily
	14	1st February – 30th April 2011		

3.3.2.2 Soil map

The European Digital Archive of Soil Maps (EuDASM) has begun through the MOSES (Monitoring the State of European Soil) activity team members of the Soil and Waste Unit (SWU) from the Institute of Environment and Sustainability (IES).The EuDASM seeks in setting up a common foundation to conserve the soil maps and also the data root inside them by adapting the modern scientific tools making it available to the worldwide research communities [224]. The aim of the EuDASM effort is to acquire, manage and spread the soil data existing in the soil maps such as soil map data as well as their following proper meta-data, to the global research communities. The global soil maps are provided through the link (http://eusoils.jrc.ec.europa.eu/library/maps/maps.html).

3.3.2.3 In-situ measurements

Three locations were selected throughout the study area based on their variety in environmental and surface cover, which were:

- Sitiawan city (the biggest city in the study area laid at the south-western side), representing the urban areas.
- UTP station was established at the eastern part of the study area, selected to represent the multi-surface cover areas. As UTP is located geographically in a suburb area surrounded by multiple classes of surface cover.
- The third surface cover type selected was an agricultural scheme in Seberang Perak location, which was selected to represent the uniform vegetation cover. The measured variables were Air temperature, surface temperature and surface MC.

Air temperature values were measured at those locations at 2 m height from the ground level (according to the meteorological standards of Ta measurements for ET determination) during the satellites overpassing time (NOAA 17 and MODIS Terra mostly pass at morning between 10:00 am – 11:30 am, while NOAA 18 and MODIS

Aqua pass at afternoons around 2:00 pm – 3:00 pm in local time) in order to be used for ETo assessment.

Surface temperature and surface MC were also measured along the different locations in the form of point measurement using mini thermometers and soil moisture probes. These will be explained in subsequent sections. Measurements were achieved at three variable depths in the soil as an attempt to satisfy the researches gap represented in MC observation depth variability. 5 cm was assumed to represent the surface temperature and MC. 10 cm represented the near surface whereas 15 cm was achieved at the agricultural field only in an attempt to examine the moisture value at plant roots. Figure 3.4 shows the three parts of the study are where the field measurements were taken.

Figure 3. 4: The three locations where measurements were conducted

The objectives of measuring surface temperature Ts and surface MC can be summarized in the following:

To produce corrected satellite Ts through applying in-situ measurements of Ts at the same time as the satellites overpass over the study area. This kind of application is made to simulate the absolute atmospheric correction in which, the path radiance is corrected using calibration target where, regression is used to predict correct value on image [225]. Moreover, the application is also meant to correlate the measured Ts within three different depths on the soil to examine the efficiency of the split window technique in the retrieval of Ts, thus, more accurate Ts value is used for moisture and ETo extraction. The Ts correlation is also used to compensate the Ta in case of a missed value when applying variable for ET estimation.

The aim of moisture measurements conducted at field is to generate an accurate surface moisture content MC through the universal triangle technique in two different depths, 5 cm to represent the surface MC and 10 cm to represent the sub-surface MC. Therefore, to estimate the moisture coefficients in the universal triangle method, in-situ measurements of moisture must be achieved at same time of the spatial variable (NDVI and Ts) acquisition.

3.3.3 Laboratory works

3.3.3.1 Oven method for soil moisture determination:

This test is conducted to calculate the water content of the study area's different soils by drying out samples to constant mass at a specific temperature. The MC of the given soil is then defined as the percentage, indicated as a percent, of the mass of the pore water to the mass of the soil. Three major parts are availed for the test:

Weighing device: A scale or balance responsive to 0.1 % of the mass of the tested sample, with a capacity comparable to, or higher than, the wet mass of the sample under test. In this study, a balance model AND GF-6000 (with accuracy of 0.1 g and maximum weight 6100 g) was used for measuring soil sample before and after drying.

Drying device: An oven or any other appropriate thermostatically governed heating device efficient at sustaining a temperature of 110 ± 5°C and above. Mostly, the samples used were left one day inside the oven for complete dryness. The oven used was a large drying oven ELE International (with heating range 20^{o}C to 250^{o}C).

Trays: Any container or any other carrier, that will not be damaged by the drying temperature, and is also ideal for maintaining the tested sample without loss when allowing water to evaporate. Most of the test samples were poured in containers with a 100 g volume. Figure 3.5 shows the laboratory facilities that were used for MC determination through the oven method. The differences in soils color at the containers represent the variation in soil types along the three measurement depths 5cm, 10cm and 15cm.

Figure 3. 5: Oven method tools provided for the study

3.3.3.2 Particle Size Distribution (PSD) test

The particle size of the tested soil samples was measured using a laser based particle size analyzer, namely Mastersizer 2000 of Malvern Instruments Ltd. It utilizes Fraunhofer diffraction of light formed by particles with a diameter larger than the incident laser beam wavelength. A combination of an optical filter, lens and photo detector coupled with a computer loaded with Mastersizer software enables one to compute the particle size distribution from the diffraction data and store it as volume percentage against the particle size. Particle size distribution profile for one of the soil samples is presented in Figure 3. 6.

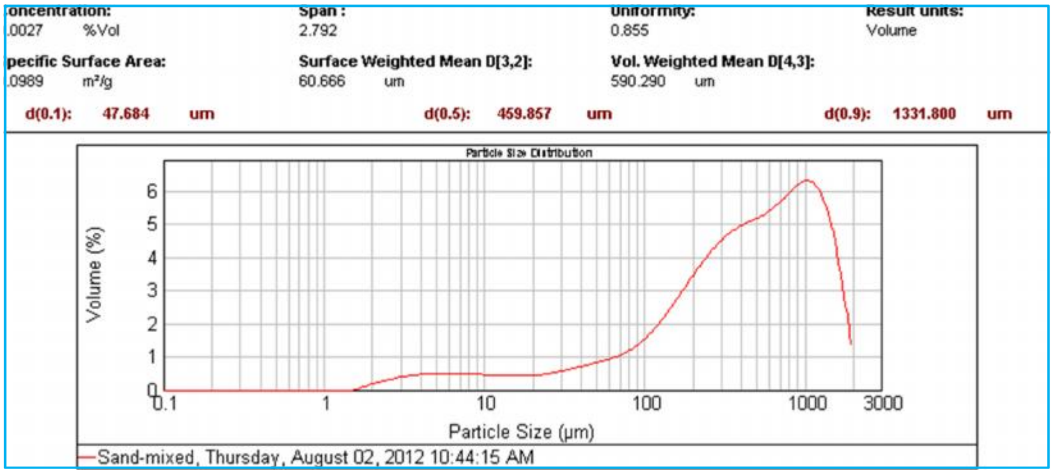

oncentration: .0027 %Vol

Span : 2.792

Uniformity: 0.855

Result units: Volume

pecific Surface Area: .0989 m²/g

Surface Weighted Mean D[3,2]: 60.666 um

Vol. Weighted Mean D[4,3]: 590.290 um

d(0.1): 47.684 um

d(0.5): 459.857 um

d(0.9): 1331.800 um

Figure 3. 6: Particle size distribution profile for soil's sample

3.4 Instrumentations

The validation of the study algorithms was based mainly on the data that used to be collected in-situ using sophisticated hand-held instruments, which are mentioned in the next paragraphs.

3.4.1 On-field Instruments

Beside the moisture determination using the oven method at UTP location, measurements of MC were done also using a PMS 714 soil moisture meter (Heavy duty probe, probe length: 20 cm) at Sitiawan and Seberang Perak locations. The meter is a hand-held sensitive moisture probe used for immediate result in moisture. Its usefulness is based on employing neutron dispersing. The process is non-destructive, and is particularly responsive to MC within the whole target substance, not only on the surface.

Two types of mini thermometers (with probe length 20 cm and sensitivity 0.5 ^{o}C) were used for soil surface temperature as well as the air temperature at height 2 m, recording immediate temperature readings during satellite overpass time. Figure 3.7 shows the types of surface moisture and temperature devices used throughout the investigation. The probe length in all devices was staged into three depths 5cm, 10cm and 15 cm for accurate insertion.

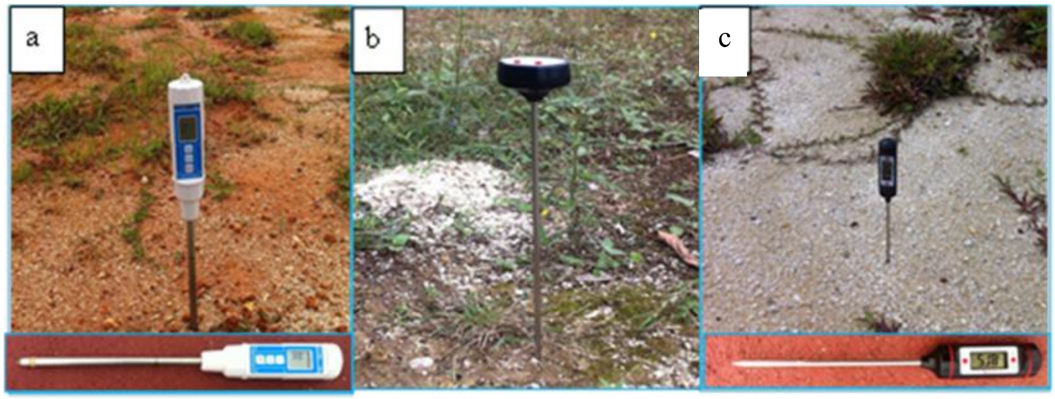

Figure 3. 7: In-situ measurement devices for (a) MC and (b and c) surface and air Ts.

3.4.1 Satellites

High temporal resolution satellites were employed intentionally to produce sufficient correlation's points with the in-situ measured parameters.

3.4.1.1 AVHRR

The Advanced Very High Resolution Radiometer is a space-borne sensor set out on the National Oceanic and Atmospheric Administration (NOAA/AVHRR) group of polar orbiting systems. AVHRR instruments determine the reflectance of the planet in 5 relatively broad (one day standard) spectral bands. The first two are concentrated about the red (0.6 µm, 500 THz) and near-infrared (0.9 µm, 300 THz) parts, the third one is situated around 3.5 µm and the last two deal with the thermal emission released by the earth, about 11 and 12 µm respectively [226].

The goal of the instrument is basically to observe and determine the thermal emission (cooling) of the planet. These sensors have demonstrated to be beneficial with regard to a number of some other applications. AVHRR data are specifically applicable to study climate change and environmental deterioration simply because of relatively long history of data (20 years). Table 3.3 below shows the series of the AVHRR satellites since the first launch (source: http://www.jpss.noaa.gove).

Table 3.3: Series of AVHRR Satellites.

Satellite name	Launch date	Service start	Service end
TIROS-N	13 Oct 1978	19 Oct 1978	30 Jan 1980
NOAA-6	27 Jun 1979	27 Jun 1979	16 Nov 1986
NOAA-7	23 Jun 1981	24 Aug 1981	7 Jun 1986
NOAA-8	12 Mar 1983	3 May 1983	31 Oct 1985
NOAA-9	12 Dec 1984	25 Feb 1984	11 May 1994
NOAA-10	17 Sep 1986	17 Nov 1986	17 Sep 1991
NOAA-11	24 Sep 1988	8 Nov 1988	13 Sep 1994
NOAA-12	13 May 1991	14 May 1991	15 Dec 1994
NOAA-14	30 Dec 1994	30 Dec 1994	23 may 2007
NOAA-15	13 May 1998	13 May 1998	present
NOAA-16	21 Sep 2000	21 Sep 2000	present
NOAA-17	24 Jun 2002	24 Jun 2002	present
NOAA-18	20 May 2005	30 Aug 2005	present
NOAA-19	6 Feb 2009	2 Jun 2009	present
MetOP-A	19 Oct 2006	20 Jun 2007	Present

3.4.1.2 MODIS

The Moderate-resolution Imaging Spectroradiometer MODIS is a scientific instrument released into Earth orbit by NASA in 1999 on board Terra (EOS AM) Satellite, as well as in 2002 on board the Aqua (EOS PM) satellite. The devices catch data within 36 spectral bands which range in wavelength from 0.4 µm to 14.4 µm and at various spatial resolutions (2 bands at 250 m, 5 bands at 500 m and 29 bands at 1 km). Collectively, the instruments picture the whole planet each from 1 to 2 days. They are developed to supply measurements in large-scale global dynamics such as alterations in Earth's cloud cover, radiation budget and processes occurring in the oceans, on land and in the lower atmosphere. MODIS scientific information is availed to the public through various World Wide Web sites and FTP records ("Direct Broadcast at MODIS Website" http://modis.gsfc.nasa.gov/data/directbrod/).

3.4.1.3 LANDSAT TM/ETM+

Landsat 7, which was launched in 1999, is actually the seventh satellite of the Landsat program. Its main purpose is to recharge the worldwide database of satellite photos, offering up-to-date and cloud-free images. The Landsat program is managed and worked by the USGS, and data from Landsat 7 is gathered and distributed by the USGS.

The principal instrument on board Landsat is the Enhanced Thematic Mapper Plus (ETM+). It has a spectral resolution of 8 bands and spatial resolution of 30 m whereas one panchromatic band’s spatial resolution is 15 m beside thermal bands with resolution of 60 m (http://en.wikipedia.org/w/index.php?title=Landsat_7&oldid=539728566).

3.5 Softwares

Softwares were used for images’ pre-processing and processing based on their pixel’s spectral signatures. Softwares were also used as data display mechanisms.

3.5.1 ENVI

ENVI is a software used for the creation, analysis, and display of all sorts of digital imagery. ENVI's full image-processing package incorporates innovative, yet easy-to-use, spectral tools, geometrical correction, terrain analysis, radar analysis, raster and vector GIS features, intensive support for images from a wide range of sources, and even more. ENVI handles frequent image processing problem areas like input of non-standard data types, viewing and analysis of large images, as well as simple extensions of analysis abilities (add-on functions). The program includes important tools necessary for image processing throughout multiple disciplines, and it has the flexibility to permit execution of customized analysis techniques.

ENVI softwares were specifically used in this study for pre-processing the acquired NOAA and MODIS images, which were acquired in the form of level 1B processed data, that needs geometric, radiometric and atmospheric correction.

3.5.2 ArcGIS software

ArcGIS is a geographic information system (GIS) for dealing with maps and geographical data. It is usually employed for: generating and utilizing maps; putting together geographical data; studying mapped information; expressing and obtaining geographical information; using maps and geographic data within a range of applications; and handling geographic information within a database. The system offers an infrastructure for producing maps and geographic information accessible throughout an organization, across a community, and online availability.

ArcGIS 10 software was used in this study for relative processing of the images using the spatial analysis tools in order to manipulate the raster images for moisture and ET extraction via the spatial analyst features (Raster calculator, Equations, etc.). Figure 3.8 shows the integration between the two software's environments, remote sensing and GIS through which, the studied images were processed and analyzed to produce the moisture and ET_o maps beside performing the spatial, statistical analysis as well as the validation. Moreover, ArcGIS was used to achieve the spatial statistics of the determined MC and ET maps as well as the final maps and layouts produced in ArcGIS environment.

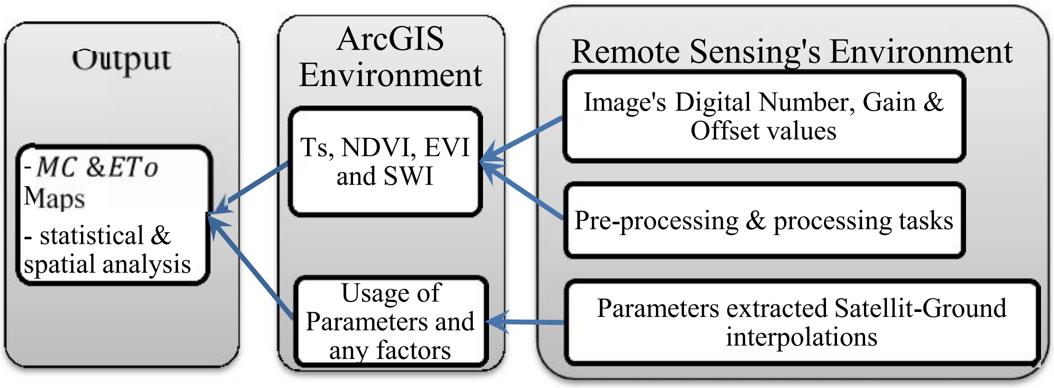

Figure 3. 8: Chart explains the process integration of the used softwares

3.5.3 SPSS

SPSS Statistics is a software program employed for statistical investigation. Which is considered as the most commonly used applications for statistical analysis in social science. It is used by market experts, health investigators, survey companies, government, education researchers, marketing companies as well as others. Along with statistical analysis, information management (case selection, file re-shaping, producing derived data) and data records (a metadata dictionary is saved in the data file) are features of the base software [227].

Along the study, the IBM SPSS software was used to statistically validate the resultant MC and ET values which are mostly correlated against the real measured parameters, from which, the standard statistics, correlation relationships and a nova test were examined.

3.5.4 Moisture Parameters generation

To extract the MC parameters from the 2nd order polynomial equation of UT, at least 9 satellite images must be used to solve the mathematics problems effectively. A complete study of such systems of equations (with 9 unknowns) belongs to the subject of linear algebra.

The implications for solving mathematics problems are that, if there is a problem involving *n* unknowns, then if there is a possibility to extract from the problem enough information to write *n* independent linear equations for the *n* unknowns, then it will be possible to obtain a unique solution to the problem. If there is not enough information available to write *n* independent linear equation for the *n* unknowns, then it will not be possible to obtain a unique solution to the problem [228].

In this study, Mathcad 14.0 M030 version was used so as to determine values of the moisture parameters in the Universal Triangle (Equation 2.27). The polynomial equation of the Universal Triangle has 9 (a_1 - a_9) parameters, so that, Ts and NDVI from 9 satellite images used to be extracted and solved with 9 surface moisture observations at same time, then the equations applied imposed into a matrix form for the parameters to be extracted using the mentioned software in the following formula:

$$A := \begin{bmatrix} a_{11} & \cdots & a_{19} \\ \vdots & \ddots & \vdots \\ a_{9} & \cdots & a_{99} \end{bmatrix} \quad B := \begin{bmatrix} b_{11} \\ \vdots \\ b_{91} \end{bmatrix} \qquad 3.1$$

$$A \times X := B, \qquad X := lsolve\,(A,B); \text{ So:}$$

$$X := (X_{11} \quad .. \quad X_{19})$$

3.6 Spatial data Processing

Spatial data processing is a series of integrated algorithms, applied to the acquired image to georeference the image coordinates, enhance the visual interpretation, calibrate the data and resize the volume of data through the subsetting applications, beside many other effective applications.

3.6.1 Images Pre-processing

3.6.1.1 Calibration and Georeferencing

Calibration utilities provided by ENVI software used to apply calibration elements to AVHRR Advanced Very High Resolution Radiometer (NOAA), TM Thematic Mapper; a Landsat sensor. Variety of atmospheric correction methods are accustomed to correct sensor radiance for atmospheric effects by mathematically modeling the physical tendencies of the radiation as it passes through the atmosphere.

AVHRR Calibration

The AVHRR calibration utility, which is a task equipped with ENVI 4.8, was used in this study to calibrate AVHRR data (Level 1B) from the NOAA-17, and -18 satellites. Normally, bands 1 and 2 are calibrated to percent reflectance and bands 4, and 5 are calibrated to brightness temperature, in degrees Kelvin through internal iterations include: Displaying AVHRR Header Information, Saving Header Info to ASCII Files, Calibrating AVHRR Data, Building AVHRR Geometry Files (through using the task AVHRR Build Geometry File) and then Georeferencing AVHRR Data.

Selection of desired output map projection is an important issue. Consideration must be given to which map projection is suitable for the location and extent of the image. Some projections tend to be more suitable for AVHRR scale images than others. Is always recommended that not to use UTM and State Plane projections for images that cover areas greater than UTM or State Plane zones. If either of such projections is chosen, then the resulting registration will likely be geographically corrected although the map coordinates in areas furthest from the origin are going to be well beyond normal maximum values for these projections. With images projected to Geographic Lat/Long, pixels possess constant degree units however, not essentially length units, since the size of a longitude degree deviates with latitude. This leads to severe distortion across most AVHRR-scale images.

Map projections which are suitable for AVHRR-scale images include stereographic, transverse Mercator, or conic projections. Stereographic projections are generally useful for images with equal N-S and E-W extent. Transverse Mercator projections are frequently useful for images with greater N-S extent. Conic projections are frequently useful for images with greater E-W extent.

Landsat Calibration

Landsat Calibration task in ENVI pre-processing tools (data specific utilities), is used to convert Landsat MSS, TM, and ETM+ “Enhanced Thematic Mapper”; a Landsat-7 sensor digital numbers to spectral radiance, a measure of the amount of electromagnetic radiation leaving a spot on the surface. More specifically, it is the pace in which light energy is emitted in a certain direction per unit of projected surface area. The standard unit is W/m^2. Most remote sensing devices directly measure radiance. or exoatmospheric reflectance (reflectance above the atmosphere) using published post-launch gain In ENVI, a value that is multiplied by the pixel value to scale it into physically meaningful units of radiance: Radiance = DN * gain + offset and offset in the context of remote sensing: A static correction value is added to or subtracted from every pixel in an image, typically through the use of image arithmetic (Band Math in ENVI). A variable is added to the gain in a regression equation for sensor calibration [229].

The spectral radiance ($L\lambda$) was determined using specific equations. ENVI determines the calibration parameters from the metadata and populates the dialog accordingly. Most Landsat GeoTIFF data now comes with metadata, if the steps: File > Open External File > Landsat > GeoTIFF with Metadata are followed to open data, ENVI will automatically determine the calibration parameters.

MODIS Data

The acquisition of ready-product of MODIS included different satellite’s packages mentioned as: MODIS-based daily composites of land surface temperature (Ts; Bands 31 and 32; MOD11A1 and MYD11A1products at 1-km resolution) as well as surface reflectance with the red (R), near infrared (NIR), and blue (B) bands (SR; MOD09 and MYD09 products at 500-m resolution). All acquired from the Level 1 and Atmosphere Archive and Distribution System website (LAADS; http://ladsweb.nascom.nasa.gov).

3.6.1.2 Enhancement

Image enhancement as a pre-processing task, is fundamentally required because it is very common to have image values concentrated in a fairly narrow range. So, the enhancement tends to improve the contrast between features in an image and also to improve the visual separability of surface features. This involves manipulating the range of input digital values to create a new range of output values.

Histogram Stretch (linear), is one of the direct ways that was used in the study to enhance the satellite images, so that the effective upper and lower cutoff values could be established. Upper and lower histogram values were set to maximum & minimum limits respectively and balance of the data were expanded linearly to fill up the extended display range as in Figure 3.9.

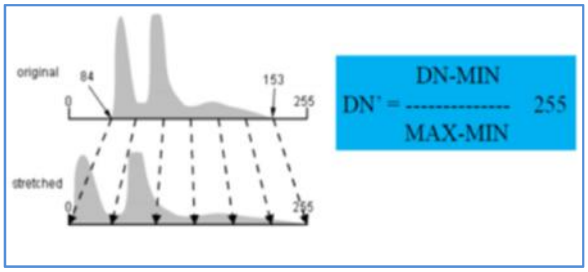

Figure 3. 9: Linear stretch enhancement [225].

3.6.1.1 Clouds and atmospheric correction

The nature of remote sensing mandates that solar radiation passes through the atmosphere prior to being collected by the device.

Due to this, remotely sensed images contain details about the atmosphere and also the earth’s surface. For consideration of quantitative analysis of surface reflectance, the percentage of radiant energy reflected by a body to the energy incident on it, generally denoted as being a percentage, eliminating the impact of the atmosphere is a significant pre-processing step. To compensate for atmospheric consequences, properties like the quantity of water vapor, distribution of aerosols, and scene visibility has to be recognized. Since direct measurements of such atmospheric properties are hardly ever available, there are methods that infer them from their imprint on hyperspectral / radiance data. These properties are used to restrict highly precise models of atmospheric radiation transfer to generate an estimate of the true surface reflectance. Furthermore, atmospheric corrections of this type can be applied on a pixel-by-pixel basis since each pixel in a hyperspectral image that includes an independent measurement of atmospheric water vapor assimilation bands [230, 231].

The model used for atmospherically correcting AVHRR and Landsat images within the study, was The Fast Line-of-sight Atmosphere Analysis of Spectral Hypercubes (FLAASH), which is a physics-based method to atmospheric correction that employs numerous metadata about time, location, and plenty of other parameters to develop a radiative transfer model using MODTRAN4. FLAASH is capable of producing highly precise surface reflectance results although requires large user inputs.

FLAASH can handle hyperspectral sensors (HyMAP, AVIRIS, HYDICE, HYPERION, Probe-1, CASI, and AISA) and multispectral sensors (ASTER, AVHRR, GeoEye, IRS, Landsat, QuickBird, RapidEye, SPOT and WorldView-2). Water vapor and aerosol retrieval are only feasible once the image contains bands in proper wavelength positions.

Cloud contamination is a frequent problem when dealing with satellite images of Malaysian areas [232]. Although the study area was small with respect to the MODIS, AVHRR and even Landsat scenes, some images were fully or partially covered by clouds. Clouds and their shadow prevent extraction of the spatial information either within the optical portion or the thermal one. In this particular study, the issue was to exclude the cloud contaminated area from Landsat images, or to exclude the entire image for AVHRR and MODIS images. These were achieved either through a subjective removal of the scene (which resulted in data volume reduction shown in Table 3.4) or through building a mask layer for extracting the clouds along with shadows via ENVI masking tools.

3.6.1.2 Bands selection and image Subset

Among the five bands of AVHRR, the optical bands 1 (0.58 - 0.68 µm) and 2 (0.72- 1.00 µm) which are within the red and the infrared regions respectively, were used for NDVI and surface emissivity generation. The two thermal bands 4 (10.3-11.3 µm) and 5 (11.5-12.5 µm) were used for Ts estimation.

Both MODIS Aqua and Terra have the same band dimensions and characteristics so that, band 1 (0.62-0.67 µm) within the red portion, band 2(0.84-0.876 µm) within the infrared portion were used for NDVI generation. Band 3 (0.459-0.479 µm) within the blue range was also added to the both mentioned bands to generate the EVI. On the other hand, Bands 31(10.78-11.28 µm) and band 32 (11.77-12.27 µm) within the thermal range, were used to estimate Ts. Band 3 (0.63-0.69 µm) within the red portion and band 4 (0.75-0.9 µm) within the infrared portion, were used for NDVI and emissivity generation for Landsat 7, while the second thermal band 6-II (11.5-12.5 µm) was used for the brightness temperature estimation.

Table 3. 4: The effective (cloud free) images used in the study.

Sensor	Total number	Period of acquisition	No. of Cloud-free images
NOAA/AVHRR 17,18	90	1st June – 30th August 2009	38
	60	2nd February – 30th April 2011	18
	60	1st June – 30th August 2012	19
Landsat ETM+	2	20th September 2001 19th June 2002	2
MODIS Terra/Aqua	22	1st June – 30th August 2012	36
	14		

Among the images pre-processing tasks, spatial subsetting is mentioned, which is a function that is usually used to limit the image for further processes. It is possible to select spatial subsets using many methods.

Two types of subsets were applied at the study's images according to the ground measurements facilities provided at the area, which are:

- The study area subset: This task was achieved by using Perak Tengah and Manjung area's boundaries (administrative), and then masking the study area from the satellite images according to those boundaries.
- The three locations subset: Subset areas of 10 pixels by 10 pixels (10 km x 10 km) were delineated surrounding each weather station. Any spatial computation performed within each subset area was assumed to represent the average value of the sub area pixels in order to simulate and integrate the spatial findings with the point measurements of MC and surface temperature measured in situ. This kind of process follows up the image's size reduction concept [225], in which, the block averaging process is used.

Block averaging is the process of reducing image size by averaging a square matrix of adjacent pixels as in Figure 3.10. There are no dropped or missing pixels, as is the case with decimated imagery. The net effect is that details are obscured, but the overall appearance of the image is improved.

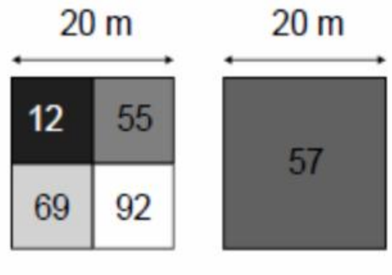

Figure 3. 10: Example of block averaging for point measurements simulation [225].

3.6.1 Images processing

This represents the higher order of the spectral manipulation so that numerical formulas and relationships could be produced from the images when processed.

3.6.1.1 NDVI

Vegetation indices could be classified as an image enhancement process, which are used for boosting the spectral contrast between the red and NIR parts of the electromagnetic spectrum. It can also be used to determine the vigor and biomass on the healthy and non-healthy vegetation. A large number of vegetation indices are being used in many aspects of the environmental and meteorological applications, especially those with regard to the land surface issues. Figure 3.11 represents the three different images of NDVI generated from three different satellites over the study area, in an attempt to show the potentials of the satellites in detecting the vegetation distribution and intensity. In which, Equation 2.6 was used within ENVI environment to produce the NDVI from the optical/infrared.

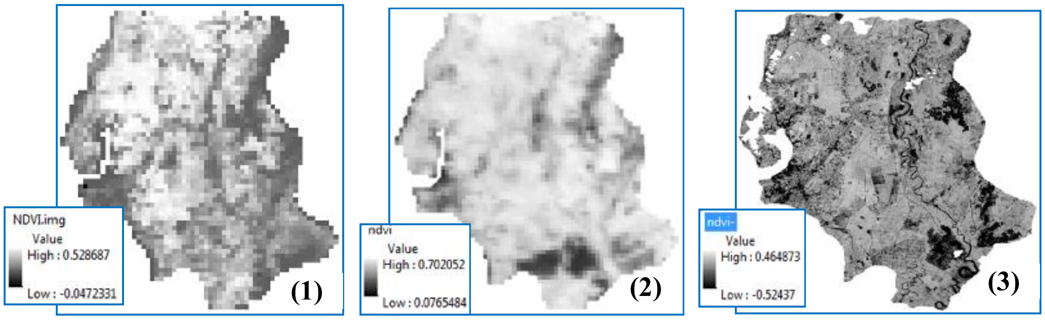

Figure 3. 11: NDVI from (1) AVHRR, (2) MODIS and (3) Landsat 7

High values of NDVI (0.70 and above) denote a surface that is fully covered by vegetation. The low NDVI on the other hand, denotes bare soil or urban areas while the negative values denote clouds or water bodies.

3.6.1.2 MODIS EVI

EVI was developed to optimize the vegetation signal with improved sensitivity in high biomass regions and improved vegetation monitoring through a de-coupling of the canopy background signal and a reduction in atmosphere influences.

3.6.1.3 LST from split window (NOAA)

The AVHRR channels 4 and 5 (10.3-11.3 µm and 11.5-12.5 µm) were used for deriving surface temperature with regard to daytime passes. Beside the brightness temperature from channels 4 and 5, the temperatures produced are dependent on the surface emissivity and the coefficients determined by the influence of the atmospheric conditions beside other related parameters on the thermal spectral radiance and its transmissivity in channels 4 and 5.

To generate the Ts map, the raster calculator from ArcGIS was used to process all the parameters at level of image pixels. Figure 3.12 shows the steps and procedures that were followed to produce the Ts map within the ArcGIS environment, beside the surface temperature rectification using the field observations.

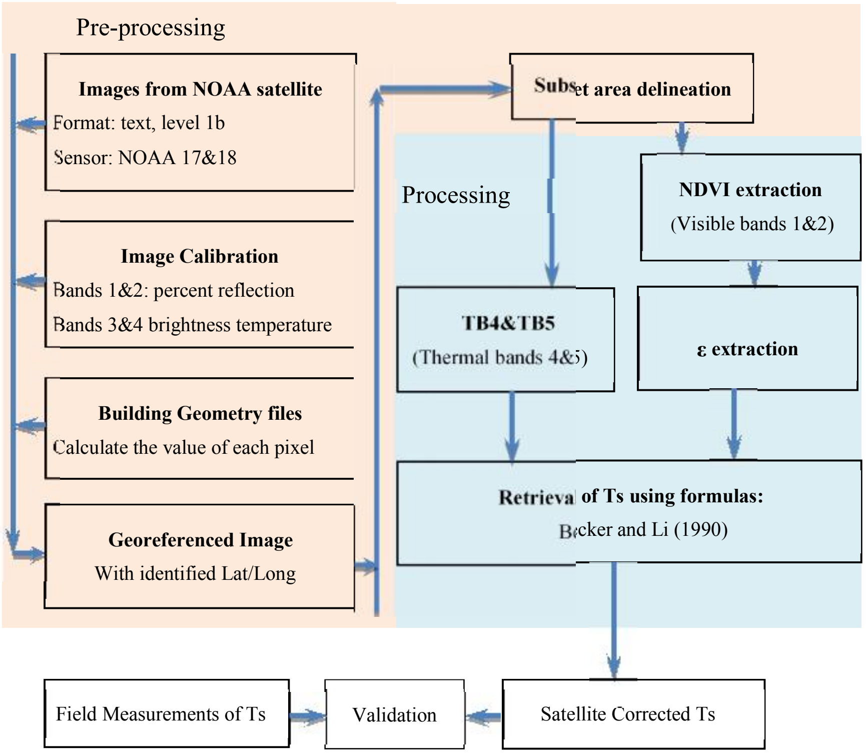

Figure 3.12: Steps of Ts extraction and rectification by in-situ measurements of Ts.

The common formula of the split-window algorithm can be written as the following:

$$Ts = T_4 + A(T_4 - T_5) + B \qquad 3.2$$

Where:

Ts is the land surface temperature, T4 and T5 are the brightness temperature for channel 4 and 5 respectively, A and B represent the coefficients determined by the influence of the atmospheric conditions beside other related parameters on the thermal spectral radiance and its transmissivity in channels 4 and 5.

The parameters A0, P and M proposed by Becker [233] could be used in a simplified way with the two coefficients A and B:

$$A = (M - P)/2 \qquad 3.3$$

$$B = A_0 + T_4(P - 1) \qquad 3.4$$

Where the parameters A0, P and M are being determined by Becker [233] as:

$$A_0 = 1.274$$

$$P = 1 + 0.15616\frac{(1-\varepsilon)}{\varepsilon} - 0.482\frac{\Delta\varepsilon}{\varepsilon} \qquad 3.5$$

$$M = 6.26 + 3.98\frac{(1-\varepsilon)}{\varepsilon} + 38.33\frac{\Delta\varepsilon}{\varepsilon} \qquad 3.6$$

Using Sobrino [149] formula:

$$T_S = T_4 + 1.06(T_4 - T_5) + 0.46(T_4 - T_5)^2 + 53(1 - \varepsilon_4) - 53\Delta\varepsilon \qquad 3.7$$

Ts Estimation by Uliveri [234]:

$$T_S = T_4 + 1.8(T_4 - T_5) + 48(1 - \varepsilon_4) - 75\Delta\varepsilon \qquad 3.8$$

The resultant corrected-Ts maps are shown in Figure 3.13 in which temperature over urban areas take relatively higher values than areas which were fully and partially covered by vegetation. This relationship could be assigned to latent heat flux canopy resistance to transpiration and soil moisture as in Lo et al.; Voogt and Oke; Chudnovsky et al. [235-237], producing a typical Universal Triangle that was presented before by Weng [238]. In a Universal triangle, the vegetation radiometric temperatures are constantly in close proximity to air temperature, however the surface radiant temperature above bare soil may vary based on the soil water content. This means that the spatial variation in surface radiant temperature will likely be small (with the exception of emission from underlying bare soil) over the full vegetation, but will vary from warm to cold while surface moisture availability ranges from zero to one for bare soil.

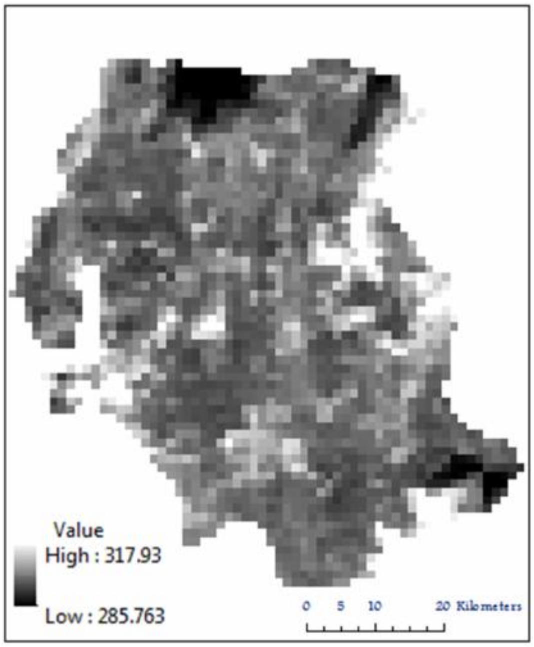

Figure 3.13: Satellite corrected-Ts map generated from AVHRR at depth 5 cm.

3.6.1.1 *Surface temperature for MODIS*

MODIS Land Surface Temperature and Emissivity (Ts/ε) products with their two common types Aqua MODIS (e.g. MYD11A1 products) and Terra-MODIS (e.g. MOD11A1 products), provided per-pixel temperature and emissivity values daily at LAADS Web (http://ladsweb.nascom.nasa.gov/), which is the web interface to the Level 1 and Atmosphere Archive and Distribution System (LAADS). The objective of LAADS is usually to supply fast and simple usage of MODIS Level 1, Atmosphere and Land data products and Land information products as in Figure 3.14.

The search for MODIS Level 1, Atmosphere and Land data products and VIIRS Level1, are always via product’s name, temporal window, collection, and spatial coordinates. So as to enable rapid and dynamic access to the data that is provided to the user immediately or within 24 to 48 hours for some packages other than Ts.

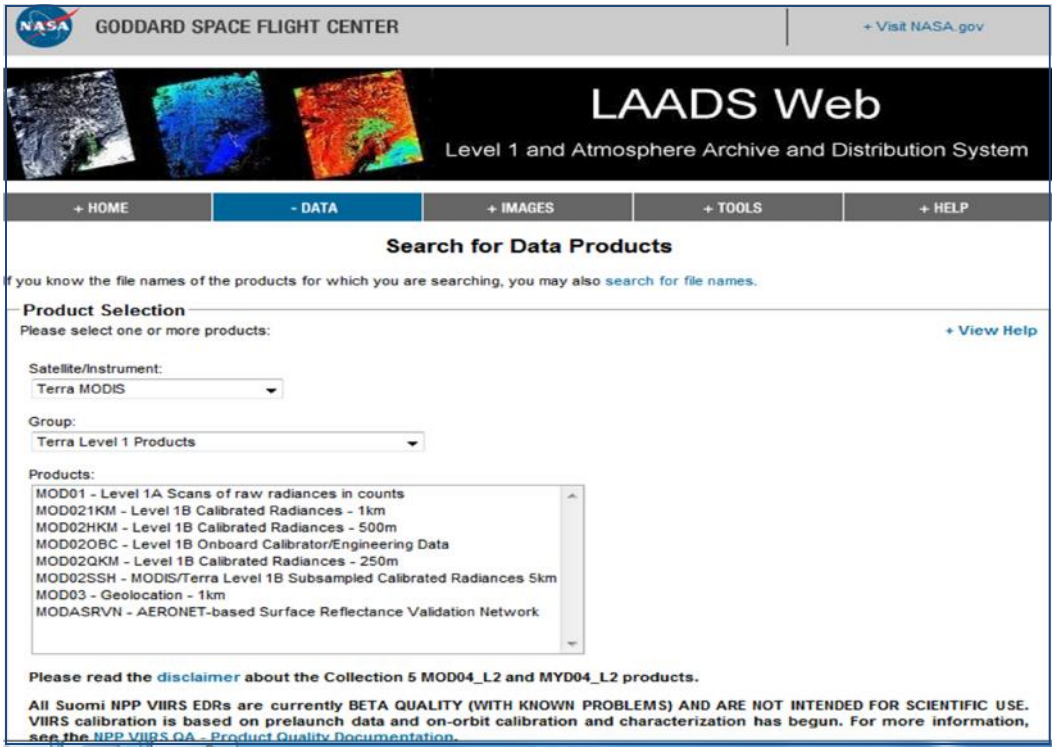

Search for Data Products

f you know the file names of the products for which you are searching, you may also search for file names.

Product Selection

Please select one or more products:

Satellite/Instrument: Terra MODIS

Group: Terra Level 1 Products

Products:

- MOD01 - Level 1A Scans of raw radiances in counts
- MOD021KM - Level 1B Calibrated Radiances - 1km
- MOD02HKM - Level 1B Calibrated Radiances - 500m
- MOD02OBC - Level 1B Onboard Calibrator/Engineering Data
- MOD02QKM - Level 1B Calibrated Radiances - 250m
- MOD02SSH - MODIS/Terra Level 1B Subsampled Calibrated Radiances 5km
- MOD03 - Geolocation - 1km
- MODASRVN - AERONET-based Surface Reflectance Validation Network

Please read the disclaimer about the Collection 5 MOD04_L2 and MYD04_L2 products.

All Suomi NPP VIIRS EDRs are currently BETA QUALITY (WITH KNOWN PROBLEMS) AND ARE NOT INTENDED FOR SCIENTIFIC USE. VIIRS calibration is based on prelaunch data and on-orbit calibration and characterization has begun. For more information, see the NPP VIIRS QA - Product Quality Documentation.

Figure 3.14: LAADS webpage where Ts and ε data are provided at daily bases.

3.6.1.1 LST from LANDSAT

The digital number values corresponding to the thermal Band 6–I and Band 6–II of the Landsat images were used to compute spectral radiance L_λ. The brightness temperature TB was then computed using the spectral radiance L_λ and calibration coefficients form LANDSAT calibration data. Finally the land surface temperature Ts was derived from the brightness temperature of Band 6 and the surface emissivity derived from the NDVI image.

The Land surface temperature Ts could be produced from Landsat satellite's Thermal-IR data using the Stefan-Boltzmann Equation [239], stated as;

$$B = \varepsilon \sigma T^4 = \sigma T_B^4$$
$$\therefore T = \frac{1}{\varepsilon^{1/4}} T_B \qquad 3.9$$

Where, σ is Stefan Boltzmann Constant (5.67×10^{-8} $Wm^{-2}K^{-4}$), B is amount of radiation emitted (Wm^{2}), T represents surface temperature (^{o}K), ε is the land surface emissivity. *TB* could be determined in two approaches; either from the image digital numbers (0-255) via LANDSAT look-up tables [240] and transformation equations, or using a relationship that resembles the Planck Formula with two free parameters displayed as [241, 242]:

$$T_B = \frac{K_2}{\ln\left(\frac{K_1}{L_\lambda} + 1\right)} \tag{3.10}$$

Where, $L\lambda$ represents the spectral radiance and K_1, K_2 are calibration constants so that;

$$K_1 = \frac{c_1}{\lambda^5}; \quad K_2 = \frac{c_2}{\lambda} \tag{3.11}$$

Where, c_1 and c_2 are constants, $c_1=1.19104346\text{x}10^{-16}$ ($W\text{-}m^{2}$) and $c_2=1.438768\text{x}10^{4}$ ($\mu m\text{-}K$) and λ is the mean wave length. The spectral radiance values could be determined from the digital number of image pixels [239],through the relationship;

$$L_\lambda = \left(\frac{L_{\lambda\max} - L_{\lambda\min}}{Q_{C\max} - Q_{C\min}}\right)\left(\mathrm{DN} - Q_{C\min}\right) + L_{\lambda\min} \tag{3.12}$$

Where, $L\lambda$ is the spectral radiance in the sensor's aperture (W/m^{2}-ster-μm), DN represents the digital number of image pixels. $QC\ max$ is the maximum quantized calibrated pixel value (equivalent to Lλ max) in DN, $Qc\ min$ is the minimum quantized calibrated pixel value (equivalent to Lλ min) in DN, Lmax is the spectral radiance which is scaled to $QC\ max$ (W/m^{2}-ster-λm), $Lmin$ is the spectral radiance which is scaled to $QC\ min$ (W/m^{2}-ster-λm). Figure 3.15 shows sample generated by Ts map from Landsat TB and ε images with spatial accuracies of 60 m.

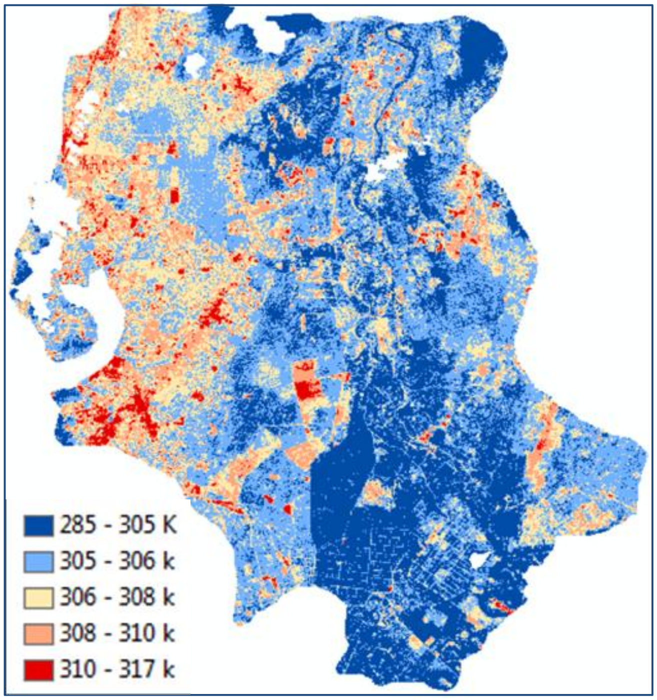

Figure 3. 15: Ts map produced by Landsat 7 band 6-II.

3.6.1.1 Classification

The purpose of the classification procedure is usually to sort out all pixels within a digital image into one of many land cover classes, or "themes". This classified data will then be utilized to generate thematic maps of the land cover within an image. Usually, multispectral data is employed to execute classification and, certainly, the spectral pattern present within the data for every pixel is utilized as being the numerical basis for classification [243]. The aim of image classification would be to determine and depict, being a distinctive gray level (or color) of the features occurring within an image with regards to the object or kind of land cover.

Image classification is probably the most crucial procedure of digital image analysis. It is extremely vital to possess a "pretty picture" or even an image, displaying a degree of colors showing various features of the actual terrain, however it is quite pointless realize the colors' mean is realized. Two main classification techniques are supervised classification and unsupervised classification.

Supervised Classification

With supervised classification, we determine types of the details classes (i.e., land cover type) of interest within the image. These are generally called "training sites". The image processing software system is then utilized to produce a statistical depiction of the reflectance for every information class. This phase is usually known as "signature analysis" and could incorporate creating a characterization as easy as the mean or even the rage of reflectance on each bands, or as difficult as comprehensive analyses of the mean, variances and covariance of overall bands. When a statistical characterization is achieved for every information class, the image will be classified by analyzing the reflectance for every pixel and deciding on which of the signatures is similar to most as shown in Figure 3.16.

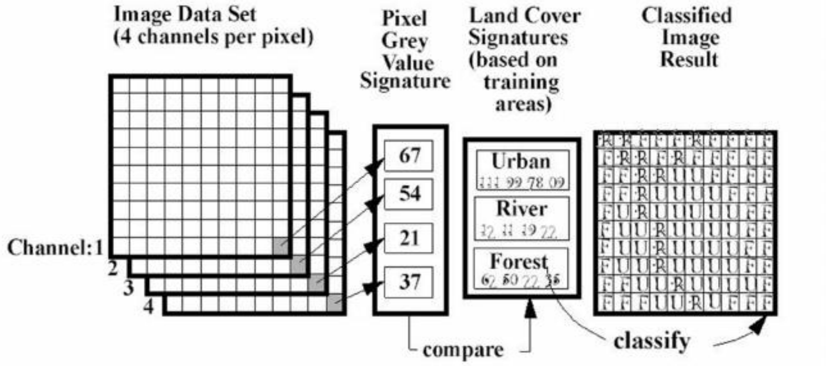

Figure 3.16: Sample of classified image’s layers.

Maximum likelihood Classification

The study tended to use the maximum likelihood Classification, which is a mathematical determination criterion to help in the classification of overlapping signatures; pixels are designated to the class of greatest probability. This classifier is considered to provide better outcomes than the other types like: parallelepiped classification and Minimum distance Classification, but it is significantly slower due to extra calculations. This considers that classes within the input data use a Gaussian distribution and these signatures were properly picked; this, however, is not usually a reasonable assumption.

The classification was achieved in the study to produce a thematic map of the study area (see Figure 3.2) to verify subjectively, the Ts distribution and its correlation to the urban and impervious surfaces as well as correlating the surface moisture distribution to the vegetation covers.

Unsupervised Classification

Unsupervised classification is a technique that investigates numerous unidentified pixels and splits into a number of categories based on natural categories within the image values. In contrast to supervised classification, unsupervised classification does not need analyst-specified training information. The fundamental assumption is always that values in a provided cover type must be close to each other within the measurement space (i.e. have similar gray levels), while data in various classes must be relatively properly separated (i.e. have completely different gray levels) [243].

Unsupervised classification is now ever more popular in agencies associated with long term GIS database servicing. Nowadays, there are systems which use clustering procedures that are very quick in the nature of functional variables. As a result it is starting to become simple to training of GIS analysis has been simplified with an overall knowledge of remote sensing to attempt classifications that fulfill standard map accuracy requirements. With ideal ground truth precision evaluation methods, this tool can offer a tremendously rapid method of generating good quality land cover data on a continuous basis.

3.7 Methodologies

This section presents the applied methodologies towards the assessment of surface moisture and ET_o in the form of flow charts for more clarifications.

3.7.1 Moisture content

Along the two applied moisture algorithms UT and TI, the MC extraction process was conducted through four stages which were data collection and preparation, data processing, results and finally the validation. This included the spatial dataset as well as the measurements that were carried out on field.

3.7.1.1 Universal Triangle – for both NOAA and LANDSAT

The strategy that followed for surface moisture assessment was dependent mainly on the extraction of NOAA and Landsat satellite's Ts beside the NDVI. These two variables represent the spatial parameters shared on the universal triangle method. In addition, these findings were compiled with in-situ measurements of Ts in order to correct the surface value, and also to reserve some ground Ts values for work validation. The second measured value was the surface MC, whose role was to enable determination of the moisture parameters within the algorithm, and also moisture validation used some part of the data.

The chart represented by Figure 3.17 shows the steps achieved towards the surface MC extraction via universal triangle method alongside satellite's-based Ts and satellite's-corrected Ts.

The spatial formula to extract MC in Equation 2.38 could be expanded in terms of a second order polynomial as in Chauhan et al. [94]:

$$MC = a_{00} + a_{10}NDVI^{*} + a_{20}NDVI^{*2} + a_{01}Ts^{*} + a_{02}Ts^{*2} + a_{11}NDVI^{*}Ts^{*} + a_{22}NDVI^{*2}Ts^{*2} + a_{12}NDVI^{*}Ts^{*2} + a_{21}NDVI^{*2}Ts^{*} \quad 3.13$$

Where

Ts: the observed surface temperature, $Ts^{*} = \frac{T-T_o}{T_S-T_o}$ 3.14

NDVI: the observed NDVI, $NDVI^{*} = \frac{NDVI-NDVI_o}{NDVI_S-NDVI_o}$ 3.15

Through the use of these regression relationships to NOAA/LandSAT measurements, daily MC estimations at NOAA temporal resolution can be acquired and a half monthly field MC acquisition could be conducted for LandSAT.

The measured Ts and MC on field were conducted at three variable depths (5 cm, 10 cm and 15 cm into soil) in order to examine the moisture depth influences, and then applied to the model to produce MC parameters based on each depth influence. This made the technique applicable for any area that has both vegetation cover and bare soil with no constraint [93].

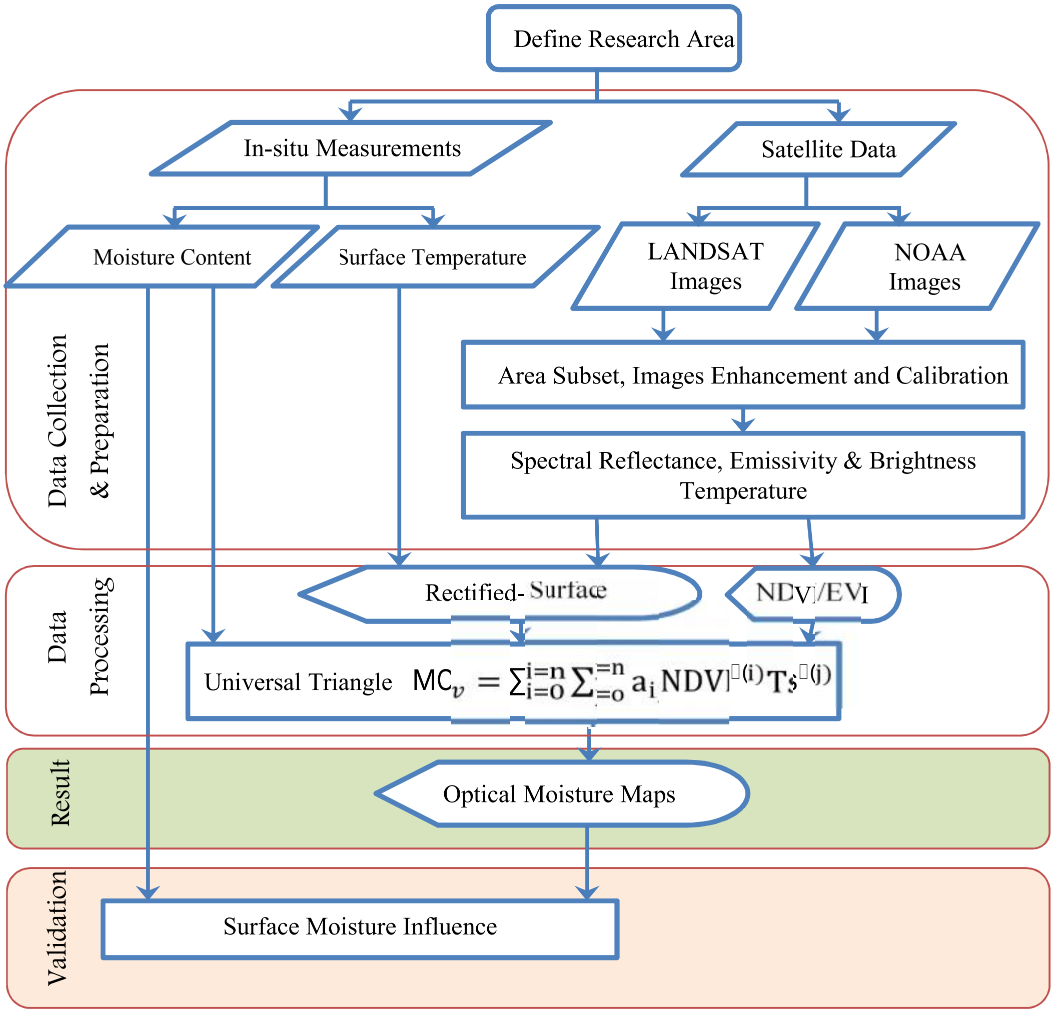

Figure 3. 17: Moisture content retrieval from satellite images & in-situ measurements.

3.7.1.2 Thermal Inertia

In order to produce surface MC using the TI method, MODIS’s Surface temperature values over study area for the entire period were downloaded directly from web source of LAADS (mentioned in section 3.6.1.1). The NDVI measurements were made with a combined red and near-infrared radiometer, developed at the NASA/Goddard Space Flight Center, which measures the reflected radiation in the bands (0.58-0.68 μm) and (0.73-1.1 μm).

Further, the EVI was established to improve the vegetation signal with improved sensitivity in higher biomass regions and enhanced vegetation tracking via de-coupling of the canopy background signal in addition to a reduction in environment influences. It was generated from the RED, NIR and Blue channels of MODIS satellite with supportive coefficients for correcting the environmental resistance in Red channel, correction coefficient for atmospheric resistance in Blue channel and canopy background brightness correction factor.

The samples were collected from the soil of each type of the surface cover among the three selected partitions of the study area (full vegetated, urban and multi-cover surfaces) in order to determine the upper and lower moisture values which represented in the soil's field (FC) capacity and the permanent wilting point (PWP) respectively. A particle size distribution (PSD) test was applied to the collected samples using Master-sizer 2000 device facilitated by UTP laboratories. Consequently, soil's structure was classified into the standard classes (sand, silt and clay) with different percentages for surface cover type. A hydraulic calculator for soil properties was then used, which is an open-source software based on the physical concept of soil water characteristics triangle as in Figure 3.18, produced by the U.S. Department of Agriculture (USDA) [244], was used to determine the values of FC and PWP according to the percentage of the soil's components sand and clay.

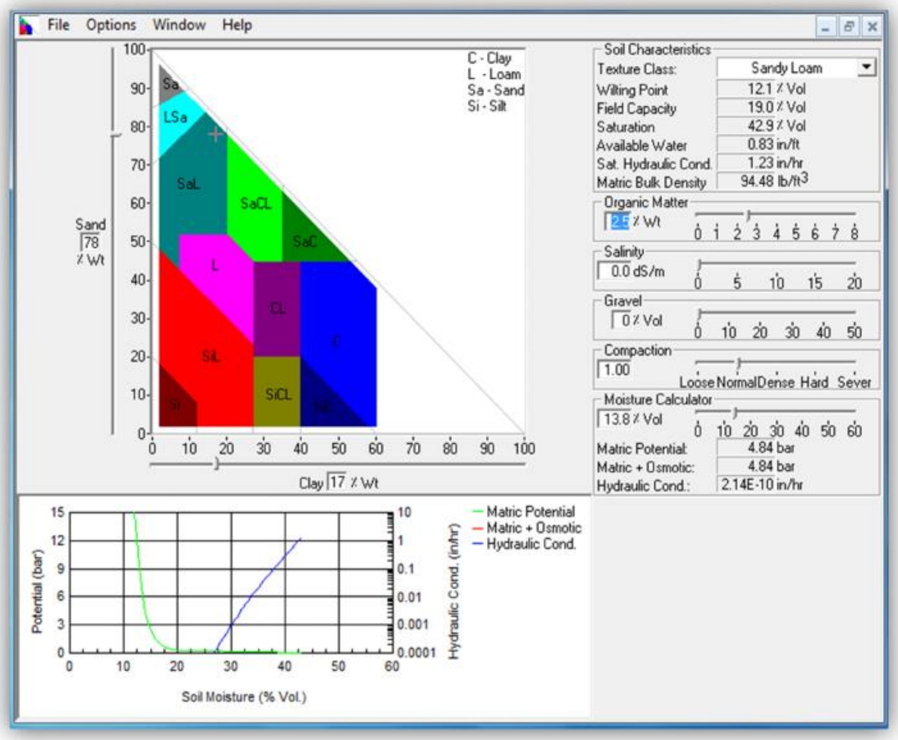

Sand 78 % Wt

Clay 17 % Wt

Soil Characteristics

Texture Class: Sandy Loam

Wilting Point 12.1 % Vol

Field Capacity 19.0 % Vol

Saturation 42.9 % Vol

Available Water 0.83 in/ft

Sat. Hydraulic Cond. 1.23 in/hr

Matric Bulk Density 94.48 lb/ft3

Organic Matter 2.5 % Wt

Salinity 0.0 dS/m

Gravel 0 % Vol

Compaction 1.00

Moisture Calculator 13.8 % Vol

Matric Potential: 4.84 bar

Matric + Osmotic: 4.84 bar

Hydraulic Cond.: 2.14E-10 in/hr

Figure 3.18: Soil water characteristics triangle.

The plan chart in Figure 3.19 shows the estimation of MC_v from the daily MODIS (Aqua/Terra) images, from which, Ts and satellite's-corrected Ts, NDVI and EVI were extracted accompanied with in-situ measurements of moisture content over the three test's locations. The produced satellite's moisture values which were in terms of point measurements were validated using the moisture measurements conducted in-situ.

3.7.1.3 *Weighted Moisture map*

The MC weightage method is based fundamentally on estimating the MC for each pixel of the image based on the weight of each class of the surface cover that is exist in the pixel. This idea was introduced in this research in attempt to compensate the limitation of aggregating multiple spectral signatures within a single image pixel because of the pixel size in coarse resolution images.

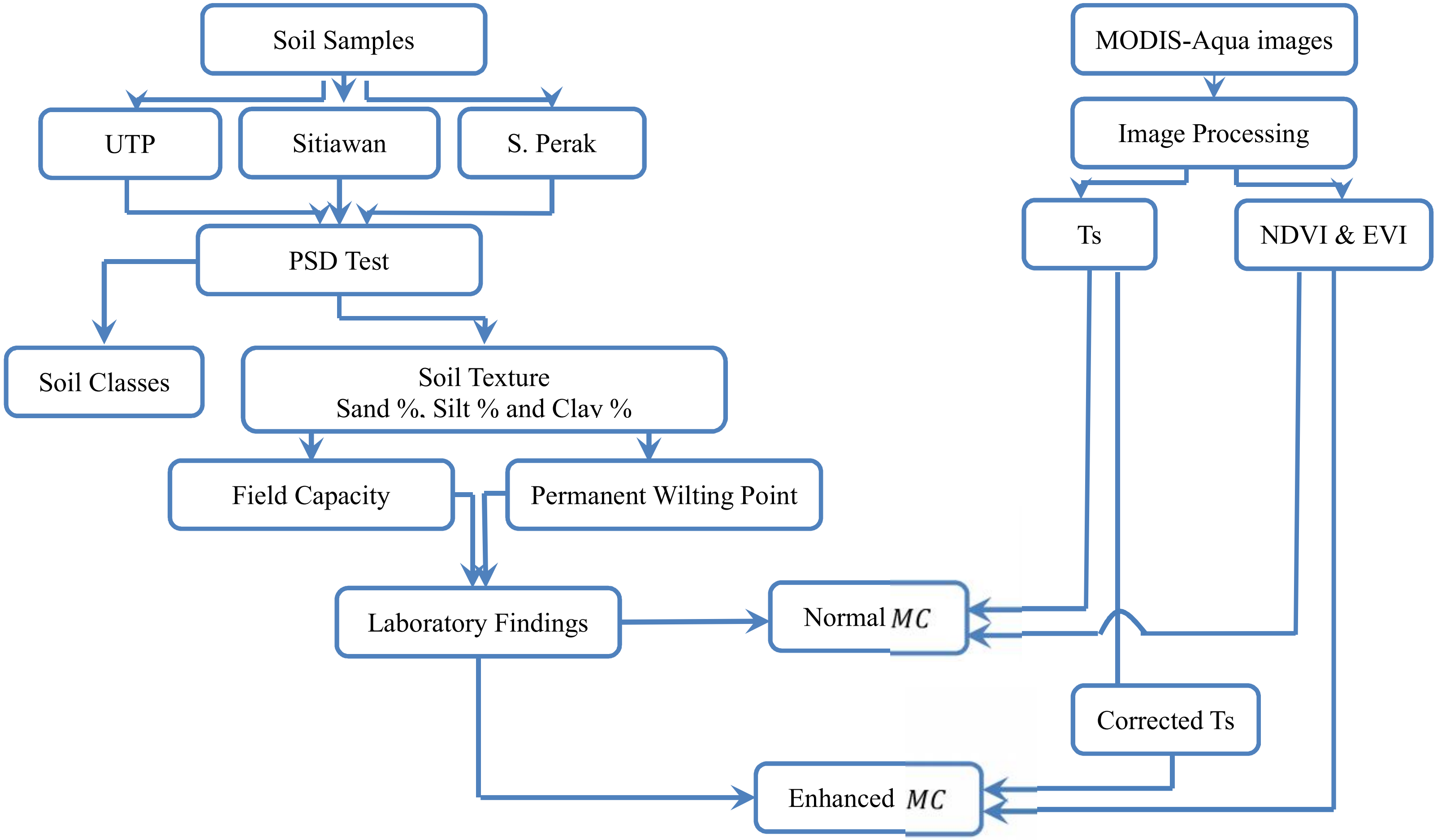

Figure 3.19: Volumetric moisture content generated from MODIS satellite and field measurements.

Derivation of weighted moisture map

Based on aforementioned information, weightage of each of the three different surface cover types in the study area was determined and inserted upon its weight in the map formation as shown in Figure 3.20. Satellite's surface moisture maps were generated using a pixel-based SWI. From the laboratory analysis of soil samples, the FC and PWP for each of the three stations were calculated. Assuming a pixel (i) at MODIS/AVHRR scale, the moisture map at pixel (i) level using the moisture boundaries over UTP station takes the value of MC_{UTP_i}, same tasks went with the moisture images generated over Sitiawan and Seberang Perak which are MC_{SITI_i} and MC_{SP_i} respectively. Thus, the following chart will explain the stepwise approach to the weighted moisture map that is proposed by the study to meet the disparity of spectral responses of surface cover type at MODIS or AVHRR images pixel.

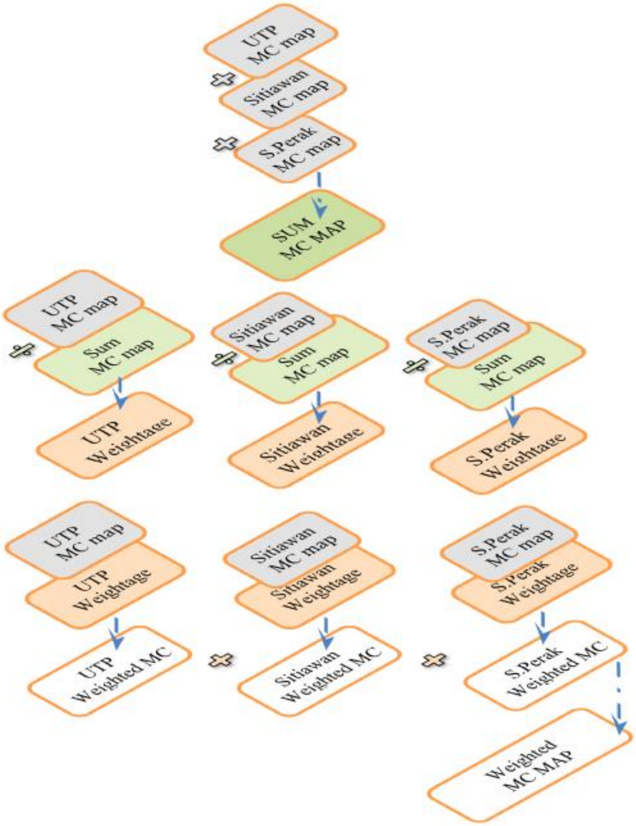

Figure 3. 20: Process steps of the weighted moisture map construction.

The total moisture map of the pixel based image was calculated as a summation of the three moisture values for each pixel (MC_{SUM_i}) then, the fraction (Fr_i) of station's moisture share within the pixel was calculated as a percentage of the pixel moisture value of the particular station to the total moisture at the pixel. Equations 3.16 to 3.23 mathematically describe the steps towards the weighted moisture estimation over the study area.

$$MC_{SUM_i} = \sum_{i=1}^{n} (MC_{UTP_i}, MC_{SITI_i}, MC_{SP_i}, ..., MC_n) \tag{3.16}$$

$$Fr_{UTP_i} = {MC_{UTP_i}} \big/ {MC_{SUM_i}} \tag{3.17}$$

$$Fr_{SITI_i} = {MC_{SITI_i}} \big/ {MC_{SUM_i}} \tag{3.18}$$

$$Fr_{SP_i} = {MC_{SP_i}} \big/ {MC_{SUM_i}} \tag{3.19}$$

The weightage (W_i) of each surface cover type for the single pixel was determined by applying the fraction of each station to the corresponding full moisture pixel which was generated by MC high and low boundaries FC and PWP. Finally, the moisture (MC_i) for each image pixel was calculated as a summation of the three different weightages of moisture pixels.

$$W_{UTP_i} = Fr_{UTP_i} \times MC_{UTP_i} \tag{3.20}$$

$$W_{SITI_i} = Fr_{SITI_i} \times MC_{SITI_i} \tag{3.21}$$

$$W_{SP_i} = Fr_{SP_i} \times MC_{SP_i} \tag{3.22}$$

$$MC_i = W_{UTP_i} + W_{SITI_i} + W_{SP_i} \tag{3.23}$$

More clarification is shown in Figure 3.21, where the MC is extracted according to the percentage of the surface cover types that are available within this pixel as a result of weighting process. On the other hand, the same image pixel in its ordinary extraction process produces MC value from lumped surface cover features.

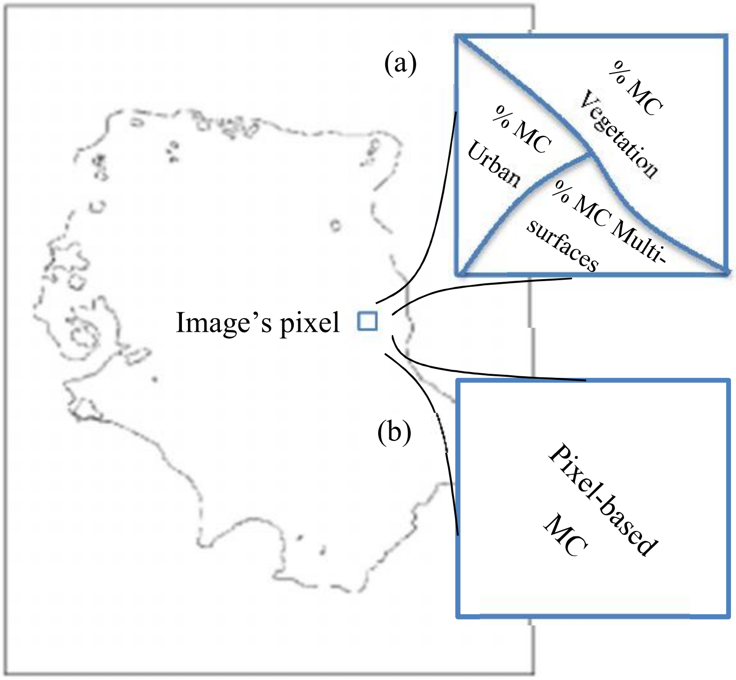

Figure 3. 21: MC extraction based on (a) pixel segmentation process and (b) the ordinary pixel-based MC.

3.7.1 Evapotranspiration

The research intended to generate a local ET estimation algorithm over the study area concerning the influence of the satellite's surface temperature in terms of correction of satellite's Ts via in-situ measurements of Ts throughout correlation relationships among satellite's Ts and Ts collected from ground measurements. In addition, the algorithm intended to address the soil MC impact on the magnitude of the ET through incorporating the satellite's resultant MC from the three sensors (AVHRR, MODIS and Landsat) into the ET extracted map. Figure 3.22 shows the selected methods for ETo retrieval.

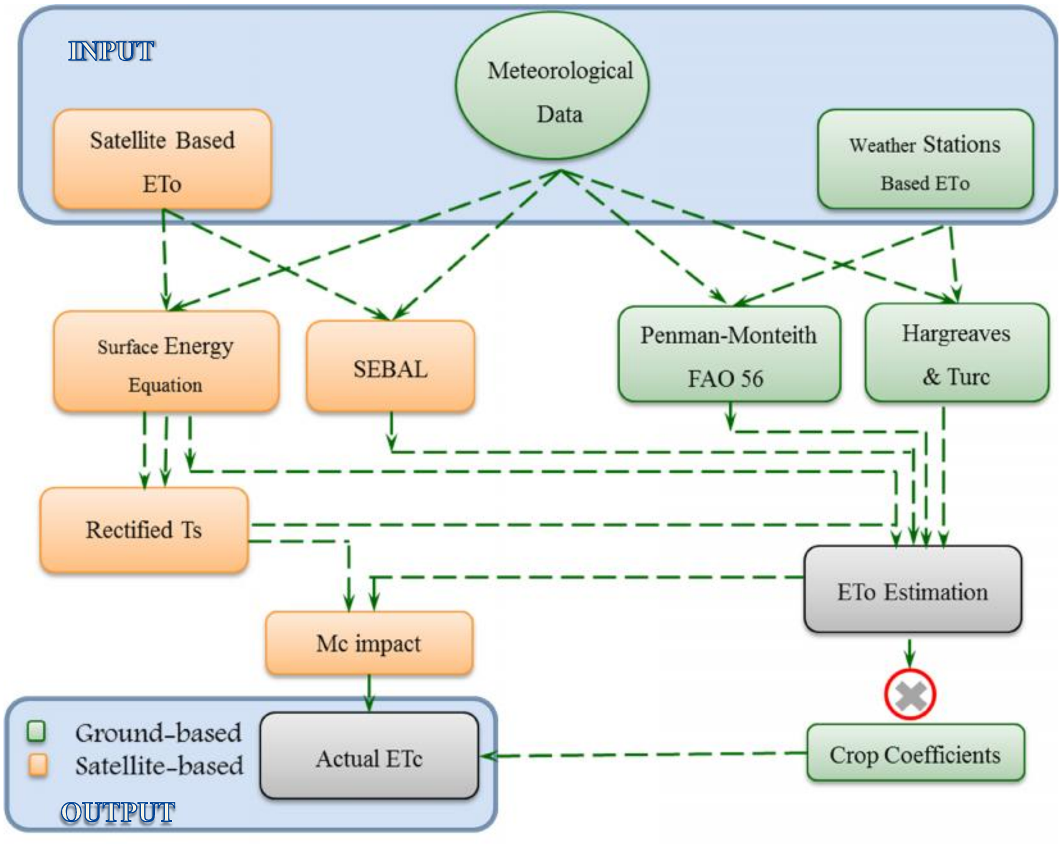

Figure 3.22: Energy budget equation with modified parameters for ET_o assessment.

3.7.1.1 Meteorological Determination of ET_o

Three of the most effective and widely applied methods for ET_o calculation were used in this study for generating ground measurements of ET_o as reference values for validating the spatial ET_o. Those methods are Penman-Monteith from FAO Hargreaves and Turc Equations. The selection of these three approaches can be justified as follows:

Firstly, The Penman-Monteith method consists of all variables which govern energy exchange as well as related latent heat flux (ET) through standard areas of vegetation. The majorities of the variables are calculated or could be easily determined from weather information. The formula can be employed for the direct computation of any crop ET_o since the surface and aerodynamic resistances are usually crop specific. The panel of specialists suggested the usage of the Penman-Monteith collaboration technique being a new standard for reference ET$_o$ and also recommended on processes for computation of the numerous parameters. The FAO Penman-Monteith technique originated by identifying the reference crop being a hypothetical crop with a presumed height of 0.12 m using a surface resistance of 70 s m^{-1} plus an albedo of 0.23, tightly comparable to the evaporation of an extension surface of green grass of standard height, positively developing and effectively watered,. The technique overcomes weak points of the earlier FAO Penman approach and offers values much more consistent with actual crop water use data globally.

Secondly, two of the essential methods were also used in order to verify the ET$_o$ extracted from images, namely, Hargreaves and Turc. They have been very essential for the evaluation of ET$_o$ acquired by indirect approaches. Hargreaves is classified as the best method that simulates the lysimeter measurements in its accuracies while the Turc method was developed based on humid regions so it was selected due to its adjacency to the study area climate. On the other hand, the proposed Energy Balance equation and SEBAL model were also estimated as being pixel-based ET$_o$ algorithms, using the ENVI and the ArcGIS environments. ET$_o$ Calculator version 3.1was used to achieve the calculations with accuracy and reliability. It is an open-source computer software produced by FAO [245] based on the Penman-Monteith technique in estimating ET$_o$. Figure 3.23 below shows the program interface in which location characteristics, data range, limits and meteorological data are required.

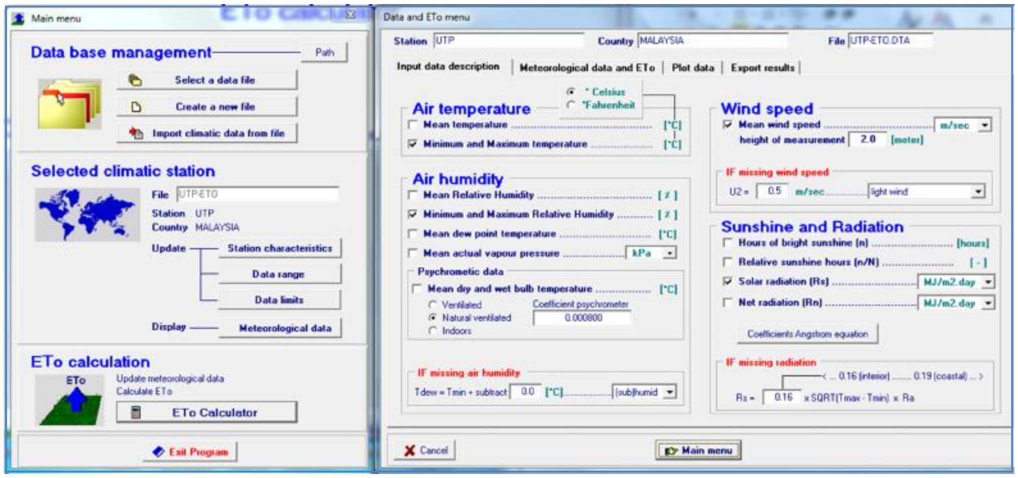

File UTP-ETO
Station UTP
Country MALAYSIA

Station UTP
Country MALAYSIA
File UTP-ETO.DTA

● °Celsius
○ °Fahrenheit
☐ Mean temperature .... [°C]
☑ Minimum and Maximum temperature .... [°C]
☐ Mean Relative Humidity .... [%]
☑ Minimum and Maximum Relative Humidity .... [%]
☐ Mean dew point temperature .... [°C]
☐ Mean actual vapour pressure .... kPa
☐ Mean dry and wet bulb temperature .... [°C]
○ Ventilated
● Natural ventilated
○ Indoors
Coefficient psychrometer 0.000800
Tdew = Tmin + subtract 0.0 [°C] .... (sub)humid
☑ Mean wind speed .... m/sec
height of measurement 2.0 [meter]
U2 = 0.5 m/sec .... light wind
☐ Hours of bright sunshine (n) .... [hours]
☐ Relative sunshine hours (n/N) .... [-]
☑ Solar radiation (Rs) MJ/m2.day
☐ Net radiation (Rn) MJ/m2.day
Rs = 0.16 x SQRT(Tmax - Tmin) x Ra

Figure 3.23: The interface of ET$_o$ Calculator produced by FAO.

3.8 Validation

Data validation is ensuring that many data (whether user input variables, read from file or read from a database) tend to be valid for the meant data types and remain valid through the entire application which is operating this data. This implies that data validation, to become as effective as it can be, has to be applied at all components that obtains the data, processes them and also saves or prints the outcomes [246].

Throughout this study, two sets of validations were applied to both MC and ET values produced by the research. Statistical validation was implemented for the simulated point measurements of MC and ET, in which The Statistical Package of Social Sciences (SPSS) Computer software used. The second set was a spatial validation for the pixel-based estimates of MC and ET_o, which was achieved using the Success Rate method.

3.8.1 Statistical validation

3.8.1.1 SPSS

IBM SPSS Statistics is an incorporated group of products that handles the complete analytical procedure, from planning to data assortment to evaluation, reporting and arrangement. Using more than several completely built in modules to select from, user can carry out research to make better choices. IBM SPSS software permits educators to show efficiently, assists individuals gain essential analytical expertise and facilitates better and informative institutional investigation and decision-making [247].

The version used in this study was IBM SPSS 20, to analyze and validate the resultant moisture values from: satellite images, satellite's corrected-Ts images and MC measured in-situ, taking into account the variation in Ts and moisture depths of measurement. The software is also used to validate the ET_o findings among the modified ET_o algorithm, SEBAL, Turc, Hargreaves and Penman-Monteith formulas. Figure 3.24 Shows simple chart describing the statistical validation set of ET_o.

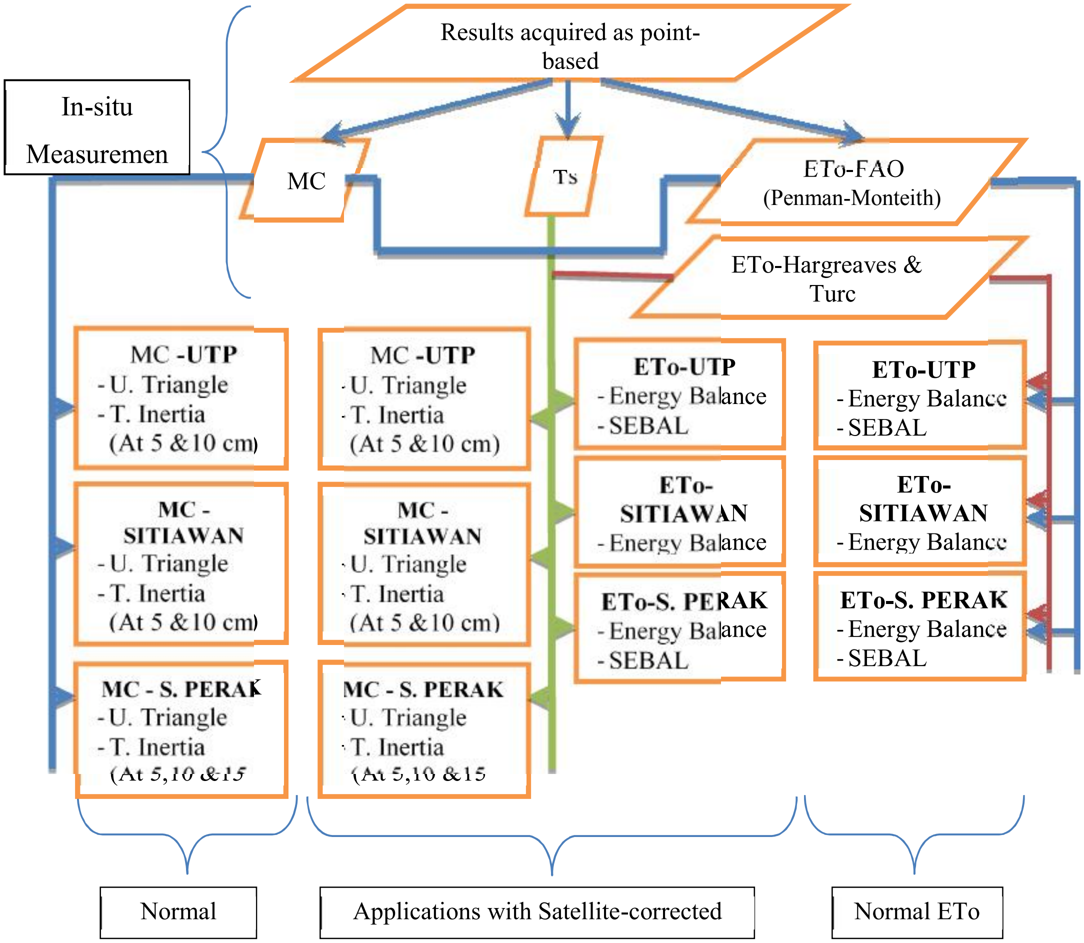

Figure 3.24: The general view of MC and ET_o validation.

3.8.1.2 Propagation of Error

Propagation of error (or propagation of uncertainty) is defined as the effects on a function by a variable's uncertainty. It is a calculus derived statistical calculation designed to combine uncertainties from multiple variables, in order to provide an accurate measurement of uncertainty [154, 248]. Every measurement has an air of uncertainty about it, and not all uncertainties are equal. Therefore, the ability to properly combine uncertainties from different measurements is crucial. Uncertainty in measurement comes about in a variety of ways: instrument variability, different observers, sample differences, time of day, etc. Typically, error is given by the standard deviation (δx) of a measurement[154].

The rule for both multiplication and division is that, the relative errors are added in quadrature. Consider the case where, the calculation is of the form:

$$x=f(a,b,c) \qquad 3.24$$

The error of propagation is f is given by

$$\frac{\delta_x}{x}=\sqrt{\left(\frac{\delta_a}{a}\right)^2+\left(\frac{\delta_b}{b}\right)^2+\left(\frac{\delta_c}{c}\right)^2} \qquad 3.25$$

MC propagation error could be estimated from Equation 2.27 which states that:

$$\mathrm{MC}=\sum_{i=0}^{i=n}\sum_{j=0}^{j=n} a_{ij}\,\mathrm{NDVI}^{(i)}\,\mathrm{Ts}^{(j)}$$

Because each measurement of MC from the UT method has an uncertainty about its mean, it can be written that, the uncertainty of δ_{MC} of the ith measurement of MC depends on the uncertainty of the ith measurements of Ts and NDVI:

$$\frac{\delta_{MC}}{MC}=\sqrt{\left(\frac{\delta_{Ts}}{Ts}\right)^2+\left(\frac{\delta_{NDVI}}{NDVI}\right)^2} \qquad 3.26$$

3.8.1 Spatial Validation

3.8.1.1 Ts-Vi validation for universal triangle

As a step to examine the relevancy of the used methodology to the universal triangle, the estimated NDVI was plotted against the satellite's-corrected surface temperature Ts. A subjective comparison was made between the resultant NDVI-Ts and the fundamental relationship of NDVI-Ts established by Carlson [119]. Figure 3.25 shows a sample universal triangle from Carlson [119].

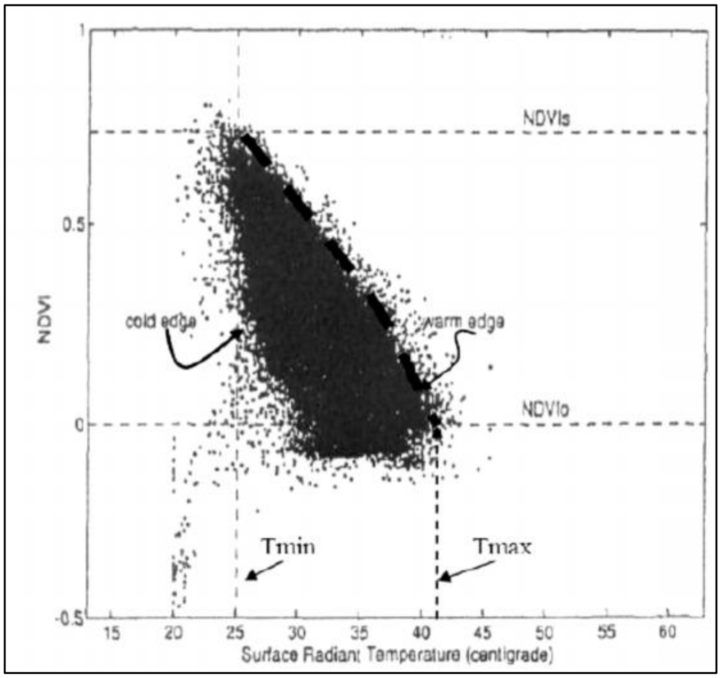

Figure 3.25: Scatterplot of satellite pixel values of NDVI and Ts [119].

3.8.1.2 Success rate validation

The second validation was performed by comparing the highest MC /ETo zones with the adjacent MC/ETo with different image (image from different satellite). The success rate curves were created and their areas under the curve (AUC) were calculated. The rate explains how well the highest moisture/ETo values meet each other [249]. So, the area under curve can assess the prediction accuracy qualitatively. To obtain the relative ranks for each prediction pattern, the calculated index values of all cells in the study area were sorted in descending order using Quantile Classification task in ArcGIS environment. Then the ordered cell values were divided into 100 classes, with accumulated 1% intervals as in Figure 3.26.

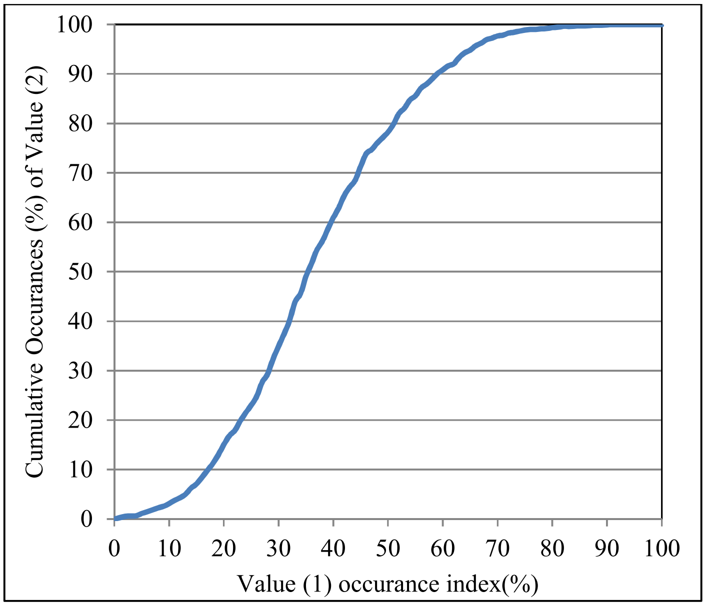

Figure 3.26: The graphical representations of the correlation sets.

Based on the aforementioned, the moisture weighted maps estimated from both AVHRR and MODIS were correlated spatially through the success rate to examine their compatibility with the moisture distribution. A spatial correlation between the generated ET_o maps from energy balance with rectification packages, and the SEBAL model, which has been applied extensively over the humid region, so it was used as spatial reference for ET_o. Moreover, further spatial correlations were made among the ET_o generated from AVHRR and MODIS images, taking into account that, each two images from different satellite, chronologically must be captured in the same day. Finally, the weighted moisture maps were correlated against ET_o maps in order to study the relationships between them, and later analyze the relation on the light of AUC strength.

CHAPTER 4
RESULTS AND DISCUSSION

Throughout this chapter, all findings that realize the objectives of the study are shown and expressed in figures and tabulated forms. The chapter covers the rectification of satellite's surface temperature by in-situ measured Ts through a linear regression, beside the reliability analysis of using the rectified Ts in processes of MC and ET extraction. In addition, the chapter introduces the retrieval of surface MC via two of the most applicable algorithms among optical/thermal remote sensing's methods, which are the universal triangle and thermal inertia methods. Moreover, the results of the weighted moisture method which is based on the concept of producing pixel values according to the weightages of surface cover classes, proposed by the study are also highlighted. Results from both methods are presented, validated and discussed along the chapter. The chapter also discusses the assessment of the ET from NOAA and MODIS satellite's images from energy balance equation, using the pre-rectified Ts and some collected meteorological data. The MC's influence in the magnitude of ET is also presented and discussed along with the statistical and the spatial validation of the methods.

4.1 Surface Temperature (Ts) Assessment

Ts was estimated from the thermal bands of both satellites NOAA and MODIS with variable considerations of the atmosphere and the emitting surface. Therefore, the equation of thermal radiation with its transfer through the atmosphere was used.

4.1.1 Split window technique for Ts extraction

In order to process the whole acquired images for surface temperature extraction, subset area has been delineated surrounding each weather station and any spatial computation performed within each subset area was assumed to represent the average value of the sub area pixels (block averaging). Figure 4.1 shows a sample of resultant surface temperatures over the three selected locations where the block averaging method was used in order to generate typical point-based measurements of Ts, MC and ET for enhanced correlation between satellite extracted and ground measured values.

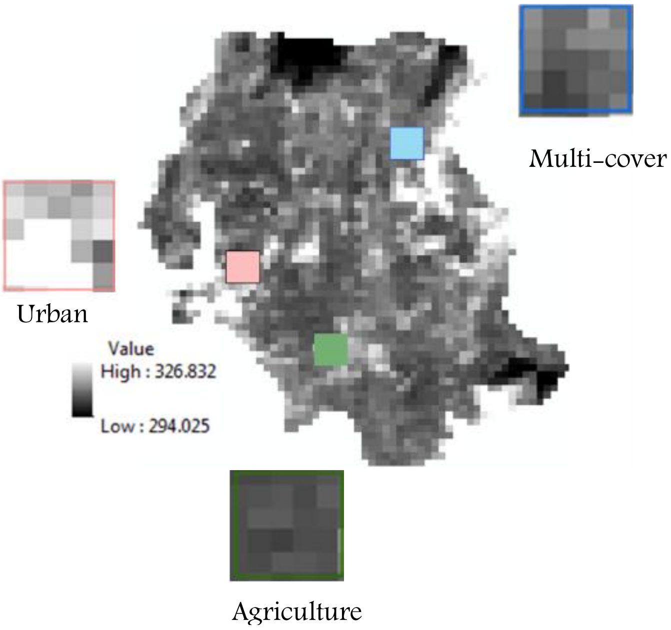

Figure 4. 1: Sample Ts map where subsets were masked and averaged to generate point measurements.

The variation of temperature values from the different locations is actually a representative of the nature of the surface cover. For example, Sitiawan area (urban area) with high up-willing emission shared by the traffic, emission from built up surfaces, roads and machines produces Ts a bit higher due to the increase in the emissivity dose, whereas Seberang Perak area (agricultural land) noticed low Ts values. It must be due to the homogenous and low emission from the surface which is shaded by vegetation cover. On the other hand, the variable types of surface cover over UTP produced different magnitudes of emissivity resulted in a slight Ts bias results in unpredicted emission manner. The extracted satellite based surface temperature showed reasonable results in terms of evaluating the split-window techniques, especially over agricultural area and areas with a uniform cover, this supports the theorem that the canopy temperature Ts will likely be near the local temperature Ta because of its low thermal mass [250]. Some analysts suggest that the split-window technique for driving surface temperature tends to overestimate actual surface temperature by 4^{o}C [251]. Table 4.1 shows example of Ts values extracted from both field measurements and satellites along UTP testing locations, where measurements were taken in concurrent times of satellites overpass.

Table 4. 1: Ts extracted from NOAA 17&18 sat. and field measurements over UTP

DAY	Measuring depth of Ts ^{o}C at field		Satellite extracted Ts ^{o}C
	5 cm	10 cm	
7-Feb-2011	22.4	20.6	25.90
9-Feb-2011	36.6	33	33.17
12-Feb-2011	38	35.2	35.91
16-Feb-2011	32	28.8	35.63
17-Feb-2011	30.1	28.3	33.06
19-Feb-2011	29.3	26.1	31.20
20-Feb-2011	30.1	28.6	34.25
21-Feb-2011	31.4	29.7	33.10
22-Feb-2011	37.5	34	31.34
27-Feb-2011	39	35	30.80
28-Feb-2011	40.3	37.8	33.20
1-Mar-2011	27.2	24.4	31.10
10-Mar-2011	30.3	28.9	33.94
23-Mar-2011	29	27.1	32.40
28-Mar-2011	38.1	34.4	30.13
30-Mar-2011	29.8	28	32.60
4-Apr-2011	30.3	27	19.56
7-Apr-2011	40.2	36.5	32.79
8-Apr-2011	35.4	31	29.81
14-Apr-2011	38.2	33.3	30.28
17-Apr-2011	33.2	27.7	24.86
19-Apr-2011	35.3	29	29.42
22-Apr-2011	37.8	34	30.49
24-Apr-2011	36	32.2	26.15

4.1.2 Satellite's corrected Ts

Satellite Ts were used in conjunction with in-situ measured Ts and MC achieved at two depths at surface 5 cm and 10 cm. The values of satellite surface temperature extracted from the images were rectified through applying a linear regression sketch with measured surface temperatures taken in-situ in the same time of images acquisition. Figures 4.2, 4.3 and 4.4 show the relationships between the two surface temperature sets for UTP, Sitiawan and Seberang Perak locations respectively. The resultant corrected Ts was integrated with NDVI and field measured MC in moisture parameters generation as in Equation 2.27 for each of the three split-window Ts. Moreover, all the ground measurements of Ts were synchronized to meet satellites overpass times.

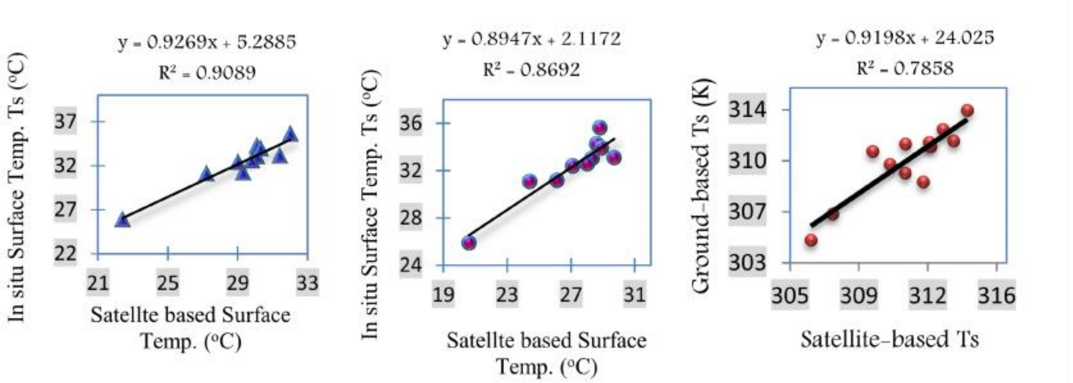

(a) (b) (c)

Figure 4. 2: Correlation of soil Ts measured in-situ and satellite Ts for temperature correction, using split-window techniques at depths (a) 5cm from NOAA, (b) 10 cm from NOAA and (c) MODIS Ts over UTP location.

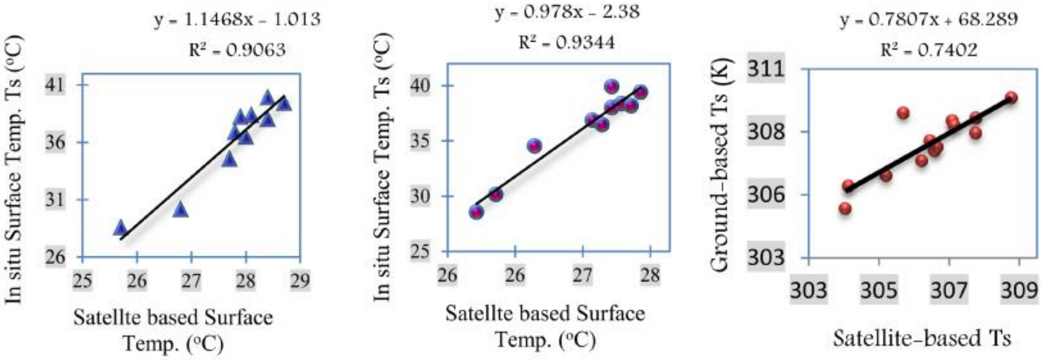

(a) (b) (c)

Figure 4. 3: Correlation of Ts measured in-situ and satellite Ts for Ts correction at depths (a) 5cm from NOAA, (b) 10 cm. from NOAA and (c) MODIS Ts at Sitiawan location.

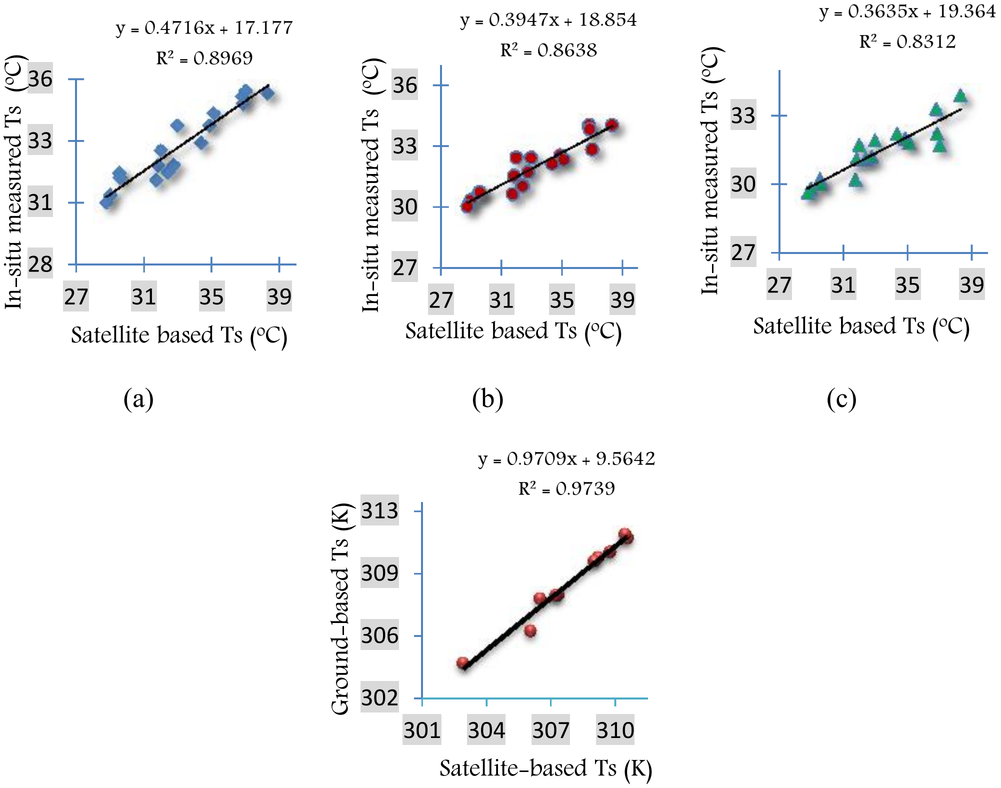

(a) (b) (c)

(d)

Figure 4. 4: Correlation of Ts measured in-situ and satellite Ts for Ts correction at depths (a) 5cm from NOAA, (b) 10 cm from NOAA, (c) 15 cm from NOAA and (d) MODIS Ts over Seberang Perak paddy field.

4.1.3 NDVI-Ts relationship

As a step to examine the accuracy of the split-window technique over different kinds of surface cover, NDVI was plotted against Ts as seen in Figure 4.5. The scaling at figures sides denotes that, all pixels' values are in the range between the 0 and below 400, which is the Ts in the absolute degrees (K) absolute. A robust negative correlation was found between NDVI and Ts particularly over the agricultural area Seberang Perak. This correlation could be attributed to latent heat flux canopy resistance to transpiration together with MC as stated by Smith and Choudhury [252], producing a typical Universal Triangle that was presented earlier by Price [193]. In the Universal Triangle, the vegetation radiometric temperatures are constantly in close proximity to air temperatures; however the surface radiant temperature above uncovered soil may differ with respect to the soil MC. This means that the spatial deviation in surface radiant temperature will probably be little over the full vegetation (aside from emission from underlying bare soil), but can vary from warm to cold when surface moisture availability ranges from zero to one for bare soil.

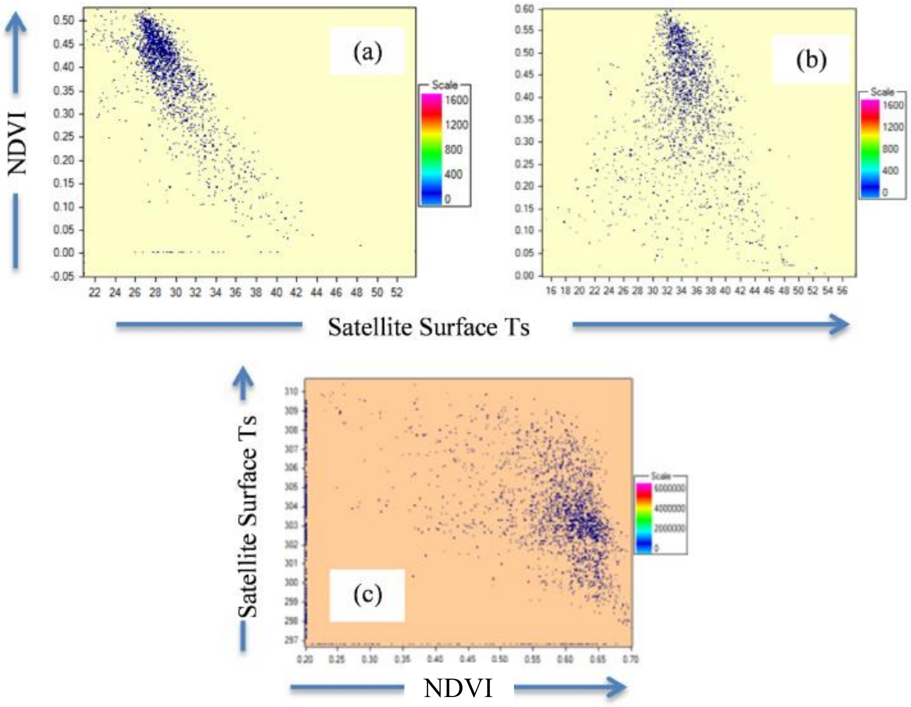

Figure 4. 5: Scatterplot between NDVI and satellite-corrected Ts over the total study area using (a) NOAA 17, (b) NOAA 18 and (c) MODIS Terra.

4.1.4 Discussion

Information about temperature correction in Figures 4.2, 4.3 and 4.4 represented a part of the study's aims, which was directed to rectify the satellite surface temperature that was produced from the diffused emissivity over the study area. Surface temperatures was measured in the fields and correlated with Ts from NOAA and MODIS in order to apply the absolute atmospheric correction for the path radiance removal. This statement confirmed and suggested by Jensen [253]as a method that shares in Ts calibration in optical sensors. As stated by Hemakumara [96] also, land surface temperature depends on factors such as ground cover and soil type. Because satellite-based Ts gives a mixed signature and reflects a combined temperature of soil and vegetation, some kinds of ground truthing which contains measurements of Ts or ε could be used to surpass the vegetation’s signal attenuation. Thus, a linear regression between satellite-based Ts and ground measurements of Ts was conducted the way which could enhance the resultant surface temperature where the temperature from satellites were extracted and unified by the bulk averaging method to enable a good comparison with the point nature of ground Ts measurements.

Additionally, it is hard to produce ground measurements with complex surface components [254-256]. For most pixels, it could be difficult to determine a pixel surface temperature with no consideration of the surface structure inside pixel in case there are significant disparities in the band emissivities and there are significant viewing shadows having a temperature drastically not the same as in other area in the pixel. This was obviously proved by Ts estimated over the urban area comparing to the one that from agricultural field of Seberang Perak.

4.2 Moisture Content

In order to retrieve the surface moisture value, two of the most applicable algorithms namely UT and TI were used based on Ts and VI.

4.2.1 Universal Triangle method

4.2.1.1 Moisture estimation from satellite's-Ts

According to the Universal Triangle, the resultant corrected Ts was used together with integrating NDVI and field measured MC that conducted as daily-based in concurrent time with the satellite's overpass. The process resulted in moisture parameters generation over each of the three locations. Table 4.2 shows the resulted regression approach parameters calculated using Equation 3.2 for multiple surface cover types, urban area and uniform vegetation cover represented by UTP, Sitiawan and Sp. Perak locations respectively.

The polynomial equation of the Universal Triangle which has 9 unknowns (a_1 - a_9), required 9 satellite images with the adjacent field moisture values, and then solved together in a form of array determination.

Figure 4.6 shows the MC maps which were generated via parameters of daily MC measured in-situ at 5 cm and 10 cm depths in conjunction with the acquired NOAA 17 satellite images in overpass times; this map is raster image produced by ArcGIS software in which each pixel represents a value of MC.

Table 4. 2: Moisture Generated Parameters from Universal Triangle Method (normal Ts)

Location	Sensor	Depth (cm)	M C Parameters								
			a_{00}	**a_{10}**	**a_{20}**	**a_{01}**	**a_{02}**	**a_{11}**	**a_{22}**	**a_{12}**	**a_{21}**
UTP	NOAA 17	**5**	0.11	0.42	0.03	-0.13	-0.27	0.33	1.12	2.59	-0.37
		10	-0.09	0.57	-0.04	-0.22	0.61	1.19	-1.66	-0.89	0.53
	NOAA 18	**5**	0.11	0.4	0.2	-0.17	0.16	0.21	-0.43	-0.73	0.48
		10	0.54	-0.35	0.06	-0.19	-0.31	0.18	-0.02	0.45	0.63
SITIAWAN	NOAA 17	**5**	-0.03	0.33	0.03	-0.12	0.07	2.49	2.08	-1.8	-2.9
		10	-0.06	0.46	-0.01	0.18	-0.21	-2.1	2.91	2.62	0.49
	NOAA 18	**5**	0.12	0.52	0.19	-0.19	0.16	0.45	0.87	-0.83	-0.9
		10	0.54	-0.36	0.2	-0.29	-0.24	0.45	-0.03	0.56	-0.26
S. PERAK	NOAA 17	**5**	0.17	0.48	-0.22	-0.16	0.26	-0.43	-0.21	-0.01	-0.71
		10	-0.1	0.56	-0.03	-0.12	0.12	0.86	0.58	-0.03	-0.43
		15	-0.07	0.66	-0.11	-0.21	0.42	0.3	0.55	-0.09	-0.74
	NOAA 18	**5**	0.13	0.37	0.22	-0.2	0.14	0.24	-0.4	-0.83	0.43
		10	0.11	0.18	0.02	0.04	-0.1	0.38	-0.11	0.46	0.57
		15	0.14	-0.61	0.8	-0.21	0.15	2.03	-0.88	-1.05	-0.38

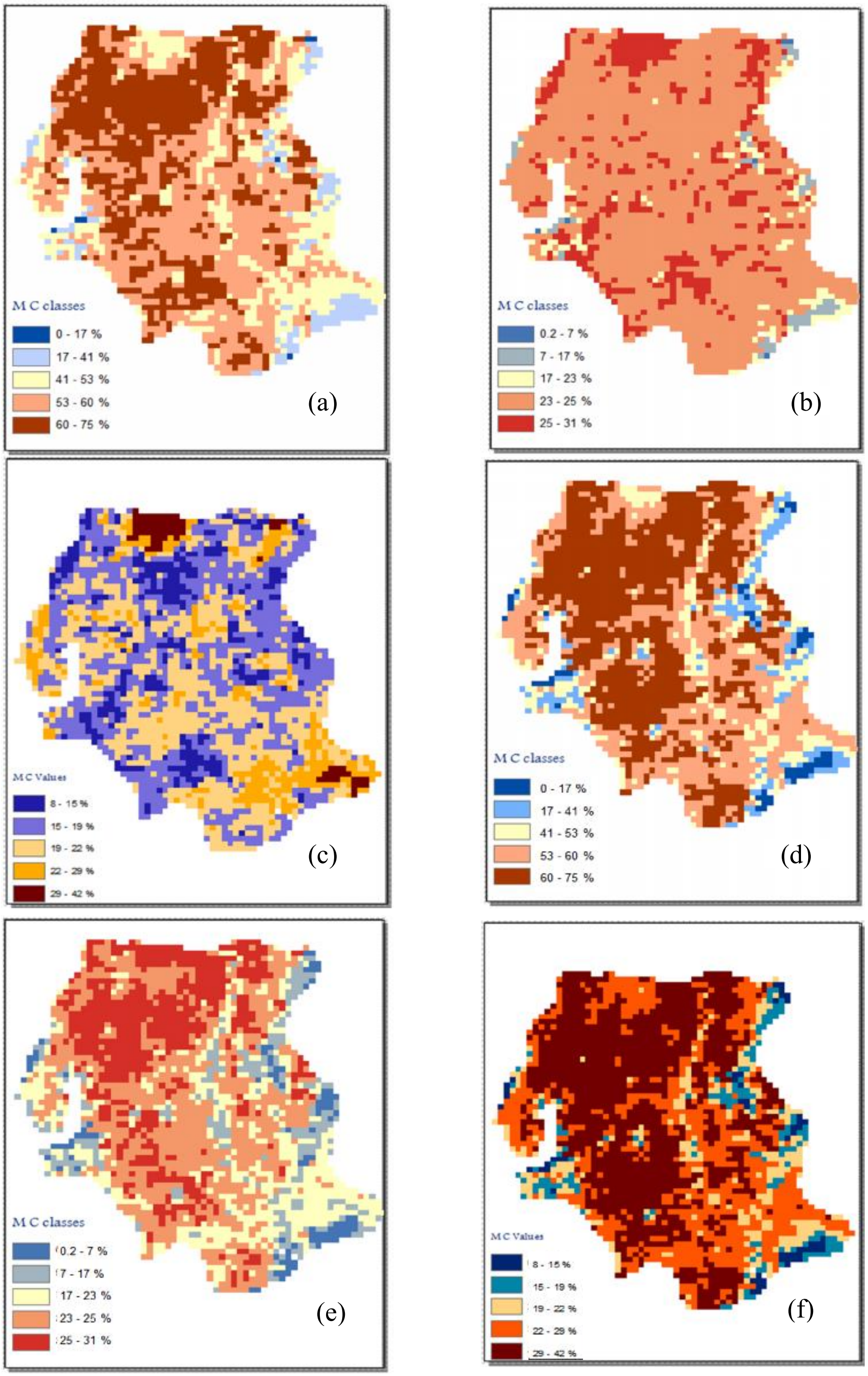

Figure 4. 6: MC generated maps using parameters from (a) UTP at 5 cm, (b) Sitiawan 5 cm, (c) Sp. Perak 5 cm, (d) UTP at 10 cm, (e) Sitiawan at 10 cm and (f) Sp. Perak at 10 cm depths using NOAA 17 Satellite images.

It could be distinguished from the browsed moisture maps that the surface MC is mainly dependent on the temperature quantum, so it decreases with the increase of Ts. This is obvious from the moisture maps that are generated according to the urban area parameters, the higher the surface temperature, the lower are the moisture values. This statement agrees with the general concept of the Universal Triangle in which the surface radiant temperature over the bare soils varies from hot to cold as the moisture status changes from dry to wet [36].

Surface roughness reduces the sensitivity of emissivity to soil moisture variations [96]. This is due to the increase of the apparent emissivity of natural land surfaces, which caused by increased emissions from impervious surfaces, roofing materials and machines over the urban areas causing an obvious reduction in MC over the area. This agrees with the general concept of TI method, which denotes dry soils and rocks always possess a lower thermal inertia while produce a higher diurnal temperature [165, 166].

The contribution of the vegetation was also significant in producing a high MC over the agricultural fields due to its low thermal mass as stated by [12].

4.2.1.2 Moisture Temperature relationship

Since the spatial distribution of MC indicated a high influence from LULC, the study plotted MC against Ts in order to examine the inverse relationship that stated by the UT and TI methods. Figure 4.7 shows scatterplots of the retrieved MC with the surface temperature along the period of measurements in which NOAA 17 images were used over UTP location as an example.

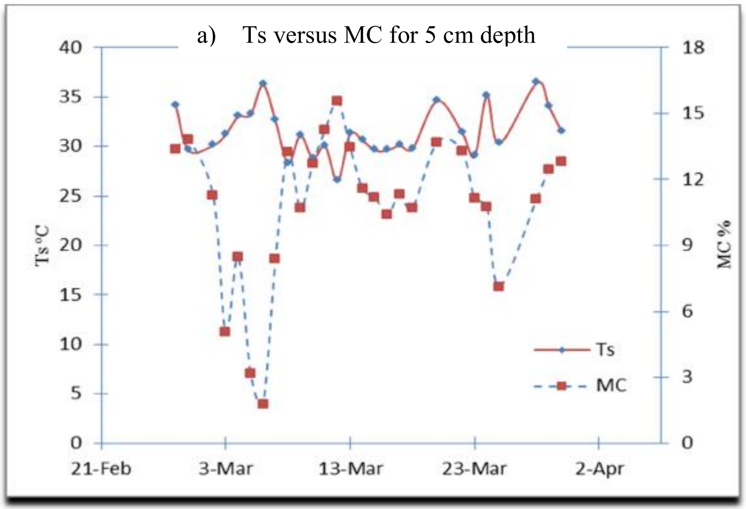
a) Ts versus MC for 5 cm depth

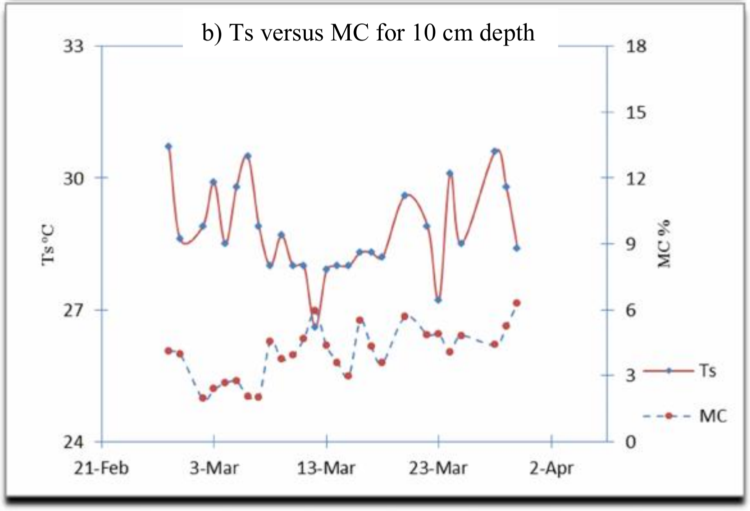
b) Ts versus MC for 10 cm depth

Figure 4. 7: Scatterplots of the retrieved MC with the surface temperature for depths (a) 5 cm and (b) 10 cm at UTP station as an example.

From the scatterplot, it is clear that the surface temperature inversely correlates the MC; this must be attributed to the MC influence in Ts magnitude along with the vegetation cover existence.

4.2.1.3 Moisture estimation from satellite's-corrected Ts

The surface rectified temperatures in turn, produced a new set of parameters when applied to the Universal Triangle method together (integrating) with the NDVI and field measured MC. Table 4.3 shows the resultant surface moisture parameters produced according to each location's measurement condition.

Although the temperature corrected Ts is a simple method to enhance the MC retrieval from space, it involved a better extraction of the surface (5cm) and sub-surface (10 cm) moisture content. Soil moisture variation and distribution over the area showed good compatibilities in terms of the LULC distribution when corrected-Ts was applied. The resultant maps in Figure 4.8 availed concise representations of surface MC distribution over the study area.

When the normal Ts moisture maps compared to their adjacent moisture maps with corrected Ts, it is observed from the status of moisture in these figures (corrected Ts against normal Ts) that the moisture values over all locations are less than those determined by the normal method within the adjacent image date and surface location. This reflects the tendency of normal Ts method to overestimate the moisture values in all LULC classes and this could be justified by the lack of precision in surface emissivity assessment via satellite's thermal bands.

Table 4. 3: MC Generated Parameters from Universal Triangle Method (corrected Ts)

Location	Sensor	Depth (cm)	M C Parameters								
			a_{00}	**a_{10}**	**a_{20}**	**a_{01}**	**a_{02}**	**a_{11}**	**a_{22}**	**a_{12}**	**a_{21}**
UTP	NOAA 17	**5**	0.03	0.44	0.06	-0.17	0.14	-0.87	0.94	0.84	0.23
		10	0.14	-0.61	0.8	-0.21	0.15	2.03	-0.88	-1.05	-0.38
	NOAA 18	**5**	0.18	-0.13	0.43	-0.11	0.25	0.01	-0.43	-0.73	0.48
		10	0.76	-0.1	0.44	-0.64	0.25	0.06	-0.38	-0.86	-0.68
SITIAWAN	NOAA 17	**5**	0.06	0.13	0.11	-0.19	0.07	0.68	0.62	0.48	-0.9
		10	-0.06	0.26	0.16	-0.14	0.1	-0.17	-2.89	4.2	-0.6
	NOAA 18	**5**	0.4	-0.43	0.2	-0.18	-0.11	0.5	0.9	-0.8	-0.65
		10	0.08	0.56	0.2	-0.21	0.14	-0.2	-0.03	0.56	-0.26
S. PERAK	NOAA 17	**5**	0.46	-0.32	0.41	0.19	-0.03	-1.96	-0.06	0.06	0.51
		10	-0.13	0.77	-0.08	-0.12	0.18	0.56	-0.9	0.81	-0.51
		15	0.1	-0.36	0.67	-0.3	0.58	-0.1	0.91	-0.62	0.68
	NOAA 18	**5**	0.13	0.37	0.22	-0.2	0.14	0.24	-0.4	-0.83	0.43
		10	0.11	0.18	0.02	0.04	-0.1	0.38	-0.11	0.46	0.57
		15	0.03	0.44	0.06	-0.17	0.14	-0.87	0.94	0.84	0.23

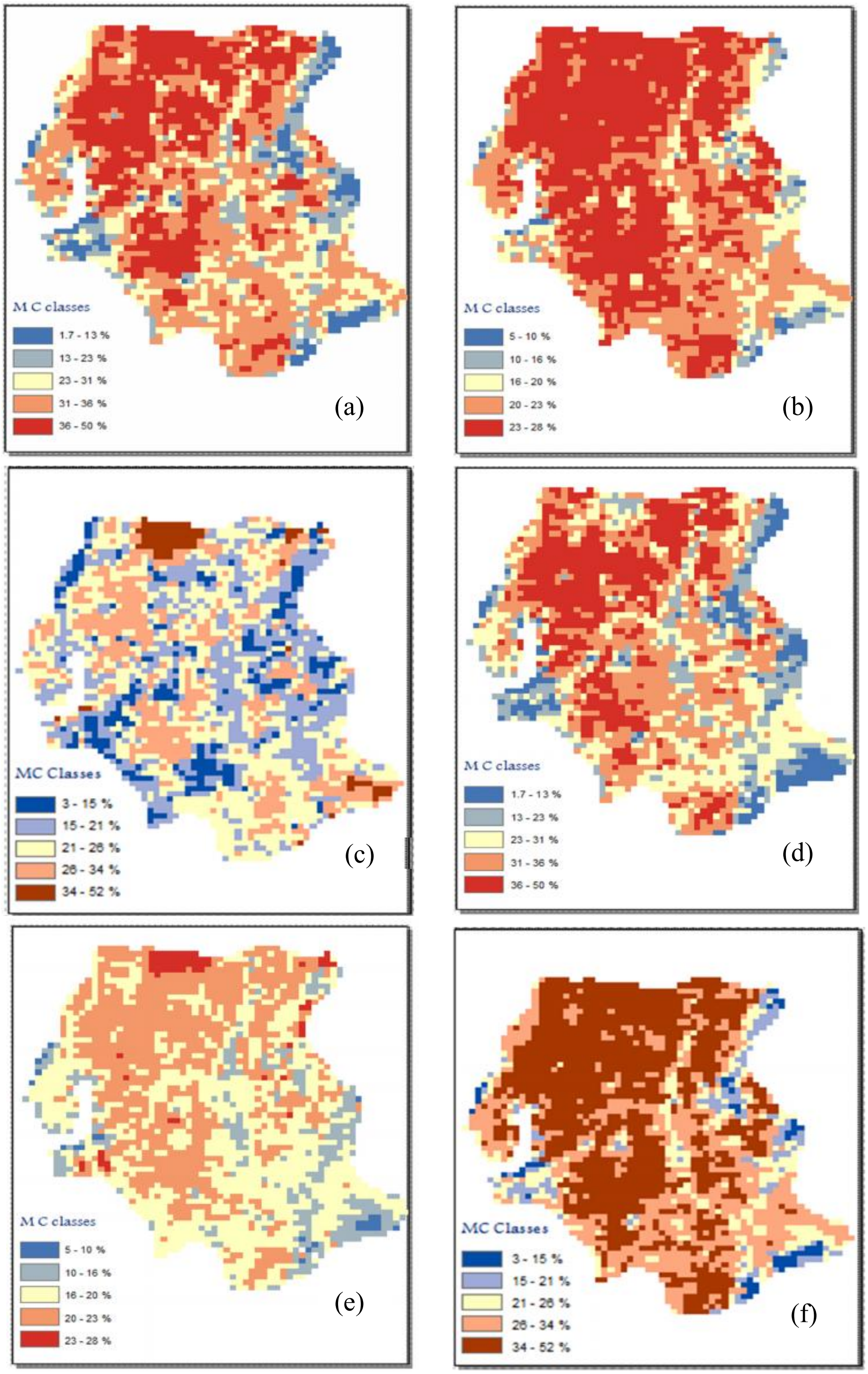

Figure 4. 8: MC maps using corrected-Ts parameters from (a) UTP at 5 cm, (b) Sitiawan 5 cm, (c) Sp. Perak 5 cm, (d) UTP at 10 cm, (e) Sitiawan at 10 cm and (f) Sp. Perak at 10 cm depths using NOAA 17 images.

4.2.1.4 Moisture depth correlation

Moisture connection along the soil strata is a very significant parameter which assists in the study and evaluation of the ground water and water table recharges as well as the assessment of the root zone MC for agricultural crops. The study examined the correlation between the acquired moisture values along the upper soil zone (5cm) and the sub-surface zone (10 cm) as an attempt to avail a threshold study of deep moisture zones, ground water, water table fluctuation studies from optical/thermal microwave remote sensing, which could be quite beneficial for the study of pore water pressure. MC is considered as a basic influencing factor in soil stability in the sloppy areas. Moreover, moisture depths correlation can assist in modelling the hydrological cycle and share in monitoring the infiltration, seepage and even the water deep percolation. Furthermore, it can also assist in the estimation of ground water storage.

Figure 4.9 shows a correlation between the values of satellite's MC at the tested depths 5 cm, 10 cm and 15 cm (for Seberang Perak field only) during the measurements period over the three classes of the study area.

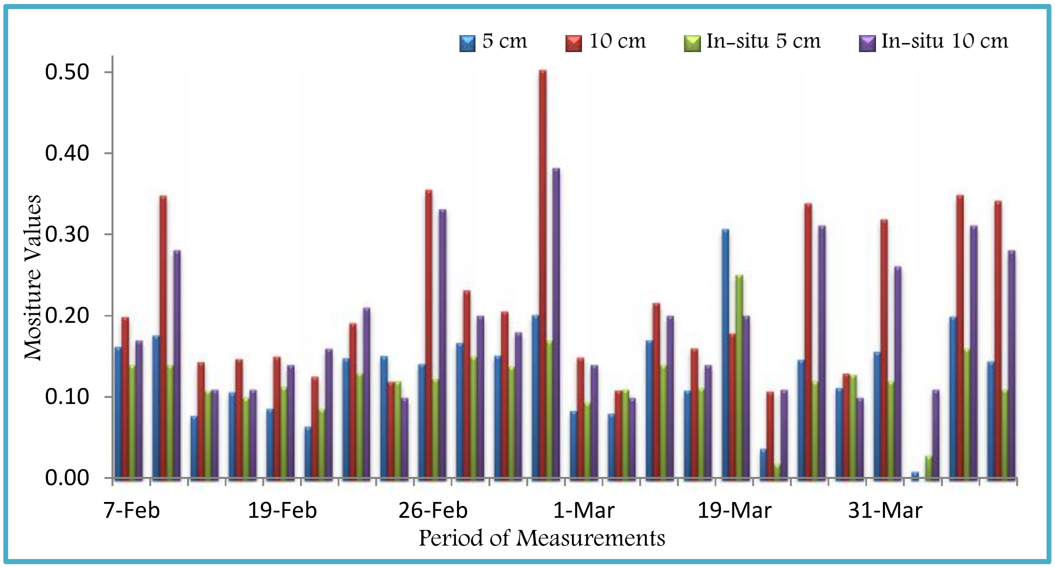

(a)

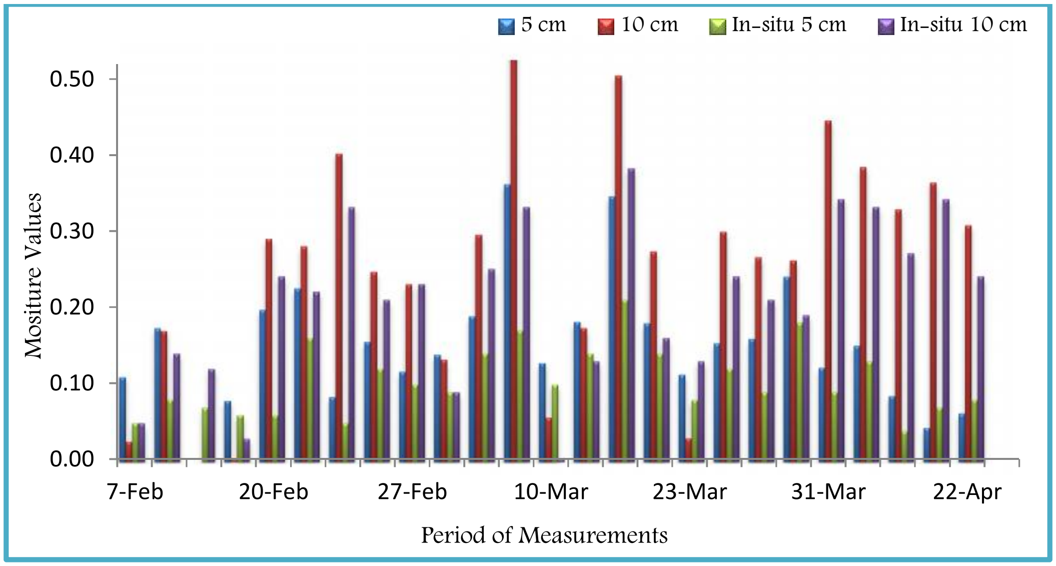

(b)

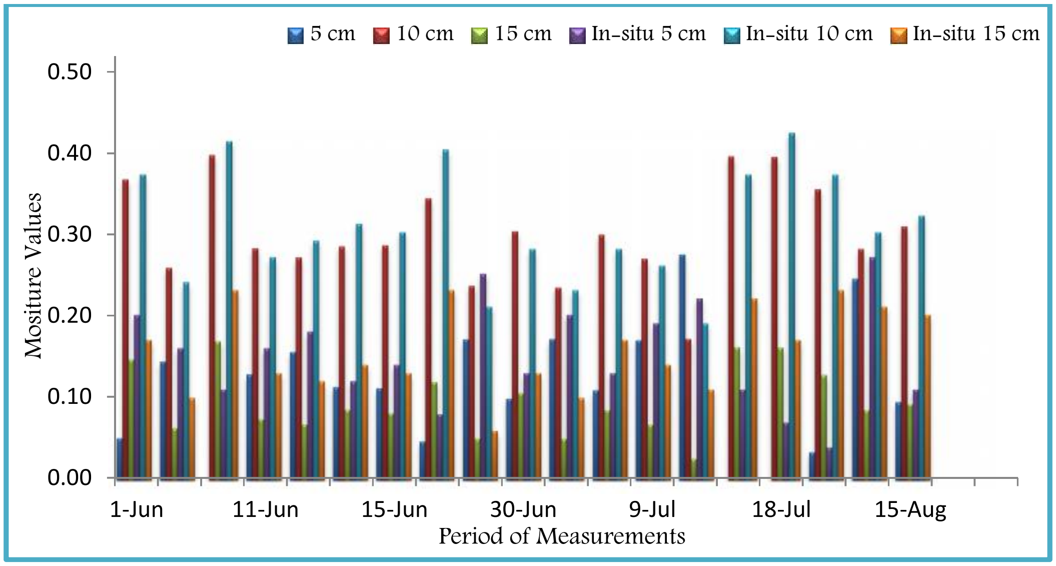

(c)

Figure 4. 9: Correlation among the values of satellite moisture content at different depths of moisture measurements for locations: (a) UTP, (b) Sitiawan and (c) Seberang Perak.

A reasonable behavior is observed along the correlations of moisture at the upper soil layers (5 cm) and the layer section right underneath it (10 cm), while the moisture at 15 cm depth over Sp. Perak paddy field shows upnormality in its values in accordance to the moisture values of 5cm above its level (depth 10 cm). This could be justified as the moisture estimation from optical/thermal satellite images is based fundamentally on the spectral responses of vegetation cover beside the emission from objects which are at the soil surface. It seems hard to assess the status of MC at deeper layers unless some other parameters related to the soil texture; hydraulic conductivity and soil heat flux are taken into account. Because MC when is much deeper than the top several centimeters, cannot be penetrated by current passive remote sensors [154].

4.2.1.5 Moisture estimation from high resolution image

The Universal Triangle algorithm has been applied to two of Landsat images to examine the potentials of Landsat satellites in estimating the surface MC. MC parameters from multi-surface cover were used at two depths of moisture and corrected Ts measurements 5cm and 10 cm as in Figure 4.10 and Figure 4.11.

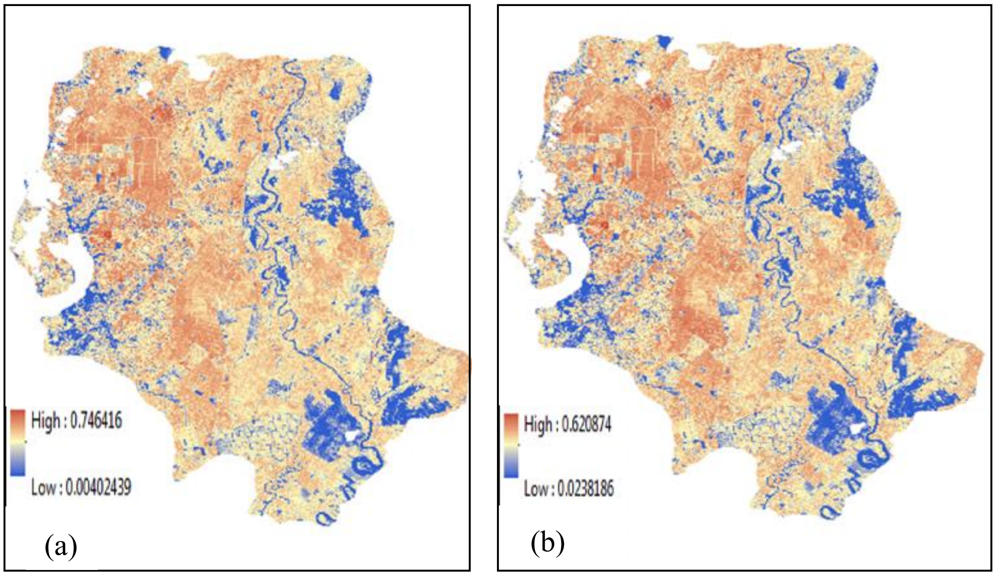

Figure 4. 10: Moisture maps at (a) 5cm and (b) 10 cm depths using Landsat ETM+ acquired in September 19, 2003.

Although the images from Figures 4.10 and 4.11 were acquired on different dates (2003 and 2010), the moisture distribution is resembles in all moisture locations, and this could be seen obviously within Landsat moisture images where the spatial resolution enables the distinction between almost all classes of surface cover in the area. Figure 4.11 shows Landsat images taken in 2010 however; robust moisture resemblance to the previous image could be noticed. This permanent distribution of

MC value is highly justified by the land use/cover influence which based on the diurnal and radiant temperatures impact over the urban and vegetation covers [6].

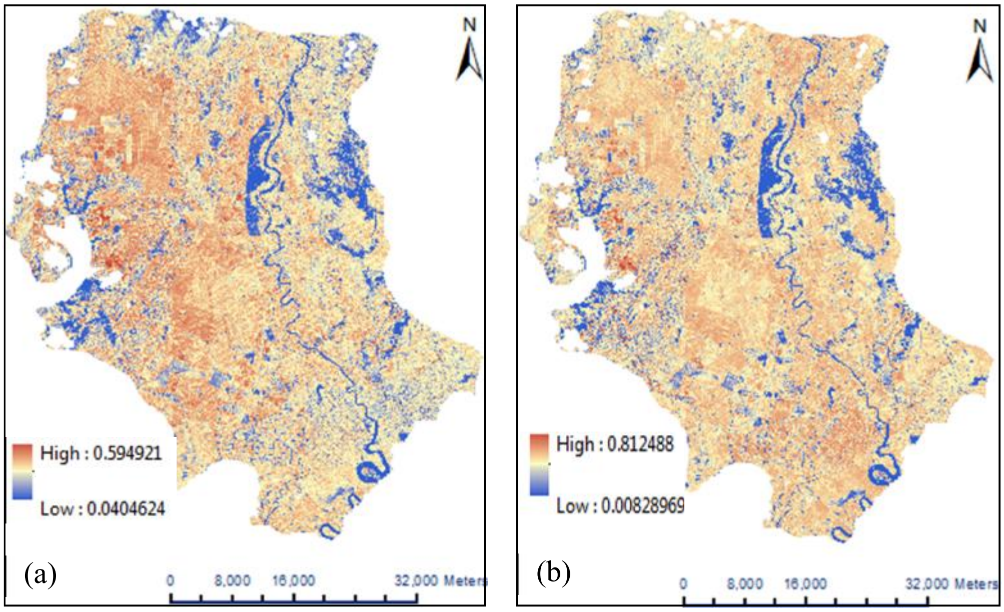

Figure 4. 11: Moisture maps at (a) 5cm and (b) 10 cm depths using Landsat L5 acquired in April 12, 2010.

4.2.2 Thermal Inertia method

The study utilized the Thermal Inertia method (TI) for soil surface moisture (MC) estimation, which is based mainly on two sets of parameters. First, the spatial set, which includes the determination of satellite's surface temperature (Ts) and the vegetation indices (VI). Second, the set of soil parameters which include the determination of soil field capacity (FC) and the permanent wilting point (PWP) as upper and lower boundaries of the soil water capacity respectively. In this study, MODIS (Aqua/Terra) images were used for estimating the spatial set (Ts and NDVI).

In-situ measurements of FC, PWP, TS and MC were conducted over each station at the time of MODIS satellites overpass. As mentioned previously in Universal Triangle method, in order to overcome the atmospheric attenuation, the satellite' Ts was rectified also by field measured values of Ts through regression plots between ground measurements of Ts and satellite's based Ts after averaging the pixel's values to single value. Figure 4.12 shows the correction of satellite's Ts in which resultant linear relationships were then used to assess the corrected Ts.

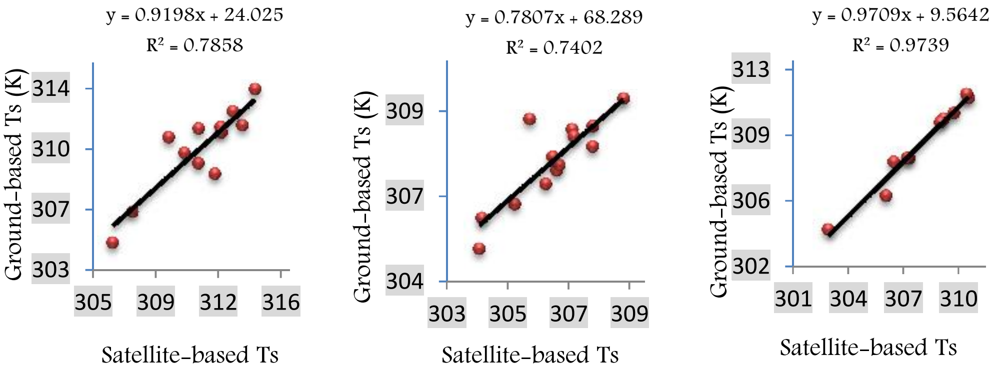

(a) (b) (c)

Figure 4. 12: Correction of satellite's Ts by field measured Ts over (a) UTP, (b) Sitiawan and (c) Sp. Perak.

4.2.2.1 Soil Wetness Index (SWI) estimation

The soil wetness index (SWI) for a given day or time (t), which represents relative surface soil moisture, is described as a fraction of surface temperature as stated in Equation 2.39 in which, the upper and lower surface temperature boundaries were determined from temperature-vegetation triangle. Therefore, Tsi_{max} represented the highest temperature along the dry edge which denotes the driest soil conditions in case of surface wetness is zero, while the wettest conditions were represented by Tsi_{min} which followed the wet edge along the Ts-Vi scatterplot. Samples of this relationship are shown in Figure 4.13.

According to the literature recommendations by Mallick et al. [169], the study used EVI with NDVI as a new vegetation index which is sensitive to leaf area index LAI more than NDVI due to the incorporation of the blue band which was found as respectively accurate in enhancing the vegetation signal with a good sensitivity in higher biomass regions and enhanced vegetation tracking via de-coupling of the canopy background signal in addition to a reduction in environment influences. These two indices were used to represent the dry temperature edge upon their linear relationship that was empirically established between them.

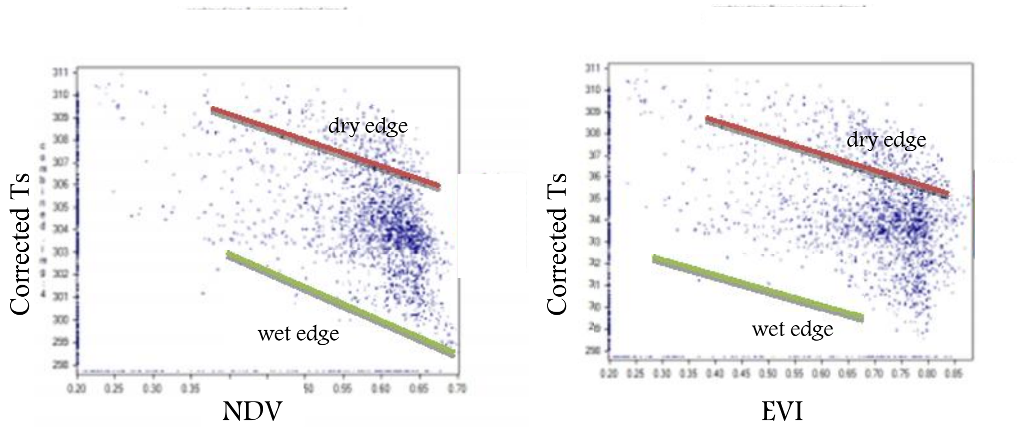

Figure 4. 13: Scatterplot between Corrected-Ts and Vi for SWI estimation (MODIS Terra) based on (1) NDVI and (2) EVI for Sp. Perak area in Aug 11, 2012.

4.2.2.2 Soil moisture boundaries

In order to determine the upper and lower moisture values which are represented in the soil's field (FC) capacity and the permanent wilting point (PWP) respectively, samples were collected from the soil of each type of the surface cover among the three selected partitions of the study area (full vegetated, urban and multi-cover surfaces). A soil classification and aggregation test was conducted to assess the particle sizes distribution of the soil samples (Master-sizer 2000 device) which is a volumetric-based analyzer with sensitivity reaching to 0.001 mm, then soils were classified into three standard groups (sand, silt and clay). Figure 4.14 shows the PSD graph for the soils of the three study area samples achieved by Mastersizer device.

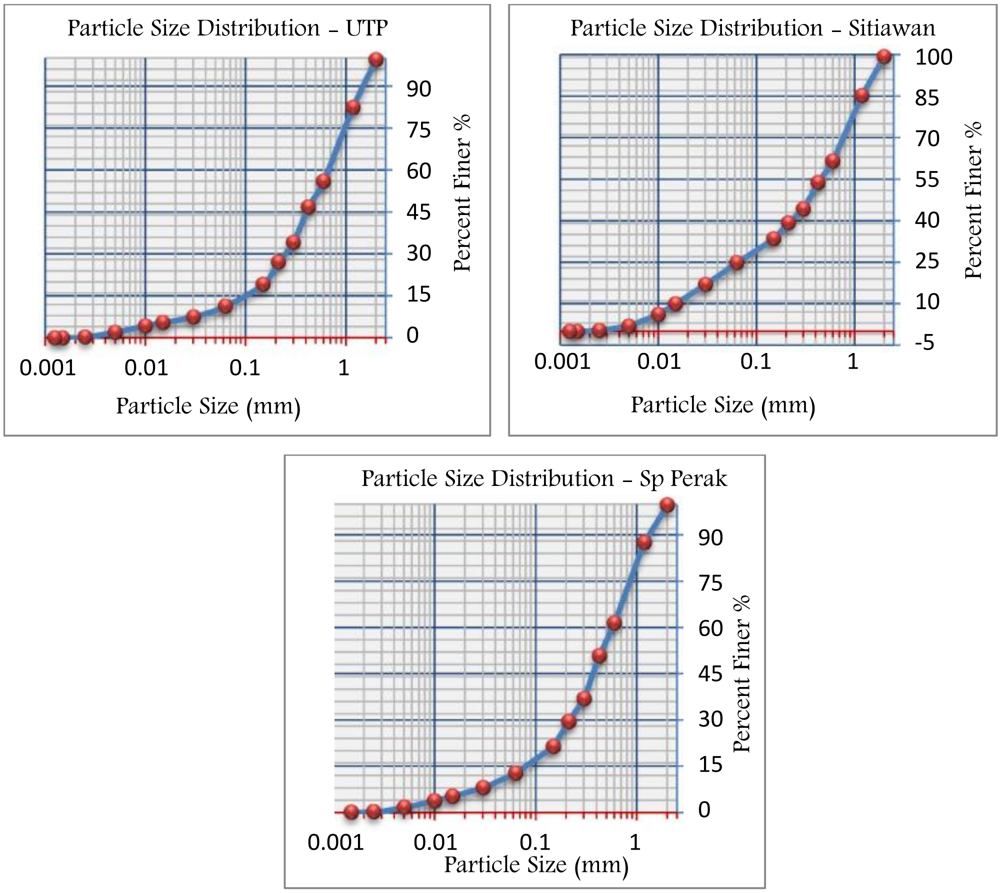

Figure 4. 14: PSD results Analysis of the soil samples of (upper left) UTP, (upper right) Sitiawan and (lower) Seberang Perak fields.

The classification system used for analyzing the soil sample was Unified Soil Classification System (USCS), in which soil is classified as: 76.2 - 4.75 mm (Gravel), 4.75 - 0.075 mm (Sand) and <0.075 mm (Silt and Clays) [257].

To estimate FC and PWP values from soil classes, a hydraulic properties calculator was used to achieve the soil class characterization. This software is an open source based on the physical concept of soil water characteristic triangle produced by (USDA). Table 4.4 shows the resultant soil samples characteristics from the PSD analysis among which, FC and PWP are determined.

Table 4. 4: Soil characteristics extracted from PSD test where FC and PWP were calculated.

	UTP				SITIAWAN				SP. PERAK			
	percent %											
	Passed	Gravel	Sand	Silt & Clay	Passed	Gravel	Sand	Silt & Clay	Passed	Gravel	Sand	Silt & Clay
Passing 4.75 mm	100.000	0.00	86.00	14.00	100.000	0.00	72.50	27.50	100.000	0.00	85.00	15.00
Passing 0.075 mm	14.000				27.500				15.000			
less than 0.075	0.000				0.000				0.000			
Field Capacity %vol.	22.6				27				22.9			
Wilting point % vol.	11.9				17.3				12.3			
Texture Class	Loamy Sand				Sandy Clay Loam				Sandy loam			
Saturation % vol.	46.9				50.9				47.3			
Available water cm/cm	0.11				0.10				0.11			
Sat. Hydraulic conductivity mm/hr	27.65				5.53				23.91			
Bulk density g/cm^3	1.41				1.3				1.4			

4.2.2.3 Soil moisture maps from NDVI & EVI

According to Equation 2.41, volumetric MC was extracted finally from thermal inertia method over the study area using daily MODIS (Aqua/Terra) images accompanied with the soil characteristics that were determined by PSD test. All these processes were performed in terms of point-based applications. Figure 4.15 shows the resultant volumetric MC's maps of the study area using SWI generated from both NDVI and EVI with different limits of moisture boundaries FC & PWP varying according to the soil class of each location. This variation yielded three moisture maps of the study area with different moisture value and spatial distribution.

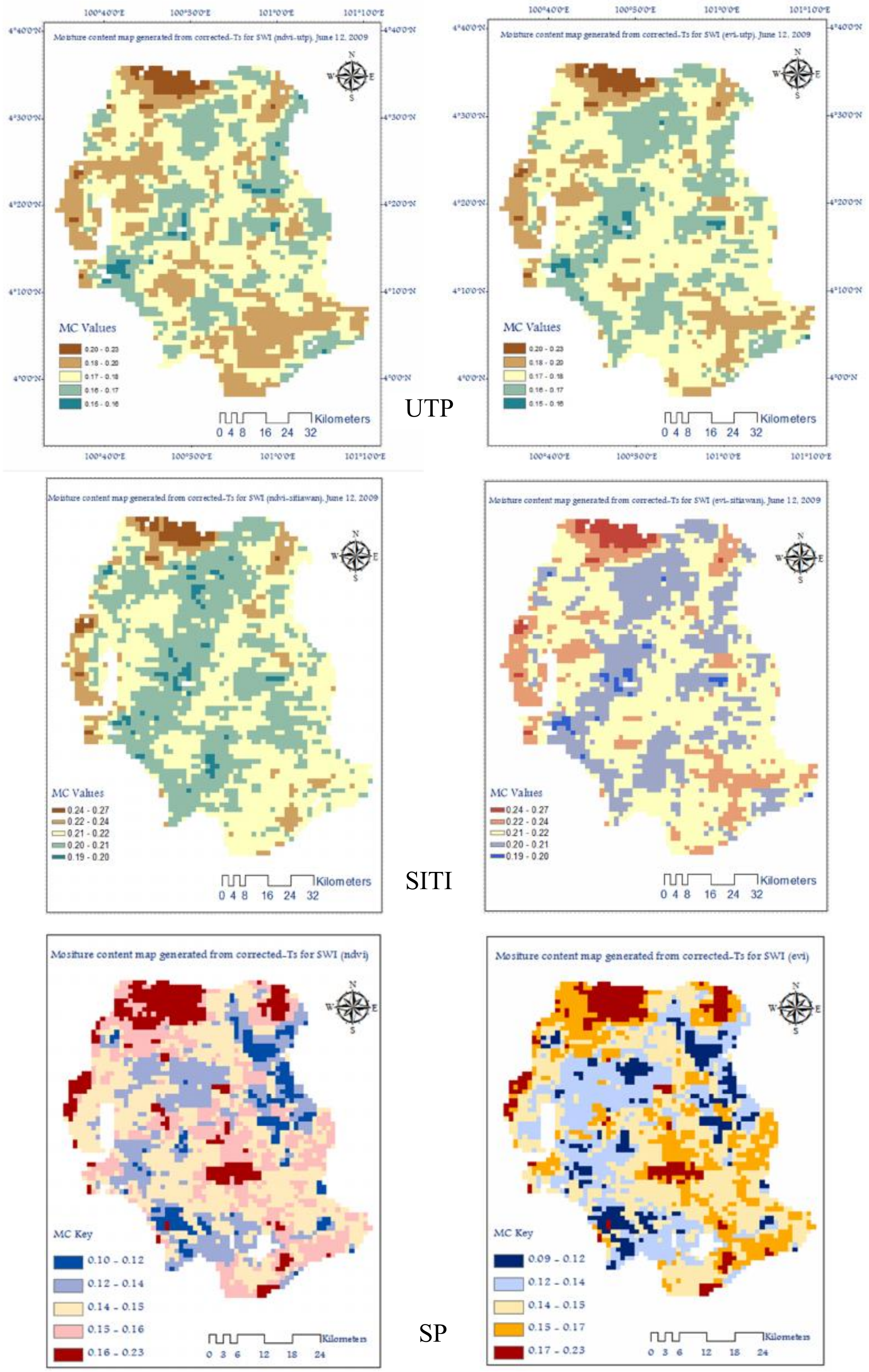

Figure 4. 15: Generated volumetric moisture maps with SWI based on NDVI (left) and EVI (right) over UTP, Sitiawan and Sp. Perak locations.

It is evident from all of the generated moisture maps that, the vegetated areas within the study area are most likely to carry much MC than the buildup areas as well as the bare soils. This could be seen most obviously in the agricultural fields whose area is covered with vegetation that is uniformly growing.

In all these sensors, the least moisture value has been noticed mainly over the built up areas or areas with impervious surfaces. It could be justified as the soil is mostly covered by cemented materials, roofing areas and asphalt layers which retain the excess water to go inside the soil underneath them. Furthermore, all these surface cover elements attached with drainages system that covey the rainfall water away before reaching the soil beneath these covers.

On the other hand, the high moisture value which is found to be equal to 0.86 when a high resolution images used (Landsat), has been noticed over the uniform green areas in all scenes. Mainly, the highest moisture values are located to the agricultural schemes which cover specifically Seberang Perak beside some other distributed locations covered by vegetation. This could be justified as follows:

- As mentioned earlier the excess water to the soil over built up areas is very seldom and rare because their surface is mostly impervious as well as the presence of the drains which are embedded along the built up areas.

- Moisture content over the built up areas is easily lost by evaporation because the surface is exposed to the direct sun illumination, wind and most of the weathering elements, while soils under the vegetated areas are shadowed by the leaves against the sun impact and weathering effects so that moisture can remain longer and maintained in large quantity.

- In the study of surface moisture-temperature relationship, its agreed that, the built up areas always have a higher surface temperature than vegetative ones, due to the up-willing emission from the asphalted surfaces roofing and etc. which causes reduction in surface moisture values, while in the vegetative areas, the surface temperature is relatively low allowing high moisture values as in [130].

From the spatial patterns and distribution of the soil MC of the two satellites (NOAA & MODIS) it can be observed that in almost all images moisture showed close resemblance with slight differences in moisture values and distribution and this change is also justifiable because:

- The overpassing time for NOAA 17 for example (10:00 -10:30 AM) is a bit earlier than MODIS Terra (10:45 -11:30 AM) at the study area's local time so this is considered as adequate time for surface moisture to get fluctuated, and mostly the earlier overpassing sensors measure the higher moisture values in case of no rainfalls between the two satellite's times.

- The spatial scale of MODIS optical bands which are being used for NDVI and EVI estimation (RED: 250 m, NIR: 250m, BLU: 500m) have their own influence on vegetation spectral signature and more accurate in representing the vegetation cover of any surface than NOAA optical bands which have a spatial resolution of 1.1 Km for all bands. This could add some advantages to MODIS image along the extraction of any surface parameter that requires the estimation of vegetation cover.

The Thermal Inertia method carries soil sampling process which means the incorporation of soil hydraulic properties in the assessment of the surface moisture. This would definitely add more dimensions in the moisture estimation method making it close to the measured value than predicted one.

With the large ground cover of every AVHRR or MODIS pixel (almost 1 km^2), the assumption is that, there is no homogeneity throughout each area equivalent to a satellite measurement. Mainly, every single area could be a mixture of vegetation, wet soil and dry soil. The surface moisture detected by satellite can also be considered as a combination of the high, moderate and low moisture values in correspondence to the surface cover type.

4.2.2.4 Moisture weighted map

The concept of the MC weighted map derivation is based fundamentally on an estimation of a pixel-based MC value over the three variable surface cover locations using one input satellite image.

Below are excerpt examples of the MC maps which were extracted as a result of the correlation between the 3 different land covers tested earlier in the study which are: the urban areas represented by Sitiawan station, the agricultural area represented by Seberang Perak paddy field and the multiple surface cover represented by UTP station. In these relationships, the weightage values of the three MC parameters were used to simulate the percentage of each surface cover among the three types within a single pixel. This was justified earlier in both satellites NOAA and MODIS which were used in this study, have relatively coarse resolutions (almost 1.0 Km) compared to the other optical sensors (Landsat, IKONOS, SPOT etc..) so that the possibility of including the three types of surface cover in a single image's pixel is surely high because of the random distribution of LULC along the study area. Figures 4.16 and 4.17 represent the moisture weighted maps from NOAA 17 and MODIS Terra satellites generated using the weightage pixel's share as described in Chapter Three.

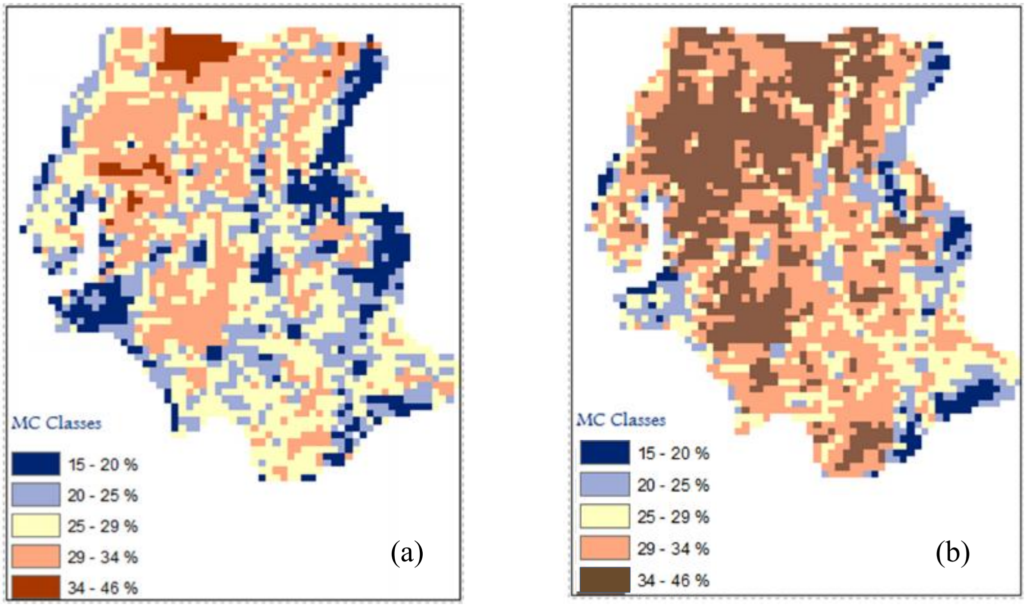

Figure 4. 16: The MC weighted maps generated from the 3 location's correlation using NOAA 17 image for Ts correction depths (a) 5 cm and (b) 10 cm.

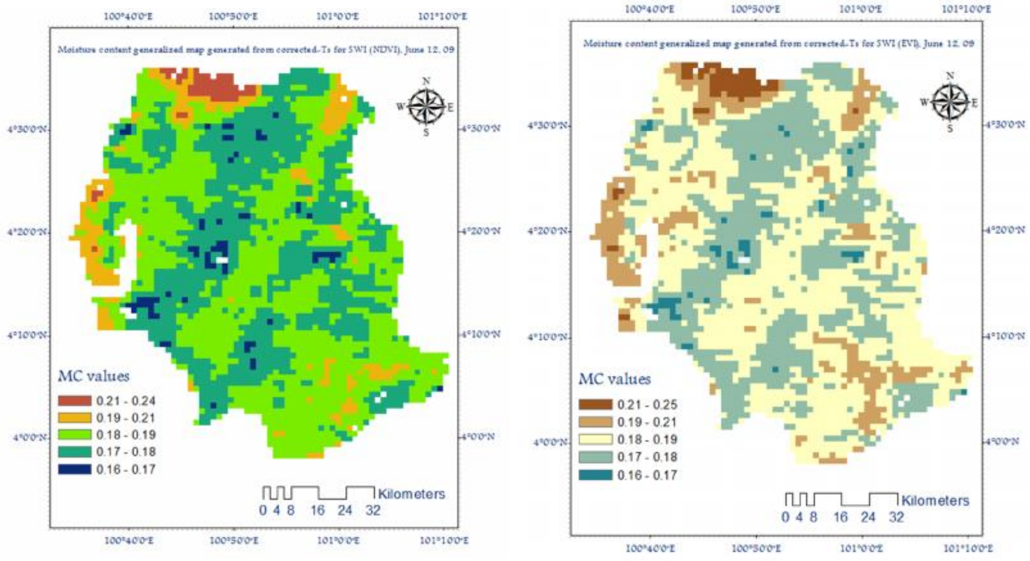

Figure 4. 17: The MC weighted maps generated from the 3 location's correlation using MODIS Terra for Ts correction depth and SWI of (left) NDVI and (right) EVI.

The MC weighted maps from NOAA/AVHRR did not show abrupt differences in the MC values along the 5 cm and the 10 cm depths in Figure 4.16, which indicate the tied correlation between the two depths of MC. However, the low MC distribution at the surface (5 cm) shows wider ranges of extension and dominancy over the urban areas and the fallow lands classes as a result of the high Ts allocation. The maps also showed a reasonable connection with a high significance between moisture estimated over the agricultural land of Seberang Perak and its in-situ measurements. That must be attributed to the uniformity of the vegetation cover represented in the cultivated crops which tend to reduce the Ts values producing a relatively high SWI over the entire area. On the other hand, a moderate relationship was found between the two sets of MC over Sitiawan area (built up area). This is certainly because soils at the urban areas get impervious due to compaction caused by traffics and human beings. Moreover, the third part which is occupied by partial vegetation cover shared with scattered patches of agricultural fields beside some residential areas producing a significant correlation along the distributed surface covers.

The MC weighted maps generated from MODIS's NDVI and EVI produced resemble MC values variation distribution along the study area. This gives a good advantage to the use of EVI as a moisture estimator from LAI and does not produce a moisture value more than the expected due to its partial contribution within the pixel.

4.2.2.5 Moisture content validation

In this research, three types of validations were used on MC assessed values. The first one was statistical validation, which was applied to the simulated point measurements of MC, where the Statistical Package of Social Sciences SPSS Software application was used. Another set was an experimental validation, whereas the satellite's MC values were plotted against the in-situ moisture values in terms of point measurements. Satellite MC was extracted from the portion of images that reserved for the validation. The third type was a spatial validation for the pixel-based estimations of MC, which was accomplished via success rate technique.

Table 4.5 shows the statistical validation of the estimated moisture values, corrected-Ts images and MC measured in-situ, considering the deviation in Ts, moisture depths of measurement and the differences in locations using SPSS 20.It could be expressed from Table 4.5 that, the MC correlation between the two sets (in-situ and satellites) measured at depth 10 cm produce R^2 higher than the one that is measured at the surface (5 cm). This is justified as that, because the MC statement at the surface is always pending to a rapid change due to its exposure to the atmospheric and evapotranspiration effects [6]. Specially, there is always a mal-synchronization between field measurements and image capturing times.

The validation of UT algorithm produced R^2 reached 0.95 for MC at 10 cm depth with very high correlation significances. On the other hand, TI method produced high accuracies with coefficient equal to 0.90 for MC generated from EVI and 0.81 for MC generated from NDVI. From the analysis of the vegetation indices it was confirmed that, EVI captures a higher LAI than NDVI which leaded to a better correlation of MC with the true values as state in Wanger [95]. In order to examine the accuracy of the proposed MC weighted method, moisture maps generated by NOAA 17 and 18 images over the different surface cover classes were compiled together according to their weightage and then correlated with the actual MC.

Table 4. 5: Validations of the retrieved MC (rectified Ts) maps over the study area using SPSS.

	measurement	Descriptive		Correlation					
		Mean	Std. Deviation	In-situ measured moisture content at depth 5 cm	Sig. (2-tailed)	In-situ measured moisture content at depth 10 cm	Sig. (2-tailed)	In-situ measured moisture content at depth 10 cm	Sig. (2-tailed)
UTP NOAA sat.	In-situ measured MC at depth 5 cm	0.12	0.04						
	In-situ measured MC at depth 10 cm	0.19	0.08						
	Satellite corrected-Ts MC at 5 cm	0.13	0.06	0.94	0.000000				
	Satellite corrected-Ts MC at 10 cm	0.21	0.11			0.95	0.000000		
UTP MODIS	In-situ measured MC	0.16	0.02						
	Corrected-Ts MC with SWI generated from (NDVI)	0.16	0.02	0.811 **	0.001376				
	Corrected-Ts MC with SWI generated from (EVI)	0.16	0.02	0.9 **	0.000066				
SITI. NOAA sat.	In-situ measured moisture content at depth 5 cm	0.10	0.05						
	In-situ measured MC at depth 10 cm	0.21	0.10						
	Satellite corrected-Ts MC at 5 cm	0.15	0.08	0.768 **	0.000005				
	Satellite corrected-Ts MC at 10 cm	0.25	0.15			0.902 **	0.000000		
SITI. MODIS sat	In-situ measured MC	0.10	0.01						
	Corrected-Ts MC with SWI generated from (NDVI)	0.21	0.01	0.663 *	0.013553				
	Corrected-Ts MC with SWI generated from (EVI)	0.21	0.01	0.681 *	0.010429				
S. Perak NOAA sat.	In-situ measured MC at depth 5 cm	0.16	0.05						
	In-situ measured MC at depth 10 cm	0.31	0.07						
	In-situ measured MC at depth 15 cm	0.16	0.05						
	Satellite corrected-Ts MC at 5 cm	0.11	0.08	0.811 **	0.000026				
	Satellite corrected-Ts MC at 10 cm	0.30	0.06			0.942 **	0.000000		
	Satellite corrected-Ts MC at 15 cm	0.10	0.04					0.76 **	0.0002
S. Perak MODIS sat	In-situ MC content	0.20	0.01						
	Corrected-Ts MC with SWI generated from (NDVI)	0.13	0.04	0.887 **	0.000276				
	Corrected-Ts MC with SWI generated from (EVI)	0.13	0.04	0.71 *	0.014400				
	**. Correlation is significant at the 0.01 level (2-tailed).								
	*. Correlation is significant at the 0.05 level (2-tailed).								

Tables 4.6 and 4.7 show a comparison between MC values generated from parameters of individual locations versus field measured MC of the same location at the two measurements depths 5 cm and 10 cm. Furthermore, weighted MC values were generated and validated by the average ground-measured MC of the three locations. Although the correlation accuracy between each specific location and its corresponding spatial MC parameter is high, the weighted MC value produced accuracies considered the best when the MC from the three locations is incorporated.

Table 4.6 comparison between MC from individual locations and the weighted values for measurements depth 5 cm.

periods		Sensor	MC from Satllite Images				MC from Field Measurements			
			Parameters Location			Weighted MC	Location of Measurement			Average MC
			UTP	Sitiawan	S. Perak		UTP	Sitiawan	S. Perak	
JUNE	1-Jun	NOAA 18	0.16	0.11	0.05	0.13	0.14	0.05	0.20	0.13
	6-Jun		0.18	0.17	0.14	0.17	0.14	0.08	0.16	0.13
	8-Jun		0.08	0.06	0.10	0.08	0.11	0.07	0.11	0.10
	11-Jun		0.11	0.08	0.13	0.11	0.10	0.06	0.16	0.11
	12-Jun		0.09	0.20	0.16	0.16	0.11	0.06	0.18	0.12
	14-Jun		0.06	0.22	0.11	0.17	0.09	0.16	0.12	0.12
	15-Jun		0.15	0.08	0.11	0.12	0.13	0.05	0.14	0.11
	21-Jun		0.15	0.16	0.05	0.14	0.12	0.12	0.08	0.11
	29-Jun		0.14	0.12	0.17	0.15	0.12	0.10	0.15	0.12
	30-Jun		0.17	0.14	0.10	0.14	0.15	0.09	0.16	0.13
JULY	4-Jul		0.15	0.19	0.17	0.17	0.14	0.14	0.20	0.16
	5-Jul		0.20	0.36	0.11	0.27	0.17	0.17	0.13	0.16
	9-Jul		0.08	0.13	0.17	0.14	0.09	0.10	0.19	0.13
	13-Jul		0.08	0.18	0.27	0.21	0.11	0.14	0.22	0.16
	17-Jul		0.17	0.34	0.11	0.26	0.14	0.21	0.11	0.15
	18-Jul		0.11	0.18	0.06	0.14	0.11	0.14	0.07	0.11
AUGUST	8-Aug		0.31	0.11	0.03	0.24	0.28	0.08	0.04	0.13
	10-Aug		0.04	0.15	0.24	0.19	0.02	0.12	0.27	0.14
	15-Aug		0.15	0.16	0.09	0.14	0.12	0.09	0.11	0.11
Average			0.14	0.17	0.13	0.16	0.13	0.11	0.15	0.13
Standard Deviation			0.06	0.08	0.06	0.05	0.05	0.04	0.06	0.02
Correlation Coeff. R										
UTP			0.88	0.01	-0.57	0.63				
Sitiawan			0.001	0.69	0.03					
S. Perak			-0.3	0	0.63					

For the weighted MC at depth 5 cm, the validation produced accuracy of 0.63 while weighted MC at depth 10 cm produced accuracy of 0.77. These correlation accuracies produced by the weighted MC give a good representation of MC statement over the whole study area despite of the disparity in surface cover. Thus, a reasonable simulation of the surface cover classes within the image's pixel in the coarse resolution images is also produced.

Table 4.7 comparison between MC from individual locations and the weighted values for measurements depth 10 cm.

periods		Sensor	MC from Satllite Images				MC from Field Measurements			
			Parameters Location			Weighted MC	Location of Measurement			Average MC
			UTP	Sitiawan	S. Perak		UTP	Sitiawan	S. Perak	
JUNE	1-Jun	NOAA 18	0.20	0.03	0.36	0.29	0.17	0.05	0.37	0.20
	6-Jun		0.35	0.17	0.26	0.28	0.28	0.14	0.24	0.22
	8-Jun		0.14	0.13	0.39	0.29	0.11	0.12	0.41	0.21
	11-Jun		0.15	0.00	0.28	0.23	0.11	0.03	0.27	0.14
	12-Jun		0.15	0.29	0.27	0.25	0.14	0.24	0.29	0.22
	14-Jun		0.13	0.28	0.28	0.25	0.16	0.22	0.31	0.23
	15-Jun		0.19	0.40	0.28	0.32	0.21	0.33	0.30	0.28
	21-Jun		0.12	0.25	0.34	0.27	0.10	0.21	0.40	0.24
	29-Jun		0.35	0.23	0.24	0.28	0.33	0.23	0.21	0.26
	30-Jun		0.23	0.13	0.30	0.24	0.20	0.09	0.28	0.19
JULY	4-Jul		0.21	0.29	0.23	0.25	0.18	0.25	0.23	0.22
	5-Jul		0.50	0.55	0.30	0.48	0.38	0.33	0.28	0.33
	9-Jul		0.15	0.06	0.27	0.21	0.14	0.00	0.26	0.13
	13-Jul		0.11	0.17	0.17	0.16	0.10	0.13	0.19	0.14
	17-Jul		0.22	0.50	0.39	0.41	0.20	0.38	0.37	0.32
	18-Jul		0.16	0.27	0.39	0.31	0.14	0.16	0.42	0.24
AUGUST	8-Aug		0.18	0.03	0.35	0.28	0.20	0.13	0.37	0.23
	10-Aug		0.11	0.30	0.28	0.26	0.11	0.24	0.30	0.22
	15-Aug		0.34	0.27	0.31	0.31	0.31	0.21	0.32	0.28
Average			0.21	0.23	0.30	0.28	0.19	0.18	0.31	0.23
Standard Deviation			0.10	0.15	0.06	0.07	0.08	0.10	0.07	0.05
Correlation Coeff. R										
UTP			0.92	0.17	-0.01	0.77				
Sitiawan			0.1	0.88	0.001					
S. Perak			-0.07	0	0.88					

It is also observable from the validation table that, he spatial MC correlates the ground measured MC best at measuring depth 10 cm (R^2 0.92 for UTP, 0.88 for Sitiawan and 0.88 for Seberang Perak) as it seen in Table 4.7. For MC at the roots zone, it has been unable to apply the weightage algorithm because MC measurements at depth 15 cm were conducted only at Seberang Perak paddy field.

Both MODIS Terra and Aqua images were also used for validating the Thermal Inertia algorithm over the whole study area parts incorporating the two values of SWI in moisture extraction (NDVI and EVI). Figures 4.18 represents an example of the experimental validation for UTP station in which, the moisture from UT from NOAA 17 satellite was validated by the in-situ data of MC at depths 5m and 10 cm. Figure 4.19 on the other hand, represents the MC from TI algorithm from MODIS satellite validated by in-situ measurements of MC where, the SWI from both NDVI and EVI was used. The full validation figures are placed in Appendix (G-2).

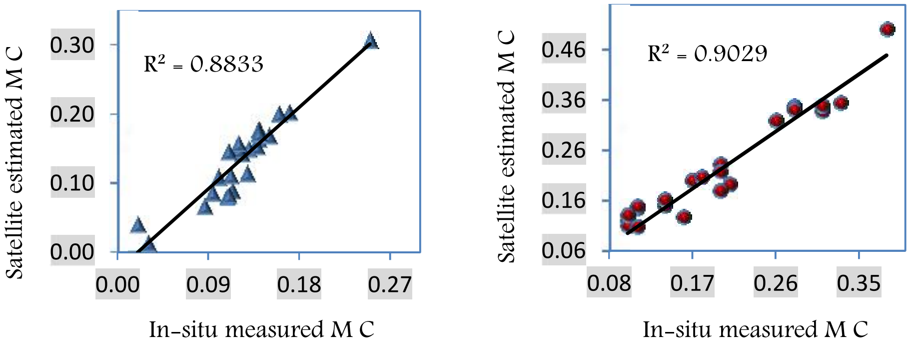

Figure 4. 18: Graphical representations of UTP moisture Validation using UT method from NOAA 17 at depths (left) 5cm and (right) 10cm.

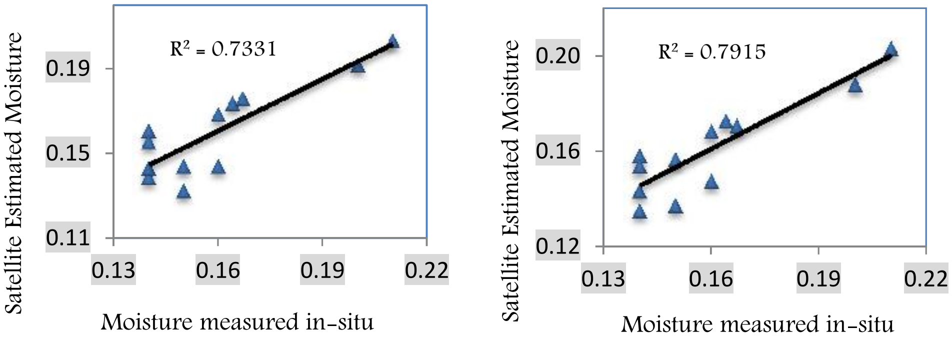

Figure 4. 19: Graphical representations of UTP moisture Validation using TI method from MODIS Terra for SWI based on (left) NDVI and (right) EVI.

4.2.2.6 Propagation of error

Base on the method described in sections 3.8.1.2 and because each measurement has an uncertainty about its mean [154], the study tended to calculate the error in the spatially assessed MC from the mean values of Ts and NDVI over each location. Tables 4.8 and 4.9 show the resultant absolute error (δ) that propagated from the UT and TI moisture algorithms using the three location's parameter for MC extraction.

Table 4.8 Error propagation estimation for UT algorithm.

Location	Depth of measurements 5 cm						Depth of measurements 10 cm					
	NDVI		Ts (K)		MC		NDVI		Ts (K)		MC	
	avg.	Error (δ)	avg.	Error (δ)	avg.	Error Propagated(δ)	avg.	Error (δ)	avg.	Error (δ)	avg.	Error Propagated(δ)
UTP	0.37	0.11	302.16	5.42	0.13	0.04	0.37	0.11	302.16	5.42	0.22	0.07
Sitiawan	0.37	0.11	304.02	5.28	0.16	0.05	0.37	0.11	304.02	5.28	0.26	0.08
S. Perak	0.28	0.10	305.57	4.50	0.13	0.05	0.28	0.10	305.57	4.50	0.30	0.11

Table 4.9 Error propagation estimation for TI algorithm.

Location	Depth of measurements 5 cm						Depth of measurements 10 cm					
	NDVI		Ts (K)		MC		NDVI		Ts (K)		MC	
	avg.	Error (δ)	avg.	Error (δ)	avg.	Error Propagated(δ)	avg.	Error (δ)	avg.	Error (δ)	avg.	Error Propagated(δ)
UTP	0.51	0.28	309.41	2.76	0.16	0.09	0.55	0.10	309.41	2.76	0.16	0.03
Sitiawan	0.57	0.05	307.51	1.08	0.21	0.02	0.63	0.11	307.51	1.08	0.21	0.04
S. Perak	0.55	0.08	308.22	2.33	0.13	0.02	0.59	0.11	308.22	2.33	0.13	0.02

A reasonable estimates of MC errors that were produced by the by the analysis of the uncertainty propagation. In UT method, the least MC errors were observed from MC parameters extracted at depth 5 cm (surface) which assured the direct influence of Ts on the quantification of MC. While, MC at depth 10 cm produced error reaches 11% when the error in Ts be around 4.5^{o} K. on the other hand, the TI method from MODIS satellite tended to generated MC errors within a homogeneous range in accordance to the Ts fluctuation. It was found that, the highest error in Ts assessment which was 2.76^{o} K over UTP location, can lead to an error of 9% of MC assessment. In all cases, it was noticed that, the temperature over the uniform vegetation cover of Seberang Perak has the uncertainty of MC estimation. This must be due to the robust triangular relationship between Ts, MC and vegetation cover as stated by Moran [12].

4.2.2.7 Spatial validation

The success rate was used as a spatial validation method in the study, which was applied to the moisture weighted maps by comparing the highest/lowest MC zone with the adjacent MC with different image (image from different satellite). The success rate curves were created and the areas under the curve were calculated. The rate explains how well the highest/lowest moisture values meet each other on accuracy qualitatively [249]. To obtain the relative ranks for each prediction pattern, the calculated index values of all cells in the study area were sorted in descending order using Quantile Classification task in ArcGIS environment. Then the ordered cell values were divided into 100 classes, with accumulated 1% intervals and characterized as base moisture map represented by MODIS Terra image captured in June 12, 2009. The other moisture map was from NOAA 17 image and has the same temporal adjacency to MODIS image (also captured in June 12, 2009). The NOAA 17 moisture map was classified according to the moisture values and then adjusted to overlay the high/low moisture at the base map by firstly removing all moisture classes except highest class and then this remaining class was converted into points to overlay at the base map from MODIS. Secondly, for low moisture validation, same procedure was applied however this time all classes were removed except the lowest moisture class and then converted into points. Figure 4.20 shows fundamental description of moisture classes overlay before the determination of the area under curve.

The aim behind validating the high and low moistures is to examine the accuracy of the two different satellites MODIS and NOAA in retrieving the moisture values under all the influencing conditions because the high moisture is mostly influenced by vegetation statement, while the low moisture amount/distribution is influenced by surface temperature mostly.

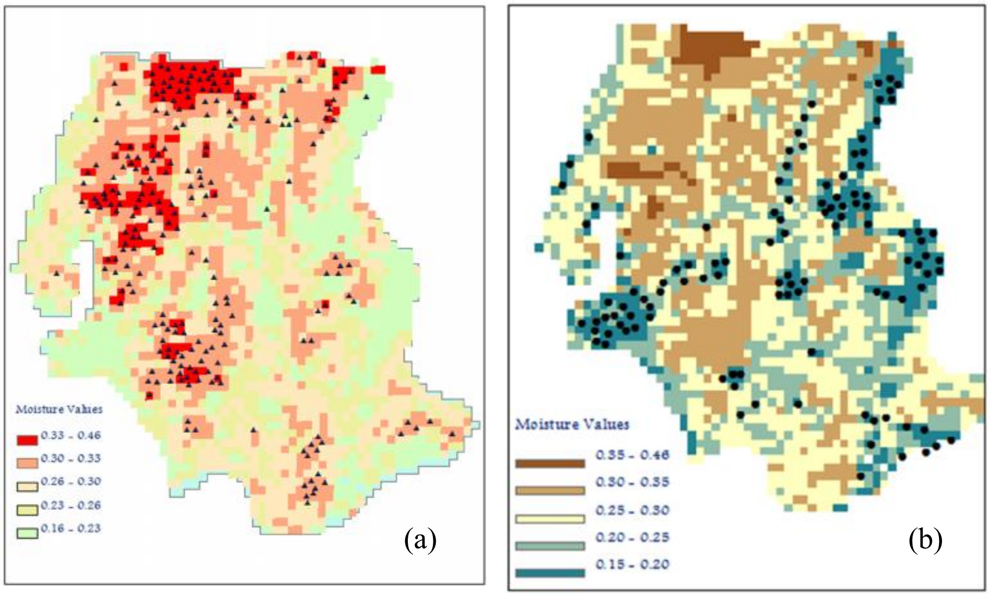

Figure 4. 20: The (a) high and (b) low MC zones converted into points for MC overlay.

Based on the aforementioned, the estimated moisture maps from both NOAA 17 and MODIS Terra were correlated spatially through the success rate to examine their compatibility with the moisture distribution taking into account their chronological equivalence. Figures 4.21 and 4.22 show the resultant AUC, in which MODIS MC maps with different SWI were used as base (MC Occurrence index %) and NOAA MC high/low classes were used as points (Cumulative M.C Occurrences %).

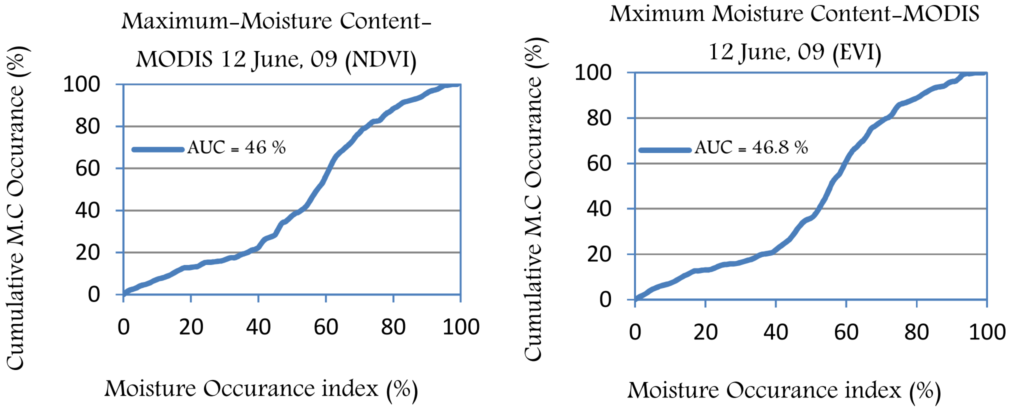

Figure 4. 21: The area under curve of high MC maps with SWI based on (left) NDVI and (right) EVI.

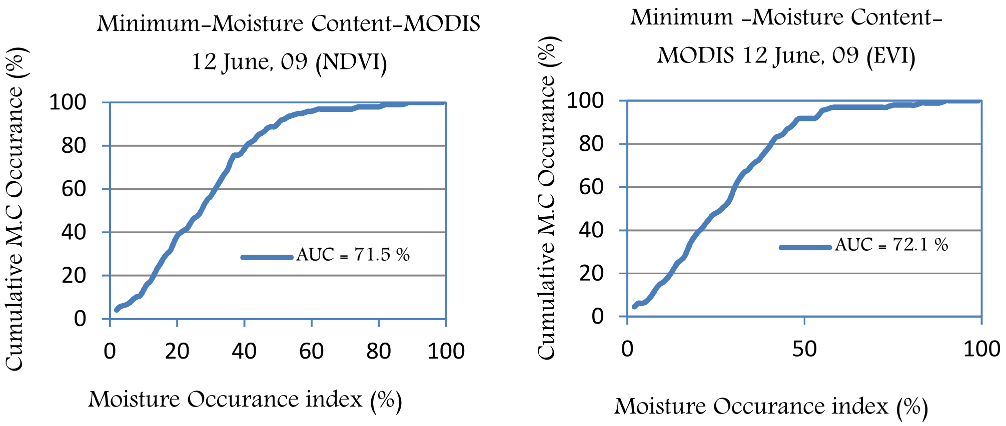

Figure 4. 22: The area under curve of low MC maps with SWI based on (left) NDVI and (right) EVI.

Spatial validations were performed in order to assure the adjacency of the acquired optical/infrared images to each other in retrieving the value and distribution of the surface MC with regard to the land uses/cover variability. However, it was found that, due to the difference in vegetation scale, the produced AUC for high MC was found to be weak (46 % for moisture based on NDVI and 46.8 % for moisture based on EVI), while the AUC for the lowest moisture which is distributed almost over the urban areas was 71.5% for moisture based on NDVI and 72.1% for moisture based on EVI. This assures that, the scale of the spatial patterns has an influence on the predicted values, so that NOAA and MODIS have the same spatial scale at the thermal bands, what led to a good agreement in estimating Ts (low moisture). On the other hand, the disparity in the spatial scale of the optical bands led to the disagreement in assessing the vegetation amount/distribution in estimating the high moisture values distribution.

4.3 Evapotranspiration

Point-based NDVI and corrected Ts calculated earlier from both NOAA/AVHRR and MODIS satellite images for surface MC's applications were used again with the same block averaging method to assess the ET_o over the three dissimilar environment partitions within the study area, which are urban, vegetation and multi-surface cover.

4.3.1 Point-based λET_{ins} assessment from Satellites

The assessment of the daily ET_o from the energy balance algorithm was achieved through the estimation of the instant latent heat flux (λET_{ins}). Which in turn involved the extraction of quite number of parameters ranged from atmospheric to meteorological which concerned the extraction of daily net radiation (R_n), sensible heat flux (H) as well as the ground heat flux (G). The daily incoming short wave radiation ($Rs\downarrow$) was the axial finding in determining (R_n), so it was estimated as a function of solar zenith angle (concerned the latitude and DOY in calculations) beside the atmospheric transmissivity which is a surface elevation-based in which GPS readings were taken because the applications assumed point-based measurements. The surface short-wave albedo (α) was estimated as atmospheric reflectance shared by the two optical bands on each sensor to represent the up willing shortwave radiation gained by satellite's sensors. Incoming long wave solar radiation was assessed from direct measurements of 2 m high air temperatures accompanied with emissivity based on the corresponding transmissivity of the air. On the other hand, the outgoing long wave radiation was assessed according to the study findings of NDVI plus normal Ts and corrected Ts, accompanied with surface emissivity extracted values.

Soil heat flux was assessed according to the resultant (R_n) in conjunction with satellite extracted NDVI, normal Ts and corrected Ts along with extracted surface albedo (α), while the sensible heat flux, was assessed as a function of the aerodynamic resistance to heat transport (r_{ah}), taking in consideration the air density, specific heat and temperature difference influences.

4.3.2 Assessment of Daily ET_o from Satellites

In order to estimate the daily ET_o from the instant latent heat flux (λET_{ins}) of energy budget algorithm, instantaneous value of the evapotranspiration (ET_{ins}) in hourly time bases was calculated based on the quantification of the latent heat vaporization and time units conversion as proposed by Nelson et al. [196] in the following relation:

$$ET_{ins} = \frac{3600 \lambda ET_{ins}}{\lambda} \qquad \text{(mm Hour -1)} \qquad 4.1$$

where; ET_{ins} is the instantaneous ET (mm/hr), 3600 is the time conversion from seconds to hours, and λ is the latent heat of vaporization or the heat absorbed when a kilogram of water evaporates (J/kg).

Finally, the daily ET_o was estimated in the form of temporal integration of the resultant instantaneous (ET_{ins}). This integration is based on the assumption that the evaporative fraction at the daily scale mostly resembles to the one that was derived instantaneously at the time of satellite's data acquisition [258]. The integration form below which was proposed by Sobrino et al. [259], was used to estimate the daily ETo using satellite potentials in collaboration with the terrestrial data.

$$ET = \int_{0}^{24} ET_{ins}(t)dt \qquad 4.2$$

$ET_{ins}(t)$: used in hourly time base.

4.3.3 Daily ET_o from SEBAL Model

ET_o from SEBAL model, was computed from the same satellite images and weather information making use of the surface energy balance as highlighted. As the satellite image supplies details for just the overpass time, SEBAL determines an instantaneous ET flux with the image time frame. Likewise, the ET flux is computed for every pixel within the image as a "residual" of the surface energy budget formula:

Hot and Cold Ts

The SEBAL method uses two "principal" pixels to correct boundary circumstances for the energy balance. They are the "hot" and "cold" pixels and so are situated on the area of interest. The "cold" pixel was chosen as being a wet, well-irrigated crop surface possessing full surface cover via vegetation. Seberang Perak paddy field was selected to provide this pixel. Surface temperature and near-surface air temperatures were thought being identical with this pixel. The "hot" pixel on the other hand, was chosen to be a dry, bare area where ET was considered to become zero, for this pixel. Parts of the urban areas of Sitiawan were selected to meet the presumption. Then finally the SEBAL ET_o values were determined through the block averaging to examine the accuracy of the research method along the meteorological-based ET_o as could be seen in Figures 4.23 and 4.24.

4.3.4 Comparison of spatial ET_o with Ordinary Methods

Three of the essential methods were used in the study in order to verify and validate the ET_o extracted from satellite images, that are the Penman-Monteith (PM) by FAO 56, Hargreaves and Turc, as they have been very essential for the evaluation of ETo estimations acquired by more indirect approaches.

As Penman-Monteith (PM) approach has successfully combined the aerodynamic approach with the energy balance method to estimate ET_o, it is considered as a global standard for estimating ET_o based on four meteorological data (temperature, wind speed, radiation and relative humidity). Thus, it was used as the reference for ET_o estimates along all the findings of ET_o, then all meteorological parameters collected from ground stations were applied in PM, Hargreaves and Turc methods with daily bases considering the satellite's overpassing time chronology. Figure 4.23 represents a comparative plots of the satellite estimated ET_o versus SEBAL model as well as the ground-based values of ET_o using the three methods, whereas, the approaches of the energy balance methods to assess ET_o, were produced from satellite based-Ts and satellite corrected-Ts. Both Satellite NOAA 17 and MODIS Terra images were captured at morning time (10:30 – 11:30 AM) when temperature and solar radiation values were relatively low.

For the mid-day session, NOAA 18 and MODIS Aqua images which have an overpass time around (2:00 – 3:00 PM) over the study area, were acquired and analyzed to extract ET_o and then plotted against the ordinary measured ET_o from PM, Hargreaves and Turc methods. The comparative plotting of the resultant ET_o can be seen in Figure 4.24 below in which, the alteration in satellites ET_o values and attitudes is very noticeable with correspondence to the ordinary ones.

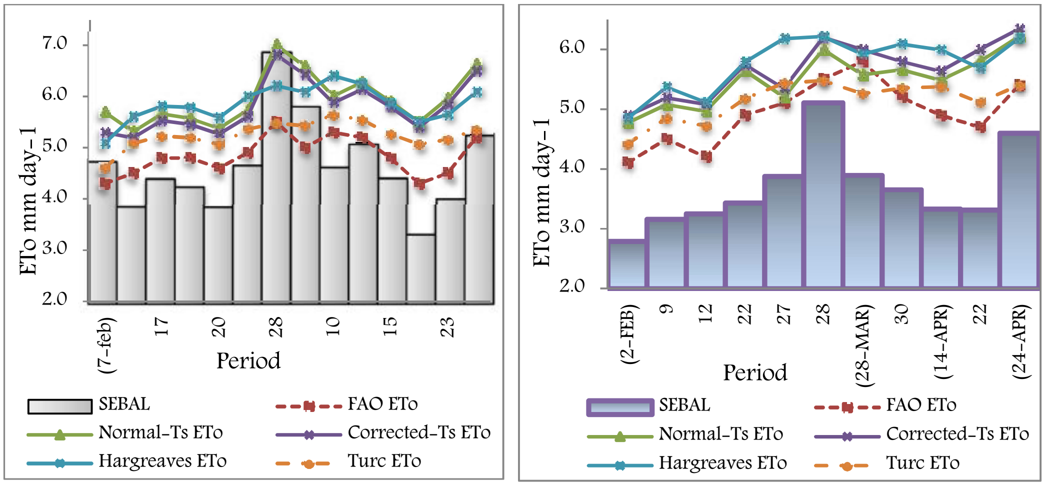

NOAA 17 at UTP

MODIS TERRA at UTP

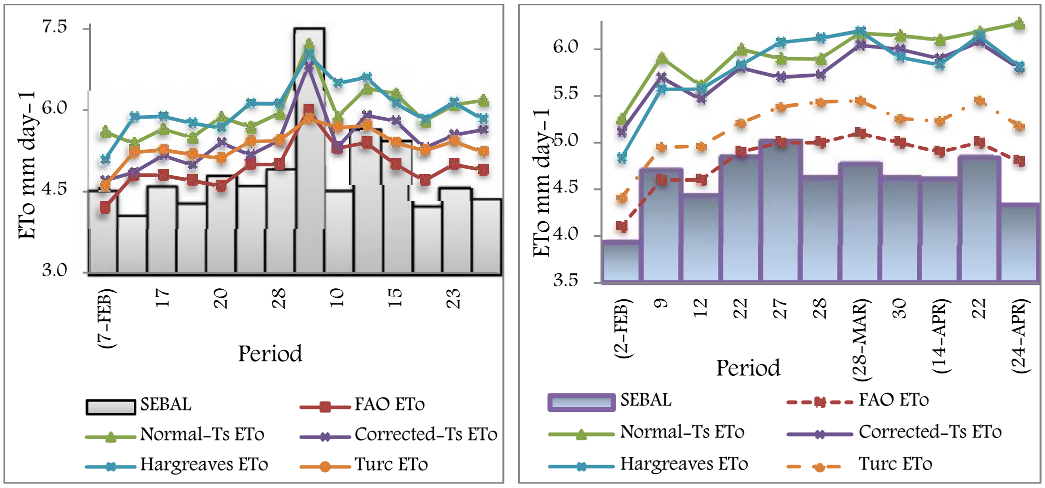

NOAA 17 at Sitiawan

MODIS TERRA at Sitiawan

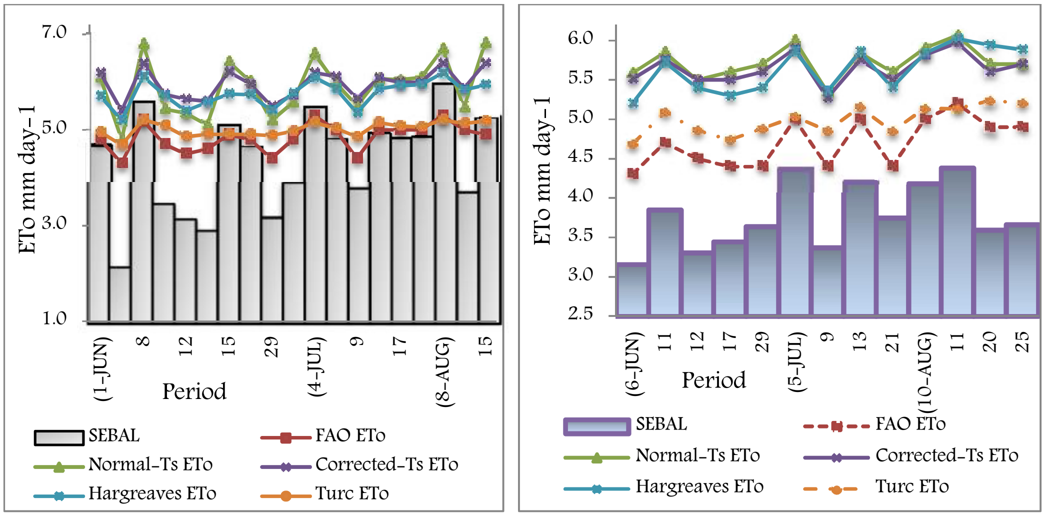

NOAA 18 at Sp. Perak

MODIS TERRA at Sp. Perak

Figure 4. 23: Scatterplots of satellite-estimated and ordinary-measured ET_o at study locations from NOAA 17and MODIS Terra.

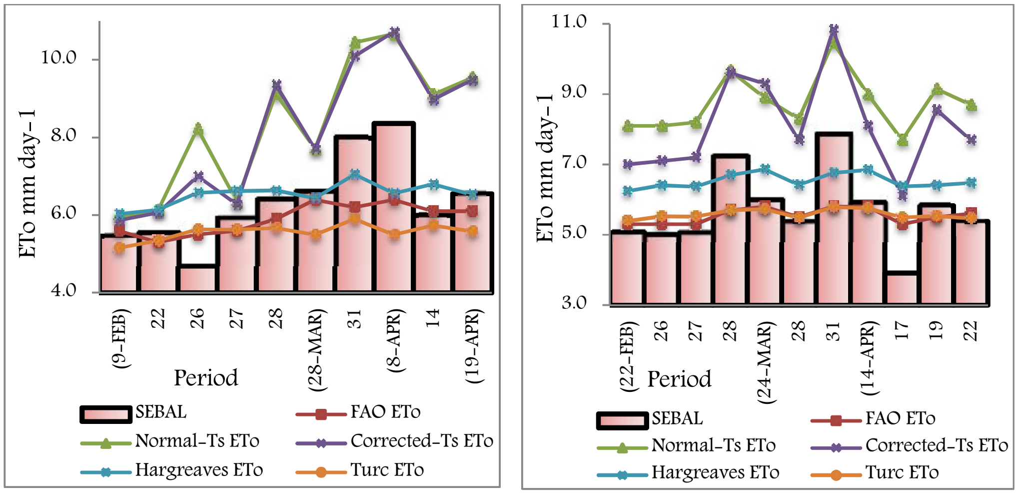

NOAA 18 at UTP NOAA 18 at Sitiawan

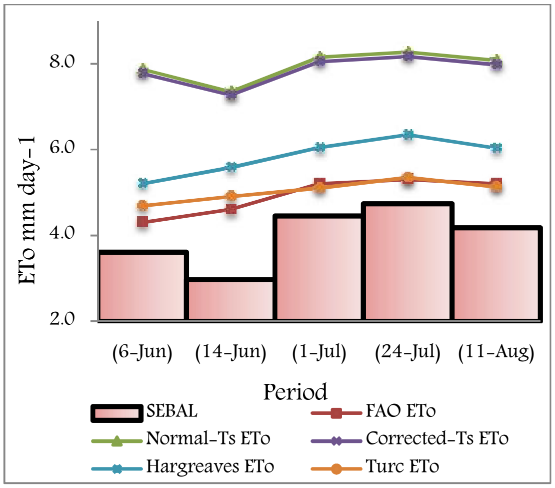

MODIS AQUA at Sp. Perak

Figure 4. 24: Scatterplots of satellite-estimated and ordinary-measured ET_o at study locations from NOAA 18 and MODIS Aqua.

4.3.5 Algorithms Validation

Statistical validation was implemented for the simulated ET_o points of measurements, in which SPSS software was used in order to estimate the standard error of the satellite datasets beside the correlation coefficient of each retrieved data when validated with PM algorithm. Table 4.10 summarizes the statistical validation of the ET_o extracted from NOAA17, MODIS Terra as morning passing satellites beside NOAA 18 as a mid-day passing satellite. Both parts of the extracted temperature were analyzed normal Ts and satellite corrected Ts, in order to examine the effectiveness of Ts rectification on the value of ET_o.

Table 4. 10: Summary of the statistical validation of satellites based ET_o.

Statistical Validation					
measurement		Descriptive		Correlation Coeff. R^2	
		Mean	Std. Deviation	ET_o from PM-FAO 56	Sig. (2-tailed)
UTP	ETo from PM-FAO 56	4.84	0.37		
	ET_o from N17 Satellite corrected-Ts	5.79	0.50	0.825 **	0.000280
	ET_o-Corrected-Ts from MODIS Terra	5.65	0.47	0.621 *	0.041530
	ET_o from N18 Satellite Corrected-Ts	8.17	1.78	0.714 *	0.020458
	ET_o from SEBAL	4.66	0.88	0.763 **	0.001488
		4.96	0.42		
SITIAWAN	ET_o from PM-FAO 56				
	ET_o from N17 Satellite corrected-Ts	5.42	0.52	0.856**	0.000095
	ET_o-Corrected-Ts from MODIS Terra	5.75	0.28	0.783 **	0.004384
	ET_o from N18 Satellite Corrected-Ts	8.11	1.36	0.825 **	0.001759
	ET_o from SEBAL	4.86	0.87	0.791 **	0.000751
		4.84	0.29		
S. PERAK	ET_o from PM-FAO 56				
	ET_o-Corrected-Ts from MODIS Aqua	7.86	0.34	0.56	0.32865
	ET_o-Corrected-Ts from MODIS Terra	5.65	0.20	0.865 **	0.000137
	ET_o from N18 Satellite Corrected-Ts	5.95	0.32	.851 **	0.000004
	ET_o from SEBAL	4.34	1.04	0.879 **	0.000001

**. Correlation is significant at the 0.01 level (2-tailed).

*. Correlation is significant at the 0.05 level (2-tailed).

Experimental validation also was conducted for the spatial datasets of ET_o with normal Ts and corrected Ts. The reserved datasets of NOAA 17 and MODIS Terra were used for field measurements of morning times, while NOAA 18 images were used for afternoon session where temperature and radiation intensity are slightly different. Figure 4.25 shows the validation of NOAA 17 and MODIS Terra satellites over the three parts of the study area for ET_o estimations under normal Ts and corrected Ts and FAO 56 ET_o as reference value.

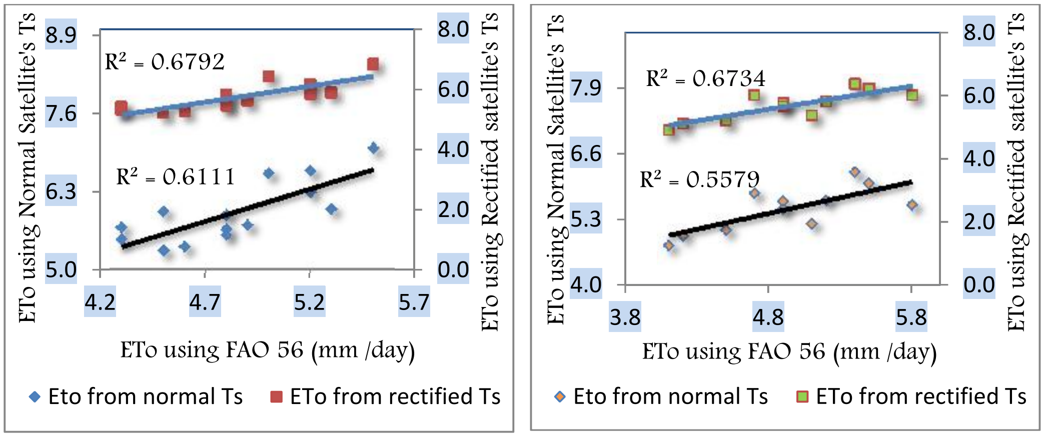

NOAA 17 at UTP MODIS Terra at UTP

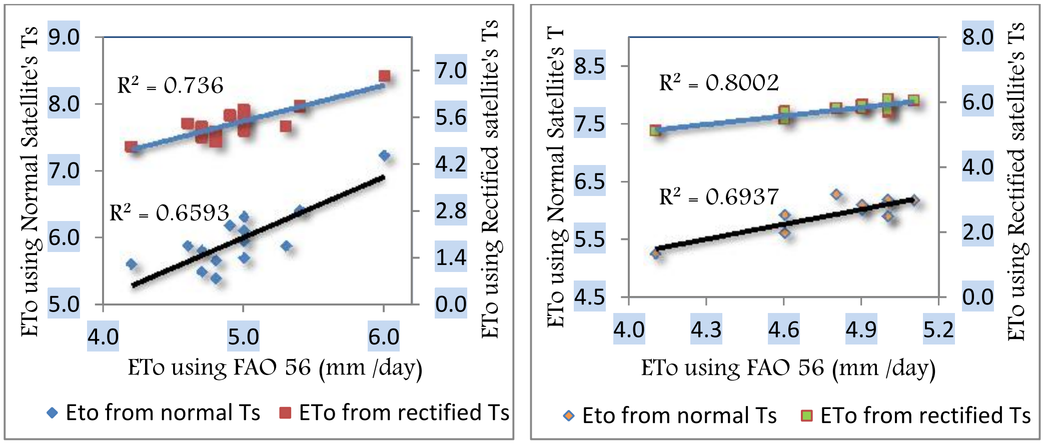

NOAA 17 at SITIAWAN MODIS Terra at SITIAWAN

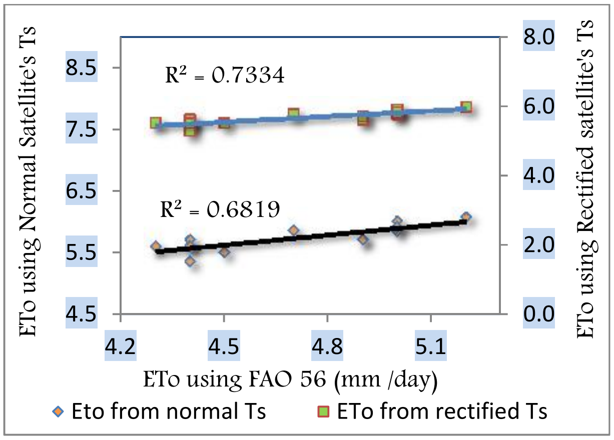

MODIS Terra at SP.PERAK

Figure 4. 25: ET_o validation using normal and rectified Ts over UTP, Sitiawan and Seberang Perak locations, from morning passing satellites.

On the other hand, validations of ET_o dataset from NOAA 18 and MODIS Aqua were also conducted, so as to examine the compatibility of these mid-day sensors with the concurrent moisture status. Figure 4.26 below shows the correlation of the ET_o based both on satellite normal-Ts and satellite corrected-Ts with FAO 56 ET_o.

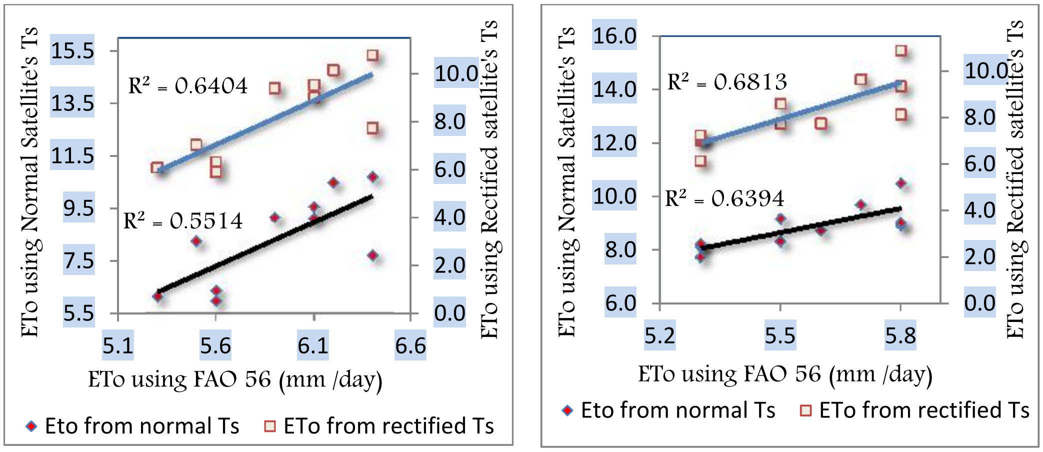

NOAA 18 at UTP

NOAA 18 at SITIAWAN

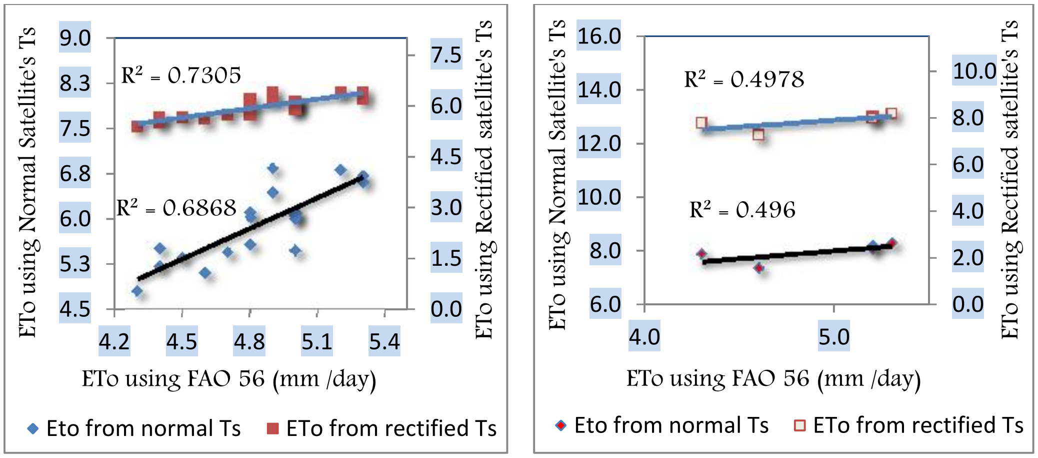

NOAA 18 at SP. PERAK

MODIS AQUA at SP. PERAK

Figure 4. 26: ETo validation using normal and rectified Ts over UTP, Sitiawan and Sp. Perak from mid-day passing satellites.

It can be noticed that the extracted ET_o produces better results when the corrected Ts is used along with the NDVI. This could be seen obviously from the validation of the resultant ET_o using the reserved satellite images with reference to the actual ET_o from FAO Penman-Monteith method.

The extracted ET_o from the images resembles the actual FAO ET_o to a very far extent, particularly from NOAA 17 MODIS Terra images whose sensors overpass the area at the morning times with an average of 6 mm day^{-1} along the three study locations. On the other hand, an overestimation of the spatial ET_o values was witnessed over the whole study areas from NOAA 18 and MODIS Aqua images, which must be due to the high Ts and solar radiation coming in the form of short waves and surface albedo acquired by those satellites during the mid-day. Simple justification is that, the field-based measurements of ET_o involve the incorporation of wind speed and relative humidity as very effective parameters influence the evaporative fraction of surface plant, while the wind speed in the spatial assessment of ET_o is only considered for assessing the ground heat flux which is a small portion of the energy flux that mostly is neglected in daily ET_o estimation.

SEBAL model in turn, produced considerable estimations of ET_a as a spatially based algorithm. This is due to the incorporation of the hot and cold pixels (located to the area of interest) in the correction of the emissivity and transmissivity values [195]. The produced ET_o by SEBAL model showed relatively low values (underestimation compared to FAO ET_o) over the three locations when images from MODIS satellite were used (both Terra and Aqua). This might be attributed to the scale disparity between the thermal bands used for Ts estimation (1 Km by 1 Km) and the optical ones used for NDVI extraction (250 m by 250 m), which may have dominated the vegetation signature causing more representation of the cold temperature (T_{cold}) which could be the lowest temperature used within the area pixels.

The temporal analysis of the resultant ET_o did not show abrupt change in ET_o attitude within the periods of measurements. This is precisely because of the shortness of the measurements time which could be assessed as four months. So that, ET_o mostly is tracked on seasons base, where the solar radiation and humidity beside the vegetation growing statements influence the ET_o leading to noticeable attitude of ET_o with time.

The validation of the extracted ET_o from satellite images produced good results in terms of their compatibility with FAO ET_o which represented the reference ET in this study. Along the statistical analysis of the extracted ET_o values, the satellite estimated

ET_o based on corrected Ts, NOAA 17 and MODIS Terra showed noticeable mean ET_o with errors less than the SEBAL model all over the three applied locations. Moreover, the ET_o correlation conducted between the mentioned sensors and FAO ET_o showed good results with coefficients ranged between 0.71 – 0.86, while NOAA18 images tended to overestimate the ET_o with an average range between 6-8 mm day^{-1} over the three locations. The whole correlations between the extracted ET_o and FAO ET_o were in a highly significance according to the level used by the study (Correlation is significant at the 0.01 level (2-tailed)). On the other hand, the produced ETo from MODIS Aqua did not show good results when correlated to FAO ET_o because insufficient volume of data was represented statistically (only 4 images represented by 4 points).

In addition, experimental validation was conducted among satellite normal-Ts ET_o, satellite corrected-Ts ET and FAO PM ET_o, in order to examine the validity and the usefulness of the temperature rectification process. All ET_o values which were estimated from satellite-corrected Ts, produced better results when compared to the actual ET_o with higher R^2, which increases the accuracy of the spatial ET_o assessment.

4.3.6 Moisture Incorporation

The final stage of the study was directed to investigate and assess the spatial impact of soil water availability in the determination of actual evapotranspiration ET_a as an attempt to overcome the complexities in estimating the actual evapotranspiration in which the crop coefficient is demanded along with the potential ET_o.

The study was presented based on a simple model developed by Jacobs et al. [202], through applying a reduction factor based on soil moisture to FAO PM Model for ET_o, for the sake of providing enhanced estimations of a. Equation 2.52 in Chapter 2 represents the estimates of ET_a which was assessed by scaling the potential evapotranspiration ETo through the reduction coefficient B which is a function of the soil moisture [202]. According to Jacobs, the reduction coefficient B was found to follow a logarithmic relationship with the MC and its accuracy was represented by R^2 equaling to 0.93.

Based on the aforementioned concepts, the weighted moisture maps from both NOAA and MODIS were combined in the Equation 2.89 to deduce ET reduction coefficients that could be used for the actual ET assessment over the study area. Thus, four types of ET maps were produced by the study when considering the MC-ET map, which are: ET_o map generated from satellite's corrected-Ts via energy balance, ETa from SEBAL model and two sets from the weighted moisture maps with moisture depth influence 5cm and 10 cm. Figure 4.27 shows the 3 examples of the resultant ET maps extracted from NOAA 17 and MODIS Terra image as examples.

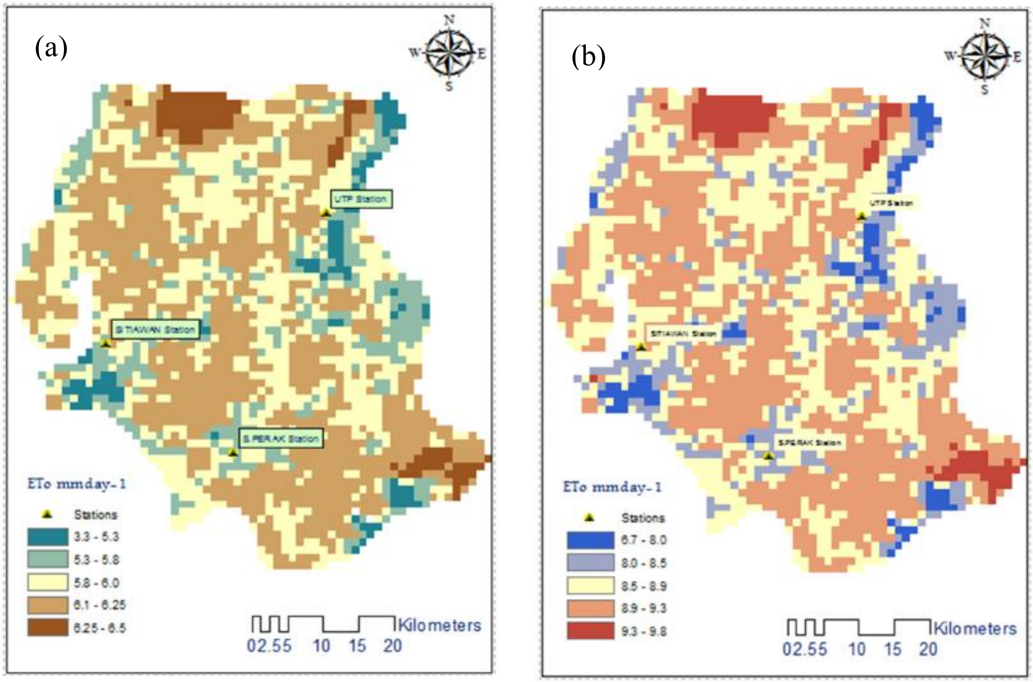

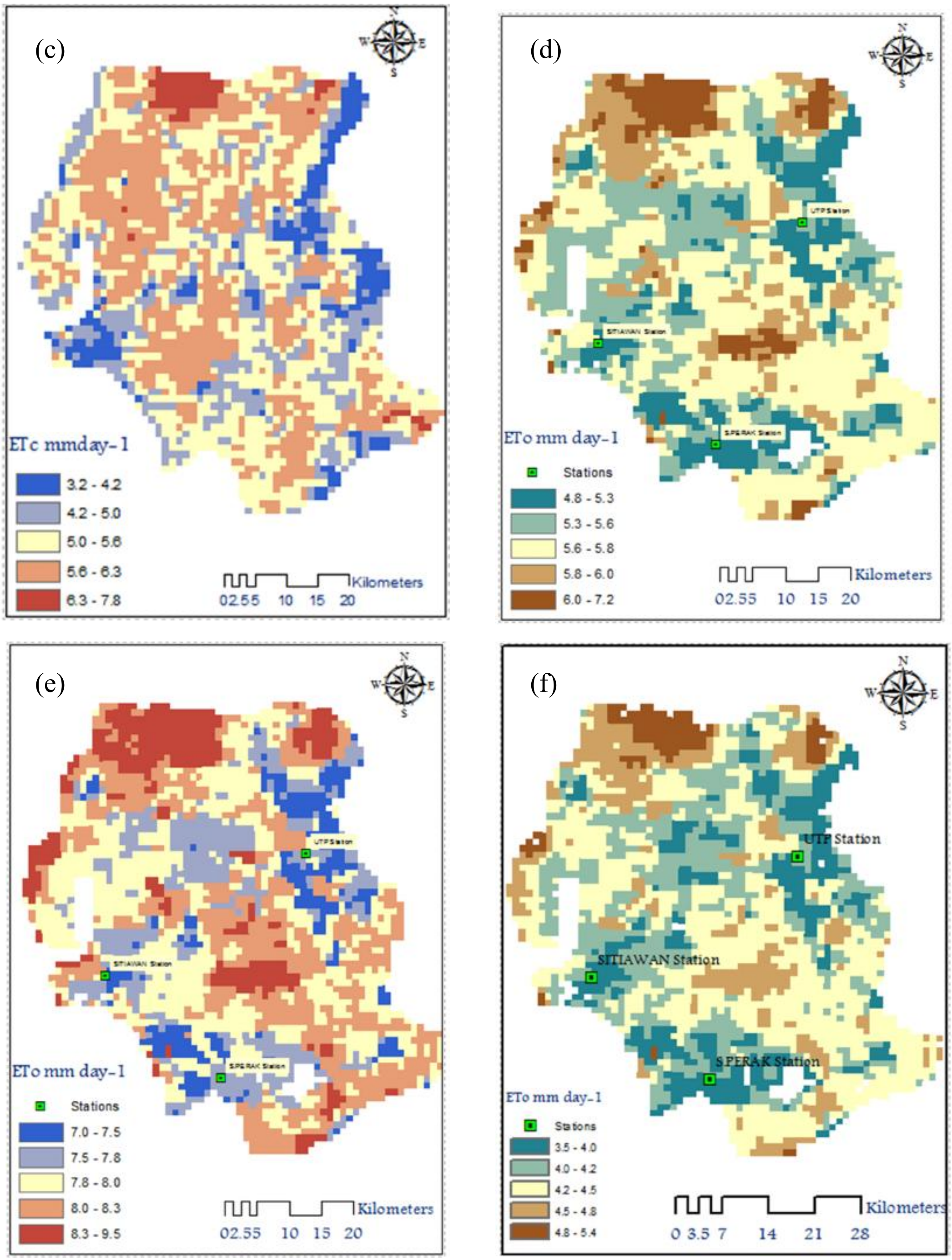

Figure 4. 27: ETo extracted from (a) Energy Balance Ts-corrected of NOAA 17, (b) SEBAL of NOAA 17, (c) Jacobs moisture model of NOAA 17, (d) Energy Balance Ts-corrected of MODIS Terra, (e) SEBAL of MODIS Terra and (f) Jacobs moisture model of MODIS Terra.

4.3.6.1 Validation

To investigate the applicability of the moisture reduction method by Jacobs in producing a perfect map of the actual ET, the resultant ET_a maps from the model were correlated against FAO ET_o in terms of point-based measured values. The validation showed considerable results for all parts of the study area. In this validation, moisture values of the three sensor's image (NOAA 17, 18 & MODIS Terra) were used together for validation over each of the three locations. Figure 4.28 shows the experimental validation conducted between FAO ET_o and the actual ET from Jacobs model, in which, the generalized moisture maps with corrected Ts were used to generate the moisture reduction coefficient B.

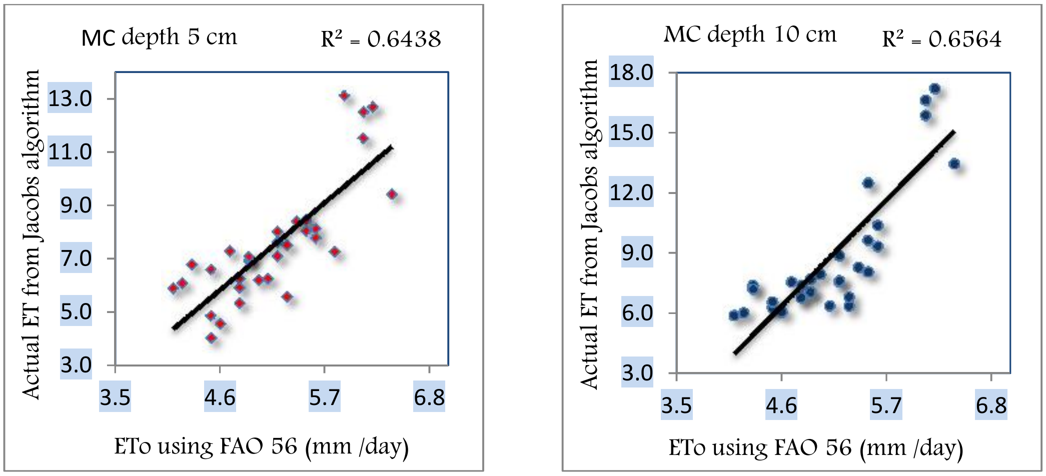

(a)

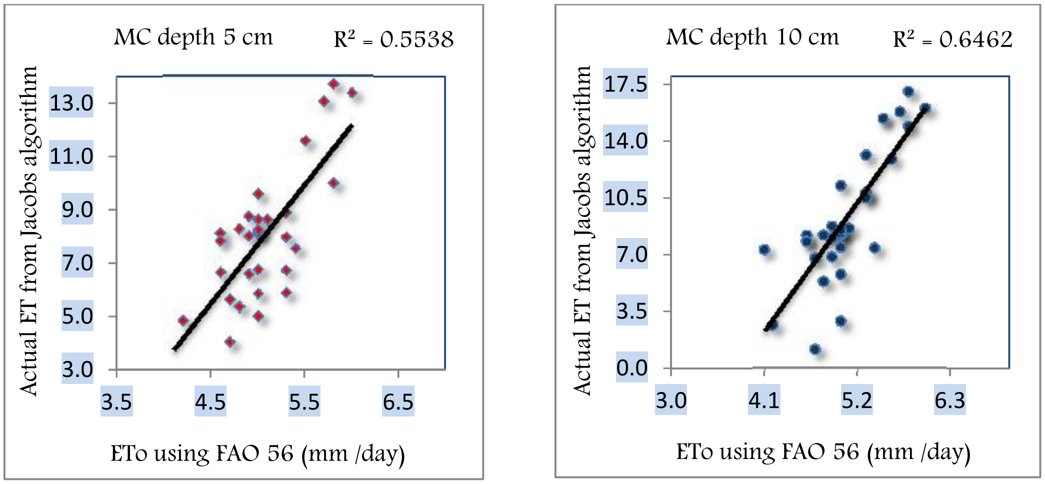

(b)

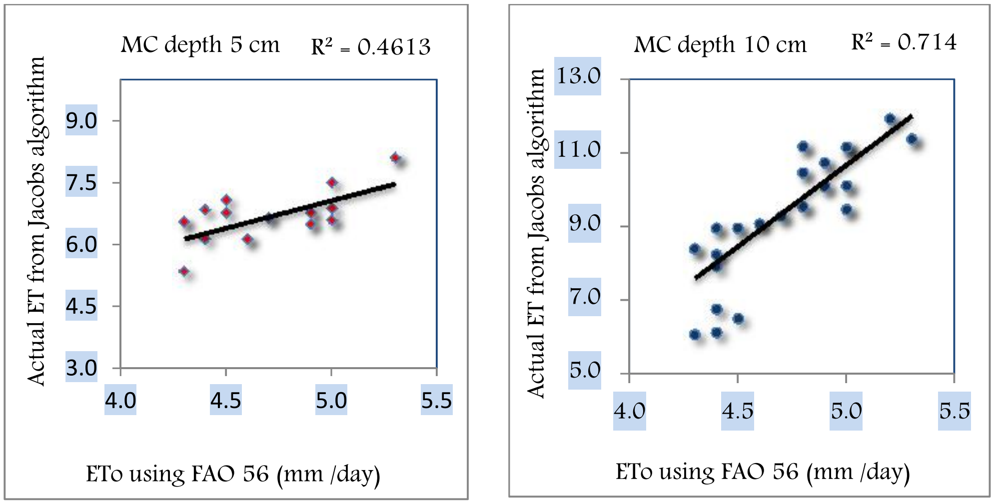

(c)

Figure 4. 28: Actual ET based on MC (5 & 10 cm depths) using Jacobs Vs FAO ETo algorithms for locations (a) UTP, (b) Sitiawan and (c) Sp. Perak.

The second part of the validation was the spatial validation of the ETa maps using success rate validation (discussed in the previous sections) in which the process involved validating the ETa over the whole study area based on each pixel's value. The Area Under the Curve AUC technique was used to rate the success of the generated ETa maps in overlapping the SEBAL ET values from the same images. The produced Jacobs methods were used with the two mentioned depths of moisture measurements 5 cm and 10 cm. In addition to that, directly applied energy balance ET_o maps with corrected Ts were used also to allow better evaluations of the weighted moisture map incorporation. Figure 4.29 shows the success rate validation of ETa from NOAA 17, 18 and MODIS Terra weighted moisture maps in which, SEBAL model for each image was used as reference ET prepared in form of ET classes (ET_o Occurrence index (%)). On the other hand, the ET_a from weighted moisture (Jacobs) and the extracted energy balance ET_o were overlaid as points of high ET class (Cumulative ET_o Occurrence (%)) to assess the area under the curve.

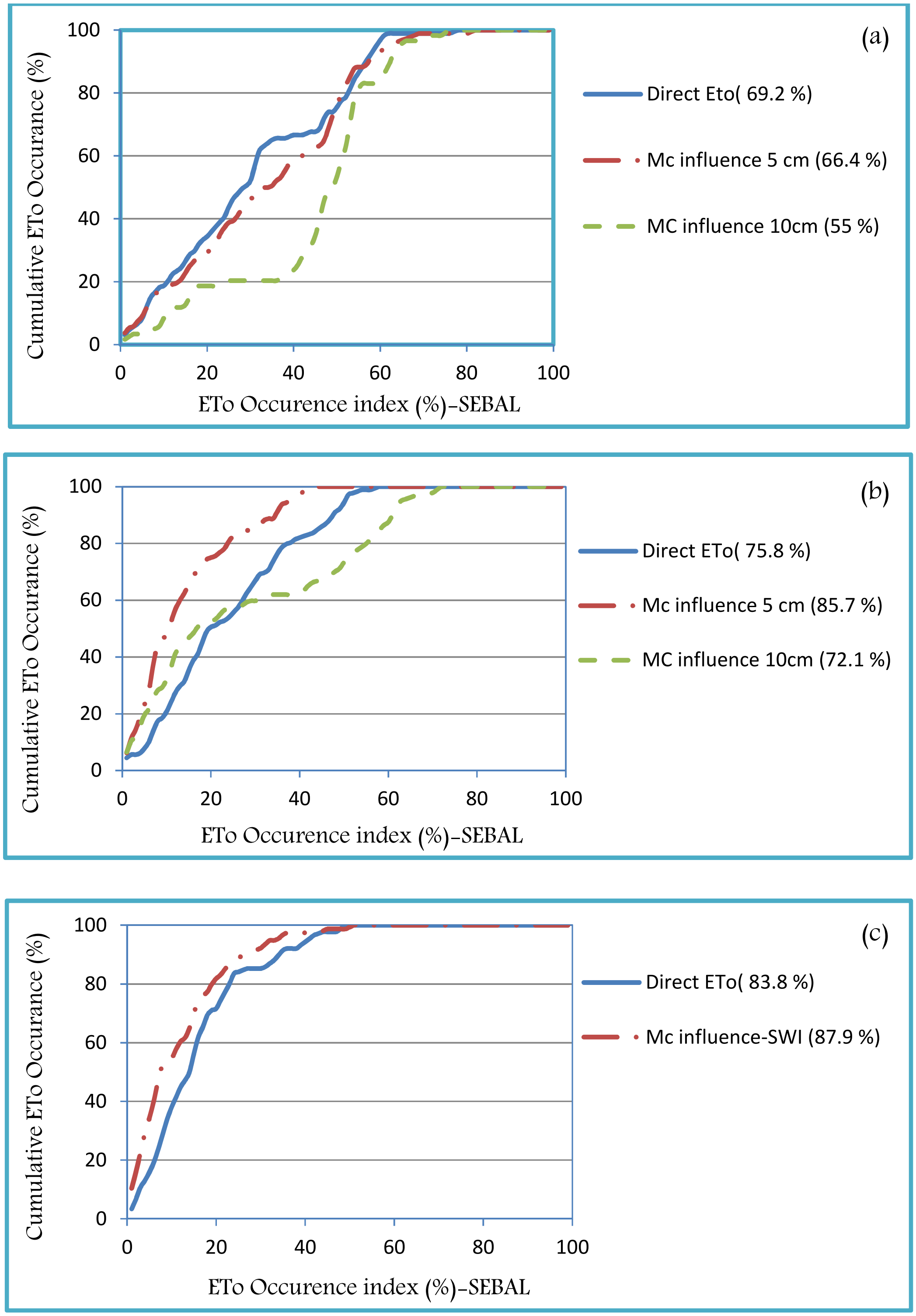

Figure 4. 29: The success rate validation of the extracted ET_o from corrected Ts as well as the moisture diffusion from (a) NOAA 17, (b) NOAA 18 and (c) MODIS Terra images.

The soil parameterization method proposed by Jacobs showed reasonable representation of the actual evapotranspiration ET_a from the water availability statement. As such, the resultant ET_a from the model was tightly correlated the ET_o from FAO which was used as a reference algorithm throughout the study. The correlation coefficients ranged between 0.55 to 0.71, which could be considered as good indicators of the methods' accuracy if the following points are considered:

- Method simplicity: With the extraction of the soil moisture map, not much effort has to be devoted to generate ETc map, so that the empirical method suggested by Jacobs provided the interface relation between the soil water content and the atmospheric water vapor status.

- No vegetation information required: The proposed method tended to generate the actual ET_a with regard to the moisture influence (reduction coefficient B), which is in turn spatially extracted as an indicator of all vegetation statements (greenness , health, age etc.) represented by the vegetation indices (NDVI, EVI, LAI, etc.) of the surface moisture algorithms.

- Traditionally, to assess the crop coefficient in such tropical area, a wide range of investigations must be conducted in order to differentiate between vegetation species and assign coefficients for them. These might be rather difficult in the tropical areas where some vegetation grows deeper inside the jungle and becomes not accessible within the plant's family.

The general indication of the resultant ET images is that the spatial distribution of ET along the study area reflects the impact of the vegetation density on ET amount, so it could be seen that the higher ET is always centered over the vegetation area, especially the uniform cover of vegetation (agricultural areas). Hence the spectral analysis and the applications of all suggested algorithms, produced results that agreed with ET estimation principles and fundamental that ET is always produced highly from vegetation cover more than bare soils and impervious surfaces [196].

The spatial validation represented in the success rate method assured the usefulness of the Jacobs method with the weighted moisture map in producing a valuable estimation of the actual evapotranspiration ET_a from the soil status and the available potential evapotranspiration ET_o. From NOAA 17 image, this validation produced an accuracy of 0.66 and 0.55 from MC depths 5 and 10 cm in Jacobs respectively. While the potential ET from corrected Ts energy balanced produced 0.69 in their spatial correlation with SEBAL model. Likewise, ETa from moisture base produced accuracies of 0.85 and 0.72 at moisture depths 5 cm and 10 cm, while the potential ET_o with corrected-Ts produced 0.75 from NOAA 18 image. Furthermore, when MODIS Terra image was used, the moisture based ETa produced accuracy of 0.87 compared to the ET_o from the potential ET_o which produced 0.83 area under curve accuracy. It could be distinguished from the browsed accuracies that, the applied Jacobs algorithm with moisture reduction coefficients is mostly in a good agreement with SEBAL model regarding the spatial distribution of the high ET values.

CHAPTER 5

CONCLUSION AND RECOMMENDATIONS

The study intended to enhance the spatial accuracy of moisture content and evapotranspiration estimation by weighting the MC produced from different surface cover classes within the image’s pixel. This chapter summarizes the achieved work with some evaluation assessment corresponding to the accuracies and statistical precisions that produced by the algorithms used. The chapter also covers the objectives that have been achieved. Finally, the study gave some recommendations which might enhance and rectify the methodology for further works in the future.

5.1 Conclusion

Images from AVHRR and MODIS satellites were acquired in order to generate a spatially enhanced MC and ET maps. The study has intended to correlate the extracted Ts from satellites with in-situ measurements in order to remove the atmospheric attenuation caused by the path radiance. The correlation between the satellite and in-situ measurements of Ts values resulted in coefficients of 90%, 90%, 86 % for Ts from NOAA over UTP, Sitiawan and Seberang Perak respectively. On the other hand, correlation of Ts from MODIS produced 78 %, 74 % and 97 % over UTP, Sitiawan and Seberang Perak respectively. Extraction of MC involved the application of two algorithms which based on the extraction of surface temperature (Ts) and vegetation indices (VI) from satellite images. Using NOAA images, surface MC was retrieved using a modified Universal Triangle (UT) method which is based mainly on a multiple-type regression relationship between MC measured in-situ and satellite Ts and NDVI values. Using MODIS images, MC was also determined based on the soil wetness index (SWI) and the upper (FC) and lower (PWP) boundaries of

MC over the three parts of the study area. Enhanced MC maps were then produced by generating a moisture weighting algorithm. This method is based on the correlation of MC from three different classes of surface cover in which, the spectral participation of each class within the single pixel is assessed based on its weightage. This, in order to avoid the aggregate spectral representation from the image pixel. The resultant MC extracted from the UT and TI methods with rectified Ts, produced accuracies of MC ranging from 0.66 to 0.95 as highest and lowest values; while the accuracy of MC generated from the ordinary MC produced accuracies ranging from 0.58 to 0.88. Both methods have been validated using in-situ measurements of MC. Furthermore, the spatial validation of MC was carried out using the success rate validation to examine the compatibility of those sensors (NOAA and MODIS). The result produced an accuracy ranging from 0.46 to 0.72.

Finally, the study succeeded in producing the actual evapotranspiration (ET_a) maps from the rectified ET_o. This is strengthened by substituting the crop coefficient in the ET_o algorithm by the weighted MC. The spatial validation using SEBAL model achieved accuracies of 0.66, 0.85 and 0.87 from NOAA 17, NOAA 18 and MODIS TERRA images respectively.

5.2 Recommendations

The study attempted to construct soil moisture maps with local criteria represented in ground truthing for data validation and surface temperature correction, to enable the application of the output algorithm in all local and regional hydrological process related to the MC, enclosing the ET as an example. However, there were some parameters that should be considered in order to significantly raise the accuracy of soil moisture estimation and application if taken in consideration for further studies.

1. The spatial multiplicity: The study analysis was based on the high temporal resolution of the satellites, but clouds allocation caused some irregularities in data flow and compatibility with field data. For future, the study suggests the use of one or

two clear (cloud free) images while multiplying the ground collection points within the study area and synchronizing data collection time with satellite overpass.

2. Pixel segments increase: The image's pixel of NOAA and MODIS (1 Km^2) could contain more than the three proposed surface covers, therefore the study suggests the portioning of multi-surface cover into bare soils, pastureland, forest, grassland and any surface cover that is expected to be available in a specific study area.

3. Natural disasters monitoring: As Malaysia is affected by two frequent natural disasters: landslides and urban floods, the study recommends applying the MC's algorithms to high spatial resolution images, so that it could be useful to monitor the moisture status over the sloppy areas and then indirectly predict the landslide occurrence possibility because MC has an effective relation with the pore water pressure. Also, the high scale moisture map could assist in forecasting the flood over the urban areas through quantifying the soil saturation.

4. A moisture intensity map could be generated using long term record of MC from wide range of satellite images and can be applied for water resources planning and managements, buildings construction, allocation of dams, roads and highways embedding, etc.

5. The use of lysimeters: Lysimeters are considered as the most effective tools for ET measurements; therefore, the study suggests their use for validating the extracted algorithms instead of FAO penman-Monteith for more precision.

REFERENCES

[1] A. K. Sahoo, "Improvement of soil moisture prediction through AMSR-E data assimilation," PhD, Graduate Faculty, George Mason University, USA, 2008.

[2] J. C. Henniker, "The depth of the surface zone of a liquid," *Reviews of Modern Physics,* vol. 21, p. 322, 1949.

[3] UNDESA, "International Decade for Action "WATER FOR LIFE"," United Nations Department of Economic and Social Affaire, Spain 2005.

[4] P. H. Gleick, "Water and conflict: Fresh water resources and international security," *International security,* vol. 18, pp. 79-112, 1993.

[5] T. Lakhankar, "Estimation of Soil Moisture Using Microwave Remote Sensing Data," PhD, The City University of New York, New York, 2006.

[6] A. A. Hassaballa, Althuwaynee, O. F., and B. Pradhan, "Extraction of soil moisture from RADARSAT-1 and its role in the formation of the 6 December 2008 landslide at Bukit Antarabangsa, Kuala Lumpur," *Arabian Journal of Geosciences,* pp. 1-10, 2013.

[7] H. L. Penman, "Natural evaporation from open water, bare soil and grass," *Proceedings of the Royal Society of London. Series A. Mathematical and Physical Sciences,* vol. 193, pp. 120-145, 1948.

[8] C. B. Tanner and W. L. Pelton, "Potential evapotranspiration estimates by the approximate energy balance method of Penman," *Journal of geophysical research,* vol. 65, pp. 3391-3413, 1960.

[9] H. F. Blaney and W. D. Criddle, "Determining consumptive use for planning water developments".USDA. Soil Conservation Service. 1966.

[10] H. L. Penman, Angus, D. E., and C. H. M. Van Bavel, "Microclimatic factors affecting evaporation and transpiration," *Irrigation of Agricultural Lands,* pp. 483-505, 1967.

[11] J. E. Christiansen, "Pan evaporation and evapotranspiration from climatic data," *Proc Amer Soc Civil Eng, J Irrig Drainage Div,* vol. 94, pp. 243-265, 1968.

[12] M. S. Moran, Peters-Lidard, Christa D.,Watts, Joseph M., and S. McElroy, "Estimating soil moisture at the watershed scale with satellite-based radar and

land surface models," *Canadian Journal of Remote Sensing,* vol. 30, pp. 805-826, 2004.

[13] E. T. Engman, "Applications of microwave remote sensing of soil moisture for water resources and agriculture," *Remote sensing of environment,* vol. 35, pp. 213-226, 1991.

[14] F. P. De Troch, Troch, P. A.,Su, Z., and D. S. Lin, "Application of remote sensing for hydrological modelling," in *Distributed hydrological modelling*, ed: Springer, 1996, pp. 165-191

[15] J. P. Walker, "Estimating soil moisture profile dynamics from near-surface soil moisture measurements and standard meteorological data," The University of Newcastle, 1999.

[16] A. M. Sadeghi, Hancock, G. D.,Waite, W. P.,Scott, H. D., and J. A. Rand, "Microwave measurements of moisture distributions in the upper soil profile," *Water Resources Research,* vol. 20, pp. 927-934, 1984.

[17] H. Qiu, "Thermal Remote Sensing of Soil Moisture," Remote Sensing, 2006.

[18] P. E. Lydolph, *The climate of the earth*: Rowman & Littlefield Publications Incorporated, 1985.

[19] P. A. Dirmeyer, "Soil moisture–muddy prospects for a clear definition," *GEWEX News,* vol. 14, pp. 11-12, 2004.

[20] R. G. Lawford, "An overview of soil moisture and its role in the climate system," 1992, pp. 9-10.

[21] C. Yu, Loureiro, C., Cheng, J. J., Jones, L. G., Wang, Y. Y., Chia, Y. P., Faillace, E., "Data collection handbook to support modeling the impacts of radioactive material in soil," ed: ANL/EAIS-8. Argonne, IL: Argonne National Laboratory, 1993.

[22] J. M. Lanicci, Carlson, Toby N., and T. T. Warner, "Sensitivity of the Great Plains severe-storm environment to soil-moisture distribution," *Monthly Weather Review,* vol. 115, pp. 2660-2673, 1987.

[23] J. Zhang and T. J. Crowley, "Historical climate records in China and reconstruction of past climates," *Journal of Climate,* vol. 2, pp. 833-849 1989.

[24] R. Bindlish, "Active and passive microwave remote sensing of soil moisture," Ph.D, Civil and Environmental Engineering, The Pennsylvania State University, Graduate School, 2000.

[25] A. C. M. Beljaars, Viterbo, Pedro, Miller, Martin J., and A. K. Betts, "The anomalous rainfall over the United States during July 1993: Sensitivity to land surface parameterization and soil moisture anomalies," *Monthly Weather Review,* vol. 124, pp. 362-383, 1996.

[26] J. Shukla and Y. Mintz, "Influence of land-surface evapotranspiration on the Earth's climate," *Science,* vol. 215, pp. 1498-1501, 1982.

[27] W. Brutsaert, "Catchment-scale evaporation and the atmospheric boundary layer," *Water Resources Research,* vol. 22, pp. 39S-45S, 1986.

[28] P. Curran and G. M. Foody, "Environmental issues at regional to global scales," John Wiley & Sons Ltd.,1994.

[29] J. Martínez-Fernández and A. Ceballos, "Temporal stability of soil moisture in a large-field experiment in Spain," *Soil Science Society of America Journal,* vol. 67, pp. 1647-1656, 2003.

[30] T. Delworth and S. Manabe, "The influence of potential evaporation on the variabilities of simulated soil wetness and climate," *Journal of Climate,* vol. 1, pp. 523-547, 1988.

[31] V. Pauwels, Hoeben, Rudi,Verhoest, Niko E. C.,De Troch, François P., and P. A. Troch, "Improvement of TOPLATS-based discharge predictions through assimilation of ERS-based remotely sensed soil moisture values," *Hydrological processes,* vol. 16, pp. 995-1013, 2002.

[32] R. D. Koster, Suarez, Max J.,Liu, Ping,Jambor, Urszula,Berg, Aaron,Kistler, Michael,Reichle, Rolf,Rodell, Matthew, and J. Famiglietti, "Realistic initialization of land surface states: Impacts on subseasonal forecast skill," *Journal of Hydrometeorology,* vol. 5, pp. 1049-1063, 2004.

[33] D. Entekhabi, Nakamura, Hajime, and E. G. Njoku, "Solving the inverse problem for soil moisture and temperature profiles by sequential assimilation of multifrequency remotely sensed observations," *Geoscience and Remote Sensing, IEEE Transactions on,* vol. 32, pp. 438-448, 1994.

[34] Z. Su, Troch, P. A.,de Troch, F. P.,Nochtergale, L., and B. Cosyn, "Preliminary Results of Soil Moisture Retrieval From ESAR (EMAC 94) and ERS-1/SAR, Part II: Soil Moisture Retrieval," 1995, pp. 7-19.

[35] A. W. Western, Green, T. R., and R. B. Grayson, "Hydrological modelling of the Tarrawarra Catchment: Use of soil moisture patterns," 1997, pp. 8-11.

[36] L. Wang, "Remote Sensing Techniques for Soil Moisture and Agricultural Drought Monitoring," 2008.

[37] A. K. Betts, Ball, John H.,Beljaars, Anton,Miller, Martin J., and P. A. Viterbo, "The land surface-atmosphere interaction: A review based on observational and global modeling perspectives," *Journal of Geophysical Research: Atmospheres (1984–2012),* vol. 101, pp. 7209-7225, 1996.

[38] C. A. Clark and P. W. Arritt, "Numerical simulations of the effect of soil moisture and vegetation cover on the development of deep convection," *Journal of Applied Meteorology,* vol. 34, pp. 2029-2045, 1995.

[39] M. J. Fennessy and J. Shukla, "Impact of initial soil wetness on seasonal atmospheric prediction," *Journal of Climate,* vol. 12, pp. 3167-3180, 1999.

[40] E.-S. National Research Council . Committee on Restoration of Aquatic*, et al.*, *Restoration of aquatic ecosystems: science, technology, and public policy*: National Academies Press, 1992.

[41] T. J. Schmugge, Jackson, T. J., and H. L. McKim, "Survey of methods for soil moisture determination," *Water Resources Research,* vol. 16, pp. 961-979, 1980.

[42] J. T. Dugan, "The relationship of the thermal regime of the soil to the extrinsic environment, with special reference to the north central United States," 1978.

[43] A. Klute, *Methods of soil analysis. Part 1. Physical and mineralogical methods*: American Society of Agronomy, Inc., 1986.

[44] J. V. Stafford, "Remote, non-contact and in-situ measurement of soil moisture content: a review," *Journal of agricultural Engineering Research,* vol. 41, pp. 151-172, 1988.

[45] L. Di, "Regional-scale soil moisture monitoring using NOAA/AVHRR data," *Climatic Modeling, and Global Environmental Change*, 1991.

[46] T. Y. Alshikaili, "Non-contact measurement of soil moisture content using thermal infrared sensor and weather variables," University of Saskatchewan, 2007.

[47] T. J. Heimovaara and W. Bouten, "A computer-controlled 36-channel time domain reflectometry system for monitoring soil water contents," *Water Resources Research,* vol. 26, pp. 2311-2316, 1990.

[48] P. R. Luney and H. W. Dill, "Uses, potentialities, and needs in agriculture and forestry," *Remote sensing with special reference to agriculture and forestry,* pp. 1-34., 1970.

[49] U. S. S. C. Service, "Aerial photo interpretation in classifying and mapping soils," Agr, Washington, D. C.,1966.

[50] V. I. Myers and W. A. Allen, "Electrooptical remote sensing methods as nondestructive testing and measuring techniques in agriculture," *Applied Optics,* vol. 7, pp. 1819-1838, 1968.

[51] J. D. Hanson, Rojas, K. W., and M. J. Shaffer, "Calibrating the root zone water quality model," *Agronomy Journal,* vol. 91, pp. 171-177, 1999.

[52] K. P. Georgakakos and O. W. Baumer, "Measurement and utilization of on-site soil moisture data," *Journal of hydrology,* vol. 184, pp. 131-152 1996.

[53] J. S. Famiglietti, Devereaux, J. A.,Laymon, C. A.,Tsegaye, T.,Houser, P. R.,Jackson, T. J.,Graham, S. T.,Rodell, M., and P. J. v. Oevelen, "Ground-based investigation of soil moisture variability within remote sensing footprints during the Southern Great Plains 1997 (SGP97) Hydrology Experiment," *Water Resources Research,* vol. 35, pp. 1839-1851, 1999.

[54] K. I. Mohr, Famiglietti, James S.,Boone, Aaron, and P. J. Starks, "Modeling soil moisture and surface flux variability with an untuned land surface scheme: A case study from the Southern Great Plains 1997 Hydrology Experiment," *Journal of Hydrometeorology,* vol. 1, pp. 154-169, 2000.

[55] B. P. Mohanty, Famiglietti, J. S., and T. H. Skaggs, "Evolution of soil moisture spatial structure in a mixed vegetation pixel during the Southern Great Plains 1997 (SGP97) Hydrology Experiment," *Water Resources Research,* vol. 36, pp. 3675-3686, 2000.

[56] B. P. Mohanty, Skaggs, Th H., and J. S. Famiglietti, "Analysis and mapping of field-scale soil moisture variability using high resolution, ground based data during the Southern Great Plains 1997 (SGP97) Hydrology Experiment," *Water Resources Research,* vol. 36, pp. 1023-1031, 2000.

[57] B. P. Mohanty and T. H. Skaggs, "Spatio-temporal evolution and time-stable characteristics of soil moisture within remote sensing footprints with varying soil, slope, and vegetation," *Advances in Water Resources,* vol. 24, pp. 1051-1067, 2001.

[58] R. Bindlish and A. P. Barros, "Parameterization of vegetation backscatter in radar-based, soil moisture estimation," *Remote Sens Environ,* vol. 76, pp. 130-137, 2001.

[59] W. P. Kustas, Jackson, Thomas J.,French, Andrew N., and J. I. MacPherson, "Verification of patch-and regional-scale energy balance estimates derived from microwave and optical remote sensing during SGP97," *Journal of Hydrometeorology,* vol. 2, pp. 254-273, 2001.

[60] A. J. Wickel, Jackson, T. J., and E. F. Wood, "Multitemporal monitoring of soil moisture with RADARSAT SAR during the 1997 Southern Great Plains hydrology experiment," *International Journal of Remote Sensing,* vol. 22, pp. 1571-1583, 2001.

[61] R. D. Koster and P. C. D. Milly, "The interplay between transpiration and runoff formulations in land surface schemes used with atmospheric models," *Journal of Climate,* vol. 10, pp. 1578-1591, 1997.

[62] W. R. Hook and N. J. Livingston, "Errors in converting time domain reflectometry measurements of propagation velocity to estimates of soil water content," *Soil Science Society of America Journal,* vol. 60, pp. 35-41 1996.

[63] J. L. Starr and I. C. Paltineanu, "Soil water dynamics using multisensor capacitance probes in nontraffic interrows of corn," *Soil Science Society of America Journal,* vol. 62, pp. 114-122, 1998.

[64] R. H. Reichle, McLaughlin, Dennis B., and D. Entekhabi, "Hydrologic data assimilation with the ensemble Kalman filter," *Monthly Weather Review,* vol. 130, pp. 103-114, 2002.

[65] E. T. Engman and R. J. Gurney, *Remote sensing in hydrology*: Chapman and Hall Ltd, 1991.

[66] T. J. Jackson, "III. Measuring surface soil moisture using passive microwave remote sensing," *Hydrological processes,* vol. 7, pp. 139-152, 1993.

[67] E. G. Njoku and D. Entekhabi, "Passive microwave remote sensing of soil moisture," *Journal of hydrology,* vol. 184, pp. 101-129, 1996.

[68] T. J. Jackson, Le Vine, David M,Hsu, Ann Y,Oldak, Anna,Starks, Patrick J,Swift, Calvin T,Isham, John D, and M. Haken, "Soil moisture mapping at regional scales using microwave radiometry: The Southern Great Plains Hydrology Experiment," *Geoscience and Remote Sensing, IEEE Transactions on,* vol. 37, pp. 2136-2151, 1999.

[69] T. Schmugge, Gloersen, P.,Wilheit, Tom, and F. Geiger, "Remote sensing of soil moisture with microwave radiometers," *Journal of geophysical research,* vol. 79, pp. 317-323 1974.

[70] T. J. Jackson and T. J. Schmugge, "Passive microwave remote sensing system for soil moisture: Some supporting research," *Geoscience and Remote Sensing, IEEE Transactions on,* vol. 27, pp. 225-235, 1989.

[71] L. Prevot, Bernard, R.,Taconet, O.,Vidal-Madjar, D., and J. L. Thony, "Evaporation from a bare soil evaluated using a soil water transfer model and remotely sensed surface soil moisture data," *Water Resources Research,* vol. 20, pp. 311-316, 1984.

[72] M. R. Smith, Newton, Richard W., and L. B. J. S. Center, *The prediction of root zone soil moisture with a water balance-microwave emission model*: Texas A & M University, 1983.

[73] K. G. Kostov and T. J. Jackson, "Estimating profile soil moisture from surface-layer measurements: a review," in *Optical Engineering and Photonics in Aerospace Sensing*, 1993, pp. 125-136.

[74] P. R. Houser, Shuttleworth, W. James,Famiglietti, James S.,Gupta,oshin V.,Syed, Kamran H., and D. C. Goodrich, "Integration of soil moisture remote sensing and hydrologic modeling using data assimilation," *Water Resources Research,* vol. 34, pp. 3405-3420, 1998.

[75] W. L. Crosson, Laymon, Charles A.,Inguva, Ramarao, and M. P. Schamschula, "Assimilating remote sensing data in a surface flux–soil moisture model," *Hydrological processes,* vol. 16, pp. 1645-1662 2002.

[76] P. J. Starks, Heathman, Gary C.,Ahuja, Lajpat R., and L. Ma, "Use of limited soil property data and modeling to estimate root zone soil water content," *Journal of hydrology,* vol. 272, pp. 131-147, 2003.

[77] G. C. Heathman, Starks, Patrick J.,Ahuja, Lajpat R., and T. J. Jackson, "Assimilation of surface soil moisture to estimate profile soil water content," *Journal of hydrology,* vol. 279, pp. 1-17, 2003.

[78] W. T. Crow and E. F. Wood, "The assimilation of remotely sensed soil brightness temperature imagery into a land surface model using ensemble Kalman filtering: A case study based on ESTAR measurements during SGP97," *Advances in Water Resources,* vol. 26, pp. 137-149, 2003.

[79] J. P. Walker and P. R. Houser, "A methodology for initializing soil moisture in a global climate model: Assimilation of near-surface soil moisture observations," *Journal of Geophysical Research: Atmospheres (1984–2012),* vol. 106, pp. 11761-11774, 2001.

[80] S. Dunne and D. Entekhabi, "An ensemble-based reanalysis approach to land data assimilation," *Water Resources Research,* vol. 41, p. W02013, 2005.

[81] S. A. Margulis, McLaughlin, Dennis,Entekhabi, Dara, and S. Dunne, "Land data assimilation and estimation of soil moisture using measurements from the Southern Great Plains 1997 Field Experiment," *Water Resources Research,* vol. 38, pp. 35-1-35-18, 2002.

[82] F. Chen, Mitchell, Kenneth,Schaake, John,Xue, Yongkang,Pan, Hua-Lu,Koren, Victor,Duan, Qing Yun,Ek, Michael, and A. Betts, "Modeling of land surface evaporation by four schemes and comparison with FIFE observations," *Journal of geophysical research,* vol. 101, pp.7251-7268, 1996.

[83] X. Liang, Wood, Eric F., and D. P. Lettenmaier, "Surface soil moisture parameterization of the VIC-2L model: Evaluation and modification," *Global and Planetary Change,* vol. 13, pp. 195-206, 1996.

[84] R. D. Koster and M. J. Suarez, "Energy and water balance calculations in the Mosaic LSM," *NASA Tech. Memo,* vol. 104606, p. 59, 1996.

[85] Y. Dai, Zeng, Xubin,Dickinson, Robert E.,Baker, Ian,Bonan, Gordon B.,Bosilovich, Michael G.,Denning, A. Scott,Dirmeyer, Paul A.,Houser, Paul R., and G. Niu, "The common land model," *Bulletin of the American Meteorological Society,* vol. 84, pp. 1013-1023, 2003.

[86] A. H. Thieken, Luecke, Andreas,Diekkrueger, Bernd, and O. Richter, "Scaling input data by GIS for hydrological modelling," *Hydrological processes,* vol. 13, pp. 611-630, 1999.

[87] P. Lachassagne, Wyns, R.,Bérard, Pierre,Bruel, Thierry,Chéry, Laurence,Coutand, Thierry,Desprats, Jean-François, and P. Strat, "Exploitation of High-Yields in Hard-Rock Aquifers: Downscaling Methodology Combining GIS and Multicriteria Analysis to Delineate Field Prospecting Zones," *Ground Water,* vol. 39, pp. 568-581, 2001.

[88] H. Schreier and S. Brown, "Scaling issues in watersheds assessments," *Water Policy,* vol. 3, pp. 475-489, 2002.

[89] C. S. Renschler, "Designing geo-spatial interfaces to scale process models: The GeoWEPP approach," *Hydrological processes,* vol. 17, pp. 1005-1017, 2003.

[90] D. M. Gates, "Introduction: biophysical ecology," in *Perspectives of biophysical ecology*, ed: Springer, 1975, pp. 1-28

[91] F. Ulaby, "Radar response to vegetation," *Antennas and Propagation, IEEE Transactions on,* vol. 23, pp. 36-45, 1975.

[92] B. E. Myhre and S. F. Shih, "Using infrared thermometry to estimate soil water content for a sandy soil," *Transactions of the ASAE,* vol. 33, pp. 1479-1486, 1990.

[93] A. A. Ahmed, "An Improved Approach For Soil Moisture Estimation By Employing Illumination-Corrected Data In A Modifed Ts-VI Method," 2011.

[94] N. S. Chauhan, Miller, S., and P. Ardanuy, "Spaceborne soil moisture estimation at high resolution: a microwave-optical/IR synergistic approach," *International Journal of Remote Sensing,* vol. 24, pp. 4599-4622, 2003.

[95] W. Wagner, Lemoine, Guido, and H. Rott, "A method for estimating soil moisture from ERS scatterometer and soil data," *Remote sensing of environment,* vol. 70, pp. 191-207, 1999.

[96] H. M. Hemakumara, *Aggregation and Disaggregation of Soil Moisture Measurements*: University of Newcastle, 2007.

[97] C. Elachi and J. J. van Zyl, *Introduction to the physics and techniques of remote sensing* vol. 28 %@ 0471783382: Wiley-Interscience, 2006.

[98] S. B. Idso, Jackson, R. D.,Reginato, R. J.,Kimball, B. A., and F. S. Nakayama, "The dependence of bare soil albedo on soil water content," *Journal of Applied Meteorology,* vol. 14, pp. 109-113, 1975.

[99] X. Hao, *Estimation of live fuel moisture and soil moisture using satellite remote sensing*, 2006.

[100] T. N. Carlson, Gillies, Robert R., and E. M. Perry, "A method to make use of thermal infrared temperature and NDVI measurements to infer surface soil water content and fractional vegetation cover," *Remote Sensing Reviews,* vol. 9, pp. 161-173, 1994.

[101] R. R. Gillies, Kustas, W. P., and K. S. Humes, "A verification of the'triangle'method for obtaining surface soil water content and energy fluxes from remote measurements of the Normalized Difference Vegetation Index (NDVI) and surface e," *Int. J. Remote Sens* vol. 18, pp. 3145-3166, 1997.

[102] R. R. Gillies and T. N. Carlson, "Thermal remote sensing of surface soil water content with partial vegetation cover for incorporation into climate models," *Journal of Applied Meteorology,* vol. 34, pp. 745-756 %@ 1520-0450, 1995.

[103] T. N. Carlson and D. A. Ripley, "On the relation between NDVI, fractional vegetation cover, and leaf area index," *Remote sensing of environment,* vol. 62, pp. 241-252, 1997.

[104] D. B. Lobell and G. P. Asner, "Moisture effects on soil reflectance," *Soil Science Society of America Journal,* vol. 66, pp. 722-727, 2002.

[105] P. J. Sellers, Berry, J. A.,Collatz, G. J.,Field, C. B., and F. G. Hall, "Canopy reflectance, photosynthesis, and transpiration. III. A reanalysis using improved leaf models and a new canopy integration scheme," *Remote sensing of environment,* vol. 42, pp. 187-216, 1992.

[106] E. A. Smith, Hsu, A. Y.,Crosson, W. L.,Field, R. T.,Fritschen, L. J.,Gurney, R. J.,Kanemasu, E. T.,Kustas, W. P.,Nie, D., and W. J. Shuttleworth, "Area-

averaged surface fluxes and their time-space variability over the FIFE experimental domain," *J Geophys Res* vol. 97, pp. 18599-18622 1992.

[107] W. G. M. Bastiaanssen, Menenti, M.,Feddes, R. A., and A. A. M. Holtslag, "A remote sensing surface energy balance algorithm for land (SEBAL). 1. Formulation," *Journal of hydrology,* vol. 212, pp. 198-212, 1998.

[108] M. M. Rahman, "Mapping surface soil moisture and roughness by radar remote sensing in the semi-arid environment," *arizona open repository* 2005.

[109] D. S. C. Liew, "Electromagnetic waves," *Centre for Remote Imaging, Sensing and Processing. Retrieved,* pp. 10-27, 2006.

[110] J. R. Jensen, Garcia-Quijano, Maria,Hadley, Brian,Im, Jungho,Wang, Zhongwu,Nel, Abraham L.,Teixeira, Eduarda, and B. A. Davis, "Remote sensing agricultural crop type for sustainable development in South Africa," *Geocarto International,* vol. 21, pp. 5-18, 2006.

[111] D. A. Pratt and C. D. Ellyett, "The thermal inertia approach to mapping of soil moisture and geology," *Remote sensing of environment,* vol. 8, pp. 151-168, 1979.

[112] W. W. Verstraeten, Veroustraete, Frank,van der Sande, Corné J.,Grootaers, Ief, and J. Feyen, "Soil moisture retrieval using thermal inertia, determined with visible and thermal spaceborne data, validated for European forests," *Remote sensing of environment,* vol. 101, pp. 299-314, 2006.

[113] J. D. Jordan and S. F. Shih, "Comparison of thermal-based soil moisture estimation techniques on a histosol," 1993.

[114] C. Ottlé and D. Vidal-Madjar, "Assimilation of soil moisture inferred from infrared remote sensing in a hydrological model over the HAPEX-MOBILHY region," *Journal of hydrology,* vol. 158, pp. 241-264, 1994.

[115] J. L. Monteith, "Evaporation and surface temperature," *Quarterly Journal of the Royal Meteorological Society,* vol. 107, pp. 1-27, 1981.

[116] S. F. Shih and E. Y. Chen, "Using GOES thermal infrared data to map freeze zones for citrus and consequences for water management," *Water Resources Research,* vol. 23, pp. 737-743, 1987.

[117] T. J. Jackson and T. J. Schmugge, "Vegetation effects on the microwave emission of soils," *Remote sensing of environment,* vol. 36, pp. 203-212, 1991.

[118] L. Wang, Qu, J. J.,Zhang, S.,Hao, X., and S. Dasgupta, "Soil moisture estimation using MODIS and ground measurements in eastern China," *International Journal of Remote Sensing,* vol. 28, pp. 1413-1418, 2007.

[119] T. Carlson, "An overview of the" triangle method" for estimating surface evapotranspiration and soil moisture from satellite imagery," *Sensors,* vol. 7, pp. 1612-1629, 2007.

[120] B. J. Choudhury and P. Pampaloni, *Passive Microwave Remote Sensing of Land--Atmosphere Interactions*: Vsp, 1995.

[121] T. W. Owen, Carlson, T. N., and R. R. Gillies, "An assessment of satellite remotely-sensed land cover parameters in quantitatively describing the climatic effect of urbanization," *International Journal of Remote Sensing,* vol. 19, pp. 1663-1681, 1998.

[122] G. G. S. Pegram, "A nested multisite daily rainfall stochastic generation model," *Journal of hydrology,* vol. 371, pp. 142-153, 2009.

[123] A. A. Van de Griend and M. Owe, "Microwave vegetation optical depth and inverse modelling of soil emissivity using Nimbus/SMMR satellite observations," *Meteorology and Atmospheric Physics,* vol. 54, pp. 225-239, 1994.

[124] E. Valor and V. Caselles, "Mapping land surface emissivity from NDVI: Application to European, African, and South American areas," *Remote sensing of environment,* vol. 57, pp. 167-184, 1996.

[125] J. C. Eidenshink and J. L. Faundeen, "The 1 km AVHRR global land data set: first stages in implementation," *International Journal of Remote Sensing,* vol. 15, pp. 3443-3462, 1994.

[126] R. Lee, Kastens, D. L.,Price, K. P., and E. A. Martinko, "Forecasting corn yield in Iowa using remotely sensed data and vegetation phenology information," 1999.

[127] A. Kondoh and A. Higuchi, "Relationship between satellite-derived spectral brightness and evapotranspiration from a grassland," *Hydrological processes,* vol. 15, pp. 1761-1770, 2001.

[128] I. Sandholt, Rasmussen, Kjeld, and J. Andersen, "A simple interpretation of the surface temperature/vegetation index space for assessment of surface moisture status," *Remote sensing of environment,* vol. 79, pp. 213-224, 2002.

[129] H. Q. Liu and A. Huete, "A feedback based modification of the NDVI to minimize canopy background and atmospheric noise," *Geoscience and Remote Sensing, IEEE Transactions on,* vol. 33, pp. 457-465, 1995.

[130] M. S. Moran, Clarke, T. R.,Inoue, Y., and A. Vidal, "Estimating crop water deficit using the relation between surface-air temperature and spectral vegetation index," *Remote sensing of environment,* vol. 49, pp. 246-263, 1994.

[131] A. A. Van de Griend and M. Owe, "On the relationship between thermal emissivity and the normalized difference vegetation index for natural surfaces," *Int J Remote Sens* vol. 14, pp. 1119-1131, 1993.

[132] Z. Wan, "MODIS land-surface temperature algorithm theoretical basis document (LST ATBD)," *Institute for Computational Earth System Science, Santa Barbara,* p. 75, 1999.

[133] Y. H. Kerr, Lagouarde, Jean Pierre,Nerry, Françoise, and C. Ottlé, "Land surface temperature retrieval techniques and applications," *Thermal Remote Sensing in Land Surface Processing,* p. 33, 2004.

[134] W. G. M. Bastiaanssen, Pelgrum, H.,Droogers, P.,de Bruin, H. A. R., and M. Menenti, "Area-average estimates of evaporation, wetness indicators and top soil moisture during two golden days in EFEDA," *Agricultural and forest meteorology,* vol. 87, pp. 119-137, 1997.

[135] T. R. McVicar and D. L. B. X. Jupp, *Using AVHRR data and meteorological surfaces as covariates to spatially interpolate moisture availability in the Murray-Darling Basin*: CSIRO Land and Water, 1999.

[136] Z. Wan*, et al.*, "Using MODIS land surface temperature and normalized difference vegetation index products for monitoring drought in the southern Great Plains, USA," *International Journal of Remote Sensing,* vol. 25, pp. 61-72, 2004.

[137] M. F. McCabe and E. F. Wood, "Scale influences on the remote estimation of evapotranspiration using multiple satellite sensors," *Remote sensing of environment,* vol. 105, pp. 271-285, 2006.

[138] G. R. Diak and T. R. Stewart, "Assessment of surface turbulent fluxes using geostationary satellite surface skin temperatures and a mixed layer planetary boundary layer scheme," *Journal of Geophysical Research: Atmospheres (1984–2012),* vol. 94, pp. 6357-6373, 1989.

[139] R. C. Vining and B. L. Blad, "Estimation of sensible heat flux from remotely sensed canopy temperatures," *Journal of Geophysical Research: Atmospheres (1984–2012),* vol. 97, pp. 18951-18954, 1992.

[140] F. Kimura and Y. Shimizu, "Estimation of Sensible and Latent Heat Fluxes from Soil Surface Temperature Using a Linear Air-Land Heat Transfer Model," *Journal of Applied Meteorology,* vol. 33, pp. 477-489, 1994.

[141] G. R. Diak and M. S. Whipple, "Improvements to models and methods for evaluating the land-surface energy balance and 'effective'roughness using radiosonde reports and satellite-measured 'skin'temperature data," *Agricultural and forest meteorology,* vol. 63, pp. 189-218, 1993.

[142] R. Crago, Sugita, Michiaki, and W. Brutsaert, "Satellite-derived surface temperatures with boundary layer temperatures and geostrophic winds to estimate surface energy fluxes," *Journal of geophysical research,* vol. 100, pp. 25447-25,451, 1995.

[143] G. A. Meehl, "Influence of the land surface in the Asian summer monsoon: External conditions versus internal feedbacks," *Journal of Climate,* vol. 7, pp. 1033-1049, 1994.

[144] A. Sinha, "Relative influence of lapse rate and water vapor on the greenhouse effect," *Journal of Geophysical Research: Atmospheres (1984–2012),* vol. 100, pp. 5095-5103, 1995.

[145] R. D. Jackson, Reginato, R. J., and S. B. Idso, "Wheat canopy temperature: a practical tool for evaluating water requirements," *Water Resources Research,* vol. 13, pp. 651-656, 1977.

[146] V. Caselles and J. Sobrino, "Determination of frosts in orange groves from NOAA-9 AVHRR data," *Remote sensing of environment,* vol. 29, pp. 135-146, 1989.

[147] H. Kerdiles, Grondona, M.,Rodriguez, R., and B. Seguin, "Frost mapping using NOAA AVHRR data in the Pampean region, Argentina," *Agricultural and forest meteorology,* vol. 79, pp. 157-182, 1996.

[148] A. R. Harris and I. M. Mason, "An extension to the split-window technique giving improved atmospheric correction and total water vapour," *International Journal of Remote Sensing,* vol. 13, pp. 881-892, 1992.

[149] J. A. Sobrino, Li, Zhao-Liang, and M. P. Stoll, "Impact of the atmospheric transmittance and total water vapor content in the algorithms for estimating satellite sea surface temperatures," *Geoscience and Remote Sensing, IEEE Trans Geosci Remote Sens* vol. 31, pp. 946-952, 1993.

[150] T. J. Klesspies and L. M. McMillin, "Retrieval of precipitable water from observations in the split-window over varying surface temperature," *Journal of Applied Meteorology,* vol. 29, pp. 851-862, 1990.

[151] G. J. Jedlovec, "Precipitable Water Estimation from High-Resolution Split Window Radiance Measurements," *Journal of Applied Meteorology,* vol. 29, pp. 863-877, 1990.

[152] Z. Wan and J. Dozier, "A generalized split-window algorithm for retrieving land-surface temperature from space," *Geoscience and Remote Sensing, IEEE Transactions on,* vol. 34, pp. 892-905, 1996.

[153] Z. Qin, Dall'Olmo, Giorgio,Karnieli, Arnon, and P. Berliner, "Derivation of split window algorithm and its sensitivity analysis for retrieving land surface temperature from NOAA-advanced very high resolution radiometer data," *Journal of Geophysical Research: Atmospheres (1984–2012),* vol. 106, pp. 22655-22670, 2001.

[154] H. H. Ku, "Notes on the use of propagation of error formulas," *Precision Measurement and Calibration, NBS SP 3D0,* vol. 1, pp. 331-341, 1969.

[155] H. Wang, Li, Xiaobing,Long, Huiling,Xu, Xu, and Y. Bao, "Monitoring the effects of land use and cover type changes on soil moisture using remote-sensing data: A case study in China's Yongding River basin," *Catena,* vol. 82, pp. 135-145, 2010.

[156] J. Song, Wesely, ML,Coulter, RL, and E. Brandes, "Estimating watershed evapotranspiration with PASS. Part I: Inferring root-zone moisture conditions using satellite data," *Journal of Hydrometeorology,* vol. 1, pp. 447-461, 2000.

[157] X. Zhan, Miller, Shawn,Chauhan, Narinder,Di, Liping,Ardanuy, Philip, and S. Running, "Soil moisture: visible/infrared imager/radiometer suite algorithm theoretical basis document," *Raytheon Systems Company, Maryland, Version,* vol. 5, 2002.

[158] K. Nishida, Nemani, Ramakrishna R.,Running, Steven W., and J. M. Glassy, "An operational remote sensing algorithm of land surface evaporation," *Journal of Geophysical Research: Atmospheres (1984–2012),* vol. 108, 2003.

[159] L. Jiang and S. Islam, "An intercomparison of regional latent heat flux estimation using remote sensing data," *International Journal of Remote Sensing,* vol. 24, pp. 2221-2236, 2003.

[160] K. Wang, Li, Zhanqing, and M. Cribb, "Estimation of evaporative fraction from a combination of day and night land surface temperatures and NDVI: A new method to determine the Priestley–Taylor parameter," *Remote sensing of environment,* vol. 102, pp. 293-305, 2006.

[161] Q. K. Hassan, Bourque, Charles P. A.,Meng, Fan-Rui, and R. M. Cox, "A wetness index using terrain-corrected surface temperature and normalized difference vegetation index derived from standard MODIS products: an evaluation of its use in a humid forest-dominated region of eastern Canada," *Sensors,* vol. 7, pp. 2028-2048, 2007.

[162] S. Stisen, Sandholt, Inge,Norgaard, Anette,Fensholt, Rasmus, and K. H. Jensen, "Combining the triangle method with thermal inertia to estimate regional evapotranspiration—Applied to MSG-SEVIRI data in the Senegal River basin," *Remote sensing of environment,* vol. 112, pp. 1242-1255, 2008.

[163] Y. Yao, Qin, Qiming,Ghulam, Abduwasit,Liu, Shaomin,Zhao, Shaohua,Xu, Ziwei, and H. Dong, "Simple method to determine the Priestley–Taylor parameter for evapotranspiration estimation using Albedo-VI triangular space from MODIS data," *Journal of Applied Remote Sensing,* vol. 5, pp. 053505-053505-16, 2011.

[164] H. Nieto, Sandholt, Inge,Aguado, Inmaculada,Chuvieco, Emilio, and S. Stisen, "Air temperature estimation with MSG-SEVIRI data: Calibration and validation of the TVX algorithm for the Iberian Peninsula," *Remote sensing of environment,* vol. 115, pp. 107-116, 2011.

[165] Y. Xue and A. P. Cracknell, "Advanced thermal inertia modelling," *Remote Sensing,* vol. 16, pp. 431-446, 1995.

[166] J. A. Sobrino and M. H. El Kharraz, "Combining afternoon and morning NOAA satellites for thermal inertia estimation 2. Methodology and application," *Journal of geophysical research,* vol. 104, pp. 9455-9465, 1999.

[167] D. S. Mitra and T. J. Majumdar, "Thermal inertia mapping over the Brahmaputra basin, India using NOAA-AVHRR data and its possible geological applications," *International Journal of Remote Sensing,* vol. 25, pp. 3245-3260, 2004.

[168] V. Tramutoli, Claps, Pierluigi,Marella, Mauro,Pergola, Nicola, and C. Sileo, "Feasibility of hydrological application of thermal inertia from remote sensing," 2000, pp. 16-18.

[169] K. Mallick, Bhattacharya, Bimal K., and N. K. Patel, "Estimating volumetric surface moisture content for cropped soils using a soil wetness index based on surface temperature and NDVI," *Agricultural and forest meteorology,* vol. 149, pp. 1327-1342, 2009.

[170] P. K. Thapliyal, Pal, P. K.,Narayanan, M. S., and J. Srinivasan, "Development of a time series-based methodology for estimation of large-area soil wetness over India using IRS-P4 microwave radiometer data," *Journal of Applied Meteorology,* vol. 44, pp. 127-143, 2005.

[171] R. R. Nemani and S. W. Running, "Estimation of regional surface resistance to evapotranspiration from NDVI and thermal-IR AVHRR data," *Journal of Applied Meteorology,* vol. 28, pp. 276-284, 1989.

[172] E. F. Lambin and D. Ehrlich, "The surface temperature-vegetation index space for land cover and land-cover change analysis," *International Journal of Remote Sensing,* vol. 17, pp. 463-487, 1996.

[173] R. Nemani, Pierce, Lars,Running, Steve, and S. Goward, "Developing satellite-derived estimates of surface moisture status," *Journal of Applied Meteorology,* vol. 32, pp. 548-557, 1993.

[174] T. N. Carlson, Gillies, Robert R., and T. J. Schmugge, "An interpretation of methodologies for indirect measurement of soil water content," *Agricultural and forest meteorology,* vol. 77, pp. 191-205, 1995.

[175] L.-A. Dupigny-Giroux and J. E. Lewis, "A moisture index for surface characterization over a semiarid area," *PE & RS- Photogrammetric Engineering & Remote Sensing,* vol. 65, pp. 937-945, 1999.

[176] S. N. Goward, Xue, Yongkang, and K. P. Czajkowski, "Evaluating land surface moisture conditions from the remotely sensed temperature/vegetation index measurements: an exploration with the simplified simple biosphere model," *Remote sensing of environment,* vol. 79, pp. 225-242, 2002.

[177] L. Jiang and S. Islam, "Estimation of surface evaporation map over southern Great Plains using remote sensing data," *Water Resources Research,* vol. 37, pp. 329-340, 2001.

[178] Q. K. Hassan and C. P. A. Bourque, "Estimating daily evapotranspiration for forests in Atlantic Maritime Canada: application of MODIS imagery," 2006, p. 11.

[179] A. Vidal and C. Devaux-Ros, "Evaluating forest fire hazard with a Landsat TM derived water stress index," *Agricultural and forest meteorology,* vol. 77, pp. 207-224, 1995.

[180] C. Wang, Qi, Shuhua,Niu, Zheng, and J. Wang, "Evaluating soil moisture status in China using the temperature-vegetation dryness index (TVDI)," *Canadian Journal of Remote Sensing,* vol. 30, pp. 671-679, 2004.

[181] R. R. Rogers and M. K. Yau, "A Short Course in Cloud Physics, International Series in Natural Philosophy," ed: Butterworth Heinemann, Burlington, MA, 1989.

[182] C.-h. Juan, *Application of remote sensing techniques at different scales of observation on wetland evapotranspiration*, 2001.

[183] R. G. Allen*, et al.*, "FAO Irrigation and drainage paper No. 56," *Rome: Food and Agriculture Organization of the United Nations,* pp. 26-40, 1998.

[184] D. Raes, "The ETo calculator: Evapotranspiration from a reference surface, Reference manual, Version 3.1. FAO," *Land and water devision, Rome, Italy,* 2009.

[185] S. Lerer, "Estimation of actual evapotranspiration using remote sensing data for the Yucatan Peninsula, Mexico," Wetlands 30, (1) 1-13,2008.

[186] S. Shahidian, Serralheiro, R. P.,Serrano, João,Teixeira, José,Haie, Naim, and F. Santos, "Hargreaves and other reduced-set methods for calculating evapotranspiration," 2012.

[187] G. H. Hargreaves and R. G. Allen, "History and evaluation of Hargreaves evapotranspiration equation," *Journal of irrigation and drainage engineering,* vol. 129, pp. 53-63, 2003.

[188] G. H. Hargreaves and Z. A. Samani, "Estimating potential evapotranspiration," *Journal of the Irrigation and Drainage Division,* vol. 108, pp. 225-230, 1982.

[189] L. Turc, "Evaluation des besoins en eau d'irrigation, évapotranspiration potentielle," *Ann. agron,* vol. 12, pp. 13-49, 1961.

[190] J. Lu, Sun, Ge,McNulty, Steven G., and D. M. Amatya, "A COMPARISON OF SIX POTENTIAL EVAPOTRANSPIRATION METHODS FOR REGIONAL USE IN THE SOUTHEASTERN UNITED STATES1," *JAWRA Journal of the American Water Resources Association,* vol. 41, pp. 621-633, 2005.

[191] D. T. Jensen, Hargreaves, G. H.,Temesgen, B., and R. G. Allen, "Computation of ETo under nonideal conditions," *Journal of irrigation and drainage engineering,* vol. 123, pp. 394-400, 1997.

[192] C.-h. Tan, "Regional Scale Evapotranspiration Estimation using Vegeation Index and Surface Temperature from NOAA Satellite AVHRR Data " PhD, Graduate School, University of Florida, 1998.

[193] J. C. Price, "Using spatial context in satellite data to infer regional scale evapotranspiration," *Geoscience and Remote Sensing, IEEE Transactions on,* vol. 28, pp. 940-948, 1990.

[194] D. Courault, Seguin, Bernard, and A. Olioso, "Review on estimation of evapotranspiration from remote sensing data: From empirical to numerical

modeling approaches," *Irrigation and Drainage systems,* vol. 19, pp. 223-249, 2005.

[195] W. G. M. Bastiaanssen, *Regionalization of surface flux desities and moisture indicators in composite terrain: a remote sensing approach under clear skies in Mediterranean climates*: Landbouwuniversiteit te Wageningen, 1995.

[196] B. C. Nelson, Ralf Waters,Kimberly, Idaho,Richard Allen,Masahiro Tasumi,Ricardo Trezza,Wageningen, the Netherlands, and W. Bastiaanssen, "Surface Energy Balance Algorithms for Land (SEBAL)," in *Advanced Training and Users Manual*, N. E. S. g. f. t. R. Company, Ed., ed. Idaho: The Idaho Department of Water Resources, 2002.

[197] S. Chatterjee, "Estimating evapotranspiration using remote sensing: A hybrid approach between MODIS derived enhanced vegetation index, Bowen ratio system, and ground based micro-meteorological data," Wright State University, 2010.

[198] F. Jacob, Olioso, Albert,Gu, Xing Fa,Su, Zhongbo, and B. Seguin, "Mapping surface fluxes using airborne visible, near infrared, thermal infrared remote sensing data and a spatialized surface energy balance model," *Agronomie,* vol. 22, pp. 669-680, 2002.

[199] S. Liang, Strahler, Alan, and C. Walthall, "Retrieval of land surface albedo from satellite observations: A simulation study," 1998, pp. 1286-1288

[200] S. Khan, Hafeez, M. M.,Rana, Tariq, and S. Mushtaq, "Enhancing water productivity at the irrigation system level: a geospatial hydrology application in the Yellow River Basin," *Journal of Arid Environments,* vol. 72, pp. 1046-1063, 2008.

[201] M. M. Hafeez, *Water accounting and productivity at different spatial scales in a rice irrigation system*: Cuvillier, 2003.

[202] J. M. Jacobs, Mergelsberg, Shannon L.,Lopera, Andres F., and D. A. Myers, "Evapotranspiration from a wet prairie wetland under drought conditions: Paynes Prairie Preserve, Florida, USA," *Wetlands,* vol. 22, pp. 374-385, 2002.

[203] W. W. Verstraeten*, et al.*, "Assessment of evapotranspiration and soil moisture content across different scales of observation," *Sensors,* vol. 8, pp. 70-117, 2008.

[204] W. J. Timmermans, Kustas, William P.,Anderson, Martha C., and A. N. French, "An intercomparison of the surface energy balance algorithm for land (SEBAL) and the two-source energy balance (TSEB) modeling schemes," *Remote sensing of environment,* vol. 108, pp. 369-384, 2007.

[205] J.-P. Lagouarde, Jacob, Frédéric,Gu, Xing Fa,Olioso, Albert,Bonnefond, Jean-Marc,Kerr, Yann,McAneney, K. John, and M. Irvine, "Spatialization of sensible heat flux over a heterogeneous landscape," *Agronomie-Sciences des Productions Vegetales et de l'Environnement,* vol. 22, pp. 627-634, 2002.

[206] W. G. M. Bastiaanssen, Noordman, E. J. M.,Pelgrum, H.,Davids, G.,Thoreson, B. P., and R. G. Allen, "SEBAL model with remotely sensed data to improve water-resources management under actual field conditions," *Journal of irrigation and drainage engineering,* vol. 131, pp. 85-93, 2005.

[207] Z. Su, "The Surface Energy Balance System (SEBS) for estimation of turbulent heat fluxes," *Hydrology and Earth System Sciences Discussions,* vol. 6, pp. 85-100, 2002.

[208] G. B. Senay, Budde, Michael,Verdin, James P., and A. M. Melesse, "A coupled remote sensing and simplified surface energy balance approach to estimate actual evapotranspiration from irrigated fields," *Sensors,* vol. 7, pp. 979-1000, 2007.

[209] F. Gellens-Meulenberghs, "Evapotranspiration and surface heat fluxes over Belgium: outcome and perspectives," *Agronomie,* vol. 20, pp. 857-868, 2000.

[210] G. J. Roerink, Su, Z., and M. Menenti, "S-SEBI: A simple remote sensing algorithm to estimate the surface energy balance," *Physics and Chemistry of the Earth, Part B: Hydrology, Oceans and Atmosphere,* vol. 25, pp. 147-157, 2000.

[211] W. W. Verstraeten, Veroustraete, Frank, and J. Feyen, "Estimating evapotranspiration of European forests from NOAA-imagery at satellite overpass time: Towards an operational processing chain for integrated optical and thermal sensor data products," *Remote sensing of environment,* vol. 96, pp. 256-276, 2005.

[212] M. S. Moran, Rahman, A. F.,Washburne, J. C.,Goodrich, D. C.,Weltz, M. A., and W. P. Kustas, "Combining the Penman-Monteith equation with

measurements of surface temperature and reflectance to estimate evaporation rates of semiarid grassland," *Agricultural and forest meteorology,* vol. 80, pp. 87-109, 1996.

[213] W. Mauser and S. Schädlich, "Modelling the spatial distribution of evapotranspiration on different scales using remote sensing data," *Journal of hydrology,* vol. 212, pp. 250-267, 1998.

[214] R. J. Granger, "Satellite-derived estimates of evapotranspiration in the Gediz basin," *Journal of hydrology,* vol. 229, pp. 70-76, 2000.

[215] H. A. Cleugh, Leuning, Ray,Mu, Qiaozhen, and S. W. Running, "Regional evaporation estimates from flux tower and MODIS satellite data," *Remote sensing of environment,* vol. 106, pp. 285-304, 2007.

[216] G. D'Urso, *Simulation and management of on-demand irrigation systems: a combined agrohydrological and remote sensing approach*: Wageningen Univ., 2001.

[217] P. L. Nagler, Cleverly, James,Glenn, Edward,Lampkin, Derrick,Huete, Alfredo, and Z. Wan, "Predicting riparian evapotranspiration from MODIS vegetation indices and meteorological data," *Remote sensing of environment,* vol. 94, pp. 17-30, 2005.

[218] P. Nagler, Jetton, Amity,Fleming, John,Didan, Kamel,Glenn, Edward,Erker, Joseph,Morino, Kiyomi,Milliken, Jeff, and S. Gloss, "Evapotranspiration in a cottonwood (Populus fremontii) restoration plantation estimated by sap flow and remote sensing methods," *Agricultural and forest meteorology,* vol. 144, pp. 95-110, 2007.

[219] A. A. Hassaballa and A. B. Matori, "The estimation of air temperature from NOAA/AVHRR images and the study of NDVI-Ts impact: Case study: The application of split-window algorithms over (Perak Tengah & Manjong) area, Malaysia," in *International Conference on Space Science and Communication (IconSpace)*, Malaysia, 2011, pp. 20-24

[220] JPM, "Basic Population Characteristics By Administrative Districts," Kuala Lumpur, 2010.

[221] Perak. (2012). *Town & Districts, Geography & Climate, Economy*. Available: http://www.malaysia-hotels.net/perak/index.html

[222] S. Senthil-Kumar. *European Digital Archive on Soil Maps of the world (EuDASM)*.

[223] ARSM, "Agensi Remote Sensing Malaysia," Kementerian Sains, Teknologi dan Inovasi Remote Sensing Data Processing and Distribution Division, Kuala Lumpur

[224] S. K. Selvaradjou, Montanarella, O.,Spaargaren, and D. Dent. (2005). *European Digital Archive of Soil Maps (EuDASM) - Soil Maps of Asia DVD-ROM version*.

[225] J. R. Jensen, *Introductory Digital Image Processing* vol. Third Edition. University of Carolina: Pearson Prentice Hall, 2005.

[226] B. A. Baum, "On the retrieval and analysis of multilevel clouds. ," 1992.

[227] G. Argyrous. *Statistics for Research: With a Guide to SPSS, SAGE*.

[228] D. Agostino, "QED Insight [mathematics, science, education, and more]," in *qedinfinity* vol. 2013, ed: QED infinity, 2010.

[229] G. Chander, Markham, Brian L., and D. L. Helder, "Summary of current radiometric calibration coefficients for Landsat MSS, TM, ETM+, and EO-1 ALI sensors," *Remote sensing of environment,* vol. 113, pp. 893-903, 2009.

[230] S. M. Adler-Golden, Matthew, Michael W.,Bernstein, Lawrence S.,Levine, Robert Y.,Berk, Alexander,Richtsmeier, Steven C.,Acharya, Prabhat K.,Anderson, Gail P.,Felde, G., and J. Gardner, "Atmospheric correction for short-wave spectral imagery based on MODTRAN 4," 1999, pp. 61-69

[231] M. W. Matthew, Adler-Golden, Steven M.,Berk, Alexander,Richtsmeier, Steven C.,Levine, Robert Y.,Bernstein, Lawrence S.,Acharya, Prabhat K.,Anderson, Gail P.,Felde, Gerald W., and M. L. Hoke, "Status of atmospheric correction using a MODTRAN4-based algorithm," 2000, pp. 199-207.

[232] A. N. Matori*, et al.*, "Study of regional monsoonal effects on landslide hazard zonation in Cameron Highlands, Malaysia," *Arabian J Geosci,* vol. 5, pp. 1069-1084, 2011.

[233] F. Becker and Z.-L. Li, "Temperature-independent spectral indices in thermal infrared bands," *Remote sensing of environment,* vol. 32, pp. 17-33, 1990.

[234] C. Ulivieri, Castronuovo, M. M.,Francioni, R., and A. Cardillo, "A split window algorithm for estimating land surface temperature from satellites," *Advances in Space Research,* vol. 14, pp. 59-65, 1994.

[235] J. A. Voogt and T. R. Oke, "Effects of urban surface geometry on remotely-sensed surface temperature," *International Journal of Remote Sensing,* vol. 19, pp. 895-920, 1998.

[236] A. Chudnovsky, Ben-Dor, E., and H. Saaroni, "Diurnal thermal behavior of selected urban objects using remote sensing measurements," *Energy and Buildings,* vol. 36, pp. 1063-1074, 2004.

[237] C. P. Lo, Quattrochi, Dale A., and J. C. Luvall, "Application of high-resolution thermal infrared remote sensing and GIS to assess the urban heat island effect," *International Journal of Remote Sensing,* vol. 18, pp. 287-304, 1997.

[238] Q. Weng, "A remote sensing? GIS evaluation of urban expansion and its impact on surface temperature in the Zhujiang Delta, China," *International Journal of Remote Sensing,* vol. 22, pp. 1999-2014, 2001.

[239] R. P. Gupta, *Remote sensing geology*: Springer Verlag, 2003.

[240] B. L. Markham and J. L. Barker, "Landsat MSS and TM post-calibration dynamic ranges, exoatmospheric reflectances and at-satellite temperatures," *EOSAT Landsat technical notes,* vol. 1, pp. 3-8, 1986.

[241] J. R. Schott and W. Volchok, "Thematic Mapper thermal infrared calibration," *Photogramm Eng Remote Sens* vol. 51, pp. 1351-1357, 1985.

[242] G. E. Wukelic, Gibbons, D. E.,Martucci, L. M., and H. P. Foote, "Radiometric calibration of Landsat Thematic Mapper thermal band," *Remote Sens Environ* vol. 28, pp. 339-347, 1989.

[243] T. M. Lillesand and R. W. Kiefer, "Remote sensing and image interpretationWiley," *New York,* 1994.

[244] USDA, "Soil Water Characteristics Triangle 6.02.74, Hydraulic Properties Calculator," ed: Agricultural Research Service.

[245] FAO, "ETo Calculator version 3.1 for Evapotranspiration from a reference surface," in *FAO Land and Water Digital Media Series* vol. N 36, ed. Rome. Italy: FAO, 2009.

[246] S. Richard. (2013). *The Art Of Data Validation*. Available: http://petesqbsite.com/sections/express/issue10/datavalidation.html

[247] IBM. *IBM SPSS*. Available: http://www01.ibm.com/software/analytics/spss/products/statistics/

[248] D. A. Skoog*, et al.*, *Instrumental analysis*: Brooks/Cole, Cengage Learning, 2007.

[249] S. Lee and B. Pradhan, "Landslide hazard mapping at Selangor, Malaysia using frequency ratio and logistic regression models," *Landslides,* vol. 4, pp. 33-41, 2007.

[250] L. Prihodko and S. N. Goward, "Estimation of air temperature from remotely sensed surface observations," *Remote sensing of environment,* vol. 60, pp. 335-346, 1997.

[251] S. N. Kalluri and R. O. Dubayah, "Comparison of atmospheric correction models for thermal bands of the advanced very high resolution radiometer over FIFE," *Journal of Geophysical Research: Atmospheres (1984–2012),* vol. 100, pp. 25411-25418, 1995.

[252] R. Smith and B. Choudhury, "Analysis of normalized difference and surface temperature observations over southeastern Australia," *Remote Sensing,* vol. 12, pp. 2021-2044, 1991.

[253] J. R. Jensen, *Remote Sensing of the Environment: An Earth Resource Perspective 2/e*: Pearson Education India, 2009.

[254] J. Dozier and S. G. Warren, "Effect of viewing angle on the infrared brightness temperature of snow," *Water Resources Research,* vol. 18, pp. 1424-1434, 1982.

[255] J. Labed and M. Stoll, "Angular variation of land surface spectral emissivity in the thermal infrared: laboratory investigations on bare soils," *Remote Sensing,* vol. 12, pp. 2299-2310, 1991.

[256] W. Rees and S. James, "Angular variation of the infrared emissivity of ice and water surfaces," *International Journal of Remote Sensing,* vol. 13, pp. 2873-2886, 1992.

[257] B. M. DAS, *Principles of Geotechnical Engineering*. division of Thomson Canada Limited: Thomson, 2006.

[258] W. G. M. Bastiaanssen, "SEBAL-based sensible and latent heat fluxes in the irrigated Gediz Basin, Turkey," *Journal of hydrology,* vol. 229, pp. 87-100, 2000.

[259] J. A. Sobrino, Gomez, M.,Jiménez-Muñoz, J. C., and A. Olioso, "Application of a simple algorithm to estimate daily evapotranspiration from NOAA–AVHRR images for the Iberian Peninsula," *Remote sensing of environment,* vol. 110, pp. 139-148, 2007.

LIST OF PUBLICATIONS

Journals

- Hassaballa A. A., Matori A. B., Shafri H. Z. M. (2013), Surface Moisture Content Retrieval from Visible/Thermal Infrared Images and Field Measurements. *Caspian Journal of Applied Sciences Research* CJASR (ISI: Thomson Reuters), (2), pp. 182-189.
- Hassaballa A. A., Matori A. B., Shafri H. Z. M. (2013), Generation of Extensive Moisture Content's Map using Weighted Moisture Values over Multi-surface Cover Types. *Research Journal of Applied Sciences, Engineering and Technology, MAXWELL* (ISI: Thomson Reuters/Elsevier Scopus), accepted.
- Hassaballa A. A. and A. B. Matori (2011), The Use and Evaluation of Split-Window Techniques for NOAA/AVHRR Surface Temperature Extraction over Different Surface Covers: case study (Perak Tengah & Manjong) area, Malaysia. International Journal of Civil & Environmental Engineering IJCEE-IJENS Vol: 11 No: 05, P: 23-28.

Conferences

- Hassaballa A. A. and Matori A. B. (2013), Surface and Near-surface Moisture Content Assessment using Multi-Temporal Satellite Images over Perak Tengah and Manjung Regions, Malaysia. International Symposium on Digital Earth-ISDE13 (Scopus/ EI Compendex/ Inspec), 26-29 August, Kuching, Sarawak, Malaysia.
- Hassaballa, A.A.; Matori, A.B. and Shafri, H. Z. M. (2012), Surface/Sub-surface Moisture Content Modeling Using NOAA/AVHRR, LANDSAT/ETM+ Images and In-situ Measurements. International Conference on Civil, Offshore & Environmental Engineering (ICCOEE) 12 – 14 June, Kuala Lumpur Convention Center, Malaysia.
- Hassaballa, A.A.; Matori, A.B. and Shafri, H. Z. M. (2012), Surface Moisture Content Retrieval from Visible/Thermal Infrared Images and Field Measurements.

International Conference on Civil Engineering (AICCE' 12), 28th – 30th August, Penang, Malaysia.

- Hassaballa, A.A.; Matori A.B. (2011), The Estimation of Air Temperature from NOAA/AVHRR Images and the study of NDVI-Ts impact, Case Study: The Application of Split-Window Algorithms over (Perak Tengah & Manjong) area, Malaysia. IEEE International Conference on Space Science and Communication (IconSpace), 12-13 July, Page(s): 20 – 24.
- Hassaballa, A.A.; Matori, A.B. (2011), Study on Surface Moisture Content, Vegetation Cover and Air Temperature Based on NOAA/AVHRR Surface Temperatures and Field Measurements. National Postgraduate Conference (NPC), 19th – 20th September, Malaysia, Page(s): 1 – 5. Copyrights: 978-1-4577-1884-7/11/$26.00 ©2011 IEEE.
- Hassaballa, A.H. Rezaur, R.B., Abdalla, S.H., and Adlan, M.N. (2010), Irrigation water management using remotely sensed data. The 1st International Conference on Sustainable Building and Infrastructure-ICSBI. Kuala Lumpur, Malaysia, 15-17 June.
- Hassaballa, A.A., Rezaur, R.B., and Matori, A.B. (2010), Extracting land surface temperature and Normalized Difference Vegetation Index from Landsat-7 image for estimating soil moisture in Perak State. The 1st International Conference on Sustainable Building and Infrastructure-ICSBI. Kuala Lumpur, Malaysia, 15-17 June.

APPENDIX A

SATELLITE EXTRACTED AND FIELD MEASURED TS

Tables represent the satellites extracted Ts versus in-situ measured Ts at times of satellites overpass.

Table A1 Extraction and measurements of Ts over UTP station from NOAA 17& 18.

DAY	Measuring depth of Ts ^{o}C at field		Satellite extracted Ts ^{o}C
	5 Cm	10 Cm	
7-Feb-2011	22.4	20.6	25.90
9-Feb-2011	36.6	33	33.17
12-Feb-2011	38	35.2	35.91
16-Feb-2011	32	28.8	35.63
17-Feb-2011	30.1	28.3	33.06
19-Feb-2011	29.3	26.1	31.20
20-Feb-2011	30.1	28.6	34.25
21-Feb-2011	31.4	29.7	33.10
22-Feb-2011	37.5	34	31.34
27-Feb-2011	39	35	30.80
28-Feb-2011	40.3	37.8	33.20
1-Mar-2011	27.2	24.4	31.10
10-Mar-2011	30.3	28.9	33.94
23-Mar-2011	29	27.1	32.40
28-Mar-2011	38.1	34.4	30.13
30-Mar-2011	29.8	28	32.60
4-Apr-2011	30.3	27	19.56
7-Apr-2011	40.2	36.5	32.79
8-Apr-2011	35.4	31	29.81
14-Apr-2011	38.2	33.3	30.28
17-Apr-2011	33.2	27.7	24.86
19-Apr-2011	35.3	29	29.42
22-Apr-2011	37.8	34	30.49
24-Apr-2011	36	32.2	26.15

Table A2 Extraction and measurements of Ts over SITIAWAN station from NOAA 17& 18.

DAY	Measuring depth of Ts ^{o}C at field		Satellite extracted Ts ^{o}C
	5 Cm	10 Cm	
7-Feb-2011	26.8	26	29.34
12-Feb-2011	33.8	33.7	27.8
16-Feb-2011	28.4	27	35.27
17-Feb-2011	27.7	26.8	33.27
19-Feb-2011	28.4	27.2	34.95
20-Feb-2011	28.1	27.3	34.17
21-Feb-2011	27.8	27	34.36
22-Feb-2011	33.4	30	13.3
26-Feb-2011	34.9	34	21.5
27-Feb-2011	38.3	33.2	30.9
28-Feb-2011	37	31.4	25.3
1-Mar-2011	25.7	25	26.26
10-Mar-2011	28.6	27.1	34.41
23-Mar-2011	27.9	27.2	34.65
28-Mar-2011	35.3	34	26.8
30-Mar-2011	28.7	27.5	36.15
31-Mar-2011	36.2	34	22.9
4-Apr-2011	34.5	29	22.7
7-Apr-2011	32.8	30.2	16.4
8-Apr-2011	35	33.1	20.4
14-Apr-2011	40.2	36.6	30.0
17-Apr-2011	38.6	34.5	26.4
19-Apr-2011	39.8	34.6	29.7
22-Apr-2011	41.1	35.2	34.7
24-Apr-2011	37.7	32.5	24.8

Table A3 Extraction and measurements of Ts over SEBERANG PERAK field from NOAA 18.

DAY	Measuring depth of Ts ^{o}C at field			Satellite extracted Ts ^{o}C
	5 Cm	10 Cm	15 Cm	
1-Jun-2012	30.8	30.3	29.8	28.95
6-Jun-2012	34.8	34	33.3	36.75
11-Jun-2012	35	32.8	31.7	36.95
12-Jun-2012	34.5	33.8	32.2	36.79
14-Jun-2012	31.7	31	31.1	32.37
15-Jun-2012	31.7	30.7	30.2	29.50
21-Jun-2012	31.4	30.6	30.2	31.70
29-Jun-2012	30.5	30	29.6	28.73
30-Jun-2012	33.6	32.5	32	34.82
4-Jul-2012	34.1	32.3	31.8	35.06
5-Jul-2012	32.9	32.1	32.2	34.32
9-Jul-2012	33.2	32.6	31	34.75
13-Jul-2012	32	31.7	31.20	32.72
17-Jul-2012	32	31.5	31.1	31.78
18-Jul-2012	33.6	32.4	31.9	32.93
10-Aug-2012	34.9	34	33.9	38.26

Table A4 Extraction and measurements of Ts over UTP station from MODIS TERRA.

Year	Sensor	Date	Pixel's Average Vale						
			NDVI	EVI	Ts				Ts (measured)
					MIN	AVG	MAX	T corrected	
2011	Terra	2-Feb	0.54	0.58	297.22	311.00	317.21	311.04	
		9-Feb	0.62	0.63	299.65	310.07	314.55	308.71	309.75
		12-Feb	0.57	0.61	299.82	310.85	315.31	311.81	311.15
		22-Feb	0.83	0.62	300.80	309.19	312.11	310.41	310.65
		27-Feb	0.22	0.34	294.36	312.77	316.78	313.44	312.15
		28-Feb	0.33	0.48	300.88	314.00	314.59	308.99	313.45
		28-Mar	0.40	0.50	299.74	312.08	314.00	311.81	311.25
		30-Mar	0.51	0.56	302.55	311.76	314.60	308.71	308.55
		14-Apr	0.13	0.43	300.66	313.30	316.45	311.22	311.35
		22-Apr	0.88	0.48	298.55	312.14	314.13	309.74	310.95
		24-Apr	0.08	0.51	299.40	310.84	315.15	307.82	309.15
	Aqua	21-Feb	0.94	0.70	300.62	306.05	311.08	303.58	304.55
		17-Apr	0.61	0.68	300.17	307.17	312.22	305.05	306.35

Table A5 Extraction and measurements of Ts over SITIAWAN station MODIS TERRA.

Year	Sensor	Date	Pixel's Average Vale						
			NDVI	EVI	Ts				Ts (measured)
					MIN	AVG	MAX	Ts Corrected	
2011	Terra	2-Feb	0.54	0.48	296.90	306.58	315.72	307.64	307.25
		9-Feb	0.66	0.74	297.85	304.13	310.41	305.72	305.85
		12-Feb	0.52	0.61	299.06	306.45	312.12	307.53	307.65
		22-Feb	0.61	0.70	301.38	308.77	311.21	309.35	309.35
		27-Feb	0.54	0.49	300.62	307.75	314.89	308.55	307.95
		28-Feb	0.58	0.53	298.16	305.69	313.22	306.94	308.75
		24-Mar	0.66	0.78	297.10	307.09	311.51	308.03	308.45
		28-Mar	0.50	0.53	301.57	306.66	314.04	307.70	307.40
		30-Mar	0.52	0.68	300.12	305.20	312.35	306.56	306.26
		14-Apr	0.53	0.66	300.00	307.76	312.88	308.56	308.55
		22-Apr	0.55	0.65	300.60	307.14	313.67	308.07	308.25
	Aqua	21-Feb	0.60	0.56	300.54	304.04	310.10	305.65	304.95
		17-Apr	0.60	0.79	300.59	306.22	311.54	307.35	306.85

Table A6 Extraction and measurements of Ts over SEBERANG PERAK field from MODIS.

Year	Sensor	Date	Pixel's Average Vale						Field-Measured Ts
			NDVI	EVI	Ts				
					MIN	MAX	AVG	Corrected Tavg	K
2012	Terra	6-Jun	0.66	0.59	300.10	310.41	309.15	309.72	309.85
		12-Jun	0.57	0.74	299.16	308.08	306.01	306.67	305.75
		29-Jun	0.65	0.52	299.50	308.70	302.88	303.63	303.95
		5-Jul	0.57	0.45	301.58	312.61	309.70	310.25	310.15
		9-Jul	0.46	0.51	301.12	311.14	308.97	309.54	309.65
		13-Jul	0.57	0.75	300.30	308.76	307.28	307.90	307.75
		21-Jul	0.58	0.69	297.64	306.05	305.12	305.81	
		10-Aug	0.48	0.57	301.58	311.20	307.18	307.81	307.75
		20-Aug	0.46	0.58	302.32	312.87	310.51	311.04	310.95
	Aqua	14-Jun	0.61	0.64	301.12	311.80	310.40	310.93	311.15
		11-Aug	0.43	0.45	299.80	312.02	306.44	307.09	307.55

APPENDIX B

SATELLITE'S SURFACE TEMPERATURE CORRECTION

Simple regression between satellite Ts and ground measured Ts was used in order to rectify satellite Ts.

B1. NOAA 17 surface temperature correction

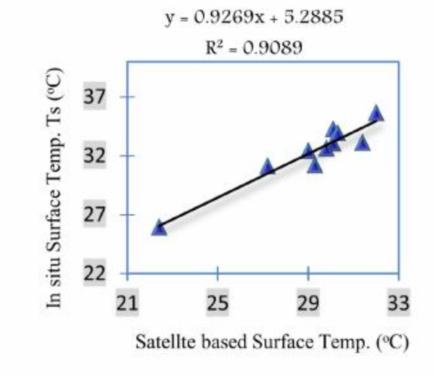

5 cm depth at UTP

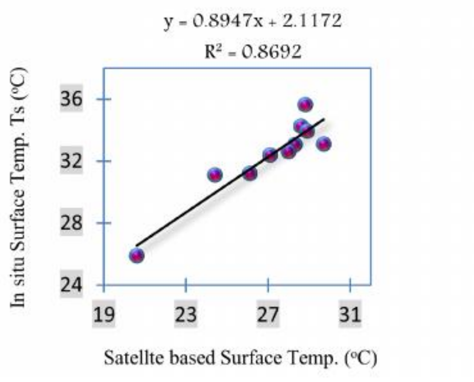

10 cm depth at UTP

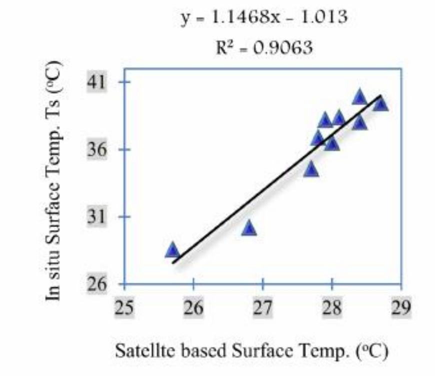

5 cm depth at Sitiawan

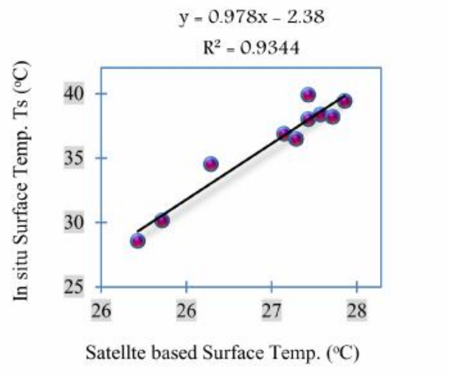

10 cm depth at Sitiawan

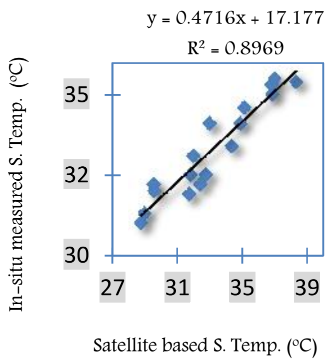

5 cm at S. Perak

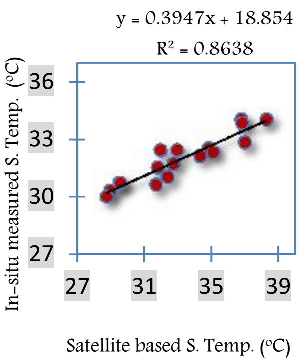

10 cm at S. Perak

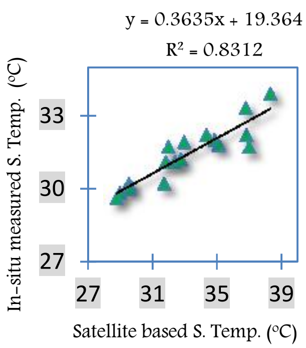

15 cm at S. Perak

B2. NOAA 18 surface temperature correction

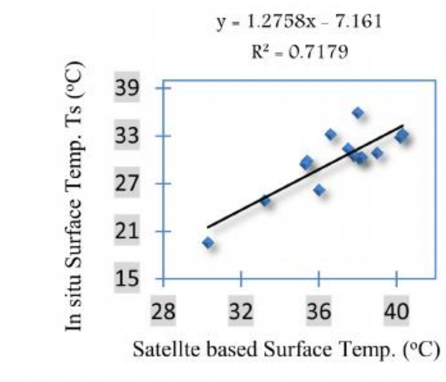

5 cm depth at UTP

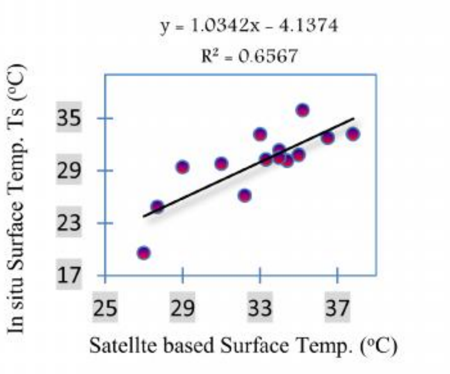

10 cm depth at UTP

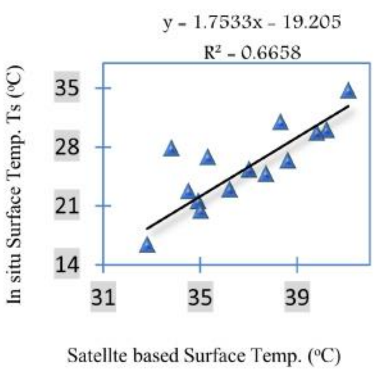

5 cm depth at Sitiawan

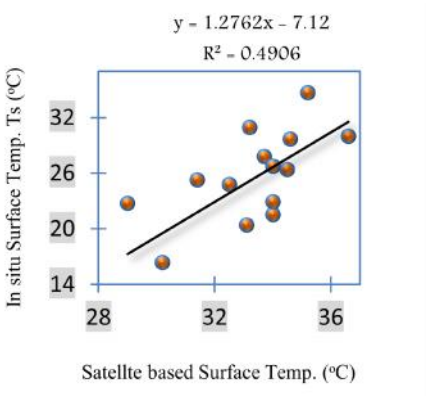

10 cm depth at Sitiawan

B3. MODIS Terra surface temperature correction

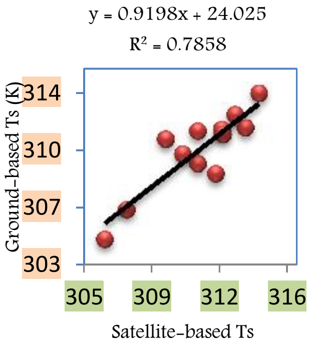

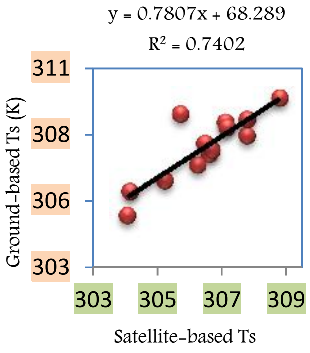

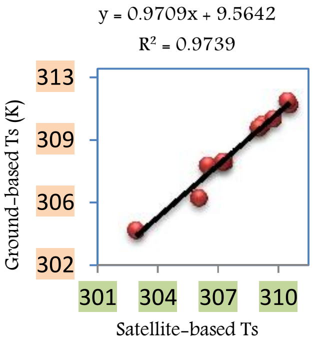

UTP **SITIAWAN** **S. PERAK**

APPENDIX C

MOISTURE PARAMETERS CALCULATION

Tables below represent the calculation of surface soil moisture through the extraction of moisture parameters from satellite’s NDVI and Ts over the study area.

C1. FINAL MOISTURE CALCULATIONS FOR-UTP

periods			Parameters Calculation								Generated MC Values				INSITU		
		Sensor	NDVI*	NDVI*2	T*	T*2	NDVI* x T*	NDVI*2 x T*2	NDVI* x T*2	NDVI*2 x T*	MC				MC		
											5 cm	10 cm	15 cm		5 cm	10 cm	15 cm
FEBRUARY	7-Feb	N17	0.39	0.15	0.65	0.43	0.26	0.07	0.17	0.10	0.16	0.20			0.14	0.17	
	9-Feb	N18	0.51	0.27	0.51	0.26	0.26	0.07	0.13	0.14	0.18	0.35			0.14	0.28	
	16-Feb	N17	0.30	0.09	0.46	0.21	0.14	0.02	0.06	0.04	0.08	0.14			0.11	0.11	
	17-Feb	N17	0.36	0.13	0.35	0.12	0.13	0.02	0.04	0.05	0.11	0.15			0.10	0.11	
	19-Feb	N17	0.32	0.10	0.45	0.21	0.14	0.02	0.07	0.05	0.09	0.15			0.11	0.14	
	20-Feb	N17	0.26	0.07	0.41	0.17	0.11	0.01	0.04	0.03	0.06	0.13			0.09	0.16	
	21-Feb	N17	0.37	0.14	0.65	0.42	0.24	0.06	0.16	0.09	0.15	0.19			0.13	0.21	
	22-Feb	N18	0.60	0.36	0.66	0.44	0.40	0.16	0.26	0.24	0.15	0.12			0.12	0.10	
	26-Feb	N18	0.34	0.12	0.57	0.32	0.19	0.04	0.11	0.07	0.14	0.35			0.12	0.33	
	27-Feb	N18	0.56	0.32	0.59	0.35	0.33	0.11	0.20	0.19	0.17	0.23			0.15	0.20	
	28-Feb	N17	0.42	0.17	0.56	0.31	0.23	0.05	0.13	0.10	0.15	0.21			0.14	0.18	
	28-Feb	N18	0.51	0.26	0.36	0.13	0.18	0.03	0.07	0.09	0.20	0.50			0.17	0.38	
MARCH	1-Mar	N17	0.31	0.10	0.46	0.21	0.14	0.02	0.07	0.04	0.08	0.15			0.09	0.14	
	10-Mar	N17	0.28	0.08	0.29	0.08	0.08	0.01	0.02	0.02	0.08	0.11			0.11	0.10	
	14-Mar	N17	0.44	0.19	0.58	0.34	0.25	0.06	0.15	0.11	0.17	0.22			0.14	0.20	
	15-Mar	N17	0.29	0.08	0.72	0.51	0.20	0.04	0.15	0.06	0.11	0.16			0.11	0.14	
	19-Mar	N17	0.41	0.17	0.91	0.82	0.37	0.14	0.34	0.15	0.31	0.18			0.25	0.20	
	23-Mar	N17	0.19	0.04	0.42	0.18	0.08	0.01	0.03	0.02	0.04	0.11			0.02	0.11	
	28-Mar	N18	0.40	0.16	0.56	0.31	0.23	0.05	0.13	0.09	0.15	0.34			0.12	0.31	
	30-Mar	N17	0.36	0.13	0.28	0.08	0.10	0.01	0.03	0.04	0.11	0.13			0.13	0.10	
	31-Mar	N18	0.47	0.22	0.55	0.31	0.26	0.07	0.14	0.12	0.16	0.32			0.12	0.26	
APRIL	8-Apr	N18	0.55	0.30	0.97	0.95	0.54	0.29	0.52	0.30	0.01	0*			0.03	0.11	
	14-Apr	N18	0.58	0.33	0.49	0.24	0.28	0.08	0.14	0.16	0.20	0.35			0.16	0.31	
	19-Apr	N18	0.39	0.15	0.56	0.32	0.22	0.05	0.12	0.08	0.14	0.34			0.11	0.28	

* MOISTURE CONTENT PRODUCED IN A NEGATIVE VALUE

C2. FINAL MOISTURE CALCULATIONS FOR-SITIAWAN

periods			Parameters Calculation								Generated MC Values				INSITU		
			NDVI*	NDVI*2	T*	T*2	NDVI* x T*	NDVI*2 x T*2	NDVI* x T*2	NDVI*2 x T*	MC				MC		
		Sensor									5 cm	10 cm	15 cm		5 cm	10 cm	15 cm
FEBRUARY	7-Feb	N17	0.32	0.10	0.14	0.02	0.04	0.00	0.01	0.01	0.11	0.03			0.05	0.05	
	16-Feb	N17	0.43	0.19	0.40	0.16	0.17	0.03	0.07	0.07	0.17	0.17			0.08	0.14	
	17-Feb	N17	0.67	0.45	0.89	0.80	0.60	0.36	0.54	0.40	*	*			0.07	0.12	
	19-Feb	N17	0.20	0.04	0.27	0.07	0.05	0.00	0.01	0.01	0.08	0.00			0.06	0.03	
	20-Feb	N17	0.38	0.15	0.55	0.30	0.21	0.04	0.12	0.08	0.20	0.29			0.06	0.24	
	21-Feb	N17	0.49	0.24	0.49	0.24	0.24	0.06	0.12	0.12	0.22	0.28			0.16	0.22	
	22-Feb	N18	0.61	0.37	0.51	0.26	0.31	0.10	0.16	0.19	0.08	0.40			0.05	0.33	
	26-Feb	N18	0.38	0.14	0.49	0.24	0.19	0.03	0.09	0.07	0.16	0.25			0.12	0.21	
	27-Feb	N18	0.34	0.12	0.62	0.38	0.21	0.05	0.13	0.07	0.12	0.23			0.1	0.23	
	28-Feb	N17	0.33	0.11	0.41	0.17	0.14	0.02	0.06	0.04	0.14	0.13			0.09	0.09	
	28-Feb	N18	0.44	0.20	0.33	0.11	0.15	0.02	0.05	0.07	0.19	0.29			0.14	0.25	
MARCH	1-Mar	N17	0.59	0.35	0.67	0.45	0.39	0.15	0.26	0.23	0.36	0.55			0.17	0.33	
	10-Mar	N17	0.38	0.15	0.21	0.04	0.08	0.01	0.02	0.03	0.13	0.06			0.1	0.004	
	14-Mar	N17	0.47	0.22	0.38	0.15	0.18	0.03	0.07	0.08	0.18	0.17			0.14	0.13	
	15-Mar	N17	0.60	0.36	0.64	0.40	0.38	0.14	0.24	0.23	0.34	0.50			0.21	0.38	
	19-Mar	N17	0.34	0.12	0.56	0.31	0.19	0.04	0.11	0.07	0.18	0.27			0.14	0.16	
	23-Mar	N17	0.33	0.11	0.09	0.01	0.03	0.00	0.00	0.01	0.11	0.03			0.08	0.13	
	24-Mar	N18	0.46	0.21	0.43	0.19	0.20	0.04	0.09	0.09	0.15	0.30			0.12	0.24	
	28-Mar	N18	0.41	0.17	0.46	0.21	0.19	0.03	0.09	0.08	0.16	0.27			0.09	0.21	
	30-Mar	N17	0.58	0.33	0.45	0.20	0.26	0.07	0.12	0.15	0.24	0.26			0.18	0.19	
	31-Mar	N18	0.67	0.44	0.36	0.13	0.24	0.06	0.09	0.16	0.12	0.44			0.09	0.34	
	14-Apr	N18	0.58	0.33	0.34	0.12	0.20	0.04	0.07	0.11	0.15	0.38			0.13	0.33	
	17-Apr	N18	0.49	0.24	0.59	0.34	0.29	0.08	0.17	0.14	0.08	0.33			0.04	0.27	
	19-Apr	N18	0.53	0.28	0.65	0.43	0.35	0.12	0.23	0.18	0.04	0.36			0.07	0.34	
	22-Apr	N18	0.45	0.20	0.67	0.44	0.30	0.09	0.20	0.13	0.06	0.31			0.08	0.24	
*	Value not defined																

C3. FINAL MOISTURE CALCULATIONS FOR-SEBERANG PERAK

periods		Parameters Calculation									Generated MC Values				INSITU		
		Sensor	NDVI*	NDVI*2	T*	T*2	NDVI* x T*	NDVI*2 x T*2	NDVI* x T*2	NDVI*2 x T*					MC		
											5 cm	10 cm	15 cm		5 cm	10 cm	15 cm
JUN																	
	1-Jun		0.54	0.29	0.49	0.24	0.26	0.07	0.13	0.14	0.05	0.36	0.15		0.20	0.37	0.17
	6-Jun		0.38	0.14	0.52	0.27	0.20	0.04	0.10	0.07	0.14	0.26	0.06		0.16	0.24	0.10
	8-Jun		0.52	0.27	0.60	0.36	0.31	0.09	0.18	0.16	0*	0.39	0.17		0.11	0.41	0.23
	11-Jun		0.43	0.18	0.48	0.23	0.21	0.04	0.10	0.09	0.13	0.28	0.07		0.16	0.27	0.13
	12-Jun		0.44	0.20	0.42	0.17	0.18	0.03	0.08	0.08	0.16	0.27	0.07		0.18	0.29	0.12
	14-Jun		0.36	0.13	0.62	0.38	0.22	0.05	0.14	0.08	0.11	0.28	0.09		0.12	0.31	0.14
	15-Jun		0.38	0.15	0.58	0.34	0.22	0.05	0.13	0.08	0.11	0.28	0.08		0.14	0.30	0.13
	21-Jun		0.42	0.17	0.64	0.41	0.27	0.07	0.17	0.11	0.05	0.34	0.12		0.08	0.40	0.23
	29-Jun		0.37	0.14	0.47	0.22	0.18	0.03	0.08	0.07	0.17	0.24	0.05		0.25	0.21	0.06
	30-Jun		0.34	0.12	0.69	0.48	0.24	0.06	0.16	0.08	0.10	0.30	0.11		0.13	0.28	0.13
JULY	4-Jul		0.37	0.13	0.49	0.24	0.18	0.03	0.09	0.07	0.17	0.23	0.05		0.20	0.23	0.10
	5-Jul		0.44	0.19	0.50	0.25	0.22	0.05	0.11	0.10	0.11	0.30	0.09		0.13	0.28	0.17
	9-Jul		0.46	0.21	0.38	0.15	0.17	0.03	0.07	0.08	0.17	0.27	0.07		0.19	0.26	0.14
	13-Jul		0.37	0.13	0.27	0.07	0.10	0.01	0.03	0.04	0.27	0.17	0.03		0.22	0.19	0.11
	17-Jul		0.47	0.22	0.66	0.44	0.31	0.10	0.20	0.15	0*	0.39	0.16		0.11	0.37	0.22
	18-Jul		0.47	0.22	0.65	0.43	0.31	0.10	0.20	0.15	0*	0.39	0.16		0.07	0.42	0.17
AUGUST	8-Aug		0.42	0.18	0.66	0.43	0.28	0.08	0.18	0.12	0.03	0.35	0.13		0.04	0.37	0.23
	10-Aug		0.53	0.28	0.23	0.05	0.12	0.01	0.03	0.06	0.24	0.28	0.09		0.27	0.30	0.21
	15-Aug		0.44	0.20	0.52	0.27	0.23	0.05	0.12	0.10	0.09	0.31	0.09		0.11	0.32	0.20

* MOISTURE CONTENT PRODUCED IN A NEGATIVE VALUE

APPENDIX D

VALUES OF MOISTURE PARAMETERS

Tables below shows the moisture parameters extracted from satellites normal-Ts as well as corrected-Ts of NOAA 17 and NOAA 18 satellites.

D1. MOISTURE PARAMETERS (NORMAL-TS) EXTRACTED FROM UNIVERSAL TRIANGLE METHOD

Location	Sensor	Depth (cm)	M C Parameters								
			a_{00}	a_{10}	a_{20}	a_{01}	a_{02}	a_{11}	a_{22}	a_{12}	a_{21}
UTP	NOAA 17	**5**	0.11	0.42	0.03	-0.13	-0.27	0.33	1.12	2.59	-0.37
		10	-0.09	0.57	-0.04	-0.22	0.61	1.19	-1.66	-0.89	0.53
	NOAA 18	**5**	0.11	0.4	0.2	-0.17	0.16	0.21	-0.43	-0.73	0.48
		10	0.54	-0.35	0.06	-0.19	-0.31	0.18	-0.02	0.45	0.63
SITIAWAN	NOAA 17	**5**	-0.03	0.33	0.03	-0.12	0.07	2.49	2.08	-1.8	-2.9
		10	-0.06	0.46	-0.01	0.18	-0.21	-2.1	2.91	2.62	0.49
	NOAA 18	**5**	0.12	0.52	0.19	-0.19	0.16	0.45	0.87	-0.83	-0.9
		10	0.54	-0.36	0.2	-0.29	-0.24	0.45	-0.03	0.56	-0.26
S. PERAK	NOAA 17	**5**	0.17	0.48	-0.22	-0.16	0.26	-0.43	-0.21	-0.01	-0.71
		10	-0.1	0.56	-0.03	-0.12	0.12	0.86	0.58	-0.03	-0.43
		15	-0.07	0.66	-0.11	-0.21	0.42	0.3	0.55	-0.09	-0.74
	NOAA 18	**5**	0.13	0.37	0.22	-0.2	0.14	0.24	-0.4	-0.83	0.43
		10	0.11	0.18	0.02	0.04	-0.1	0.38	-0.11	0.46	0.57
		15	0.14	-0.61	0.8	-0.21	0.15	2.03	-0.88	-1.05	-0.38

D2. MOISTURE PARAMETERS (CORRECTED-TS) EXTRACTED FROM UNIVERSAL TRIANGLE METHOD

Location	Sensor	Depth (cm)	M C Parameters								
			a_{00}	a_{10}	a_{20}	a_{01}	a_{02}	a_{11}	a_{22}	a_{12}	a_{21}
UTP	NOAA 17	**5**	0.03	0.44	0.06	-0.17	0.14	-0.87	0.94	0.84	0.23
		10	0.14	-0.61	0.8	-0.21	0.15	2.03	-0.88	-1.05	-0.38
	NOAA 18	**5**	0.18	-0.13	0.43	-0.11	0.25	0.01	-0.43	-0.73	0.48
		10	0.76	-0.1	0.44	-0.64	0.25	0.06	-0.38	-0.86	-0.68
SITIAWAN	NOAA 17	**5**	0.06	0.13	0.11	-0.19	0.07	0.68	0.62	0.48	-0.9
		10	-0.06	0.26	0.16	-0.14	0.1	-0.17	-2.89	4.2	-0.6
	NOAA 18	**5**	0.4	-0.43	0.2	-0.18	-0.11	0.5	0.9	-0.8	-0.65
		10	0.08	0.56	0.2	-0.21	0.14	-0.2	-0.03	0.56	-0.26
S. PERAK	NOAA 17	**5**	0.46	-0.32	0.41	0.19	-0.03	-1.96	-0.06	0.06	0.51
		10	-0.13	0.77	-0.08	-0.12	0.18	0.56	-0.9	0.81	-0.51
		15	0.1	-0.36	0.67	-0.3	0.58	-0.1	0.91	-0.62	0.68
	NOAA 18	**5**	0.13	0.37	0.22	-0.2	0.14	0.24	-0.4	-0.83	0.43
		10	0.11	0.18	0.02	0.04	-0.1	0.38	-0.11	0.46	0.57
		15	0.03	0.44	0.06	-0.17	0.14	-0.87	0.94	0.84	0.23

APPENDIX E

MOISTURE CONTENT MAPS

The following figures represent the extracted moisture content maps over the study area partitions, acquired from NOAA 17, 18 and MODIS Terra and Aqua satellite images.

E1. MOISTURE CONTENT MAPS FROM NOAA 18 OVER UTP LOCATION

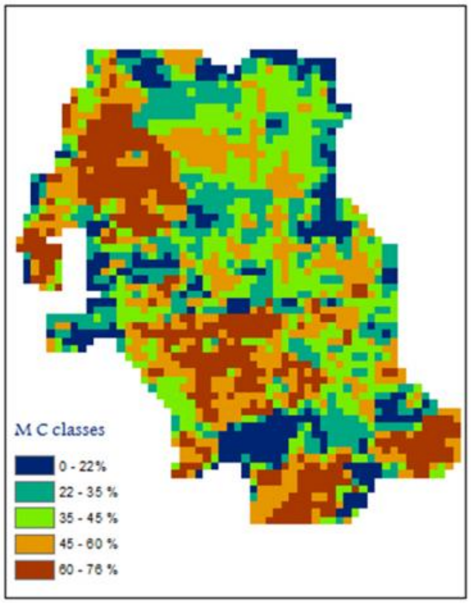

Normal Ts at 5 cm depth

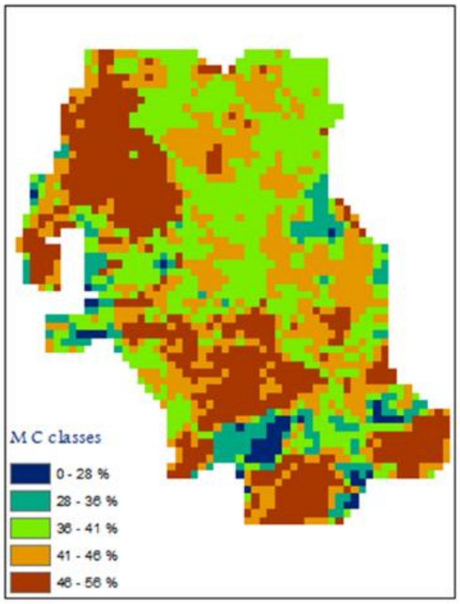

Normal Ts at 10 cm depth

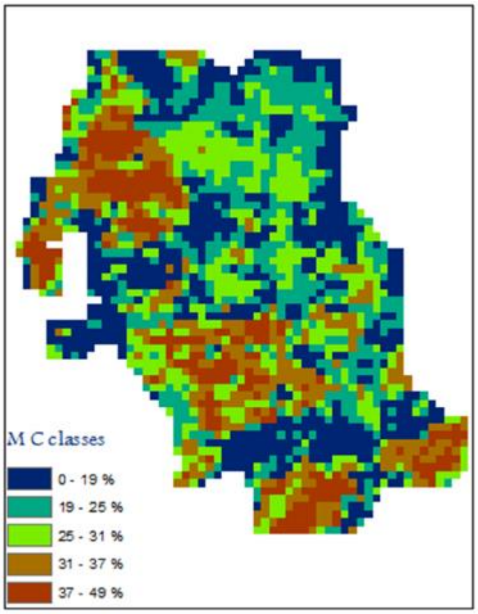

Corrected Ts at 5 cm depth

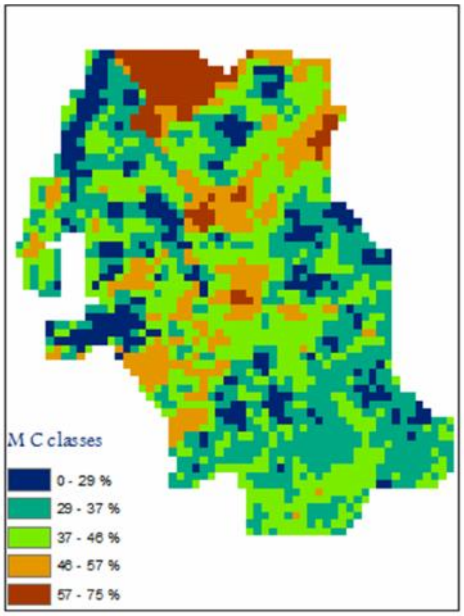

Corrected Ts at 10 cm depth

E2. MOISTURE CONTENT MAPS FROM NOAA 18 OVER SITIAWAN LOCATION

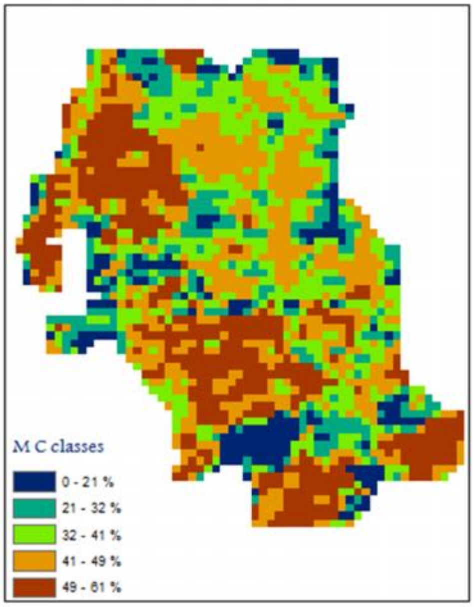

Normal Ts at 5 cm depth

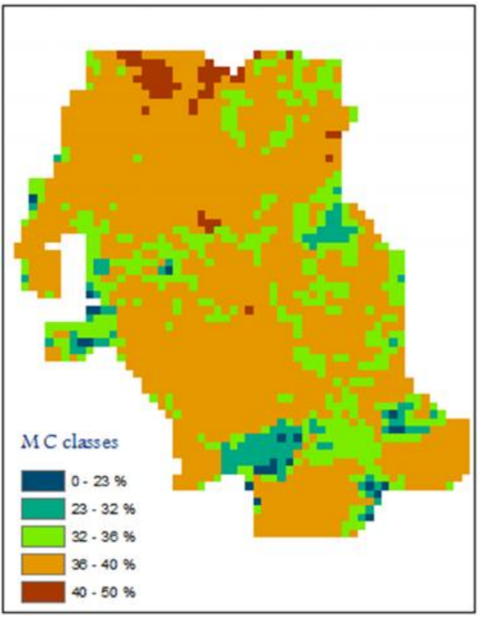

Normal Ts at 10 cm depth

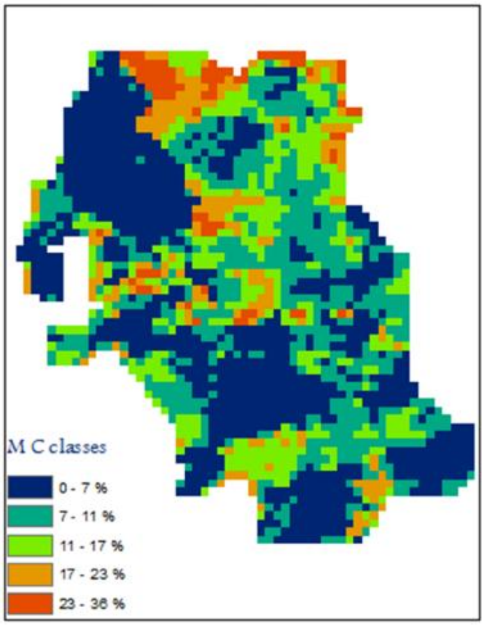

Corrected Ts at 5 cm depth

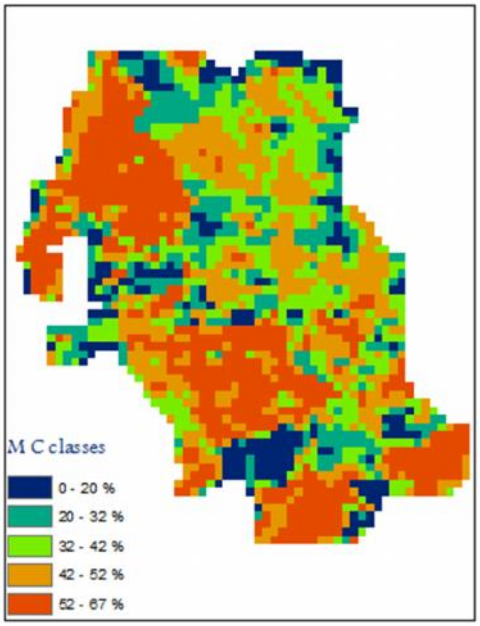

Corrected Ts at 10 cm depth

E3. MOISTURE CONTENT MAPS FROM NOAA 17 OVER UTP LOCATION

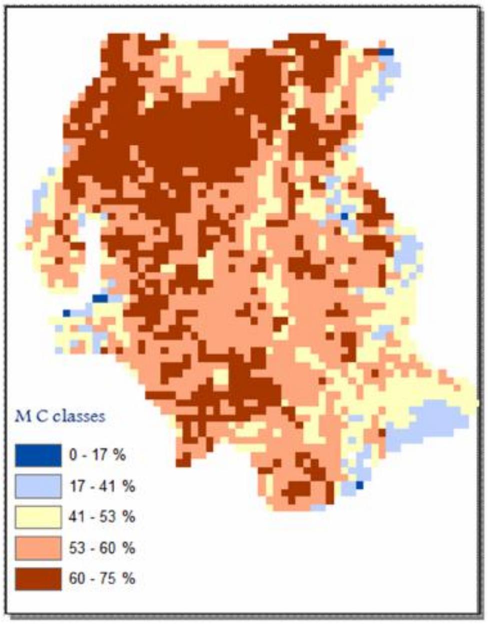

Normal Ts at 5 cm depth

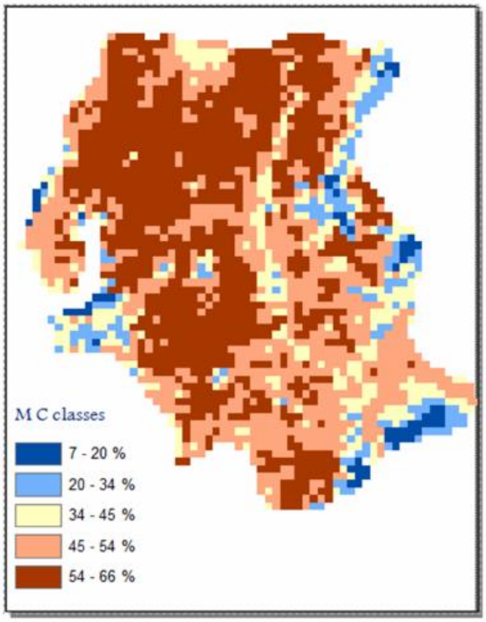

Normal Ts at 10 cm depth

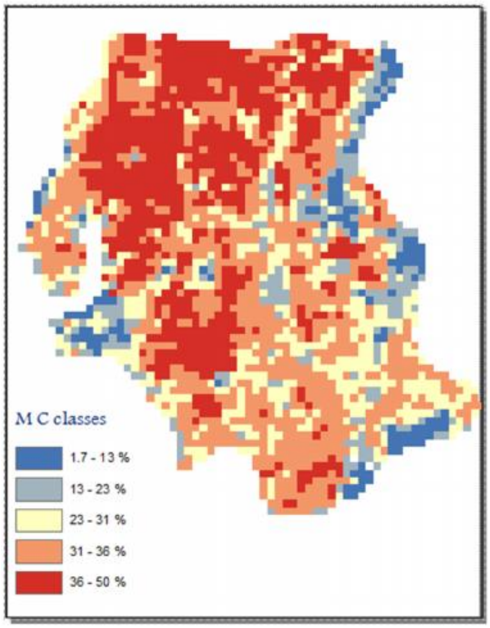

Corrected Ts at 5 cm depth

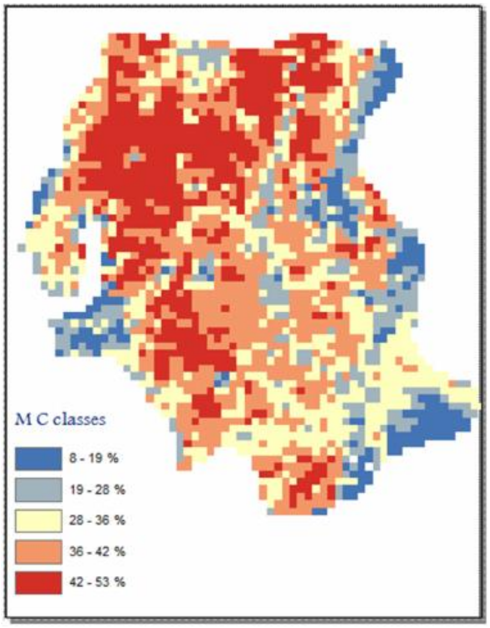

Corrected Ts at 10 cm depth

E4. MOISTURE CONTENT MAPS FROM NOAA 17 OVER SITIAWAN LOCATION

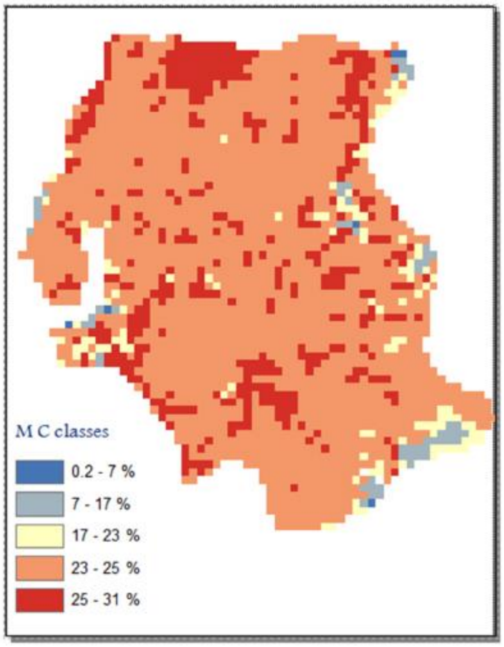

Normal Ts at 5 cm depth

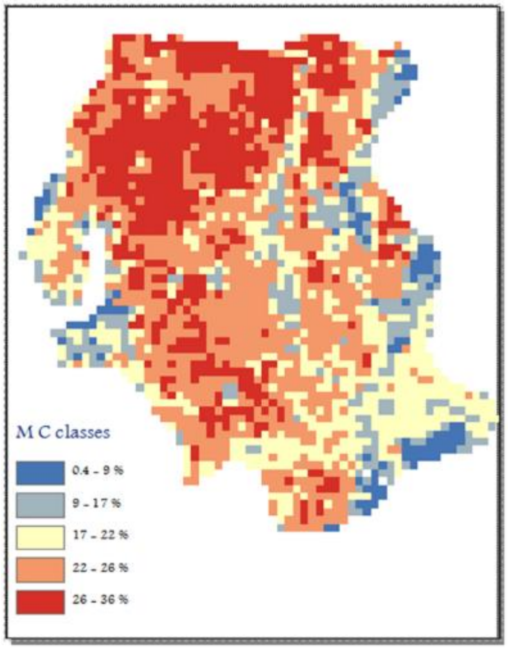

Normal Ts at 10 cm depth

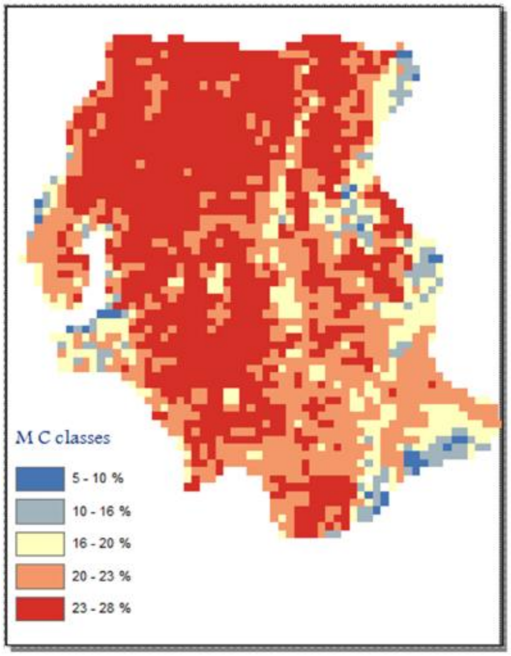

Corrected Ts at 5 cm depth

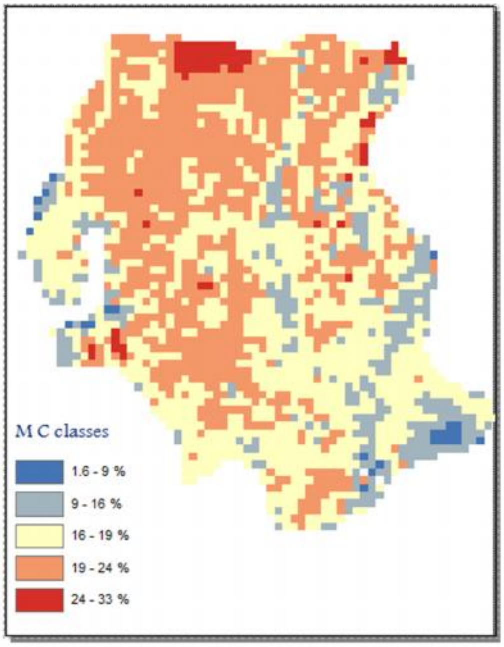

Corrected Ts at 10 cm depth

E5. MOISTURE CONTENT MAPS FROM NOAA 17 OVER S. PERAK LOCATION

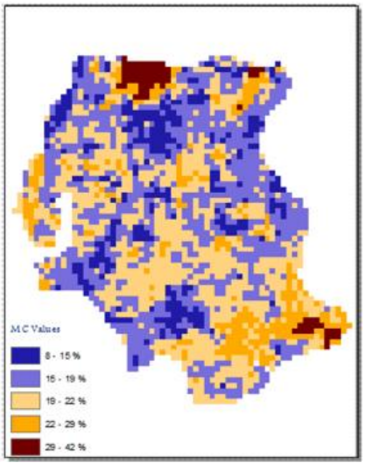

Normal Ts at 5 cm depth

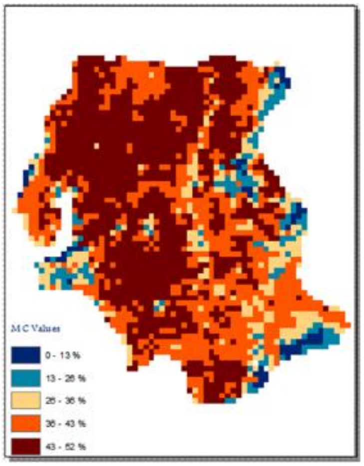

Normal Ts at 10 cm depth

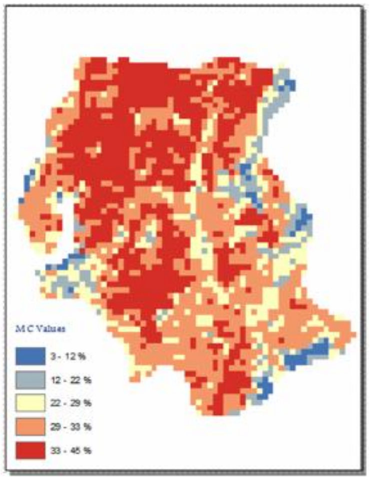

Normal Ts at 15 cm depth

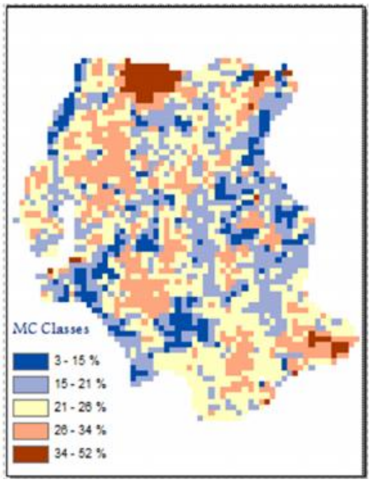

Corrected Ts at 5 cm depth

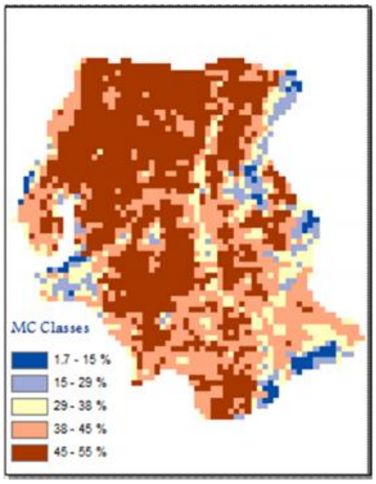

Corrected Ts at 10 cm depth

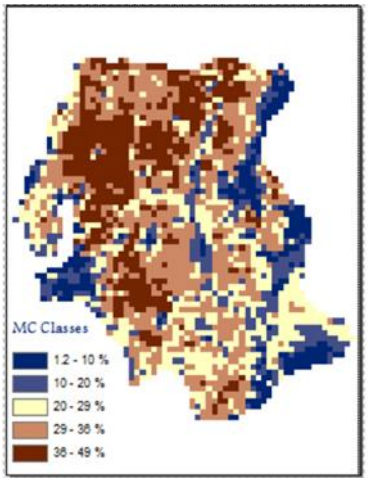

Corrected Ts at 15 cm depth

E6. MOISTURE CONTENT MAPS FROM MODIS TERRA OVER UTP LOCATION

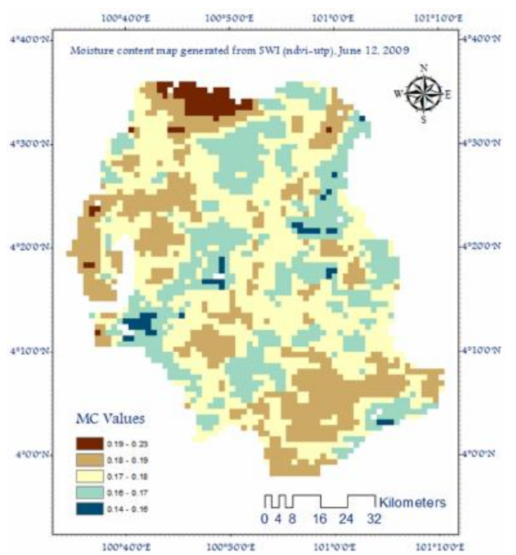

Normal Ts at 5 cm depth

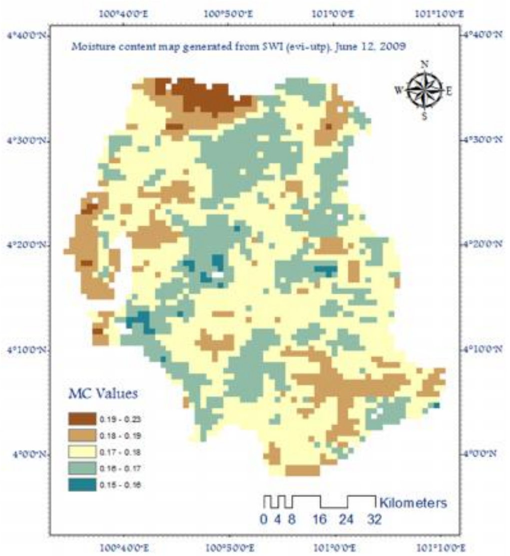

Normal Ts at 10 cm depth

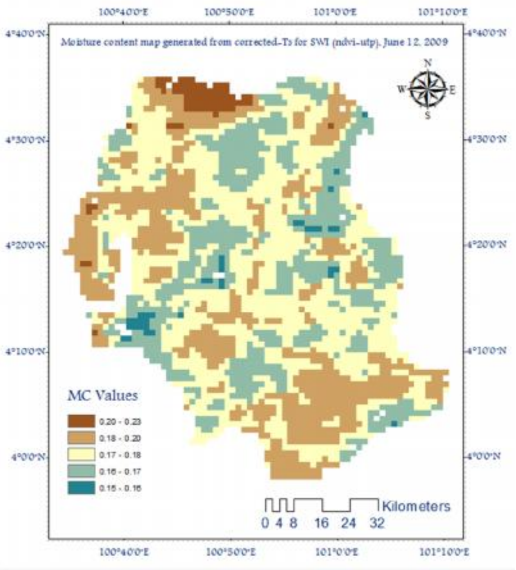

Corrected Ts at 5 cm depth

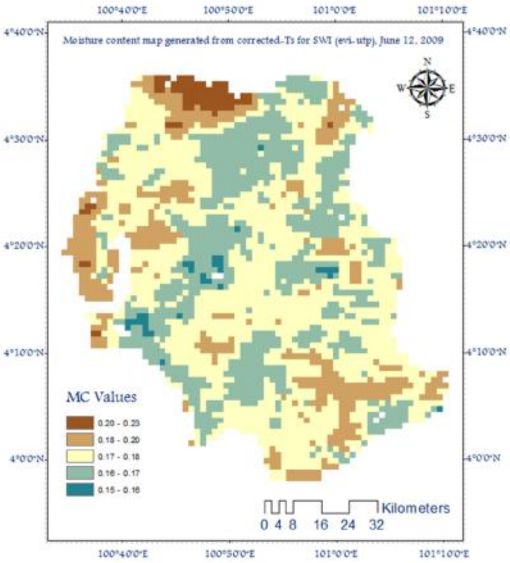

Corrected Ts at 10 cm depth

E7. MOISTURE CONTENT MAPS FROM MODIS TERRA OVER SITIAWAN LOCATION

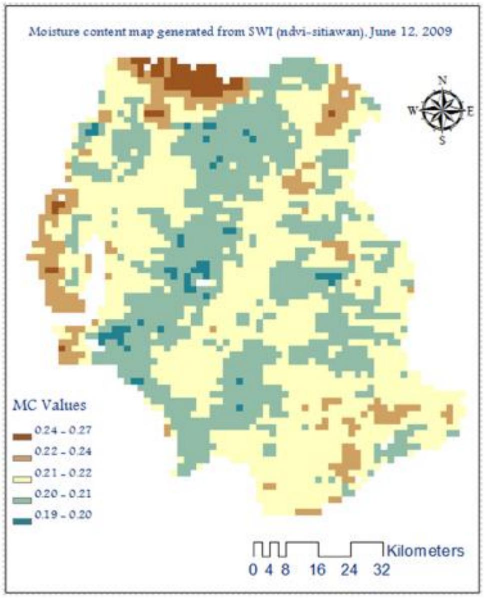

Normal Ts at 5 cm depth

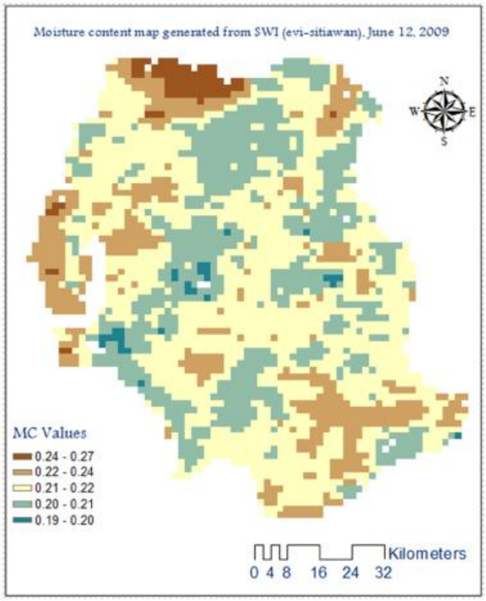

Normal Ts at 10 cm depth

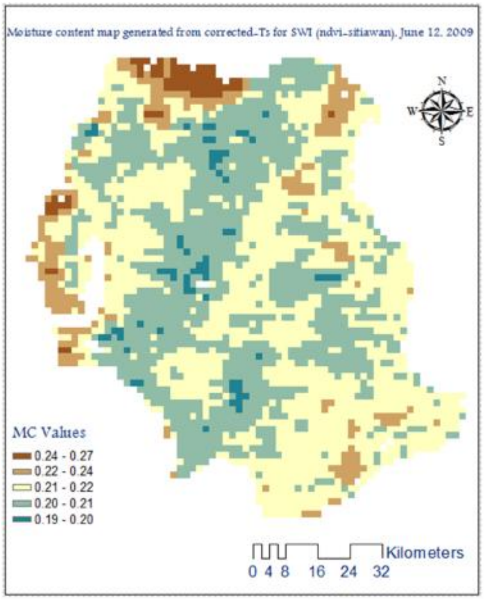

Corrected Ts at 5 cm depth

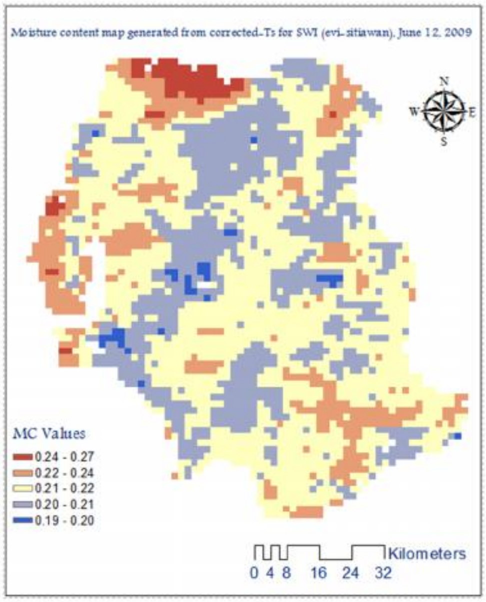

Corrected Ts at 10 cm depth

E8. MOISTURE CONTENT MAPS FROM MODIS TERRA OVER S. PERAK LOCATION

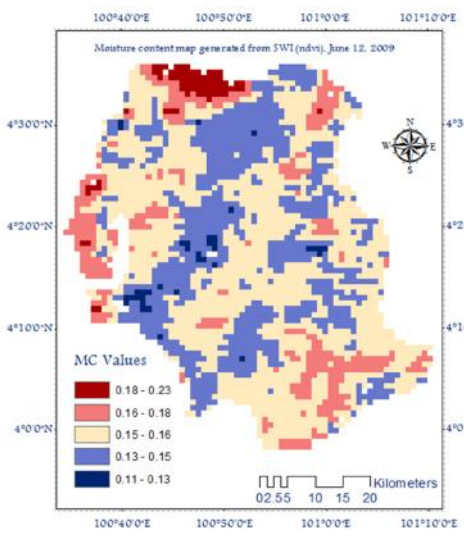

Normal Ts with NDVI base

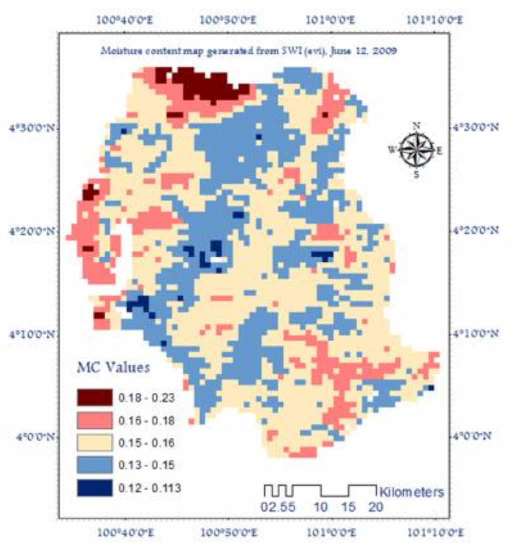

Normal Ts with EVI base

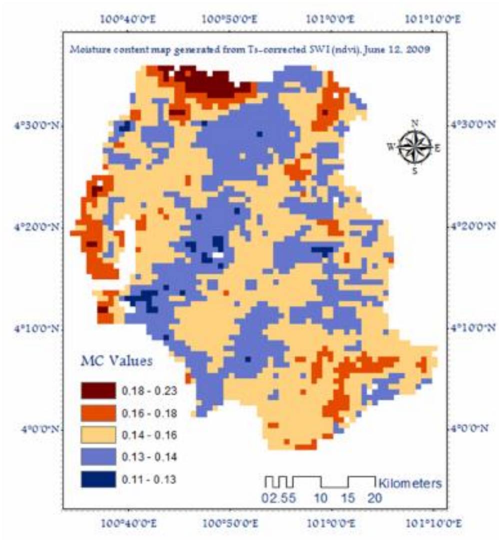

Corrected Ts with NDVI base

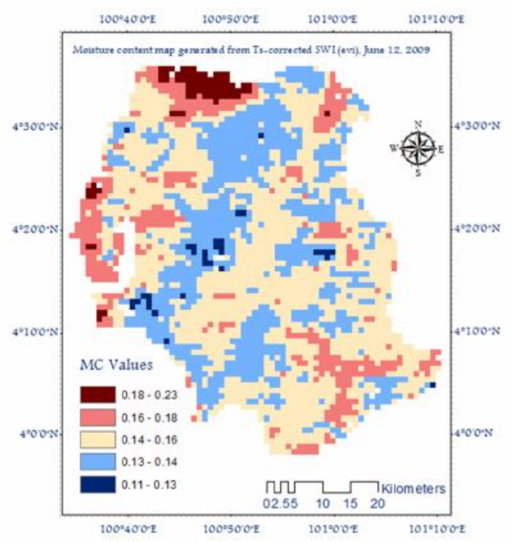

Corrected Ts with EVI base

E9. MOISTURE CONTENT MAPS FROM LANDSAT FROM THE UNIVERSAL TRIANGLE METHOD

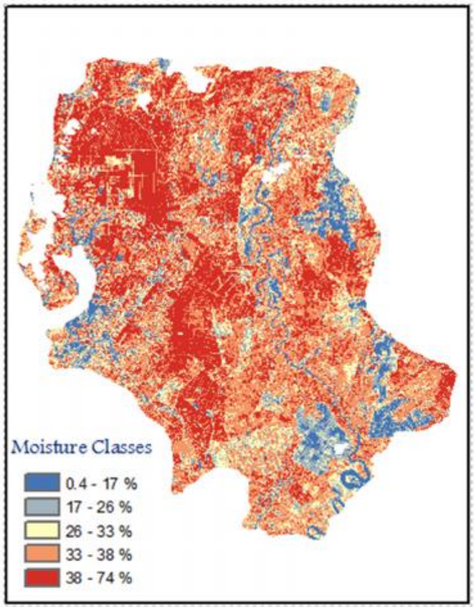

5 cm moisture depth from ETM+

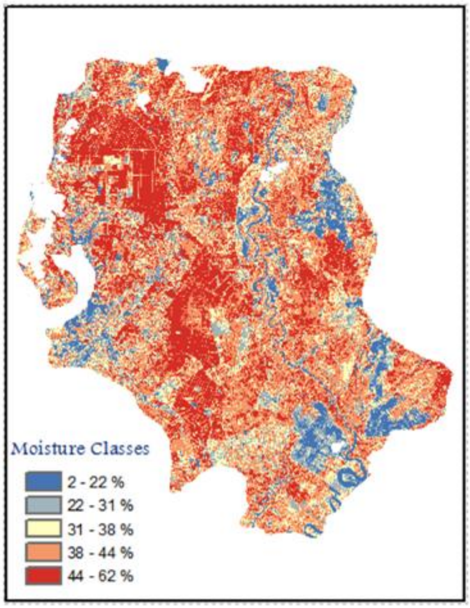

10 cm moisture depth from ETM+

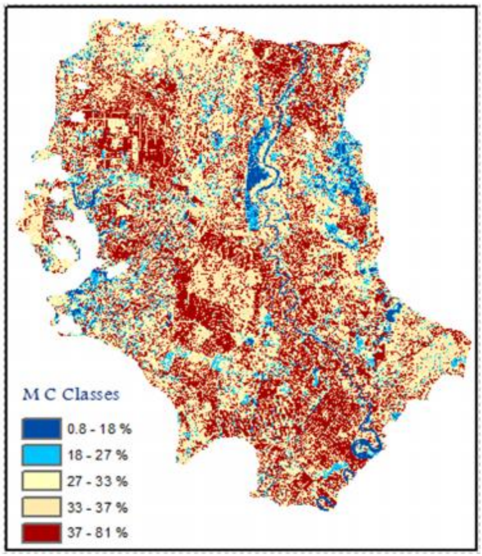

5 cm moisture depth from L5

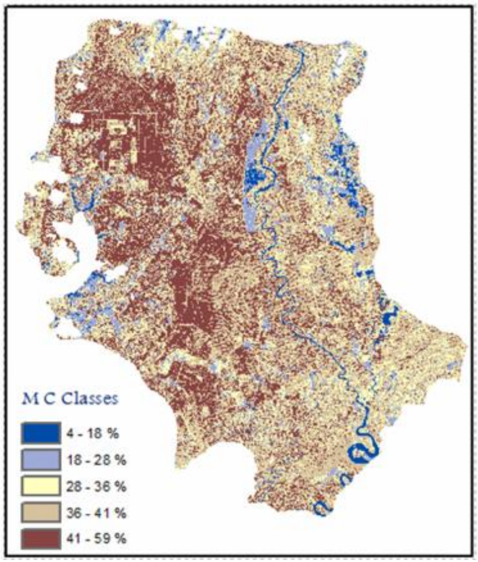

10 cm moisture depth from L5

APPENDIX F

GENERALIZED MOISTURE CONTENT’S MAPS

Below are the moisture content maps extracted as a result of the correlation between the 3 different land covers tested earlier in the study.

F1. The generalized moisture map generated from the 3 locations correlation using NOAA 17 image.

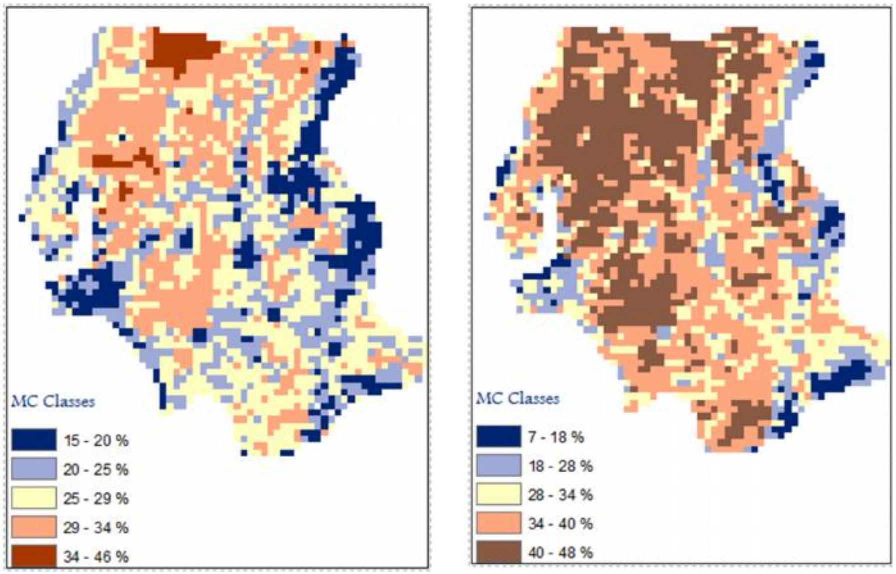

5 cm moisture depth **10 cm moisture depth**

F2. The generalized moisture map generated from the 3 locations correlation using MODIS TERRA image.

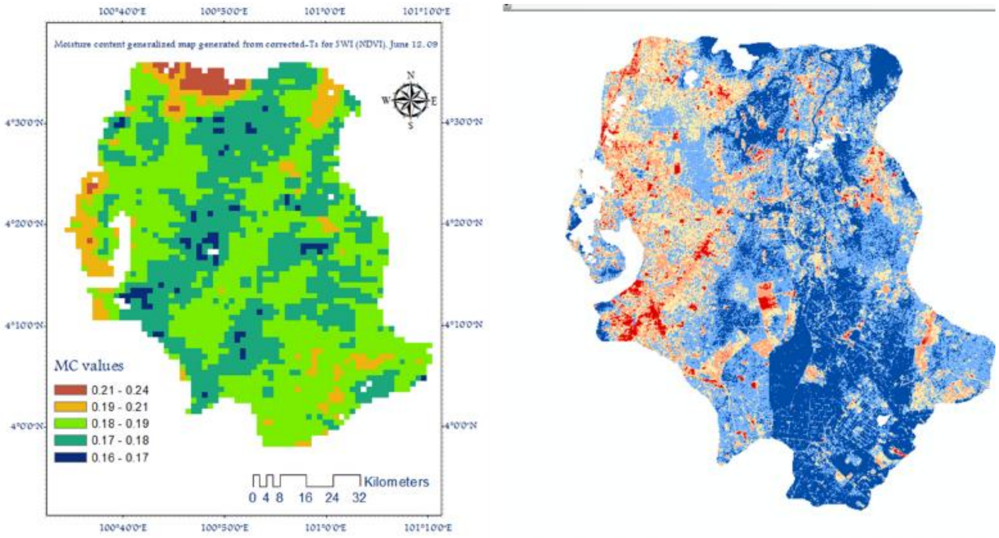

Moisture with NDVI base **Moisture with EVI base**

APPENDIX G

MOISTURE CONTENT VALIDATION

The first type of validation is graphical representations of NDVI when plotted against the surface temperature in order to simulate the universal triangle method and understand the distribution of the surface temperature with respect to the vegetation cover.

G1. VALIDATION USING TEMPERATURE-VEGETATION TRIANGLE

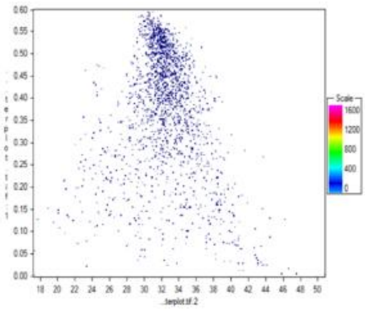

Normal Ts from NOAA 18

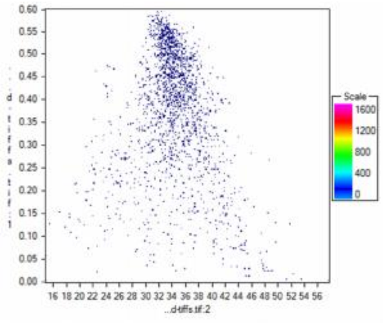

Corrected Ts from NOAA 18

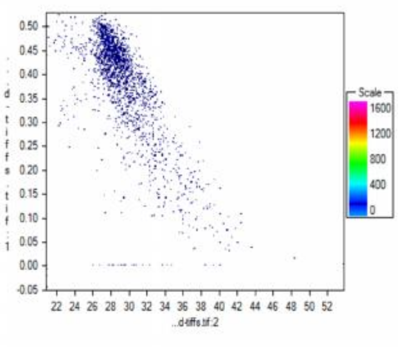

Normal Ts from NOAA 17

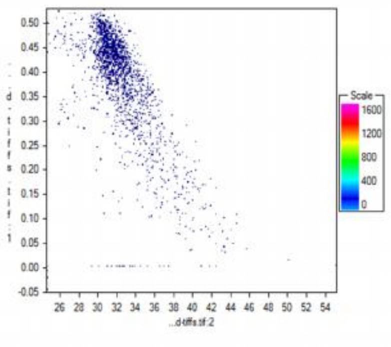

Corrected Ts from NOAA 17

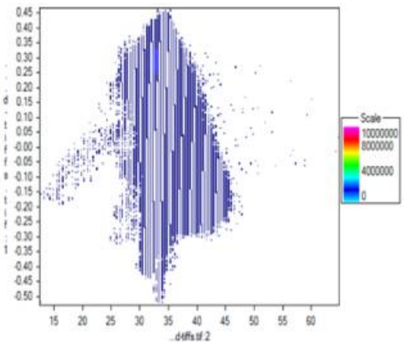

Corrected Ts from ETM+

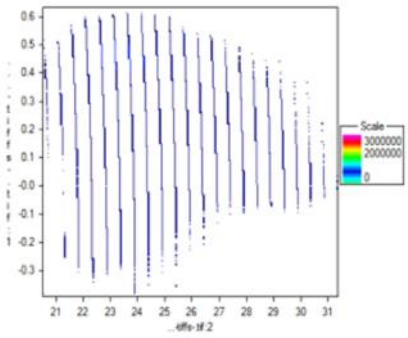

Corrected Ts from L5

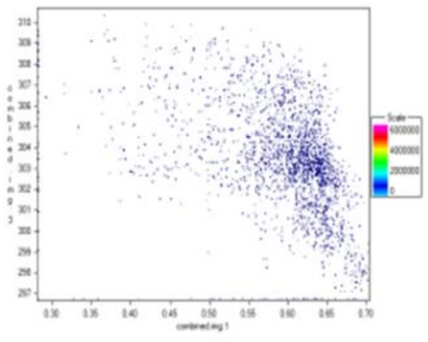

Normal Ts from MODIS T

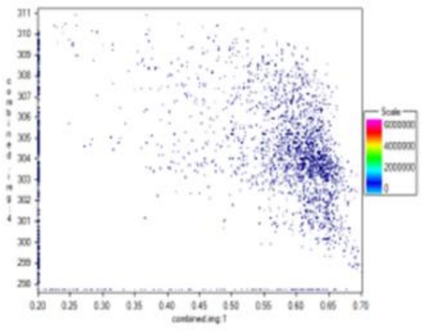

Corrected Ts from MODIS T

G2. VALIDATION USING EXPERIMENTAL DATA RESERVATION

G 2.1 Universal Triangle Method from NOAA 17 & 18 Over Utp Location

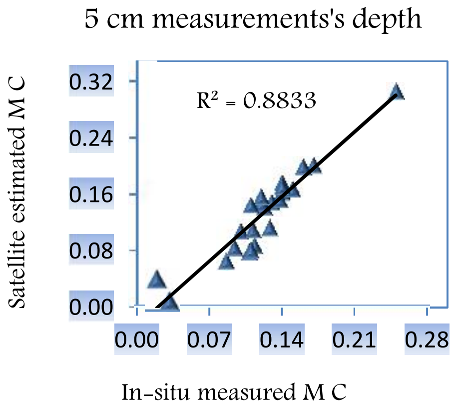

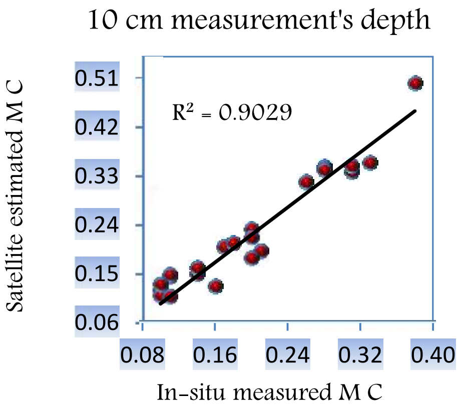

G 2.2 Universal Triangle Method from NOAA 17 & 18 Over Sitiawan Location

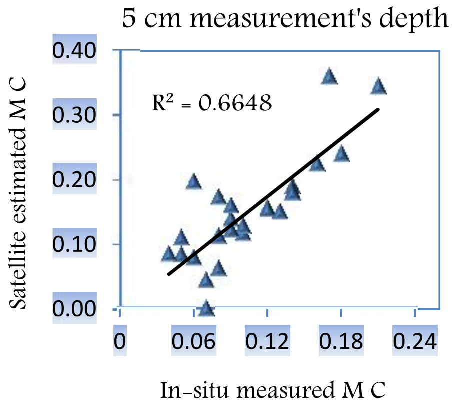

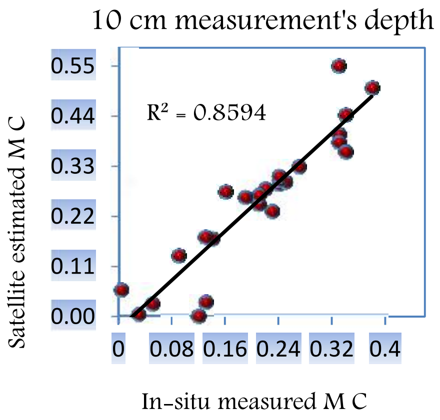

G 2.3 Universal triangle method from NOAA 17 & 18 over s. perak location

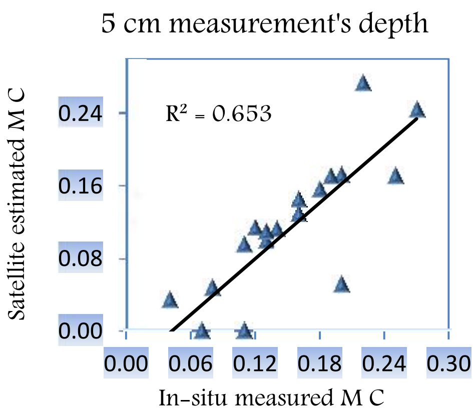

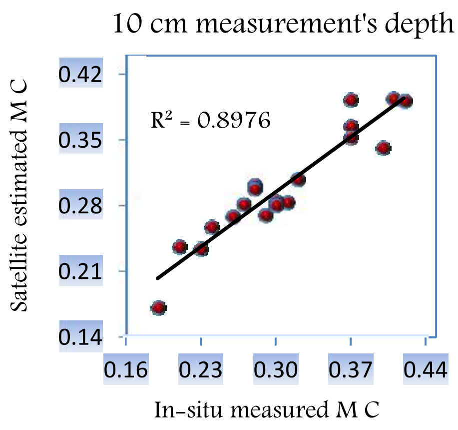

G 2.4 THERMAL INERTIA METHOD FROM MODIS TERRA & AQUA OVER UTP LOCATION

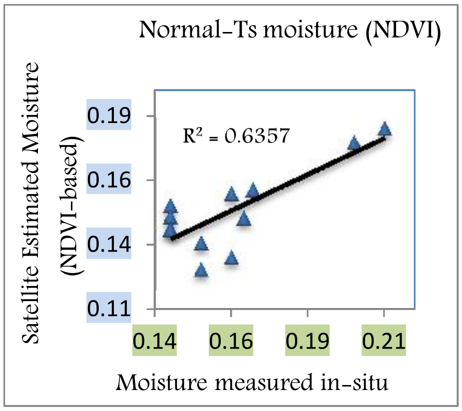

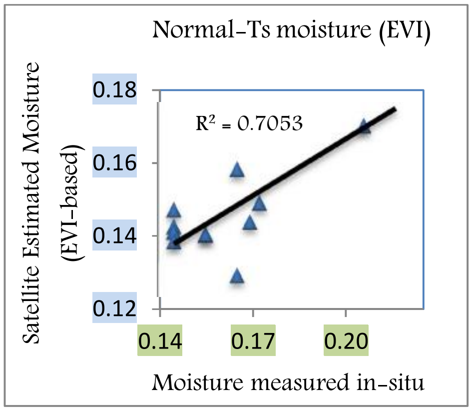

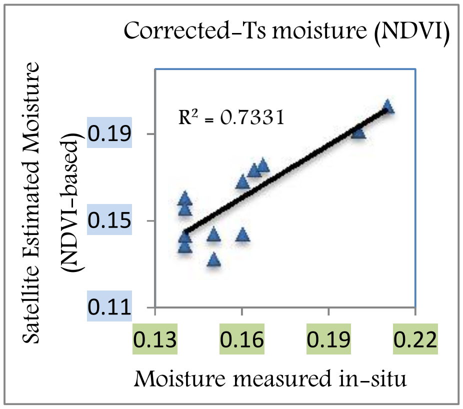

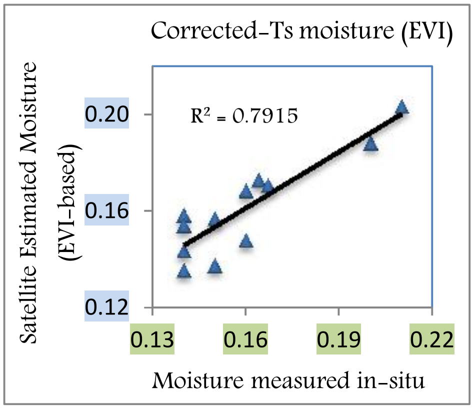

G 2.5 THERMAL INERTIA METHOD FROM MODIS TERRA & AQUA OVER SITIAWAN LOCATION

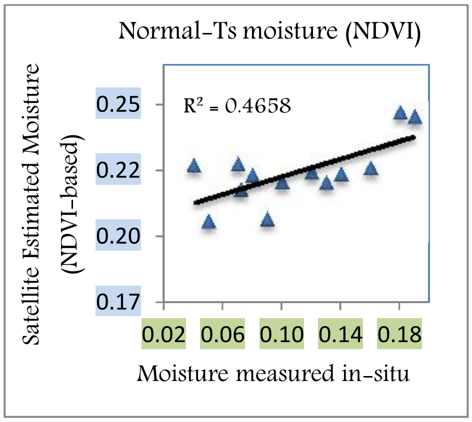
Normal-Ts moisture (NDVI)

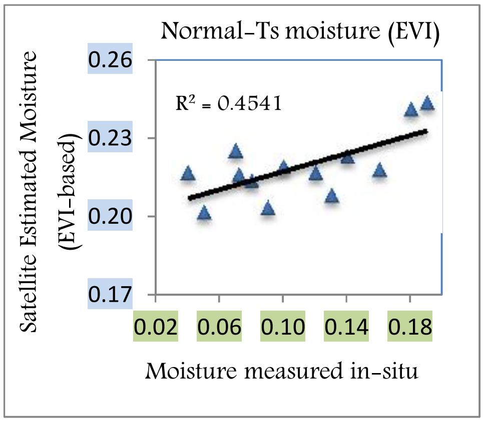
Normal-Ts moisture (EVI)

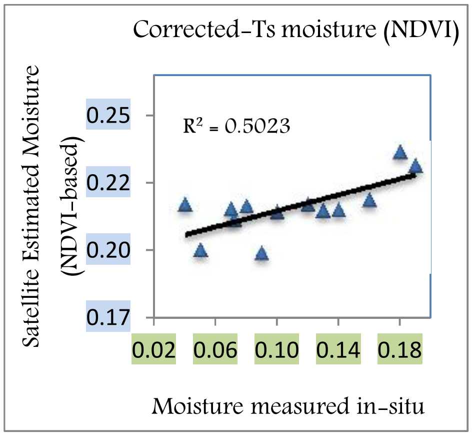
Corrected-Ts moisture (NDVI)

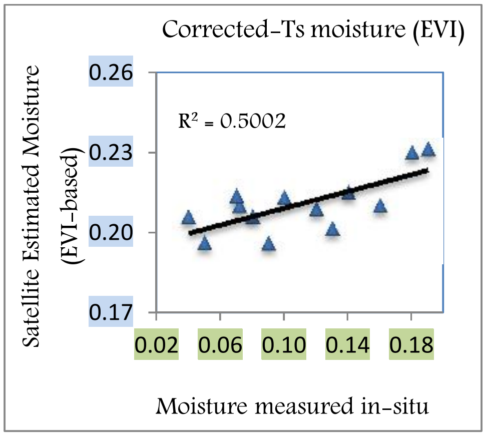
Corrected-Ts moisture (EVI)

G 2.6 THERMAL INERTIA METHOD FROM MODIS TERRA & AQUA OVER S. PERAK LOCATION

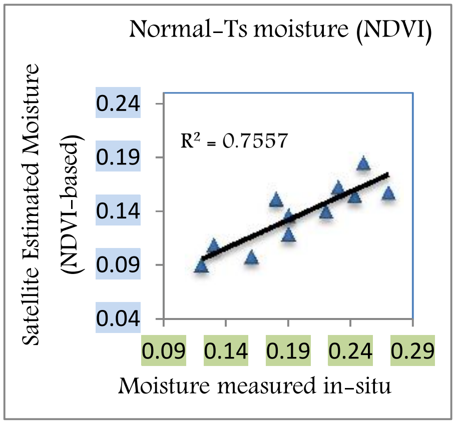
Normal-Ts moisture (NDVI)

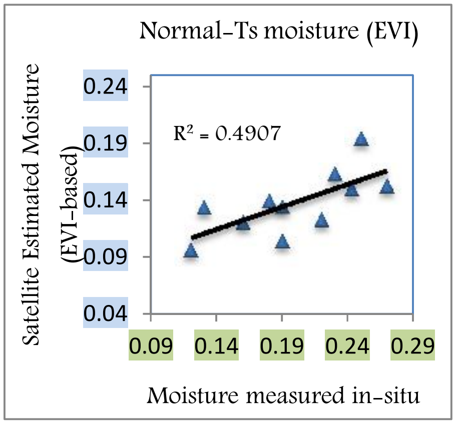
Normal-Ts moisture (EVI)

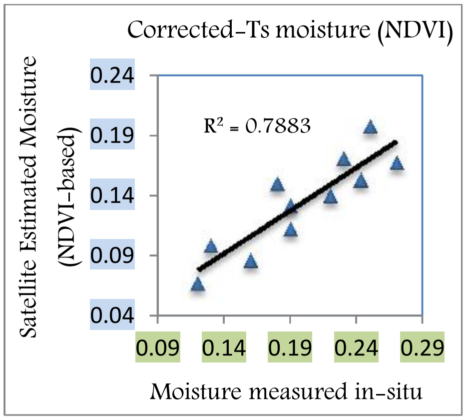

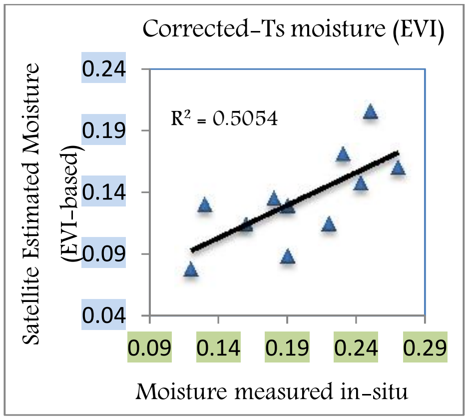

G 2.7 MOISTURE DEPTH CORRELATIONS FROM NOAA 17 & 18 OVER UTP LOCATION

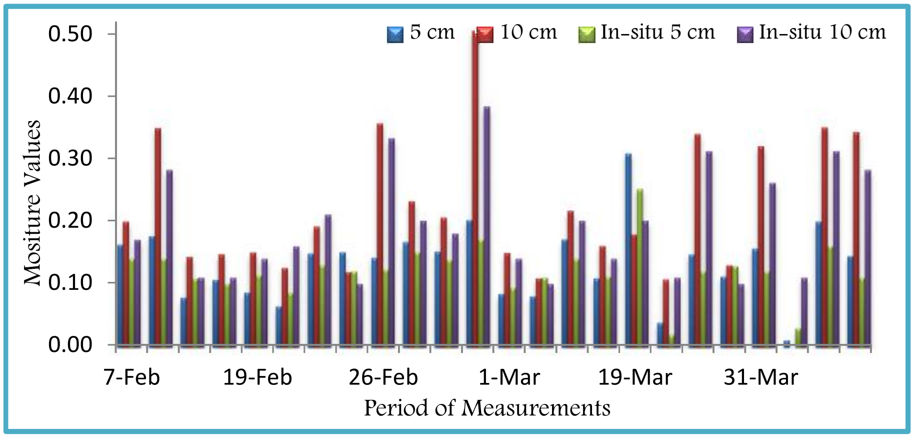

G 2.8 MOISTURE DEPTH CORRELATION FROM NOAA 17 & 18 OVER SITIAWAN LOCATION

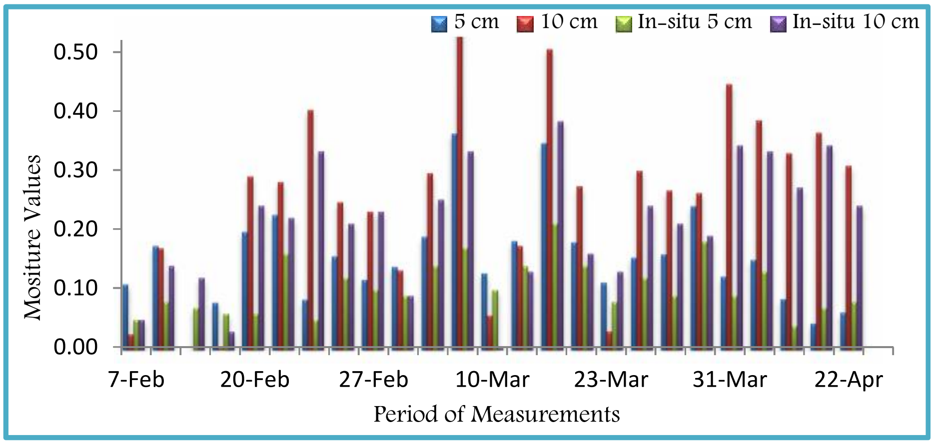

G 2.9 MOISTURE DEPTH CORRELATIONS FROM NOAA 17 & 18 OVER S. PERAK LOCATION

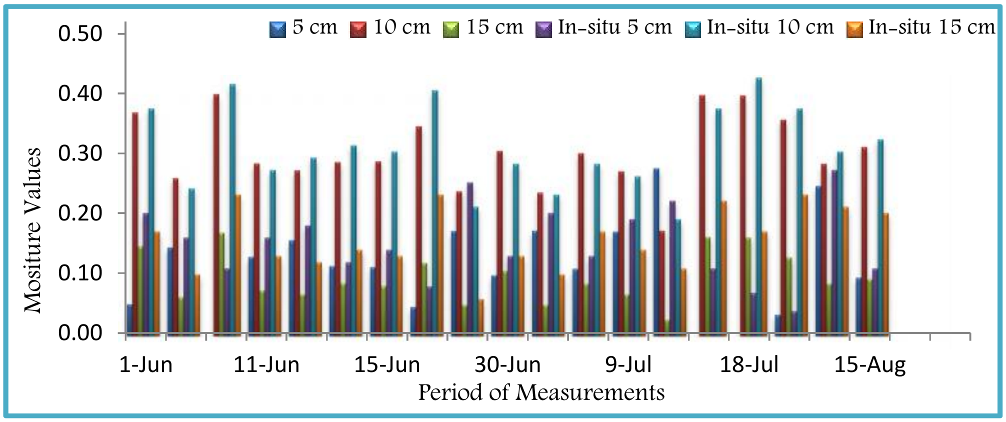

G 2.10 SURFACE MOISTURE SETS COMPARISON FROM MODIS TERRA & AQUA OVER UTP LOCATION.

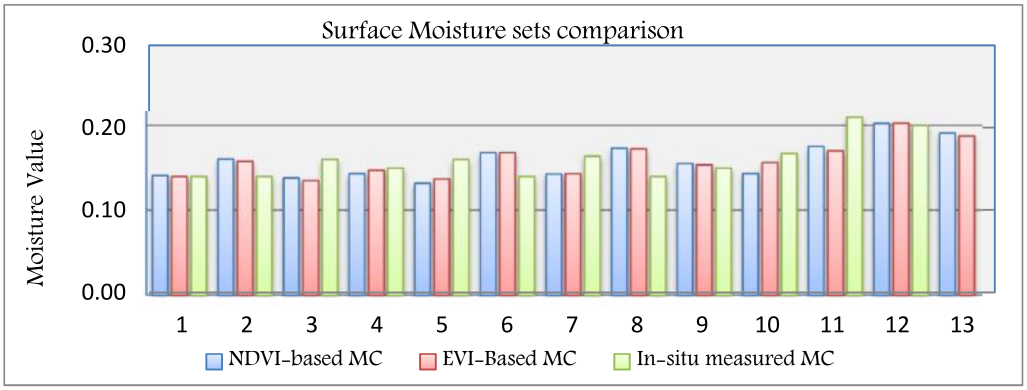

G 2.11 SURFACE MOISTURE SETS COMPARISON FROM MODIS TERRA & AQUA OVER SITIAWAN LOCATION.

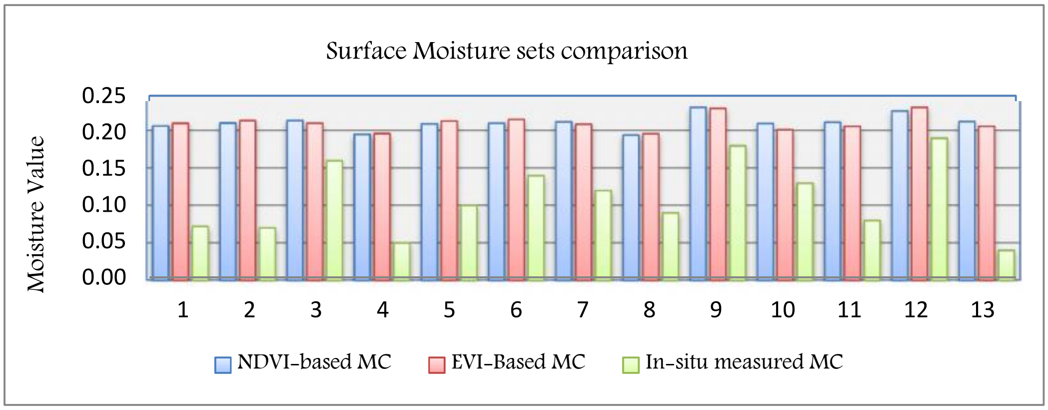

G3. 1 VALIDATION OF MC (CORRECTED Ts) USING SPSS

		Descriptive		Correlation					
	measurement	Mean	Std. Deviation	In-situ measured moisture content at depth 5 cm	Sig. (2-tailed)	In-situ measured moisture content at depth 10 cm	Sig. (2-tailed)	In-situ measured moisture content at depth 10 cm	Sig. (2-tailed)
UTP NOAA sat.	In-situ measured MC at depth 5 cm	0.12	0.04	0.94	0.000000	0.95	0.000000	0.76 **	0.0002
	In-situ measured MC at depth 10 cm	0.19	0.08						
	Satellite corrected-Ts MC at 5 cm	0.13	0.06						
	Satellite corrected-Ts MC at 10 cm	0.21	0.11	0.811 **	0.001376				
UTP MODIS	In-situ measured MC					0.902 **	0.000000		
	Corrected-Ts MC with SWI generated from (NDVI)	0.16	0.02						
	Corrected-Ts MC with SWI generated from (EVI)	0.16	0.02	0.9 **	0.000066				
SITI. NOAA sat.	In-situ measured moisture content at depth 5 cm			0.768 **	0.000005				
	In-situ measured MC at depth 10 cm	0.21	0.10						
	Satellite corrected-Ts MC at 5 cm	0.15	0.08						
	Satellite corrected-Ts MC at 10 cm	0.25	0.15	0.663 *	0.013553				
SITI. MODIS sat.	In-situ measured MC					0.942 **	0.000000		
	Corrected-Ts MC with SWI generated from (NDVI)	0.21	0.01						
	Corrected-Ts MC with SWI generated from (EVI)	0.21	0.01	0.681 *	0.010429				
S. Perak NOAA sat.	In-situ measured MC at depth 5 cm			0.811 **	0.000026				
	In-situ measured MC at depth 10 cm	0.31	0.07						
	In-situ measured MC at depth 15 cm	0.16	0.05						
	Satellite corrected-Ts MC at 5 cm	0.11	0.08						
	Satellite corrected-Ts MC at 10 cm	0.30	0.06	0.887 **	0.000276				
	Satellite corrected-Ts MC at 15 cm	0.10	0.04						
S. Perak MODIS sat.	In-situ MC content								
	Corrected-Ts MC with SWI generated from (NDVI)	0.13	0.04						
	Corrected-Ts MC with SWI generated from (EVI)	0.13	0.04	0.71 *	0.014400				
	**. Correlation is significant at the 0.01 level (2-tailed).								
	*. Correlation is significant at the 0.05 level (2-tailed).								

G3. 2 VALIDATION OF MC (NRMAL Ts) USING SPSS

	measurement	Descriptive		Correlation					
		Mean	Std. Deviation	In-situ measured moisture content at depth 5 cm	Sig. (2-tailed)	In-situ measured moisture content at depth 10 cm	Sig. (2-tailed)	In-situ measured moisture content at depth 10 cm	Sig. (2-tailed)
UTP NOAA sat.	In-situ measured MC at depth 5 cm	0.12	0.04	0.73*	0.040000	0.82**	0.000120	0.61*	0.0500
	In-situ measured MC at depth 10 cm	0.19	0.08						
	Satellite MC at 5 cm	0.23	0.23						
	Satellite MC at 10 cm	0.34	0.17	0.72**	0.002000				
UTP MODIS	In-situ measured MC	0.16	0.02			0.77*	0.012400		
	MC with SWI generated from (NDVI)	0.15	0.15						
	MC with SWI generated from (EVI)	0.15	0.15	0.823**	0.001000				
SITI. NOAA sat	In-situ measured moisture content at depth 5 cm	0.10	0.05	0.66*	0.035000				
	In-situ measured MC at depth 10 cm	0.21	0.10						
	Satellite MC at 5 cm	0.19	0.15						
	Satellite MC at 10 cm	0.38	0.11	0.72**	0.005000				
SITI. MODIS sat	In-situ measured MC	0.10	0.01			0.88**	0.000300		
	MC with SWI generated from (NDVI)	0.22	0.01						
	MC with SWI generated from (EVI)	0.23	0.12	0.58*	0.035000				
S. Perak NOAA sat.	In-situ measured MC at depth 5 cm	0.16	0.05	0.74**	0.007500				
	In-situ measured MC at depth 10 cm	0.31	0.07						
	In-situ measured MC at depth 15 cm	0.16	0.05						
	Satellite MC at 5 cm	0.22	0.23						
	Satellite MC at 10 cm	0.40	0.08	0.87**	0.000350				
	Satellite MC at 15 cm	0.36	0.09						
S. Perak MODIS sat	In-situ MC content	0.20	0.01						
	MC with SWI generated from (NDVI)	0.14	0.03						
	MC with SWI generated from (EVI)	0.14	0.03	0.687*	0.019000				

**. Correlation is significant at the 0.01 level (2-tailed).

*. Correlation is significant at the 0.05 level (2-tailed).

G4. SPATIAL VALIDATION USING SUCCESS RATE METHOD

G 4.1 The high moisture zones converted into points for moisture overlay.

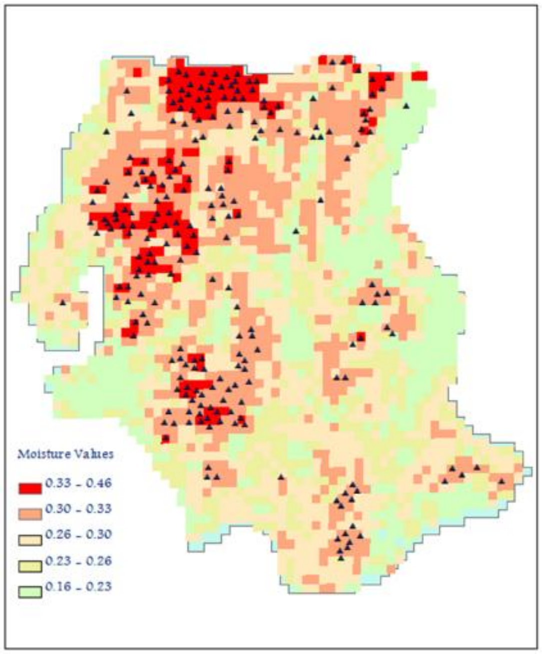

G 4.2 The low moisture zones converted into points for moisture overlay.

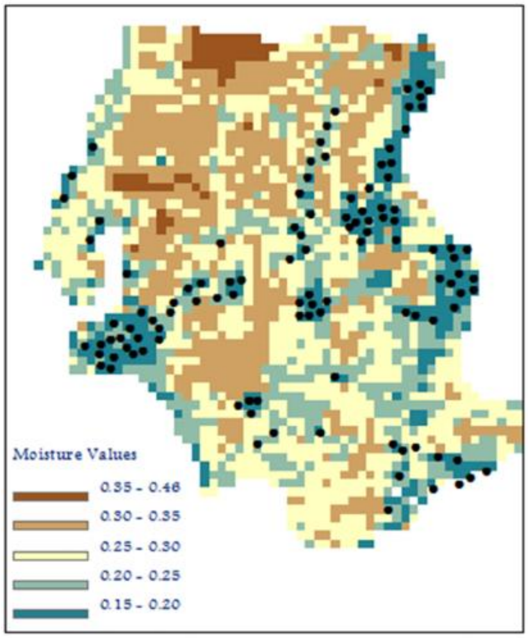

G 4.3 Area under the curve for MODIS moisture maps when overlaid at NOAA high moisture map.

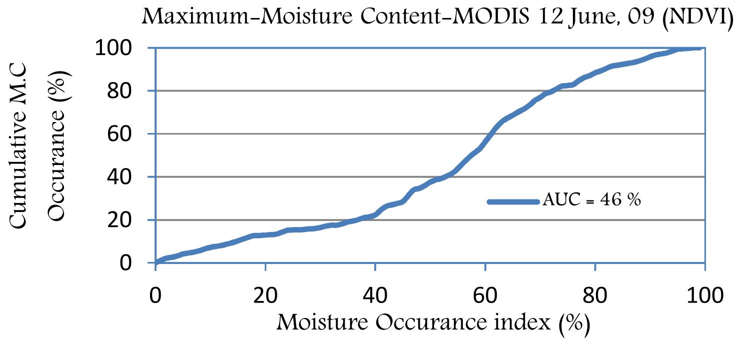

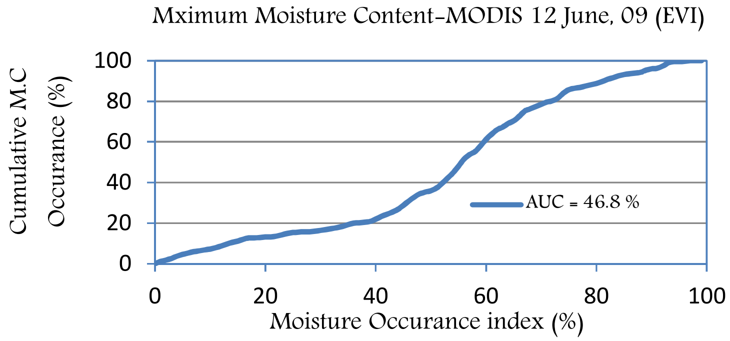

G 4.4 Area under the curve for MODIS moisture map when overlaid at NOAA low moisture map.

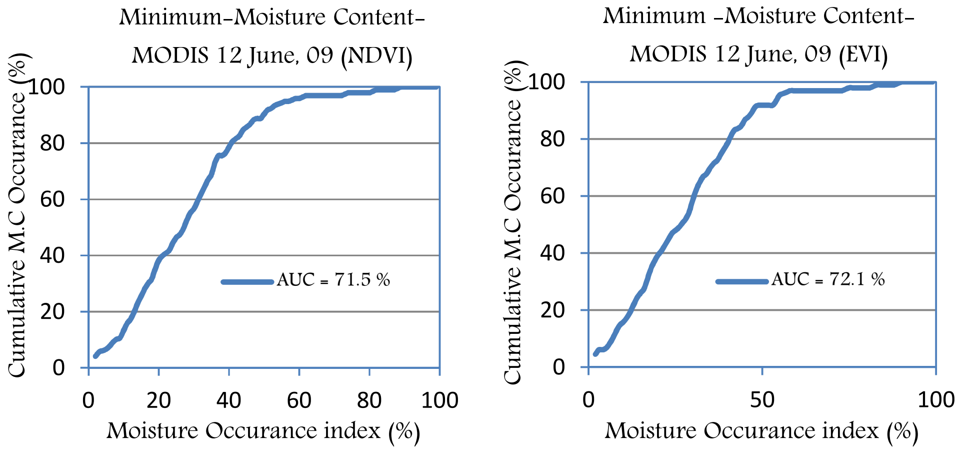

APPENDIX H

EVAPOTRANSPIRATION ANALYSIS

Tables below show the extracted ETo values from both meteorological measurements and satellites observations after scaling into point measurements.

H1.1 Overall ETo Estimated and Measured Values (m m/day) over UTP location

Utp NOAA 17 & MODIS Terra

periods		Sensor	Satellite-Based						Meteorological-Based		
			Energy Balance								
			Normal		Ts-Corrected		SEBAL		FAO 56 (PM)	Hargreaves	the Turc
			NOAA 17	TERRA	NOAA 17	TERRA	NOAA 17	TERRA			
February	2-Feb	Terra		4.8		4.9		2.8	4.1	4.8	4.4
	7-Feb	N17	5.7		5.3		4.8		4.3	5.1	4.6
	9-Feb	Terra		5.1		5.2		3.2	4.5	5.4	4.9
	12-Feb	Terra		5.0		5.1		3.3	4.2	5.1	4.7
	16-Feb	N17	5.3		5.2		3.9		4.5	5.6	5.1
	17-Feb	N17	5.7		5.5		4.4		4.8	5.8	5.2
	19-Feb	N17	5.6		5.5		4.3		4.8	5.8	5.2
	20-Feb	N17	5.4		5.3		3.8		4.6	5.6	5.1
	21-Feb	N17	5.7		5.6		4.7		4.9	6.0	5.4
	22-Feb	Terra		5.6		5.7		3.4	4.9	5.8	5.2
	27-Feb	Terra		5.2		5.3		3.9	5.1	6.2	5.4
	28-Feb	N17/Terra	7.0	6.0	6.8	6.2	6.8	5.1	5.5	6.2	5.5
MARCH	1-Mar	N17	6.6		6.4		5.8		5.0	6.1	5.4
	10-Mar	N17	6.0		5.9		4.6		5.3	6.4	5.6
	14-Mar	N17	6.3		6.1		5.1		5.2	6.3	5.5
	15-Mar	N17	5.9		5.8		4.4		4.8	5.9	5.3
	19-Mar	N17	5.5		5.4		3.3		4.3	5.5	5.1
	23-Mar	N17	6.0		5.8		4.1		4.5	5.6	5.2
	28-Mar	Terra		5.6		6.0		3.9	5.8	5.9	5.3
	30-Mar	N17/Terra	6.6	5.7	6.5	5.8	5.2	3.7	5.2	6.1	5.4
April	14-Apr	Terra		5.5		5.6		3.3	4.9	6.0	5.4
	22-Apr	Terra		5.8		6.0		3.3	4.7	5.7	5.1
	24-Apr	Terra		6.2		6.3		4.6	5.4	6.2	5.4

Utp NOAA 18 & MODIS Aqua

periods		Sensor	Satellite-Based						Meteorological-Based		
			Energy Balance								
			Normal		Ts-Corrected		SEBAL		FAO 56 (PM)	Hargreaves	the Turc
			NOAA 18	AQUA	NOAA 18	AQUA	NOAA 18	AQUA			
February	9-Feb	N18	6.0		5.9		5.5		5.6	6.0	5.2
	21-Feb	Aqua		9.6		9.7		5.1	5.7	6.7	5.7
	22-Feb	N18	6.1		6.1		5.5		5.3	6.1	5.3
	26-Feb	N18	8.2		7.0		4.7		5.5	6.6	5.6
	27-Feb	N18	6.4		6.3		5.9		5.6	6.6	5.6
	28-Feb	N18	9.1		9.4		6.4		5.9	6.6	5.7
March	28-Mar	N18	7.7		7.7		6.6		6.4	6.4	5.5
	31-Mar	N18	10.5		10.1		8.0		6.2	7.1	5.9
APRIL	8-Apr	N18	10.7		10.7		8.4		6.4	6.6	5.5
	14-Apr	N18	9.1		9.0		6.0		6.1	6.8	5.7
	17-Apr	Aqua		9.0		9.1		5.2	5.7	6.6	5.6
	19-Apr	N18	9.5		9.5		6.6		6.1	6.5	5.6

H1.2 Overall ETo Estimated and Measured Values (m m/day) over SITIAWAN location

Sitiawan NOAA 17 & MODIS Terra

periods		Sensor	Satellite-Based						Meteorological-Based		
			Energy Balance								
			Normal		Ts-Corrected		SEBAL		FAO 56 (PM)	Hargreaves	the Turc
			NOAA 17	TERRA	NOAA 17	TERRA	NOAA 17	TERRA			
February	2-Feb	Terra		5.3		5.1		3.9	4.1	4.8	4.4
	7-Feb	N17	5.6		4.7		4.5		4.2	5.1	4.6
	9-Feb	Terra		5.9		5.7		4.7	4.6	5.6	5.0
	12-Feb	Terra		5.6		5.5		4.4	4.6	5.6	5.0
	16-Feb	N17	5.4		4.8		4.1		4.8	5.9	5.2
	17-Feb	N17	5.7		5.2		4.6		4.8	5.9	5.3
	19-Feb	N17	5.5		5.0		4.3		4.7	5.8	5.2
	20-Feb	N17	5.9		5.4		4.8		4.6	5.7	5.1
	21-Feb	N17	5.7		5.2		4.6		5.0	6.1	5.4
	22-Feb	Terra		6.0		5.8		4.8	4.9	5.8	5.2
	27-Feb	Terra		5.9		5.7		5.0	5.0	6.1	5.4
	28-Feb	N17/Terra	5.9	5.9	5.4	5.7	4.9	4.6	5.0	6.1	5.4
MARCH	1-Mar	N17	7.2		6.8		7.5		6.0	7.0	5.8
	10-Mar	N17	5.9		5.3		4.5		5.3	6.5	5.7
	14-Mar	N17	6.4		5.9		5.6		5.4	6.6	5.7
	15-Mar	N17	6.3		5.8		5.4		5.0	6.1	5.4
	19-Mar	N17	5.8		5.3		4.2		4.7	5.8	5.3
	23-Mar	N17	6.1		5.5		4.6		5.0	6.1	5.4
	24-Mar	Terra		6.2		6.0		4.8	5.1	6.2	5.4
	28-Mar	Terra		6.1		6.0		4.6	5.0	5.9	5.3
	30-Mar	N17/Terra	6.2	6.1	5.6	5.9	4.4	4.6	4.9	5.8	5.2
April	14-Apr	Terra		6.2		6.1		4.8	5.0	6.1	5.5
	22-Apr	Terra		6.3		5.8		4.3	4.8	5.8	5.2

Sitiawan NOAA 18 & MODIS Aqua

periods		Sensor	Satellite-Based						Meteorological-Based		
			Energy Balance								
			Normal		Ts-Corrected		SEBAL		FAO 56 (PM)	Hargreaves	the Turc
			NOAA 18	AQUA	NOAA 18	AQUA	NOAA 18	AQUA			
February	21-Feb	Aqua		8.6		8.4			5.3	6.4	5.5
	22-Feb	N18	8.1		7.0		5.1	5.4	5.3	6.2	5.4
	26-Feb	N18	8.1		7.1		5.0		5.3	6.4	5.5
	27-Feb	N18	8.2		7.2		5.1		5.3	6.4	5.5
	28-Feb	N18	9.7		9.6		7.2		5.7	6.7	5.7
March	24-Mar	N18	8.9		9.3		6.0		5.8	6.9	5.7
	28-Mar	N18	8.3		7.7		5.4		5.5	6.4	5.5
	31-Mar	N18	10.5		10.8		7.9		5.8	6.8	5.8
April	14-Apr	N18	9.0		8.1		5.9		5.8	6.8	5.8
	17-Apr	N18/Aqua	7.7	8.9	6.1	8.7	3.9	5.2	5.3	6.4	5.5
	19-Apr	N18	9.2		8.6		5.8		5.5	6.4	5.5
	22-Apr	N18	8.7		7.7		5.4		5.6	6.5	5.5

H1.3 Overall ETo Estimated and Measured Values (m m/day) over S. PERAK location

S. Perak NOAA 18 & MODIS Aqua/Terra

periods		Sensor	Satellite-Based									Meteorological-Based		
			Energy Balance											
			Normal			Ts-Corrected			SEBAL			FAO 56 (PM)	Hargreaves	the Turc
			NOAA 18	AQUA	TERRA	NOAA 18	AQUA	TERRA	NOAA 18	TERRA	Aqua			
June	1-Jun	N18	6.1			6.2			4.7			4.8	5.7	5.0
	6-Jun	N18/Terra/Aqua	4.8	7.9	5.6	5.4	7.8	5.5	2.2	3.2	3.6	4.3	5.2	4.7
	8-Jun	N18	6.8			6.4			5.6			5.2	6.1	5.2
	11-Jun	N18/Terra	5.4		5.9	5.7		5.8	3.5	3.9		4.7	5.7	5.1
	12-Jun	N18/Terra	5.3		5.5	5.6		5.5	3.1	3.3		4.5	5.4	4.9
	14-Jun	N18/Aqua	5.1	7.3		5.6	7.3		2.9		3.0	4.6	5.6	4.9
	15-Jun	N18	6.4			6.2			5.1			4.9	5.8	4.9
	17-Jun	Terra			5.6			5.5		3.4		4.4	5.3	4.7
	21-Jun	N18	6.0			6.0			4.7			4.8	5.7	4.9
	29-Jun	N18/Terra	5.2		5.7	5.5		5.6	3.2	3.6		4.4	5.4	4.9
	30-Jun	N18	5.6			5.7			3.9			4.8	5.8	5.0
JULY	1-Jul	Aqua		8.2			8.0				4.5	5.2	6.0	5.1
	4-Jul	N18	6.6			6.2			5.5			5.3	6.1	5.2
	5-Jul	N18/Terra	6.0		6.0	6.1		5.9	4.8	4.4		5.0	5.9	5.0
	9-Jul	N18/Terra	5.5		5.4	5.7		5.3	3.8	3.4		4.4	5.4	4.9
	13-Jul	N18/Terra	6.1		5.8	6.1		5.8	4.9	4.2		5.0	5.9	5.2
	17-Jul	N18	6.0			6.0			4.8			5.0	5.9	5.1
	18-Jul	N18	6.1			6.0			4.9			5.0	5.9	5.1
	21-Jul	Terra			5.6			5.5		3.8		4.4	5.4	4.8
	24-Jul	Aqua		8.3			8.2				4.7	5.3	6.3	5.3
AUGUST	8-Aug	N18	6.7			6.4			6.0			5.3	6.2	5.2
	10-Aug	N18/Terra	5.5		5.9	5.9		5.8	3.7	4.2		5.0	5.8	5.1
	11-Aug	Terra/Aqua		8.1	6.1		8.0	6.0		4.4	4.2	5.2	6.0	5.1
	15-Aug	N18	6.8			6.4			5.2			4.9	5.9	5.2
	20-Aug	Terra			5.7			5.6		3.6		4.9	5.9	5.2
	25-Aug	Terra			5.7			5.7		3.7		4.9	5.9	5.2

H 2. Scatterplots for the measured and satellites estimated ETo.

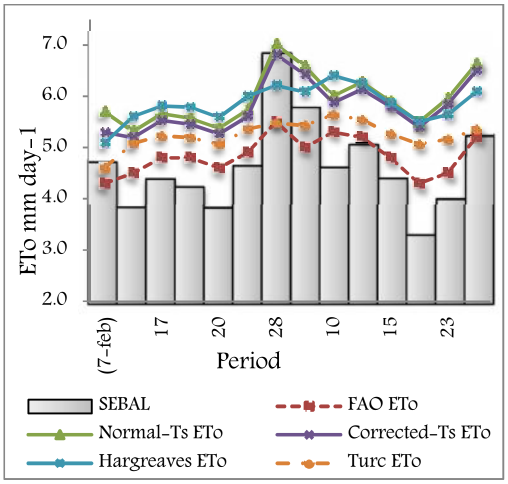

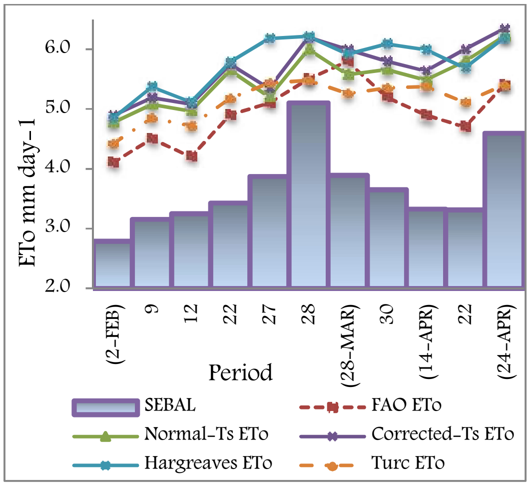

NOAA 17 at UTP

MODIS TERRA at UTP

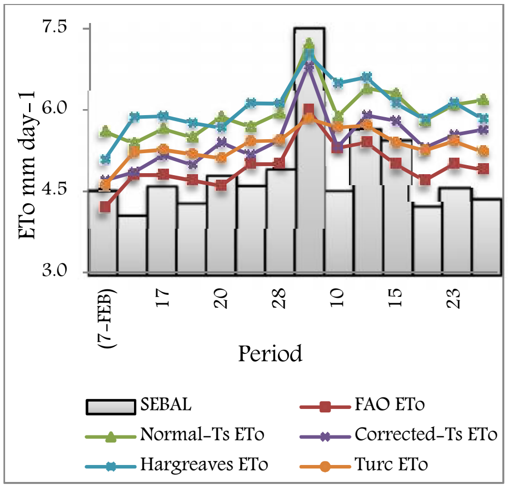

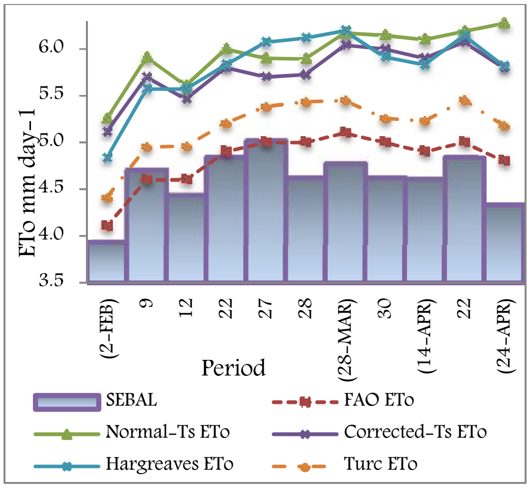

NOAA 17 at Sitiawan

MODIS TERRA at Sitiawan

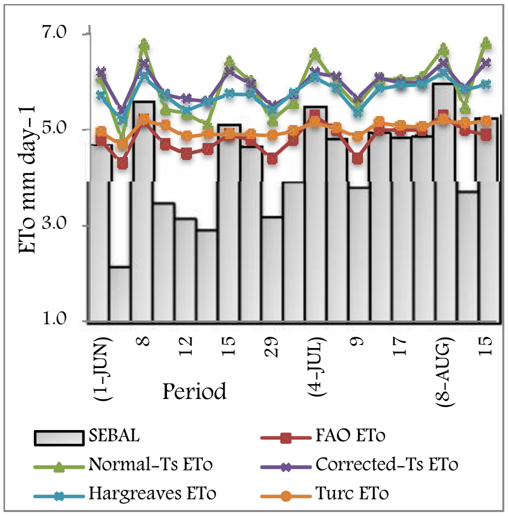

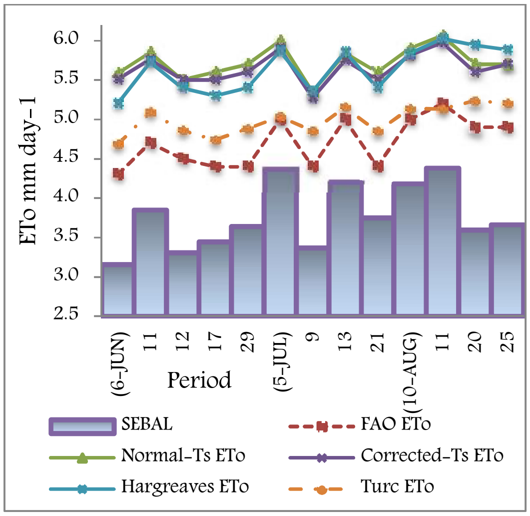

NOAA 18 at Sp. Perak

MODIS TERRA at Sp. Perak

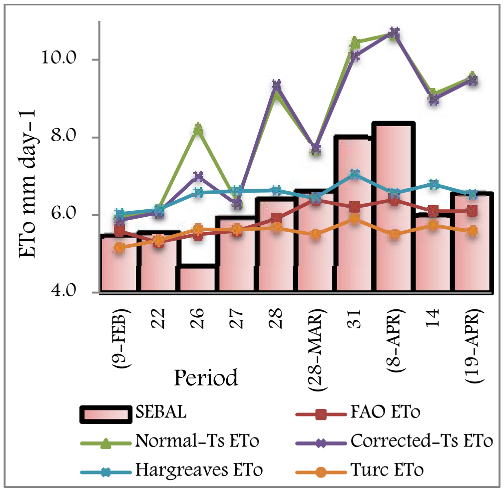

NOAA 18 at UTP

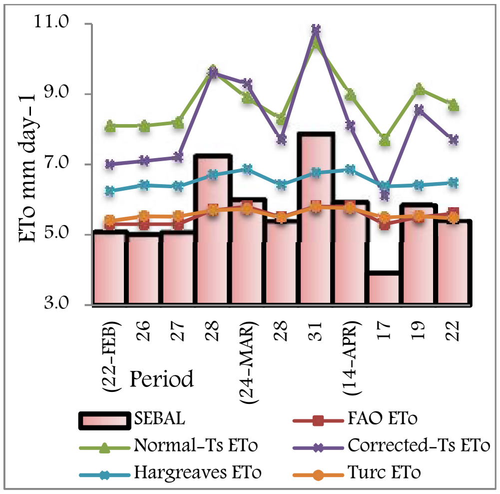

NOAA 18 at Sitiawan

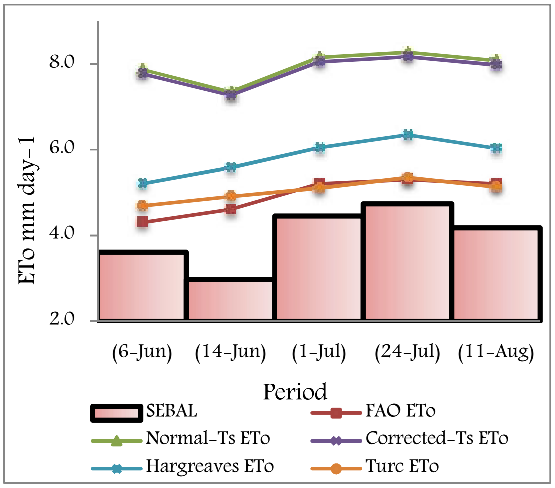

MODIS AQUA at Sp. Perak

APPENDIX I

MOISTURE INFLUENCE ON ETO

Tables below show the resultant ETo after incorporating the effect of soil moisture content.

I 1. Values of the actual ET extracted from satellites based on moisture influence over UTP location.

		Location	Satellite-Corrected Ts θ		Satellite-Corrected Ts Eto	**Reduction Coeff. B**		**Actual ET Jacobs Algorithm**		PM FAO 56
			Depth					mm day-1		mm day-1
			5 cm	**10 cm**		**5 cm**	**10 cm**	**5 cm**	**10 cm**	
N17	7-Feb	UTP	0.16	0.20	5.3	1.3	1.4	6.8	7.4	4.3
	16-Feb	UTP	0.08	0.14	5.2	0.9	1.2	4.8	6.3	4.5
	17-Feb	UTP	0.11	0.15	5.5	1.1	1.2	5.9	6.8	4.8
	19-Feb	UTP	0.09	0.15	5.5	1.0	1.2	5.3	6.7	4.8
	20-Feb	UTP	0.06	0.13	5.3	0.9	1.1	4.5	6.0	4.6
	21-Feb	UTP	0.15	0.19	5.6	1.2	1.4	6.9	7.7	4.9
	28-Feb	UTP	0.15	0.21	6.8	1.2	1.4	8.4	9.6	5.5
	1-Mar	UTP	0.08	0.15	6.4	1.0	1.2	6.2	7.9	5.0
	10-Mar	UTP	0.08	0.11	5.9	0.9	1.1	5.6	6.3	5.3
	14-Mar	UTP	0.17	0.22	6.1	1.3	1.4	8.0	8.8	5.2
	15-Mar	UTP	0.11	0.16	5.8	1.1	1.3	6.2	7.4	4.8
	19-Mar	UTP		0.18	5.4	0.0	1.3	0.0	7.2	4.3
	23-Mar	UTP	0.04	0.11	5.8	0.7	1.1	4.0	6.2	4.5
	30-Mar	UTP	0.11	0.13	6.5	1.1	1.2	7.1	7.5	5.2
N18	9-Feb	UTP	0.18	0.35	5.9	1.3	1.8	7.7	10.3	5.6
	22-Feb	UTP	0.15	0.12	6.1	1.2	1.1	7.5	6.8	5.3
	26-Feb	UTP	0.14	0.35	7.0	1.2	1.8	8.4	12.4	5.5
	27-Feb	UTP	0.17	0.23	6.3	1.3	1.5	8.1	9.3	5.6
	28-Feb	UTP	0.20	0.50	9.4	1.4	2.1	13.1	19.3	5.9
	28-Mar	UTP	0.15	0.34	7.7	1.2	1.7	9.4	13.4	6.4
	31-Mar	UTP	0.16	0.32	10.1	1.3	1.7	12.7	17.1	6.2
	8-Apr	UTP			10.7	0.0	0.0	0.0		6.4
	14-Apr	UTP	0.20	0.35	9.0	1.4	1.8	12.5	15.8	6.1
	19-Apr	N18	0.14	0.34	9.5	1.2	1.7	11.5	16.6	6.1
TERRA	2-Feb	UTP	0.14	0.14	4.9	1.2	1.2	5.9	5.8	4.1
	9-Feb	UTP	0.16	0.16	5.2	1.3	1.3	6.6	6.5	4.5
	12-Feb	UTP	0.14	0.14	5.1	1.2	1.2	6.1	6.0	4.2
	22-Feb	UTP	0.14	0.15	5.7	1.2	1.2	7.0	7.0	4.9
	27-Feb	UTP	0.13	0.14	5.3	1.2	1.2	6.2	6.3	5.1
	28-Feb	UTP	0.17	0.17	6.2	1.3	1.3	8.0	8.0	5.5
	28-Mar	UTP	0.14	0.14	6.0	1.2	1.2	7.2		5.8
	30-Mar	UTP	0.17	0.17	5.8	1.3	1.3	7.6	7.6	5.2
	14-Apr	UTP	0.16	0.15	5.6	1.3	1.2	7.0	7.0	4.9
	22-Apr	UTP	0.14	0.16	6.0	1.2	1.3	7.3	7.5	4.7
	24-Apr	UTP	0.18	0.17	6.3	1.3	1.3	8.4	8.3	5.4

I 2. Values of the actual ET extracted from satellites based on moisture influence over SITIAWAN location.

		Location	Satellite-Corrected Ts θ		Satellite-Corrected Ts ETo	Reduction Coeff. B		Actual ET Jacobs Algorithm		PM FAO 56
			Depth					mm day-1		mm day-1
			5 cm	10 cm		5 cm	10 cm	5 cm	10 cm	
N17	7-Feb	SITI	0.11	0.03	4.5	1.1	0.6	4.8	2.6	4.2
	16-Feb	SITI	0.17	0.17	4.1	1.3	1.3	5.4	5.3	4.8
	19-Feb	SITI	0.08	0.00	4.3	0.9	0.3	4.0	1.1	4.7
	20-Feb	SITI	0.20	0.29	4.8	1.4	1.6	6.6	7.8	4.6
	21-Feb	SITI	0.22	0.28	4.6	1.5	1.6	6.8	7.4	5.0
	28-Feb	SITI	0.14	0.13	4.9	1.2	1.2	5.9	5.7	5.0
	1-Mar	SITI	0.36	0.55	7.5	1.8	2.1	13.4	16.0	6.0
	10-Mar	SITI	0.13	0.06	4.5	1.2	0.8			5.3
	14-Mar	SITI	0.18	0.17	5.6	1.3	1.3	7.5	7.4	5.4
	15-Mar	SITI	0.34	0.50	5.4	1.8	2.1	9.6	11.2	5.0
	19-Mar	SITI	0.18	0.27	4.2	1.3	1.6	5.6	6.7	4.7
	23-Mar	SITI	0.11	0.03	4.6	1.1	0.6	5.0	2.9	5.0
	30-Mar	SITI	0.24	0.26	4.4	1.5	1.6	6.6	6.8	4.9
N18	22-Feb	SITI	0.08	0.40	7.0	1.0	1.9	6.7	13.1	5.3
	26-Feb	SITI	0.16	0.25	7.1	1.3	1.5	8.9	10.8	5.3
	27-Feb	SITI	0.12	0.23	7.2	1.1	1.5	8.0	10.7	5.3
	28-Feb	SITI	0.19	0.29	9.6	1.4	1.6	13.0	15.8	5.7
	28-Mar	SITI	0.15	0.30	9.3	1.2	1.7	11.6	15.4	5.5
	31-Mar	SITI	0.16	0.27	10.8	1.3	1.6	13.7	17.0	5.8
	14-Apr	SITI	0.15	0.38	8.1	1.2	1.8	10.0	14.9	5.8
	17-Apr	SITI	0.08	0.33	6.1	1.0	1.7	5.9	10.5	5.3
	19-Apr	SITI	0.04	0.36	8.6	0.7	1.8		15.4	5.5
	22-Apr	SITI	0.06	0.31	7.7	0.8	1.7		12.9	5.6
TERRA	2-Feb	SITI	0.21	0.21	5.1	1.4	1.4		7.3	4.1
	9-Feb	SITI	0.21	0.21	5.7	1.4	1.4	8.1	8.2	4.6
	12-Feb	SITI	0.21	0.21	5.5	1.4	1.4	7.8	7.8	4.6
	22-Feb	SITI	0.20	0.20	5.8	1.4	1.4	8.0	8.0	4.9
	27-Feb	SITI	0.21	0.21	5.7	1.4	1.4	8.1	8.2	5.0
	28-Feb	SITI	0.21	0.22	5.7	1.4	1.4	8.1	8.2	5.0
	24-Mar	SITI	0.21	0.21	6.0	1.4	1.4	8.6	8.6	5.1
	28-Mar	SITI	0.19	0.20	6.0	1.4	1.4	8.3	8.3	5.0
	30-Mar	SITI	0.23	0.23	5.9	1.5	1.5	8.7	8.7	4.9
	14-Apr	SITI	0.21	0.20	6.1	1.4	1.4	8.6	8.5	5.0
	22-Apr	SITI	0.21	0.21	5.8	1.4	1.4	8.3	8.2	4.8

I 3. Values of the actual ET extracted from satellites based on moisture influence over S. PERAK location.

	Date	Location	Corrected-Ts Moisture Content	Satellite-Corrected Ts ETo	Reduction Coeff. B	Actual ET Jacobs Algorithm	PM FAO 56
			θ_{vNDVI}			mm day-1	mm day-1
N17	1-Jun	SP	0.36	6.2	1.8	11.2	4.8
	6-Jun	SP	0.26	5.4	1.6	8.4	4.3
	8-Jun	SP	0.39	6.4	1.9	11.9	5.2
	11-Jun	SP	0.28	5.7	1.6	9.3	4.7
	12-Jun	SP	0.27	5.6	1.6	8.9	4.5
	14-Jun	SP	0.28	5.6	1.6	9.0	4.6
	15-Jun	SP	0.28	6.2	1.6	10.1	4.9
	21-Jun	SP	0.34	6.0	1.7	10.4	4.8
	29-Jun	SP	0.24	5.5	1.5	8.2	4.4
	30-Jun	SP	0.30	5.7	1.7	9.5	4.8
	4-Jul	SP		6.2	0.0		5.3
	5-Jul	SP	0.30	6.1	1.6	10.1	5.0
	9-Jul	SP	0.27	5.7	1.6	8.9	4.4
	13-Jul	SP		6.1	0.0		5.0
	17-Jul	SP	0.39	6.0	1.9	11.1	5.0
	18-Jul	SP	0.39	6.0	1.9	11.1	5.0
	8-Aug	SP	0.35	6.4	1.8	11.4	5.3
	10-Aug	SP	0.28	5.9	1.6	9.4	5.0
	15-Aug	SP	0.31	6.4	1.7	10.7	4.9
N18	1-Jun	SP	0.36	6.2	1.8	11.2	4.8
	6-Jun	SP	0.26	5.4	1.6	8.4	4.3
	8-Jun	SP	0.39	6.4	1.9	11.9	5.2
	11-Jun	SP	0.28	5.7	1.6	9.3	4.7
	12-Jun	SP	0.27	5.6	1.6	8.9	4.5
	14-Jun	SP	0.28	5.6	1.6	9.0	4.6
	15-Jun	SP	0.28	6.2	1.6	10.1	4.9
	21-Jun	SP	0.34	6.0	1.7	10.4	4.8
	29-Jun	SP	0.24	5.5	1.5	8.2	4.4
	30-Jun	SP	0.30	5.7	1.7	9.5	4.8
	4-Jul	SP		6.2	0.0		5.3
	5-Jul	SP	0.30	6.1	1.6	10.1	5.0
	9-Jul	SP	0.27	5.7	1.6	8.9	4.4
	13-Jul	SP		6.1	0.0		5.0
	17-Jul	SP	0.39	6.0	1.9	11.1	5.0
	18-Jul	SP	0.39	6.0	1.9	11.1	5.0
	8-Aug	SP	0.35	6.4	1.8	11.4	5.3
	10-Aug	SP	0.28	5.9	1.6	9.4	5.0
	15-Aug	SP	0.31	6.4	1.7	10.7	4.9
TERRA	6-Jun	SP	0.11	5.5	1.1	6.0	4.3
	12-Jun	SP	0.13	5.5	1.2	6.5	4.5
	29-Jun	SP	0.21	5.6	1.4	7.9	4.4
	5-Jul	SP		5.9	0.0		5.0
	9-Jul	SP	0.13	5.3	1.2	6.1	4.4
	13-Jul	SP	0.11	5.8	1.1		5.0
	21-Jul	SP	0.15	5.5	1.2	6.7	4.4
	10-Aug	SP		5.8	0.0		5.0
	20-Aug	SP		5.6	0.0		4.9

APPENDIX J

EVAPOTRANSPIRATION MAPS

Figures below show the generated ETo maps of the study area according to energy balance, SEBAL and Jacobs methods.

J 1. Evapotranspiration maps Estimated from NOAA 17 Satellite

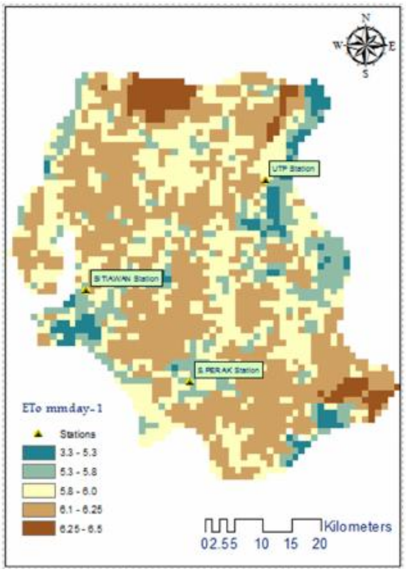

Energy Balance Ts-corrected ETo

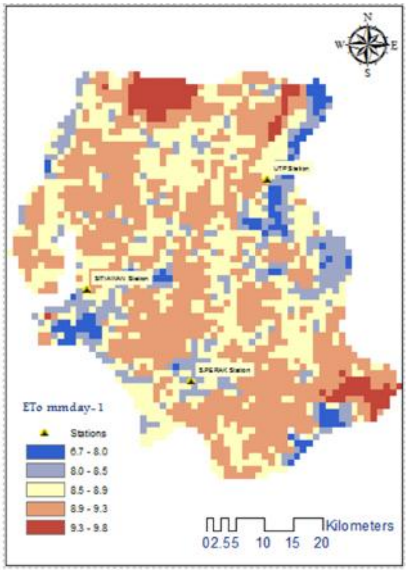

SEBAL-NOAA 17

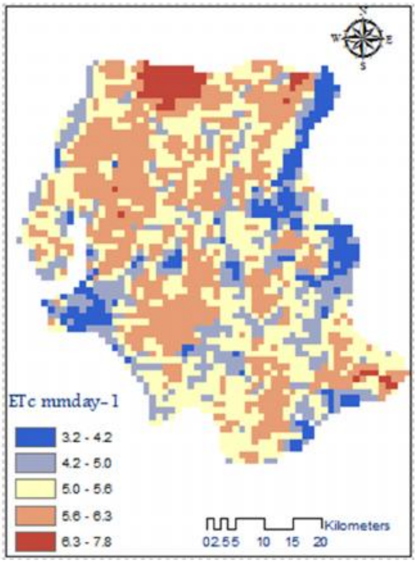

5 cm moisture depth ETo (Jacobs)

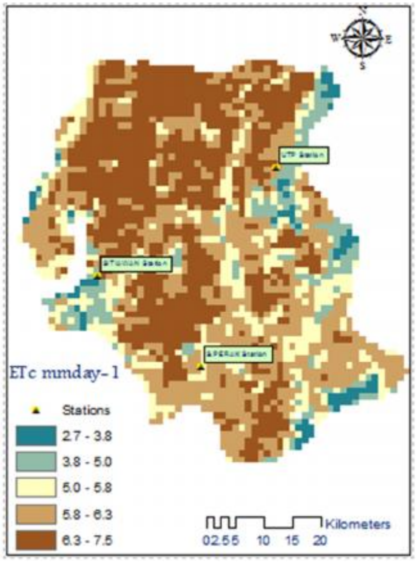

10 cm moisture depth ETo (Jacobs)

J 2. Evapotranspiration maps Estimated from NOAA 18 Satellite

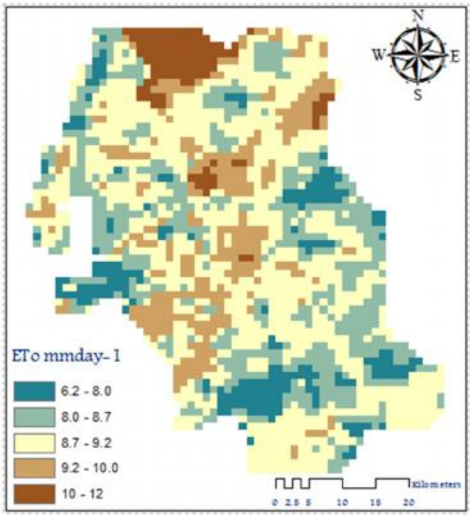

Corrected Ts ETo

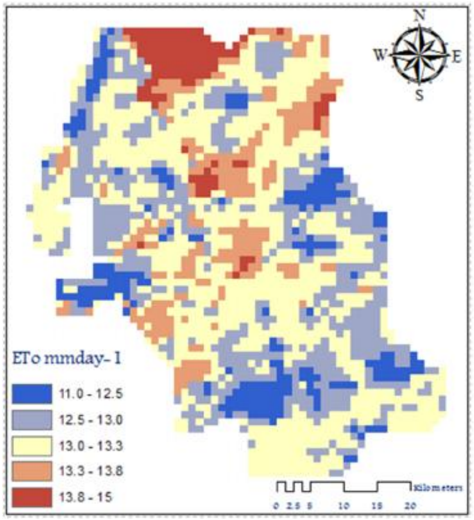

SEBAL model

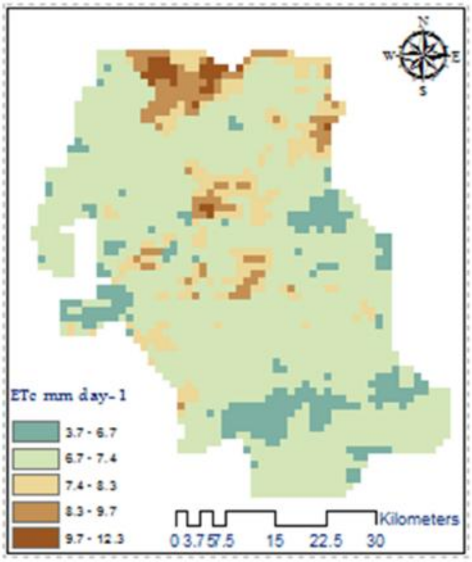

5 cm moisture depth ETo (Jacobs)

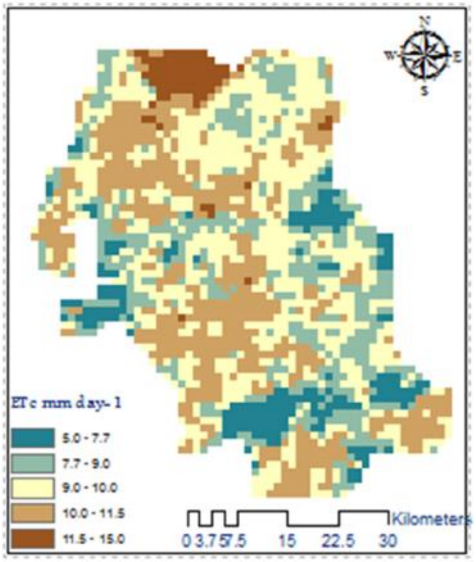

10 cm moisture depth ETo (Jacobs)

J 3. Evapotranspiration maps Estimated from MODIS TERRA Satellite

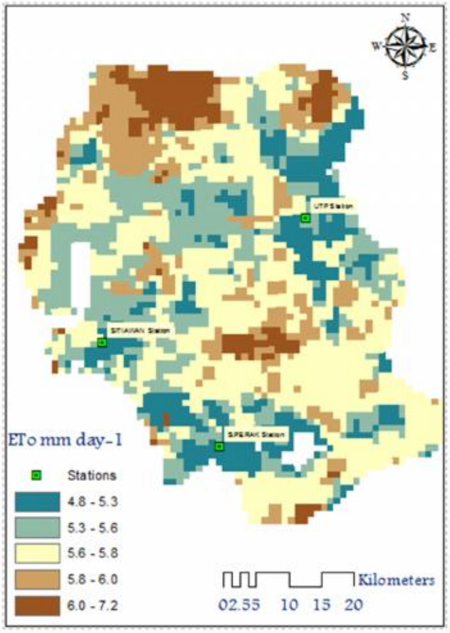

Corrected Ts ETo

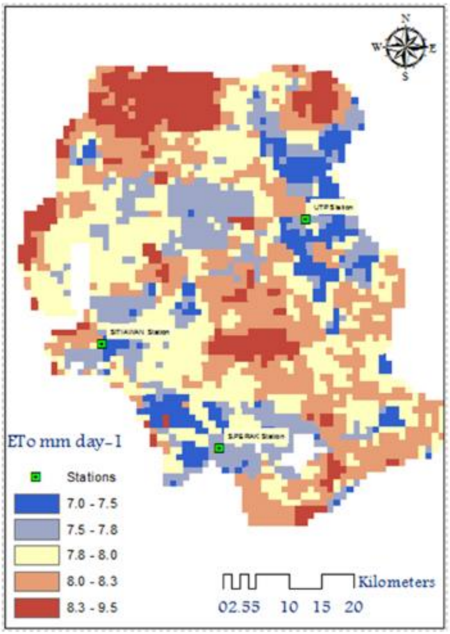

SEBAL Model

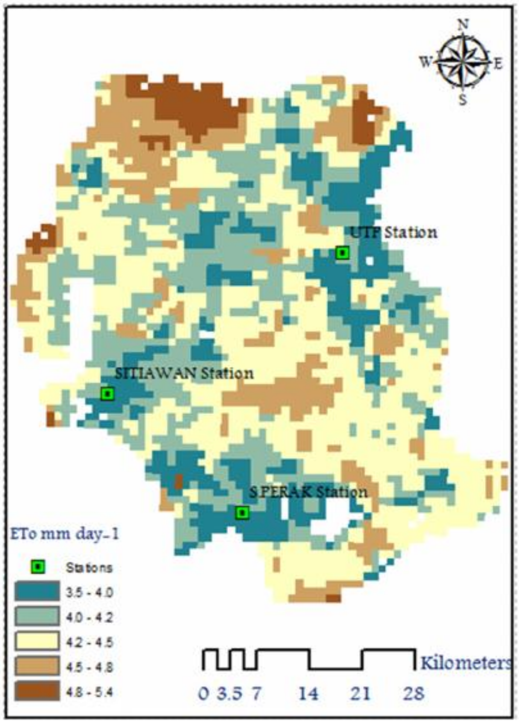

ETo (Jacobs) with SWI based on NDVI

APPENDIX K

EVAPOTRANSPIRATION VALIDATION

Three types of validation are shown in this section statistical, experimental and spatial validation.

K 1. Statistical validation of ETo using SPSS

Statistical Validation					
measurement		Descriptive		Correlation Coeff. R^2	
		Mean	Std. Deviation	ETo from PM-FAO 56	Sig. (2-tailed)
UTP	ETo from PM-FAO 56	4.84	0.37		
	ETo from N17 Satellite corrected-Ts	5.79	0.50	0.825 **	0.000280
	ETo-Corrected-Ts from MODIS Terra	5.65	0.47	0.621 *	0.041530
	ETo from N18 Satellite Corrected-Ts	8.17	1.78	0.714 *	0.020458
	ETo from SEBAL	4.66	0.88	0.763 **	0.001488
		4.96	0.42		
SITIAWAN	ETo from PM-FAO 56				
	ETo from N17 Satellite corrected-Ts	5.42	0.52	0.856**	0.000095
	ETo-Corrected-Ts from MODIS Terra	5.75	0.28	0.783 **	0.004384
	ETo from N18 Satellite Corrected-Ts	8.11	1.36	0.825 **	0.001759
	ETo from SEBAL	4.86	0.87	0.791 **	0.000751
		4.84	0.29		
S. PERAK	ETo from PM-FAO 56				
	ETo-Corrected-Ts from MODIS Aqua	7.86	0.34	0.56	0.32865
	ETo-Corrected-Ts from MODIS Terra	5.65	0.20	0.865 **	0.000137
	ETo from N18 Satellite Corrected-Ts	5.95	0.32	.851 **	0.000004
	ETo from SEBAL	4.34	1.04	0.879 **	0.000001

**. Correlation is significant at the 0.01 level (2-tailed).

*. Correlation is significant at the 0.05 level (2-tailed).

K 2. Experimental validation of ETo using reserved field and satellites data.

K 2.1 Satellites data validations for Morning overpass sensors.

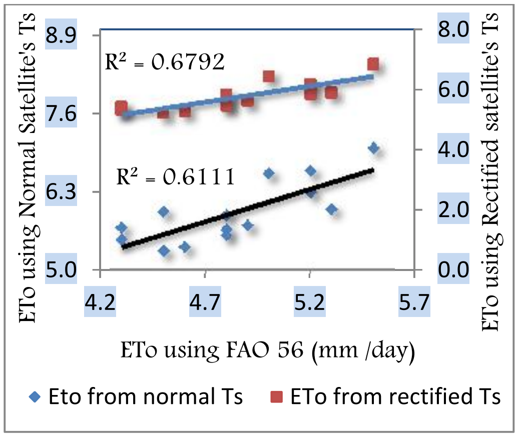

NOAA 17 at UTP

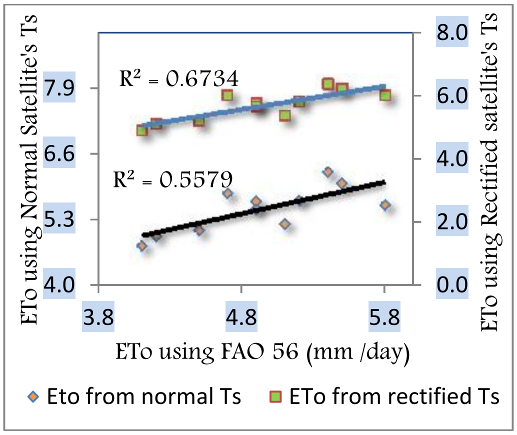

MODIS Terra at UTP

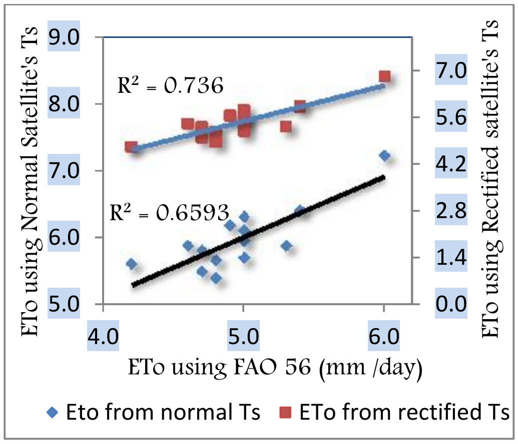

NOAA 17 at SITIAWAN

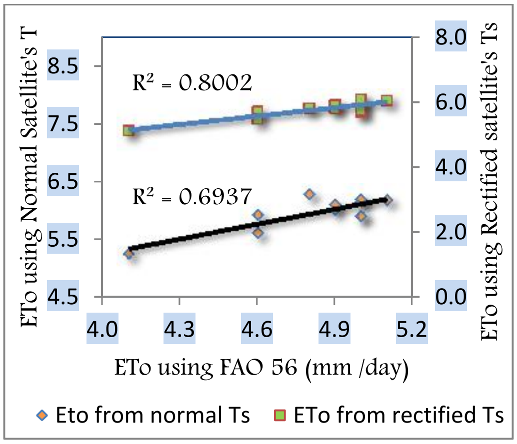

MODIS Terra at SITIAWAN

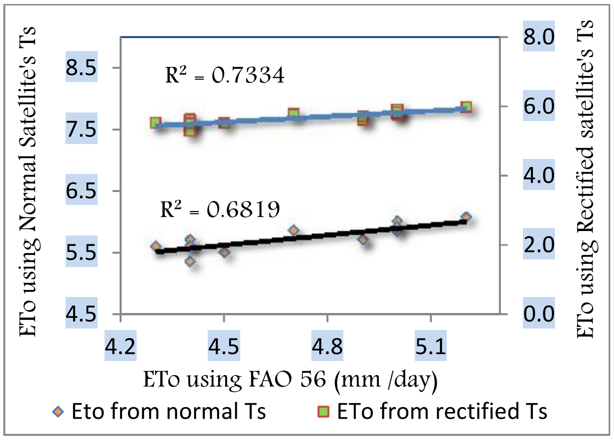

MODIS Terra at SP.PERAK

K 2.2 Satellites data validations for Afternoon overpass sensors.

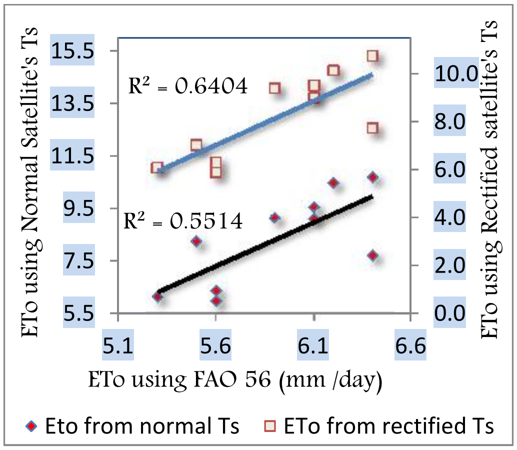

NOAA 18 at UTP

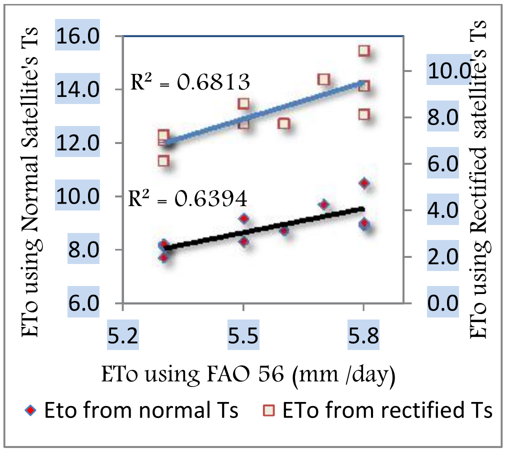

NOAA 18 at SITIAWAN

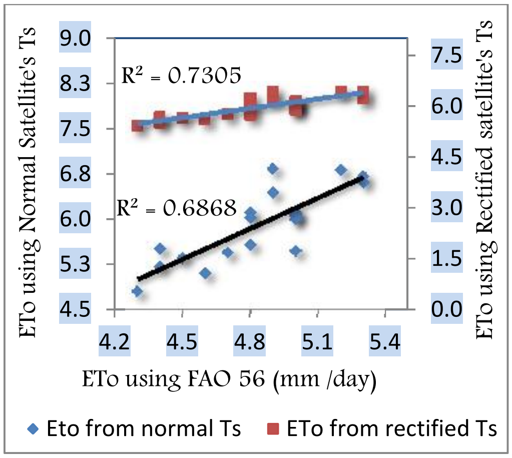

NOAA 18 at SP. PERAK

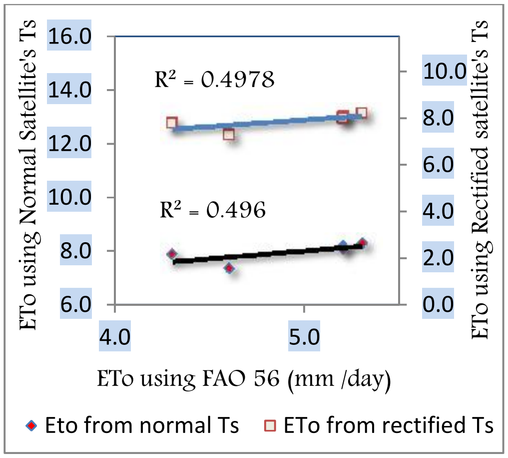

MODIS AQUA at SP. PERAK

K 2.3 Satellites data validations using Jacobs algorithm for Afternoon overpass sensors.

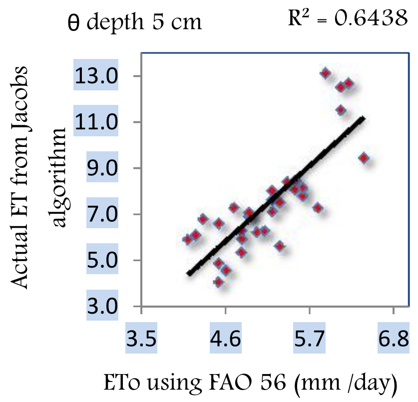

UTP ETa at 5 cm moisture depth

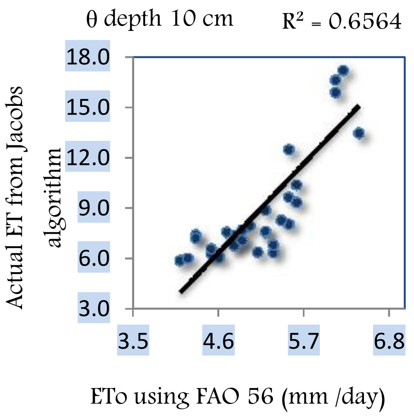

UTP ETa at 10 cm moisture depth

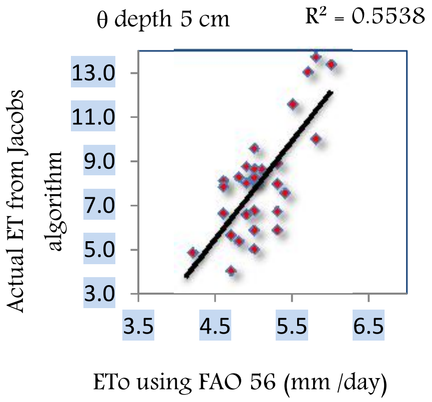

SITIAWAN ETa at 5 cm moisture depth

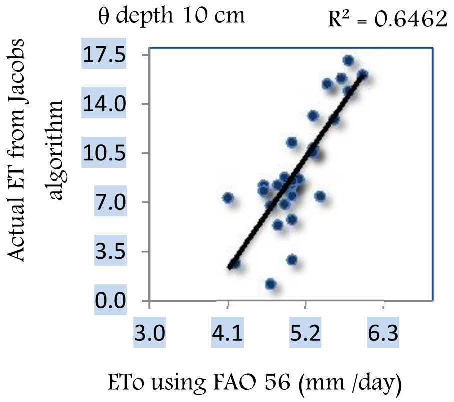

SITIAWAN ETa at 10 cm moisture depth

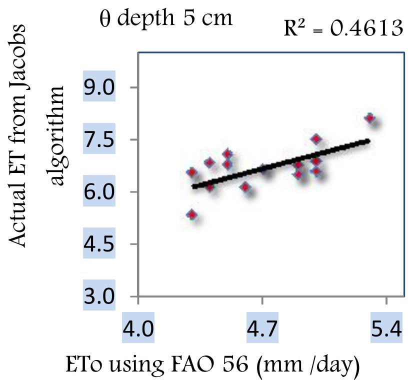

S. PERAK ETa at 5 cm moisture depth

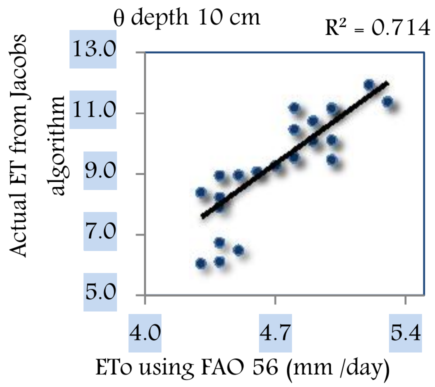

S. PERAK ETa at 10 cm moisture depth

K 3. The success rate validation of the extracted ETo from corrected Ts as well as the moisture diffusion.